

Modelling and Assessment of Restoration in Electrical Power Systems with High Penetration of Power Electronic Converters

Leonel Noris
2018



MODELLING AND ASSESSMENT OF RESTORATION IN ELECTRICAL POWER SYSTEMS WITH HIGH PENETRATION OF POWER ELECTRONIC CONVERTERS

A thesis submitted to the Delft University of Technology in partial fulfillment
of the requirements for the degree of

Master of Science in Electrical Engineering: Electrical Sustainable Energy

by

Leonel Noris

October 2018

Leonel Noris: *Modelling and Assessment of Restoration in Electrical Power Systems with High Penetration of Power Electronic Converters* (2018)

 This work is licensed by TU Delft. To view a copy of this license, visit
<https://repository.tudelft.nl/>.

Cover credits to Mr. Romeo Robles, Graphic Artist

The work in this thesis was made in the:



Intelligent Electrical Power Grids
Electrical Power Engineering
Faculty of Electrical Engineering, Mathematics & Computer Science
Delft University of Technology

Supervisors: Prof. Dr. José Luis Rueda Torres
Prof. Dr. Peter Palensky
Prof. Dr. Armando Rodrigo Mor

ABSTRACT

Power outages can damage severely critical infrastructures such as telecommunication networks, financial services, water supplies and hospitals and completely shutting down production at companies. While most power blackouts usually last from some minutes to few hours, some can last days or even weeks. Furthermore, it is likely that these kinds of events would become more recurrent due to the stranded expansion of aged Electrical Power System (EPS) infrastructures in Europe for coping with the increased societal and environmental pressure for massive deployment of adopting Renewable Energy Source (RES)-based generation, which is known for having a variable characteristic. It is expected that RES will become the dominant factor in the power grid and will gradually replace Conventional Synchronous Generation Units (CGU), and it is known that Offshore Wind Farms (OffWF) are more suitable for large-scale generation applications. However, RES, including Wind Farms (WF), are not well aligned to work with EPS that were designed fifty - to - sixty years ago, due to reduced inertia, reduced short-circuit power, and limited control capabilities that imply the integration of RES. Moreover, more grids will contain more renewables, and thus more risks of outages could arise as one fault can trigger another one as a *domino effect*, deriving in widespread disruptions, including regional blackouts.

In this context, the contemporary control systems that regulate WF inject power to the grid via Power-Electronic Interfaces (PEI), and their schemes are designed to not interfere actively with the safe and secure regulation of a large-scaled EPS. On the contrary, they are just limited to inject a predetermined power injection setpoint with a current-injection control method that assumes all the time this power has load demand to go (*grid-following* control). However, this is not the case when unplanned *islanding* or an outage arises in an EPS, as the WF currently do not possess a control system that regulates the frequency of an *island*.

This MSc Thesis Project presents the design, implementation and testing of a control system attached to type-4 Wind Turbines (WT) that can manage and tightly ensure the load and generation balance during any circumstance, including a massive blackout. This control method can successfully regulate voltage, reactive power and frequency, which can be adapted automatically to the real-time conditions of the grid. The scheme takes the *grid-following* control approach as starting point, which was modified in order to have *Grid-Forming* and *Black-Start* capabilities. The proposed new control approach for *grid-forming* and *black-start* design was implemented in DIgSILENT PowerFactory 2018, where a total of seventeen large-scaled type-4 WF are located into a three-area EPS. The Permanent-Magnet Synchronous Generator (PMSG) WF containing the proposed *grid-forming* control system are accompanied by Hydro, Nuclear and Thermal Plants, accounting CGU. Additionally, the three-area EPS also contains two HVDC Transmission Systems composed each by two Voltage-Source Converters (VSC), which also have similar *grid-forming* and *black-start* capabilities, and seven Battery-Energy Storage Systems (BESS), which give auxiliary power to the *Black-Start* Units and frequency support to the areas with loss of generation. The WF, BESS and the HVDC stations are interfaced via modelled Modular Multi-level Converter (MMC) controlled voltage sources.

The proposed *grid-forming* and *black-start* capabilities of the three-area EPS were tested with several EMT simulations reproducing severe short-circuit faults followed by a loss-of-generation scenario, the blocking of the HVDC converter stations and a massive relay protection program, resulting in the full outage and isolation of the area responsible for the largest power supply in the three-area EPS. After the blackout, the three-area EPS performed a *Restoration* plan, from the generation resetting and the reconnection of lines, transformers, etc., to the final (cold) load pick-up stage. In order to evaluate the advantage of using utility-scaled WF with *grid-forming* controllers to execute a conjunct *Black-Start* and *Restoration* plan, two operational scenarios were performed: one with 90% wind power share and another without any participation of wind power. As a consequence of the implementation of the proposed *grid-forming* control systems, the simulation results endorse that an EPS with 90% wind power share can steer a *Black-Start* and *Restoration* operation when required.

ACKNOWLEDGEMENTS

Primero quiero agradecer a mi Familia por apoyarme y creer en mí siempre. Jamás hubiera podido llegar aquí sin ustedes. A Tania, Saidé, mi Madre y mi Padre por su ejemplo, valores, autoridad, disciplina, por guiarme y fomentar mi interés por la Ingeneiría Eléctrica desde pequeño. Este trabajo está dedicado a ustedes.

I feel honoured and grateful to have met and worked with Dr. José Rueda throughout all this time. He has been an inspiration for me to get things successfully done and to keep me thrilled in the Scientific Research Path. His guidance, support and feedback was invaluable for the realisation of this Project. I also want to thank Dr. Peter Palensky for his confidence, supervision and guidance during the scheduled meetings that were part of this Work, and Dr. Armando Rodrigo Mor for being part of my Thesis Committee and for his very interesting and insightful courses in High Voltage Technology and Laboratory.

I want to highlight and thank the major share of knowledge of Dr. István Erlich (†) and the guidance and clever advice of MSc. Abdul Korai, from the Universität Duisburg-Essen. Further, all my gratitude and acknowledgment to Dr. Elyas Rakhshani for his bright counselling and feedback, and to MSc. Arcadio Perilla, Dr. José Chavez, MSc. Claudio López, and MSc. Digvijay Gusain, from TU Delft IEPG Group, Alfredo Campos, from TenneT TSO GmbH, Eric Meier, from ERCOT, and Adrian Constantin, from DIgSILENT GmbH, for their mastery, advice and teaching.

All my gratitude and acknowledgement to Mr. Roel Overakker, from Royal SMIT Transformers/3E Foundation, for the 3E Sponsorship that allowed me to travel to Germany for the purpose of completing this Investigation. And, of course, I will be forever grateful to Mexico's National Council of Science and Technology (CONACyT) and Secretariat of Energy (SENER) for granting me the scholarship that allowed me to come to study in the Netherlands from the beginning.

Finally, I feel very happy to have met during these two years all the brilliant people who were my classmates and who are now my friends.

"It's not about standing still and becoming safe. If anybody wants to keep creating they have to be about change." — Miles Davis

...

CONTENTS

1	INTRODUCTION	1
2	RESEARCH GOALS, QUESTIONS, AND MILESTONES	3
2.1	Problem Statement	3
2.2	Research Goal	3
2.3	Research Questions	3
2.4	Research Milestones	4
2.5	Thesis Outline	4
3	LITERATURE REVIEW	5
3.1	Electric Power System Blackout	5
3.2	Power Outages Around The Globe	6
3.3	Electric Power System Black-Start and Restoration	10
3.4	Main Role of Power-Electronic Interfaces	12
3.5	Voltage-Source Converters as Grid-Forming Elements	15
3.6	Wind Energy Systems and HVDC Transmission	16
3.7	Wind Energy as a Leading Source	22
3.8	Battery-Energy Storage Systems For Enhanced Support	24
4	STUDY CASE FOR BLACK-START/NETWORK RESTORATION STRATEGIES	27
4.1	Black-Start Strategy with Wind Power Plants, BESS and HVDC Transmission	27
4.2	Dynamic Simulations in DIgSILENT PowerFactory	27
4.2.1	Electromechanical Transients (RMS)-Electromagnetic Transients (EMT) Simulation Differences .	28
4.2.2	Simulation Setup and Procedure	28
4.2.3	Programming and Built-in Model Design	29
4.3	The Original PST 16 Benchmark Power System	31
4.4	Wind Turbine Control System to-be Modified	33
4.5	Power and Control System Models Modifications	35
4.5.1	Synchronous Machines and Transformers	37
4.5.2	Wind Energy Conversion Systems	39
4.5.3	Measurement, Protection and Restoration Logic-Relays	53
4.5.4	Battery-Energy Storage Systems (BESS)-Storage Systems	56
4.5.5	High-Voltage Direct-Current (HVDC) Transmission	59
4.5.6	Measurement Instruments	64
5	RESULTS/PERFORMANCE EVALUATION	65
5.1	PST 16 Benchmark System Network (100% CGU) Load Flow Analysis	65
5.2	PST 16 Benchmark System Network (100% CGU) EMT Outage followed by Restoration	68
5.3	Test of Individual Wind Farm with the Grid-Forming Control Systems	73
5.3.1	WECS Mechanical Dynamic Performance	74
5.3.2	Wind Energy Conversion Systems (WECS) Electrical Dynamic Performance	75
5.4	PST 16 Benchmark System Network (90% WF) Load Flow Analysis	76
5.5	PST 16 Benchmark System Network (90% WF) EMT Outage followed by Restoration with Optimum Wind	78
5.5.1	EMT 90% WF Case Study Dynamic Performance during Initialisation	79
5.5.2	EMT 90% WF Case Study Dynamic Performance after a Blackout	82
5.6	PST 16 Benchmark System Network (90% WF) EMT Outage followed by Restoration with Low Wind . .	94
6	CONCLUSIONS	97
6.1	Answers for Research Questions	97
6.2	Related and Future Work	99

A APPENDIX A: SYNCHRONOUS MACHINE MODELS	107
B APPENDIX B: PERMANENT-MAGNET SYNCHRONOUS GENERATOR WIND TURBINE MODELS	111
C APPENDIX C: HVDC CONVERTER STATION MODELS	121
D APPENDIX D: BESS-STORAGE MODELS	129
E APPENDIX E: RELAY PROTECTION ALGORITHMS	135
E.1 Relay Code for Protection Scheme in Zone A	135
E.2 Relay Code for Protection Scheme in Zone B/Zone C	141

LIST OF FIGURES

Figure 1.1	Power generation facilities around the Globe [1], [2], [3].	2
Figure 3.1	2003 Italy blackout [4].	7
Figure 3.2	South Australia State completely Blacked Out after one of the worst storms in 50 years took place [5].	8
Figure 3.3	Power network topology of Japan in terms of frequency, with three Line-Commutated Converters (LCC) HVDC frequency converter stations [6].	9
Figure 3.4	Typical Restoration Stages [7].	11
Figure 3.5	Sinusoidal waveforms depicted by a Modular Multi-level Converters (MMC) with 200 sub-modules [8].	13
Figure 3.6	Modular Multi-Level Converter [8].	14
Figure 3.7	d - q - o Transformation.	16
Figure 3.8	Structure of a Wind Turbine Generator System [9].	17
Figure 3.9	Structure of a Wind Power as a function of Wind Speed [10], [10].	18
Figure 3.10	Wind-to-Torque Control Plot [10].	19
Figure 3.11	Typical Offshore Wind Farm Diagram very far from Shore [9].	20
Figure 3.12	Comparison of AC and DC Transmission [11].	21
Figure 3.13	Global electricity production in year 2050 [12].	23
Figure 3.14	Circuit of a Battery without and with Parasitic Reaction Path [13], [14].	26
Figure 4.1	Flowchart describing the Simulation Procedure in DiSILENT PowerFactory (DPF). [15].	29
Figure 4.2	<i>PST 16 Benchmark System</i> original case designed in DPF. [16].	31
Figure 4.3	Wind Energy Conversion Systems [17].	33
Figure 4.4	Classical Current Control Method with Current Setpoint reference [17], [18].	34
Figure 4.5	Direct Current (DC) Voltage of the Wind Farms (WF) in <i>PST 16 Benchmark System</i> after a blackout in <i>Zone A</i>	35
Figure 4.6	The modified <i>PST 16 Benchmark System</i> overview.	36
Figure 4.7	Deep frequency excursion with <i>gov_IIEEEG1</i> after applying a Short-Circuit and disconnection of loads.	37
Figure 4.8	DPF Static Generator (ElmGenstat*) depicted as an scaled Wind Power Plant.	40
Figure 4.9	Modifications to the current control method [19].	41
Figure 4.10	Converter Current Limitation Control [17], [19], [20].	42
Figure 4.11	Reactive Power/Alternating Current (AC) Voltage Control Loop [17], [19], [20].	43
Figure 4.12	Active Power/Frequency Control Loop [17], [19], [20].	44
Figure 4.13	Control Loop of the DC Circuit encompassing the Capacitor and the Chopper [21].	46
Figure 4.14	DPF Simulation Language (DSL) Model Definition with the Formulas describing the Equation of Motion for the Permanent-Magnet Synchronous Generator (PMSG) [22].	49
Figure 4.15	Look-up Table for determining the Maximum Speed based on measured Active Power [22].	51
Figure 4.16	<i>Back-to-Back</i> philosophy with a Salient-Pole Machine as the PMSG.	52
Figure 4.17	Zoom-in of <i>Zone A</i>	53
Figure 4.18	Flowchart describing the Protection and <i>Restoration Scheme</i> [7], [23].	54
Figure 4.19	BESS-Storage System Concept [13].	57
Figure 4.20	BESS-Storage System.	58
Figure 4.21	MMC-HVDC Transmission System that interconnects <i>Zone A</i> with <i>Zone B</i> [8].	60
Figure 4.22	<i>V</i> - <i>I</i> Characteristic for a Voltage-Source Power Electronic Converter Interfaces (VSC) operating in active power control mode [24].	61
Figure 4.23	Frequency Analysis according to Nyquist Criterion [8].	63
Figure 5.1	<i>PST 16 Benchmark System</i> case overview with 100% Conventional Synchronous Power Generation Units (CGU) Active.	65
Figure 5.2	Load Flow Analysis applied to the 100% CGU <i>PST 16 Benchmark System</i> Network.	66
Figure 5.3	EMT Simulation on the 100% CGU <i>base-case</i> scenario.	68

Figure 5.4	Synchronous Generators Frequency Plots before, during and after the outage and <i>Restoration</i> events.	70
Figure 5.5	Synchronous Generators Rotor Angle Plots before, during and after the outage and <i>Restoration</i> events.	70
Figure 5.6	Synchronous Generators Active Power in Mega-Watts (MW).	71
Figure 5.7	Active Power Delivered to the Loads of <i>Area A</i> in MW.	72
Figure 5.8	AC Voltage of the busbars connected with the Loads of <i>Area A</i> in Per Unit (p. u)	72
Figure 5.9	Wind Power Plant with a rating of 900 MW.	73
Figure 5.10	WECS Mechanical Dynamic Performance.	74
Figure 5.11	WECS Electrical Dynamic Performance.	75
Figure 5.12	Load Flow Analysis applied to the 90% Wind-Share <i>PST 16 Benchmark System</i> Network.	76
Figure 5.13	EMT Simulation on the 90% Wind Share study case scenario.	78
Figure 5.14	EMT Frequency plots of the Synchronous Machines after 22 seconds of intialisation.	79
Figure 5.15	EMT Frequency Plots of the Wind Power Plants after 22 seconds of intialisation.	79
Figure 5.16	EMT Active/Reactive Power Plots of the Synchronous Machines after 22 seconds of intialisation.	80
Figure 5.17	EMT Active Power Plots of the Wind Power Plants after 22 seconds of intialisation.	80
Figure 5.18	EMT Reactive Power Plots of the Wind Power Plants after 22 seconds of intialisation.	81
Figure 5.19	EMT DC Voltage plots of the Wind Power Plants after 22 seconds of intialisation.	81
Figure 5.20	EMT Simulation on the 90% Wind Share study case scenario just after the blackouts.	82
Figure 5.21	Three-Phase Currents in the High-Voltage (HV)-side of Transformer <i>M_C12_2T</i>	83
Figure 5.22	EMT Frequency Plots of the CGU Synchronous Generators before, during and after the outage and <i>Restoration</i>	84
Figure 5.23	EMT Active/Reactive Power Plots of the Synchronous Machines before, during and after the outage and <i>Restoration</i>	84
Figure 5.24	EMT Frequency Plots of the Wind Power Plants before, during and after the outage and <i>Restoration</i>	85
Figure 5.25	EMT Active Power Plots of the Wind Power Plants before, during and after the outage and <i>Restoration</i> events.	85
Figure 5.26	EMT Reactive Power Plots of the Wind Power Plants before, during and after the outage and <i>Restoration</i> events.	86
Figure 5.27	EMT DC Voltage Plots of the Wind Power Plants before, during and after the outage and <i>Restoration</i> events.	86
Figure 5.28	Active Power of the busbars connected with the Loads of <i>Area A</i> in p. u.	87
Figure 5.29	AC Voltage of the busbars connected with the Loads of <i>Area A</i> in p. u.	87
Figure 5.30	EMT Three-phase Current of the Transformer <i>M_A1a_2T</i> , connected next to the Generator <i>A1aG</i>	88
Figure 5.31	Magnetising Flux (ϕ) vs. Magnetising Current per each phase of the Transformer <i>M_A1a_2T</i>	89
Figure 5.32	EMT Three-phase Current of the Transformer <i>M_A1a_2T</i> , connected next to the Generator <i>A1aG</i>	90
Figure 5.33	Active Power of the busbars connected with the Loads of <i>Areas B</i> and <i>C</i> in p. u.	90
Figure 5.34	AC Voltage of the busbars connected with the Loads of <i>Areas B</i> and <i>C</i> in p. u.	91
Figure 5.35	State of Charge of all the BESS-Storage Units before, during and after the outage and <i>Restoration</i> events.	91
Figure 5.36	Active Power of all the BESS-Storage Units before, during and after the outage and <i>Restoration</i> events.	92
Figure 5.37	DC Voltage of all the Batteries before, during and after the outage and <i>Restoration</i> events.	92
Figure 5.38	<i>PST Benchmark System</i> Network with 90% Wind Power after the finalisation of the EMT Simulation.	93
Figure 5.39	EMT Mechanical Power Plots of the Wind Power Plants considering substandard wind speed conditions.	95
Figure A.1	Synchronous Generator Dynamic Frame.	107
Figure A.2	Automatic Voltage Regulator System designed as a Block Definition by DPF.	108
Figure A.3	Power System Stabiliser designed as a Block Definition by DPF.	109
Figure A.4	Governor with Secondary Frequency Controller (SFC) Model [25].	110
Figure B.1	Wind Turbine Generator Dynamic Model.	111
Figure B.2	Pitch Angle Controller [22].	112
Figure B.3	Wind Power-Turbine Model.	113

Figure B.4	Wind Turbines (WT) Shaft Model.	114
Figure B.5	WT Power Reference based on Speed or Maximum Power Point Tracker (MPPT) [22].	115
Figure B.6	WT DC Busbar, Capacitor and Chopper Model [21],[26].	116
Figure B.7	Phase-Locked Loop Model [8].	117
Figure B.8	Voltage-Reactive Power Controller [21],[26].	118
Figure B.9	Current Limitation and Damping [21],[26].	119
Figure B.10	WT Voltage Modulation Limiter [21],[26].	120
Figure C.1	HVDC System Composite Frame [8].	121
Figure C.2	HVDC Active Power Control [8].	122
Figure C.3	HVDC Reactive Power Control [8].	123
Figure C.4	HVDC Voltage/Frequency Control [8].	124
Figure C.5	HVDC Frequency Sensitive Mode [8].	125
Figure C.6	HVDC Power Oscillation Damper [8].	126
Figure C.7	HVDC Fault-Ride Through Current Injection [8].	127
Figure C.8	HVDC Emergency Power Control Code [8].	128
Figure D.1	Battery-Energy Storage System Frame [13].	129
Figure D.2	Battery Frame [13].	130
Figure D.3	Electrochemical Battery Model [13].	131
Figure D.4	BESS Frequency Deviation Regulator [13].	132
Figure D.5	BESS Charge Controller [13].	133
Figure D.6	BESS Voltage/Power Regulator [13].	134

LIST OF TABLES

Table 3.1	Direct and Indirect Consequences of Blackouts [7], [27].	6
Table 3.2	Major operational challenges for Black-Start and Network Restoration strategies [28].	12
Table 3.3	Advantages of utilising BESS for Ancillary Services (AS) [29].	25
Table 4.1	Different characteristics between RMS and EMT time-domain simulations [15], [30].	28
Table 4.2	Structure of built-in Dynamic Models in DPF.	30
Table 4.3	Saturation/Magnetisation Parameters.	38
Table 4.4	Two-Quadrant Capability Curve for all the WECS.	40
Table 4.5	External Station Control with Q-Operation Mode.	41
Table 4.6	Protection Circuits and Trigger Conditions of the scaled-WT [21].	45
Table 4.7	Wind Gust DSL Common Model and Block Definition [22].	47
Table 4.8	66×49 Wind Power Matrix Array.	48
Table 4.9	Look-up Table for determining the Maximum Speed based on measured Active Power [22].	50
Table 4.10	Protection and <i>Restoration</i> System Model based on Critical Path Method (CPM) [7], [27].	55
Table 4.11	BESS-Storage System Common Model.	59
Table 4.12	Four-Quadrant Capability Curve for all the HVDC Stations.	62
Table 5.1	Load Flow Analysis applied to the 100% CGU <i>PST 16 Benchmark System</i> Network.	67
Table 5.2	Settings for the EMT Simulation.	69
Table 5.3	Output Window Results for the 90% Wind-Share Load Flow Analysis.	77
Table 5.4	Table showing defined events at the EMT initialisation.	78
Table 5.5	Table showing the DSL Protection and <i>Restoration</i> System defining the Remedial Action Schemes (RAS) for healing the grid after the disturbances.	83
Table 5.6	Settings for the different Wind Gust Common Models.	94

ACRONYMS

A	Ampère	25
AC	Alternating Current	xi
AEMO	Australian Energy Makert Operator	8
Ah	Ampère-hour	25
AS	Ancillary Services	xv
AVR	Automatic Voltage Regulator	38
BESS	Battery-Energy Storage Systems	ix
BS	Black-Start	10
BSU	BS Units	8
CGU	Conventional Synchronous Power Generation Units	xi
CIGRÉ	International Council on Large Electric Systems	29
CPM	Critical Path Method	xv
DC	Direct Current	xi
DFIG	Doubly-Fed Induction Generator	17
DPF	DIgSILENT PowerFactory	xi
DSL	DPF Simulation Language	xi
DSO	Distribution System Operator	5
e. g.	Exempli gratia	47
ElectraNet	South Australia's Transmission System Operator (TSO)	8
emf	Electro-Motive Force	18
EMT	Electromagnetic Transients	ix
ENEL	Ente Nazionale per l'Energia Elettrica-Italy's Power Utility Company	7
ENTSOE	European Network of Transmission System Operators for Electricity	22
EPC	Emergency Power Control	62
EPS	Electric Power Systems	1
EPSF	Electric Power Systems of the Future	2
F	Farad	45
FACTS	Flexible AC Transmission Systems	24
FRT	Fault-Ride Through	64
FSM	Frequency Sensitive Mode	63
GB	Giga-Byte	52
GHz	Giga-Hertz (Hz)	52
GSC	Grid-Side Converter Station	32
GSO	Generation System Operator	5
GW	Giga-Watts	7
GWh	Giga-Watt-hour	32
HiL	Hardware-in-the-Loop	99
HV	High-Voltage	xii

HVDC	High-Voltage Direct-Current	ix
Hz	Hertz	xvii
IEC	International Electrotechnical Comission	29
IEEE	Institute of Electrical and Electronics Engineers	29
IGBT	Insulated-Gate Bipolar Transistor	12
kV	kilo-Volt	6
kWh	kilo-Watt-hour	22
km	kilo-metre	7
LCC	Line-Commutated Converters	xi
LFO	Low-Frequency Oscillations	3
LV	Low-Voltage	89
MHz	Mega-Hz	52
MMC	Modular Multi-level Converters	xi
mmf	Magneto-Motive Force	49
MPPT	Maximum Power Point Tracker	xiii
ms	milli-second	25
MSc	Master of Science	3
MVA	Mega-Volt-Ampère	31
Mvar	Reactive Mega-Volt-Ampère	32
MW	Mega-Watts	xii
m/s	Metre per Second	17
NEM	National Energy Market	8
NR	Network Restoration	10
OffWF	Offshore Wind Farms	8
Ω	Ohm	26
OLTC	On-Load Tap Changer	43
OnWF	Onshore Wind Farms	20
PC	Personal Computer	53
PCC	Point of Common Coupling	25
PEI	Power Electronic Interfaces	2
PED	Power Electronic Devices	38
PEC	Power Electronic Converters	4
PI	Proportional-Integral Control	34
PID	Proportional-Integral-Derivative Control	47
PLL	Phase-Locked Loop	45
p.m.	post meridiem	7
PMSG	Permanent-Magnet Synchronous Generator	xi
POD	Power Oscillation Damping	63
PSS	Power System Stabiliser	39
PT1	First-Order Polynomial Delay Filter	59
p. u.	Per Unit	xii
PV	Photo-Voltaic	2
PWM	Pulse-Width Modulation	12

RAS	Remedial Action Schemes	xv
R&D	Research and Development	2
REI	Renewable Energy Integration	12
RES	Renewable Energy Sources	1
RfG	Requirements for Generators	22
RMS	Electromechanical Transients	ix
ROCOF	Rate of Change of Frequency	25
rpm	Rotations per Minute	18
RTDS	Real-Time Digital System	99
SCR	Short-Circuit Ratio	22
SFC	Secondary Frequency Controller	xii
SO	System Operator	1
SOC	State of Charge	25
SOS	Security of Supply	1
STATCOM	Static Synchronous Compensation	25
SVM	Space-Vector Modulation	15
TSC	Turbine-Side Converter Station	50
TSO	Transmission System Operator	xvii
UHV	Ultra-High Voltage	13
UPS	Uninterrupted Power Supplies	2
UV	Under-Voltage Relay	5
V	Volt	26
VDAPR	Voltage-Dependent Active Power Reduction	44
VSC	Voltage-Source Power Electronic Converter Interfaces	xi
WECS	Wind Energy Conversion Systems	ix
WF	Wind Farms	xi
WT	Wind Turbines	xiii

1

INTRODUCTION

Nearly every facet of modern life and society depends on electricity. It is hard to ignore the fact that the electrical grid is perhaps the most powerful lever of human activity and productivity. Electricity is everywhere. The current way of life in modern society is supported by it, from the simplest application at home to the most complex operations in frenetic cities. All primary services rely on the basic service of the power supply. From healthcare, traffic management, food conservation, to communication and finance (just to name some). It is a controllable, safe, economical, efficient and almost invisible means of transportation and delivery of energy. It is amazing how much modern society calls upon on it.

Naturally, for securing this basic service, Electric Power Systems (EPS) are very robust. However, they are also quite complex. EPS are comprised of many elements, like wires, cables, transformers, generation units, switchgears, power-electronic devices, protection and control equipment, and many other parts, which means there are a lot of possibilities that something can go wrong. This fact, together with the world's increasing population, can be translated into a larger electrical power demand, and therefore, the EPS getting closer to their technical limits [31]. As a consequence, disturbances in the EPS are always a risk for the Security of Supply (SOS), and these disturbances can be triggered by many factors [31].

It is disturbing to imagine what would happen if the power supply service is lost for a day, for a week, a month, or longer. It would certainly be chaotic. Without electricity, much of society would deteriorate and break down. An ageing grid infrastructure exacerbates the flaws on energy reliability and grid resiliency [31]. In areas with EPS designed over fifty - to - sixty years ago, even a single storm can cause large-scale cataclysms, to the likes of a power outage. Major blackouts had occurred in previous years breeding serious consequences. Business sectors have had 91 to 164 billions of Euro (€) in losses a year because of power outages [31]. Additionally, because electricity is the driving force that delivers all other elementary services, social dangers can also occur. Looting and vandalism can be widespread, causing disorder and destruction [32]. Even lives are at risks because without power life-support systems in hospitals, nursing homes and households are lost, risks of accidents due to the lost and failures of traffic lights control services, damage to electronic data and computer services, etc. [27].

That is why it is indispensable to maintain the reliability of the Electric Power Grid under all situations. And that is the job of the System Operator (SO). In Electrical Power Business, SO are the entities that manage electrical energy, from the generation stage to the distribution centres, via the transmission systems. They generate and transmit electrical power from generation plants over the electrical grid to regional or local electricity distribution operators. They do this in a reliable way to ensure good-quality electric energy. SO execute system services such as maintaining the balance between electricity supply and customer demand, secure the power supply at the required voltage system, and ensure the exchange between providers and users. Safety and reliability are a critical issue for transmission system operators. To minimise the probability of grid instability and failure, inter-national SO interconnect to each other.

Another task for the entities that manage electric power generation and supply is to optimise the transport network and integrate cleaner technologies to generate electric power, the so-called Renewable Energy Sources (RES). This has been fostered by geopolitical entities that have gotten aware that pollution and climate change are compelling problems that the Globe is facing, and addressing them requires major changes to energy infrastructures. Therefore, European laws have been created to widespread deploy and commercialise RES.

These sustainable energy sources slowly but steadily will be replacing CGU, which are known for their stiff rotor-angle, heavy masses, strong inertia, frequency and voltage regulation capabilities (advantages), but also for their high contribution to environment pollution and CO₂ emissions, especially the synchronous generators with coal and mineral resources as fuel (undesirable disadvantages).

Some examples of RES are Wind, Solar, Hydro, and Biomass Energy while some examples of new technologies de-



Figure 1.1.: Power generation facilities around the Globe [1], [2], [3].

signed to improve energy efficiency are Battery-Energy Storage Systems (BESS), Uninterrupted Power Supplies (UPS), VSC, and HVDC power transmission. All modern energy-efficiency technologies are based on Power Electronic Interfaces (PEI). For example, RES cannot be actively utilised as energy sources if there are no PEI involved [17], [19], [21]. This means that if it is intended to extensively increase the share of renewables in the future, then it is mandatory to integrate PEI extensively in the Electric Power Systems of the Future (EPSF).

Some examples of the mentioned policies and funding-research programmes are the Paris Agreement under the United Nations Framework Convention on Climate Change (Accord de Paris) [33], the Massive InteGRATion of Power Electronic Devices (MIGRATE) [34], and the PROgress on Meshed HVDC Offshore TransmissiOn Networks (PROMOTiON) [35]; the last two managed by the Europe Union (EU), and the first one by the United Nations (UN), where Europe also plays a key role.

In present-day, these agreements have taken effect already in today's EPS. By now, they have penetrated the Netherlands, Europe and the Globe, and this tendency is growing (Figure 1.1). The mentioned environment policies, improvements in technology, financial funds, trends, and business models have been conceived with the main goal of changing the role of renewables, as the main actor in the management of the EPSF. Therefore, in order to maintain reliability and dynamic stability under all circumstances, new control schemes designed for the SOS of the EPSF with fully integrated RES are required. This applies to the standard use of PEI and all upcoming new technologies. Such control schemes must assure a secure power supply even in the worst scenarios. Specifically, a mandatory demand for *grid-forming* capabilities from RES [36]. Electrical networks will connect more BESS, Photo-Voltaic (PV) systems, Wind Power Plants and HVDC links. At first glance, these two scenarios see each other as opposite but must be inclusive one with another. Thus, it is required to successfully develop new control methodologies that guarantee the stability of systems with high penetration of renewables. These new control systems will make renewables able to regulate voltage, reactive power and frequency, besides match generation/load requirements in unstable *islands* a counter-strategy for a lack of inertia in the grid as the use of CGU start to decrease.

From decades there have been successfully-proven standard control systems for maintaining the electrical grid robust, although these strategies were designed to be ruled by CGU. Fundamentally, CGU have relatively predictable operating performance. As a result, *restoration* strategies in the traditional energy paradigm are based on the assumption that the output of each synchronous machine is controllable or predictable [31]. The nature of RES is another, variable and uncertain. Such nature will have an impact in the control of the EPSF, causing major concerns and challenges in the aforementioned rotor-angle, frequency and voltage variables [37]. Although a great amount of work has been done to make power systems resilient against failures, risks of large-scale shutdowns still exist and with the massive inclusion of PEI, these risks will increase. A direct repercussion for that circumstance is that the Power Utilities' traditional way to control all generation, transmission and distribution systems is going to change [37]. Evidently this stands as well for any unexpected extreme scenarios with high instability in the electrical networks; for example, during a blackout followed by the *restoration* of the outaged network. For that, technical Research and Development (R&D) around the Globe on how to *restore* power grids quickly and effectively after outages, ruled by renewables and power electronic devices, are currently being studied.

2

RESEARCH GOALS, QUESTIONS, AND MILESTONES

2.1 PROBLEM STATEMENT

The motivation for doing this project derives from the need for automated, self-healing grids as the intricacy and susceptibility of the interconnected networks increase. After a network blackout fault occurs, the generation units should be able to self-cure, enabling it to return to conditions securely and with a rapid time, minimising losses and diminish adverse impacts on society.

2.2 RESEARCH GOAL

The main goal of this Master of Science (MSc) Thesis Project is to **model and evaluate the performance of the control system of PEI-based generation, Battery-Energy Storage Systems and HVDC transmission links in the restoration of an EPS with high penetration of renewables (90% Wind Power)** after a major outage has taken place. In detail, this investigation analyses the capabilities of new control concepts applied to WF based on type-4 PMSG WT and BESS-battery systems, for starting the *restoration* plans after a major blackout has taken place in an electrical power grid conformed by three strongly-meshed areas. For this purpose, a *Three-Area Benchmark System* was utilised for the simulations on this context. The modelled electrical network is based on the *PST 16 Benchmark System* [16], [38], [39], which was originally defined for sound research on different kinds of stability phenomena (frequency, rotor angle, voltage, Low-Frequency Oscillations (LFO)) [39]. The test electrical network will undergo short-circuit failures followed by a massive outage in one of the areas of the grid. The short-circuits take place in different zones within the same area with a zero-impedance magnitude, causing major disturbing transients that force the system to execute a protection scheme that isolates that area from the rest, creating an *island* while all the elements inside the damaged area are outaged. This scenario is the ideal setup for command a conjunct *Black-Start* and *Restoration* strategy.

The **control systems and the electrical power equipment must then perform outstandingly over normal (steady-state) operation, and, after the scenarios with high instability, all power generation units, devices and control systems must work coordinately for the successful completion of the restored grid**. Software package **DiGILENT PowerFactory 2018 (DPF)** was the main tool utilised for this research. The main power system analysis functions employed in this software were **Load Flow Analysis** and time-domain **EMT Simulations**. The study case has two different operational scenarios, based on the different share of wind energy penetration (0% and 90% share). The 0% wind share operational scenario was included to have a simulation reference of a *network restoration* in classical power systems that do not hold renewables, to have a rough idea of what to expect when tests are done in the other case. In turn, the 90% wind share operational scenario depicts a futuristic case when the gradual substitution of CGU by renewables has already occurred. It is understood that if a joint *Black-Start* and *Restoration* strategy can be performed with 90% WF (a quite difficult scenario due to the very-fast dynamic responses of VSC), other power systems with lower shares of RES should be also capable to do it with a wider margin of ease and simplicity. The *PST 16 Benchmark System* has the two HVDC transmission links and the seven BESS units actively functional in both 0% and 90% wind share operational scenarios.

2.3 RESEARCH QUESTIONS

The modifications implemented in this model must provide the appropriate frequency, voltage, and reactive power support, according to engineering practice nowadays and in the future. This context is the basis of the research questions for this project:

1. **Based on Black Start/Network Restoration TSO sequences, how to model a protection system for restoring an outaged network?**

2. What are the necessary modifications to extend the WT and BESS models used in stability studies for *Black Start*/*Network Restoration* simulation?
3. Considering the theoretical analysis and the research results, is it possible for WF BESS and Power Electronic Converters (PEC) to *restore* a network during different atmospheric conditions?

2.4 RESEARCH MILESTONES

The milestones of this research are the following:

- Prepare a theoretical review with respect to this Thesis topic. Investigate what has been done in previous research and discern among the different scientific articles what can add value to this work.
- According to what has been found during the theoretical review stage, modify and upgrade the three-area EPS with the presented WF, BESS and HVDC links. This also covers the proper implementation of their respective control systems.
- As the size and complexity of the study case is rather large, individual assessment of parts of the whole network had to be done separately, to ensure that the applied control systems operate in an expected way.
- Run **Load Flow Analyses** and **EMT Simulations** with the fully-upgraded complete EPS during steady-state (normal) conditions, as a first assessment to the control schemes for managing EPS. This was recreated for each different operational scenario.
- Run **Load Flow Analyses** and **EMT Simulations** with the fully-upgraded complete grid before, during and after the extreme event of a blackout. This was the main experiment of this Thesis Project, as this assessment can demonstrate whether or not the WF and all the PEI added to the study case are able to perform a *Black Start*/*Network Restoration*. This was recreated for each different operational scenario, but taking special attention to the one with the share of wind energy.
- With regard to the theoretical analysis and the research results, evaluate the obtained results for answer the research questions defined in [Section 2.3](#).

2.5 THESIS OUTLINE

Following the previous introductory chapter ([Chapter 1: Introduction](#)), and this Chapter, where the objectives of this Thesis Project are defined with fundamental questions for the success of this research ([Chapter 2: Research Goals, Questions and Milestones](#)), the outline of this report is comprised by the following Chapters:

- [Chapter 3: Literature review](#). Deepens in the concept of *Black-Start* and *Islanded Operation*, presents briefly some recent outages around the Globe, and explains the potential of WF and PEI in the EPSF.
- [Chapter 4: Theoretical analysis of the study cases for the study of Network Restoration](#). This chapter explains in more detail the DPF study case *PST 16 Benchmark System*. A brief explanation of the modelled electrical network and the introduced technologies used in this research. Structure of the study case with its elements and control systems for all its operational scenarios. Further, the changes applied to the study cases for the study of *Network Restoration* are explained. Step-by-step implementations in the study case in DPF to simulate all the study cases. Capabilities, assumptions and limitations of the model.
- [Chapter 5: Results/Performance evaluation](#). Test and analysis of the results of the simulations. **Load Flow Analysis** for a proper set-up, followed by the initialisation and the time-domain **EMT Dynamic Simulations**, presenting extreme contingencies, power outages, and *restoration* sequences for all the difference operational scenarios.
- [Chapter 6: Conclusions](#). At the closure, the found outcomes are summarised and based on the results, the Answers of the [Research Questions](#) are established. Besides the Conclusions for this MSc Thesis Research, Future and Related Work are briefly considered.

3

LITERATURE REVIEW

3.1 ELECTRIC POWER SYSTEM BLACKOUT

The loss of the electric power in the grid is known as **shutdown**, **power outage**, or **blackout**. Shutdowns can last for a short-term or a long-term period of time. There are many factors that could potentially derive into power outages in an EPS. Examples include faults at power stations, damage to transmission lines, substations or other parts of the distribution system, short circuits and subsequent voltage instabilities, the overloading of electricity mains, dispatch-demand imbalances, defective protection and/or redundancy schemes, etc. Nevertheless, almost none of these potential events go that far to end up in such a critical situation [27], [40]. Normally SO extinguish all potential risks and the served loads/customers/regular population would likely never notice them. When the situation is under control, protection schemes are activated in order to avoid physical damage to the network and total disruption of the system. The abundant transmission paths make strong redundancy schemes that they can even afford to lose a transmission link. This operation is known as $(N-1)$. Besides, in case an EPS is about to fail to meet the load demand, power utilities can deliberately turn off service to some areas, cutting back the supply voltage in order to preserve the healthy operation of at least part of the system. This action is known as *Load Shedding* [41].

Still, when those factors manage to get out of the statistics, uncontrolled disruptions may surge and could evolve into a massive blackout. Often is the loss of voltage support in the grid that causes inability to recover itself, leading to a voltage collapse. As the voltage falls, Under-Voltage Relay (UV) programs trip out elements, but if this procedure is not done carefully, that action reduces the ability of the system to handle the collapsing voltage. This could trigger a cascading effect in which lines trip one after the other until the system blacks out. Another potential source of disaster is when the system frequency (the average frequency of all the generation units that are online), experiences heavy deviations that surpass the frequency thresholds. Sustained operation of EPS is impossible if the system frequency fails to be kept within these strict limits [27], [42].

There are different types of power outages [43]:

- **Partial system blackout:** Blackout of a fragment of the EPS either partially, fully or with more than one portion of the system outaged.
- **Islands:** In case that part of the EPS is separated from the grid due to system splitting or through protection schemes, the isolated part of the grid has to perform the *Restoration* and operate independently. This mode of operation is named *Islanded Operation Mode*. One example of this situation is when the faulted section of the grid is interconnected to other areas through HVDC links, which even before any fault, they make the faulty area already isolated in terms of frequency.
- **Total system blackout:** The EPS in this case, it is said that it is under total blackout when all the generation of regional public services has stopped working and there is no supply of external interconnections to external networks and it is not possible for the total system to work again unless it is completely restarted.

Under certain conditions, a network component shutting down can cause current fluctuations in neighbouring segments of the network leading to a cascading failure of a larger section of the network. This may range from a building to a block, to an entire city, or to the totality of the electrical grid. Thus, changing from one type of shutdown to a more severe type of blackout [43].

The action against a power outage depends on why and what was the cause of it. In case one or more generation units shut down due to a failure in its/their system, the TSO and/or the Distribution System Operator (DSO) make repairs in the network before restarting the resources. Once they are restarted, the Generation System Operator (GSO) can begin the process of reconnecting the generator to the grid. Before closing the circuit breakers of the generator switchgear, it must be sure that all the phases of the generator match the phases of the grid. Otherwise, the generator would relapse to be tripped offline, thus failing to reconnect. This procedure is reproduced if more than one unit failed [27], [40].

If the power outage was caused by a breakdown of the local electric grid, then the TSO designates certain units to go back online under their own power and rebuild the transmission system. As the electrical network is being rebuilt, generators will be added to the system as power is required. In this scenario, it is not the GSO duty to reconnect the units to the grid but rather that of the TSO. Formerly designated to connect to the grid, the generators come online. Once the phases match, the generator can reconnect [27], [40]. These two procedures are however very general and full of assumptions. In [Section 3.3](#) detailed schemes for Restoration Strategies are explained.

Due to the basic need for electricity in the modern world, blackouts are undesirable due to the serious social, economic and industrial consequences that impact civilisation. Some of the most significant consequences and negative effects that imply a blackout are enlisted in [Table 3.1](#) [7], [27].

Direct Impacts of a Blackout	
	Food spoilage
	Manufacturing plant shutdown
	Damage to electronic data and loss of computer services
	Loss of life-support systems in hospitals, nursing homes and households
	Suspension of electrified transport
	Traffic congestion and risk of accidents due to the failure of traffic control services (both in motorways and airports)
Indirect Impacts of a Blackout	
<i>Short term</i>	
	Property losses from looting and vandalism
	Overtime payments to police and fire personnel
	Cancellation of social aids
<i>Medium term</i>	
	Cost of recovery from looting and vandalism
	Lost tax revenues during recovery period
	Consequent increase in insurance rate problems
	Incarceration of looters
<i>Long term</i>	
	Litigation costs
	Contamination due to sewage disposal
	Consequent increased disease

[Table 3.1](#).: Direct and Indirect Consequences of Blackouts [7], [27].

3.2 POWER OUTAGES AROUND THE GLOBE

A characteristic of the EPS is that the collapse of the nodes in a grid can cause a subsequent failure of the dependent nodes in other networks. This can happen recursively and can lead to a cascade of failures. In fact, a failure of a very small fraction of nodes in a grid can lead to the complete fragmentation of the system [44].

That was the case of the blackout that occurred in Italy in September of 2003. [Figure 3.1](#) shows the initial events of the outage. The root cause was a tree flashover that damaged a 380-kilo-Volt (kV) power line that was interconnected between Italy (Lavorgo) and Switzerland (Mettlen). Followed the trip of this line, another 380 kV power line interconnected between them (Soazza-Sils) also switched off because of the sudden higher load in this line due to the previous event, running at 110% of its nominal capacity [4]. Overly-phased angles hindered the reconnection of the lost lines, so the cascading effect disrupted power flow between Italy and Switzerland, France and Austria. The Soverzene-Lienz line that goes to Austria executed the UV protection scheme. Soon after, a voltage collapse in

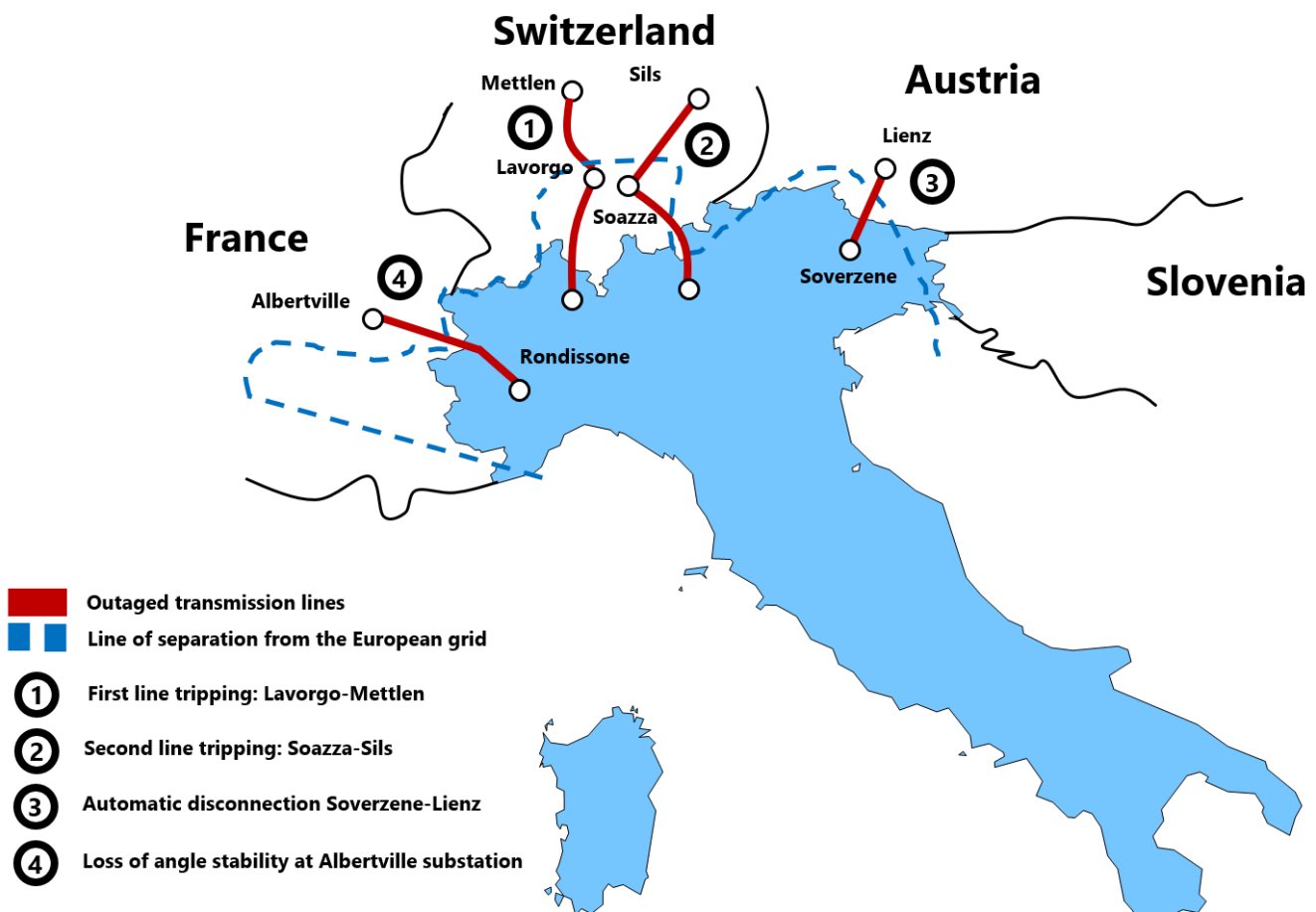


Figure 3.1.: 2003 Italy blackout [4].

Albertville substation in France took place. At this moment the main interconnection lines between the Italian and the European grids were disconnected and they became asynchronous.

The Ente Nazionale per l'Energia Elettrica-Italy's Power Utility Company (ENEL) failed to regulate the stability of the grid in the next 4 seconds, with the lines to neighbouring countries tripped one by one. Frequency collapsed, attaining 49 Hz, because of the loss of the imported power. Within the next 2.5 minutes, the frequency went further down until the under-frequency threshold of 47.5 Hz was hit and all generators were tripped according to the under-frequency protection settings. During this phase the system could not compensate for the additional loss of generation, when around 7.5-Giga-Watts (GW) of distributed power plants tripped during under-frequency operation [4], [45].

The example in Italy shows that EPS blackouts can ensue even if no human error was involved in the root cause, but the ageing protection systems and the little real experience in shutdowns for TSO (which is very little given that this phenomenon does not occur frequently) can be crucial factors for the situation to derive in this worst case. Another example is the blackout that took place in the State of South Australia on September 28th of 2016. One of the worst storms to hit Australia in 50 years knocked out twenty-three HV power pylons [46]. Tornadoes with wind speeds in the range of 190–260 kilo-metre (km)/hour occurred in areas of South Australia. Two tornadoes almost simultaneously damaged a 275 kV single-circuit and one double-circuit transmission lines, 170 km apart from each other [46]. The damage to these three transmission lines caused them to trip, and a sequence of faults in quick succession resulted in six voltage dips on the South Australia grid over a two-minute period at around 4:16 post meridiem (p.m.) [5]. A map of Australia is displayed in Figure 3.2 with the outaged zone standing out.

As the number of faults in the EPS increased, nine WF located in the South Australian Sea showed a sustained reduction in power by activating a protection function that was too sensitive. For eight of these wind power plants, the protection configuration of their WT allowed them to withstand a predetermined number of voltage dips within a period of two minutes. Yet, the activation of this protection function resulted in a significant sustained energy reduction for these WF. A sustained generation reduction of 456 MW occurred over a period of fewer than seven

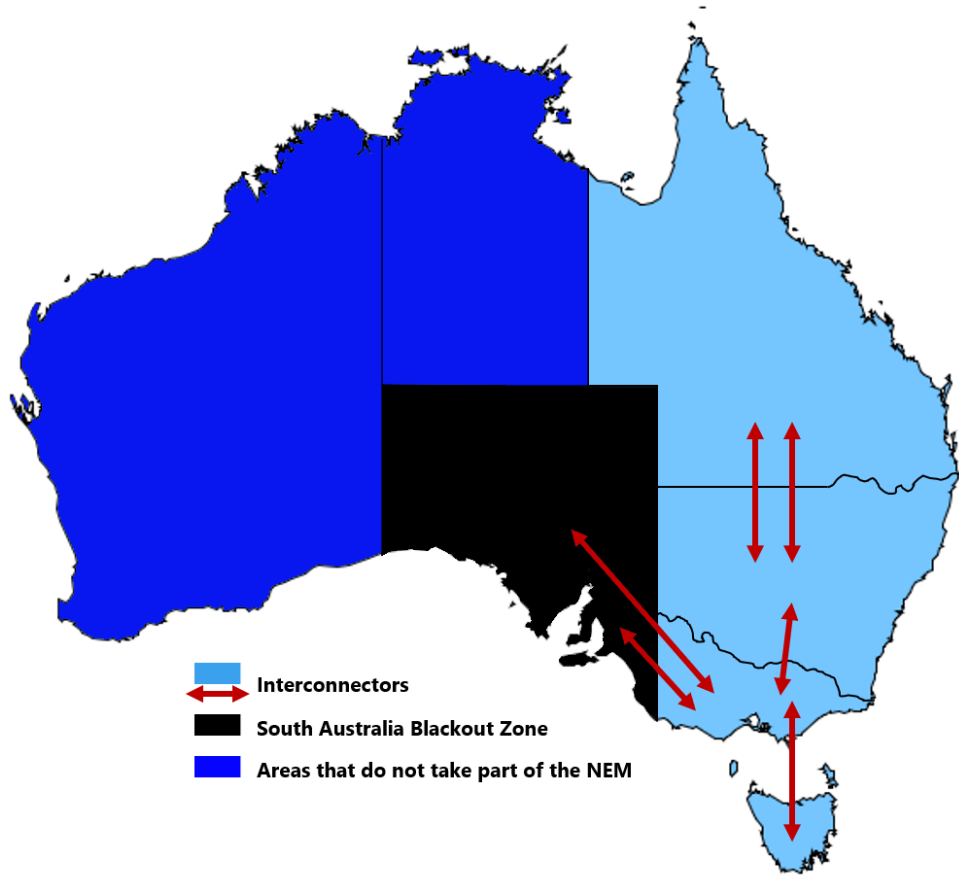


Figure 3.2.: South Australia State completely Blacked Out after one of the worst storms in 50 years took place [5].

seconds [5]. The reduction in WF output caused a significant increase in imported power flowing through the Heywood Interconnector. Roughly less-than-one second after the power loss from the last of the WF, the flow on the Victoria–South Australia Heywood Interconnector reached a preset threshold that, in turn, activated a special protection scheme, tripping off the interconnector [5]. The South Australian EPS then became fully isolated from the rest of the National Energy Market (NEM). After the programmed loss of generation protection, the remaining generation was much less than the connected load, while there was no corresponding *load-shedding* action equating the sudden loss of generation, becoming unable to keep the *isolated* system frequency [5]. As a result, all supply to the South Australian region was lost at 4:18 p.m. The Australian Energy Market Operator (AEMO) analysis showed that following system separation, frequency collapse, and the consequent outage was inevitable [5]. Immediately after the massive outage, AEMO and South Australia's TSO (ElectraNet) evaluated the state of the transmission grid, then ElectraNet put out of service the damaged transmission lines that may have been presenting a potential threat to public safety [5]. After checking what sections of the network were safe to energise, a *Restoration* scheme began at 4:30 p.m., including restart capability from one of two contracted BS Units (BSU) AS Generators from South Australia, and supply from Victoria via the Heywood Interconnector [5].

After the failure, immediate political reactions went to the jugular of the Offshore Wind Farms (OffWF) located in the coast of South Australia's State, accusing them of being the cause of the failure [46]. The official report of AEMO, however, concluded that WT successfully rode through grid disturbances. In fact, the key factor that triggered the problems was rather the action of the protection settings responding to multiple disturbances that led to the blackout [5]. After the failure, changes to the turbine control settings shortly after the event were applied in order to remove the risk of recurrence given the same number of disturbances.

Another widespread shutdown case with no prior human error involved, and to-who blame was entirely on causes of force majeure of mother earth was the major blackout and nuclear disaster that occurred in the Fukushima-Daiichi Nuclear Power Plant complex following the Earthquake and Tsunami of 2011, taking place in Tōhoku, Japan. The natural disaster wreaked havoc of such magnitude that even after seven years they have not been completely repaired. The earthquake triggered powerful tsunami waves that reached heights of up to 40.5 metres, reaching 10 km

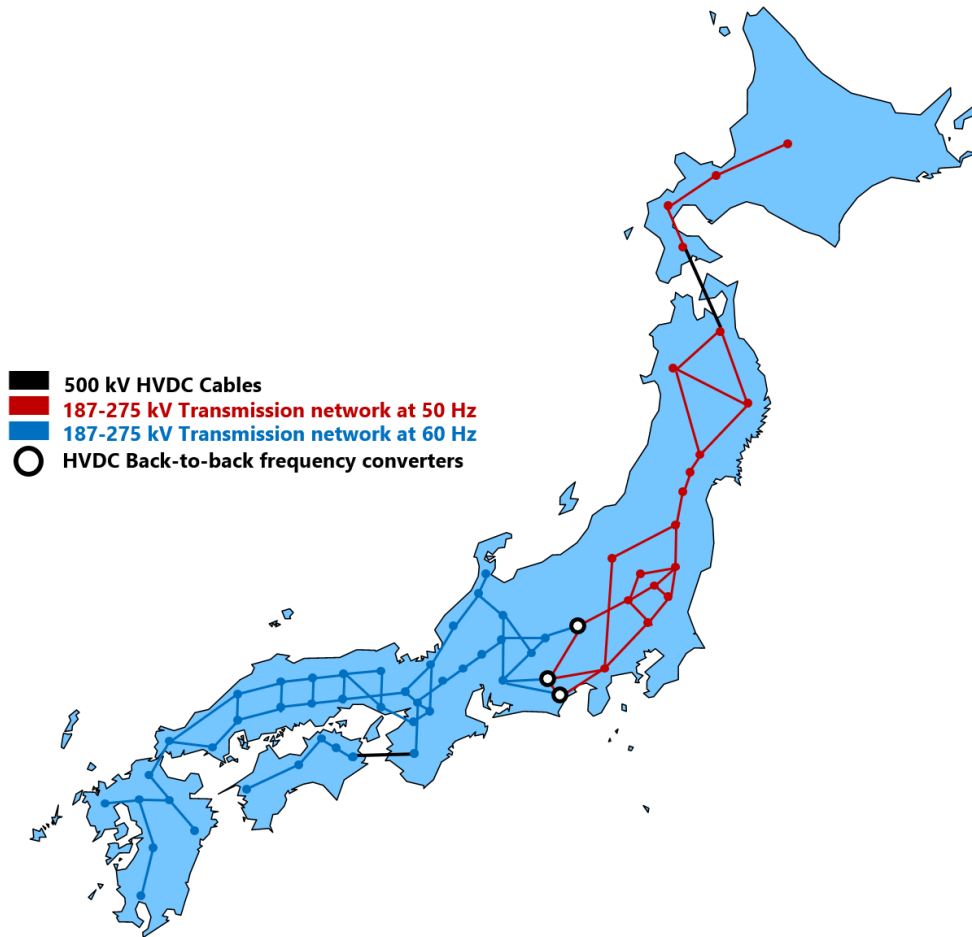


Figure 3.3.: Power network topology of Japan in terms of frequency, with three LCC HVDC frequency converter stations [6].

inland, including the nuclear facilities. It was the most powerful earthquake ever recorded in Japan [47]. The disaster resulted in the loss of about 30 GW of electricity generation capacity, or about 17.3% of Japan's total capacity at the time [48], [49]. Many of the affected fossil-fuel and hydroelectric power stations were quickly restored to operation. However, the biggest blow to Japan's energy supply on that tragic day was delivered to its nuclear power plants. The implications of this sinister brought energy policies that sought to counteract the potential threat of blackouts. The result was a new National Energy Plan introducing a reform that seeks to rebuild from scratch the EPS of Japan with features that ease the process of *restoring* a totally-outaged grid. Rather than improve the robustness of their EPS, Japan focused in developing an easy-to-rebuild grid after a potential catastrophe of such magnitude as Fukushima, as there is probably no strong enough power grid that could endure a disaster of such degree. This plan embroiled a new energy resource mix, giving priority to RES in substitution of nuclear power stations [50], [51].

The inclusion of RES was done along with the decentralisation of power generation. Japan started to switch from large-scale to small-scale power plants distributed evenly across all regions, in which case, battery-storage systems, solar and wind power could take over. Before the tsunami event, Japan's share of renewables was below the 1% of its total energy production. One of the causes it hindered the change was the infrastructure already installed and active. Another reason for avoiding the move to renewables was the high costs of purchase and construction of renewable systems. These reasons made the utilities reluctant to invest heavily in RES. After the calamity, nonetheless, that was no longer an excuse as many of the generation units got irreversibly damaged [48].

In contrast, yearly 2017 Fukushima's installed capacity in renewables had reached nearly 1.4 GW. That comes close to one large nuclear reactor. This included 925 MW of solar power, 209 MW of biomass and 174 MW of wind, with small shares for geothermal (65 MW) and small-scale hydro (17 MW) [51], [52], [53].

The country's unusual transmission network is another challenge, and one of the reasons the blackout spread out heavier. Japan's transmission grid is divided by two, with the east system running at 50 Hz and the western system at 60 Hz. Shin Shinano, Higashi-Shimizu and Sakuma Dam *back-to-back* HVDC facilities are the stations that link these two systems, as shown in Figure 3.3. One of the advantages of using HVDC links is that two grids running at different frequencies can be connected with DC power. Yet, these frequency stations use LCC thyristor

converters, which are great for bulk power transmission, but they do not have controllability for dispatch power in both directions, neither controllability of reactive power. Part of the National Energy Plan aims to replace the LCC for VSC stations too [6].

3.3 ELECTRIC POWER SYSTEM BLACK-START AND RESTORATION

The process of restore an EPS and recover it to bring it back to regular operation after a total or partial shutdown is called **Black-Start (BS)** and **Network Restoration (NR)**. The process may be done with or without relying on external power transmission networks; that depends on the kind of outage [28], [54]. These two terms are commonly used as synonyms, but there is some difference between them. BS is the action of bringing the initial units online only, while NR is rebuilding the system once some transmission is built [27], [40].

SO hold standard RAS procedures for such scenarios; however, in the practice, because of the disruptive nature of blackouts, the *Restoration* Planning rarely progress exactly as planned [7], [27]. There is always a different number of varying-interdependent activities, while new information is brought up after the failure. Besides, there is always the disclaimer that every EPS and resource mix is different. Then, depending on the system characteristics and topology, the SO may choose to first reenergise bulk transmission paths before reconnect and synchronise generation units, or the other way around [55]. Thus, system topology and resource mix will govern both BS and NR strategies.

After a full blackout, as a standard approach, all generators are set offline, and there may be physical damage to the grid itself depending on the cause of the blackout. This damage may need to be repaired before energising the transmission system. The SO will issue a notification of emergency operations to all GSO or TSO. As soon as the operators are ready, they will begin to implement their BS plans. Normally, the grid operator will coordinate with transmission owners and generators to begin powering on select power plants before beginning to rebuild the transmission grid. Lines would be energised to link substations and restore power as time goes on. More generators would be brought online and synchronised to form an electrical *island*. Eventually these *islands* will be synchronised together to restore the grid. Each step will be taken very carefully and slowly to ensure that the rebuild goes smoothly. Failure to follow the proper procedures can lead to the collapse of an *island* and the restarting of the entire process [27], [28], [40], [54], [56]. Always reminding that each *Restoration* Scheme would be different given the described factors above, a NR stage is shown in [Figure 3.4](#). The main stages of a NR are the following:

1. **Preparation: Critical-time actions.** As its name implies, time to perform appropriate actions is critical. This phase can be summarised as an optimisation problem concerning pathfinding (the selection of the best path with regard to present criterion circumstances) from some set of available alternatives., and selection of key resources and key loads to be picked up. Here it is developed a strategy for *restoring* the outaged area or grid, after a *post-mortem* study. Proper scheduling and coordination between the responsible parties and different actions are fully required, as otherwise further errors would hinder the rebuild strategy. The engineers develop a CPM [7], [56], which is a technique that helps to minimise the duration of the outage status speeding up the AS and BS. The theoretical development of the CPM is in charge of study the fastest/best transmission path to reconnect basic elements of the grid, by decomposing the sequence into several separated activities. This approach has a mathematical methodology that ensures that all the individual activities are registered and not started until others have finished, specifying which forthcoming activity has to follow a specific prior one. This planning/scheduling stage makes sure that the available resources are used as minimum and necessary as possible. CPM treats the duration of each activity as a variable, and for each activity is selected three different time duration: an optimistic time x , a most-likely time y , and a pessimistic time z . Moreover, a *Beta* (β) distribution is assumed for consider the probability of the possible duration of the activities. In this fashion, the expected time for one activity is defined by Equations 3.1 to 3.4 [7], [27].

$$t_c = \frac{(x + 4y + z)}{6} \quad (3.1)$$

$$\sigma = \frac{(y - x)}{6} \quad (3.2)$$

The expected total length of the critical path is

$$T_c = \sum t_c \quad (3.3)$$

$$\sigma_c = \left(\sum \sigma^2 \right)^{\frac{1}{2}} \quad (3.4)$$

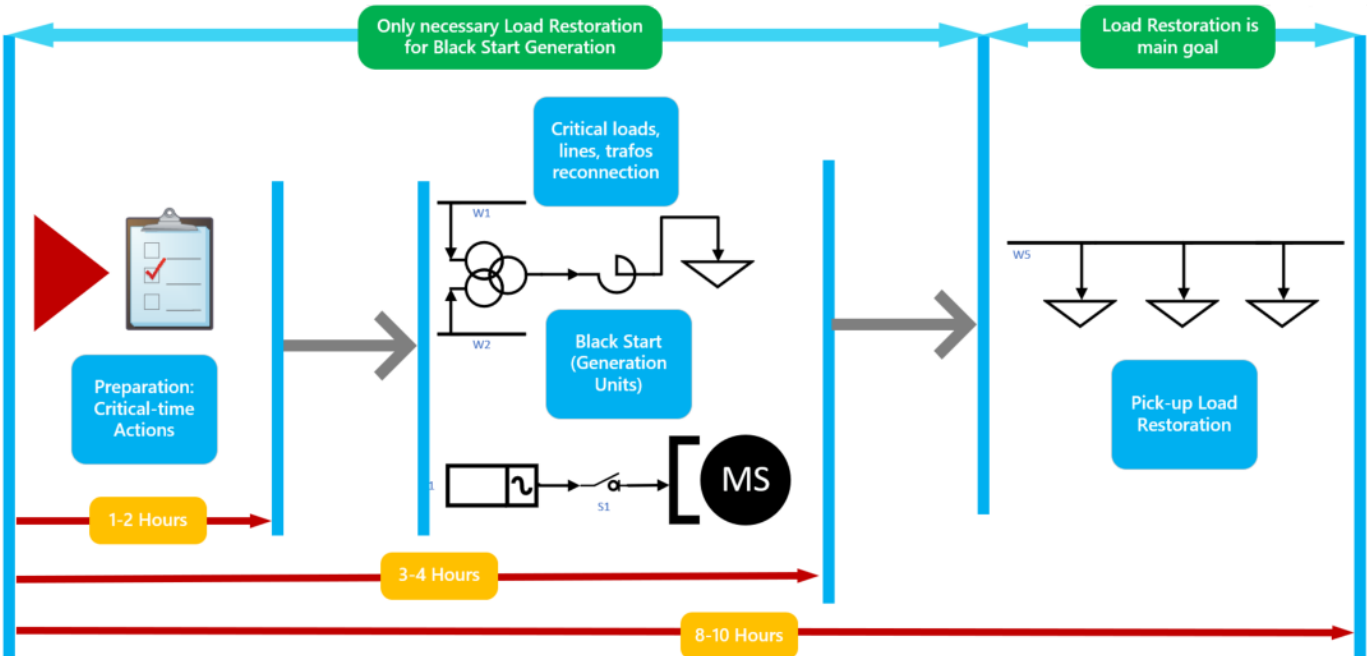


Figure 3.4.: Typical Restoration Stages [7].

This method helps to calculate a realistic time and avoid overly optimistic/pessimistic estimations of the probability of completion. The error can be eliminated by averaging many simulated trials of the near-critical paths in the BS and NR plans.

- Black-Start: Critical elements and loads for cranking power.** In the second stage, there is a need to start the generation units as soon as possible. Here, the CPM optimisation is applied. Only necessary elements are reconnected to be picked up by the first generators *restored* and synchronised. These, in turn, are reset with the help of BSU. BSU are relatively small generation units (like hydroelectric, gas turbine, diesel power plants or BESS). Due to their size, these units are not able to *restore* the majority of the load, but are used to supply power to larger generating plant to enable them to start, that is, they supply the cranking power to the larger units [7]. The priority at this stage is the reintegration of the generation units, whatever type they are, so element or load reconnection are stick to just the backbone path for the accomplishment of this stage. This is generally accomplished by cranking up elements or loads in slow increments that can be well met with the inertia or frequency response of the *restored* units [56]. It is recommended that small radial loads are *restored* before larger ones in order to maintain a relatively constant active/reactive power ratio. Whenever possible it is endorsed that lower-voltage transmission lines are energised first as very HV lines need a ton of reactive power. Reactive power is a scarce/critical resource in a BS and NR. Without it, transmission lines cannot be picked up, because when they are started to be served, they are open-ended and act as large capacitors due to the *Ferranti Effect*, which make voltage management hard [27], [54]. At this step, the EPS is very weak, as there is limited-to-none external support and limited AS. Lack of enough inertia and electromagnetic issues related to reconnection of heavy elements/generation units cause transient voltages and deep frequency variations which may delay the whole process. Further, the protection relays that are reconnected and can always trip again. That is why is very important to follow the structured strategy calculated in the previous stage.
- Network Restoration: (Cold) pick-up of all remaining elements and loads.** The third stage is in charge of *restore* the unserved loads. It is common that the integration of the loads is carried one by one. This makes the task very time-consuming, but otherwise reconnecting several elements at once (or *restoring* them in large increments) is risky because could trigger severe transients and abnormal frequency that might make the system re-incite in an outage. Common practice is that feeders equipped with frequency relays are cranked up at this phase when the system frequency tends back to stability again [27], [54]. As this stage evolves later, however, the grid is stronger as now more generation units and meshed transmission paths are engaged in the process. The effective system response rate and the responsive reserve increase with the combined capacity of these re-activated units [28], [36]. The scheduling of the load cranking and the permissible load size to be picked up will depend on the response of the rate capabilities of the generators that were getting online previously. If the whole process has reached this point, then it is allowed to *restore* loads at higher increments [56].

In real life, these stages are composed of several actions that depend on the circumstances are out of the scope of the simulations for this research, like switching interlocks and circuit breakers manually, energisation of the internal circuitry that reignites non-BS units, SO/utilities manager meetings, and the additional time it has to be taken for the coal generation units to heat themselves and further communication between the different parties relevant to the *Black-Start* plans that may increase the duration of this stage [40].

Table 3.2 categorises some of the major types of technical challenges that need to be considered during the BS and NR phases:

	<i>Black-Start Stage</i>	<i>Network Restoration Stage</i>
<i>Transient Security</i>	<ul style="list-style-type: none"> • Electromagnetic transients of BS units • Frequency response of prime movers to load pick-up • Switching transient overvoltages • Resetting the thresholds of protection for BS and for NR 	<ul style="list-style-type: none"> • Voltage stability and compensation in energising long-distance transmission lines with high or no load • Tie-line phase angles of synchronisation • Switching surges
<i>Steady-State Security</i>	<ul style="list-style-type: none"> • Active power balance • Reactive power compensation • Fault allocation 	<ul style="list-style-type: none"> • Active-Reactive power balance • Reactive power balance • Thermal stability • Voltage stability • Generation selection and line routing • Reliability

Table 3.2.: Major operational challenges for Black-Start and Network Restoration strategies [28].

3.4 MAIN ROLE OF POWER-ELECTRONIC INTERFACES

The increasing penetration of renewable-based generation units that feed power into the network do it via converter interfaces. They make possible the injection of energy from these sources despite the latter present more frequent, larger, and faster fluctuations in their generation processes. In the case of wind and solar sources, these power-electronic converters decouple the sources interfaces from the electrical grid. Therefore, when it is stated that Renewable Energy Integration (REI) will be required to participate in active and reactive power management systems, so will be PEI [18], [21]. This gives rise to many challenges to the power system. Two of the most important challenges are voltage/reactive power and frequency control. Renewables will have to manage voltage control the same way the synchronous machines currently do it. Further, is expected that the participation of the latter will be continuously reduced in the EPSF, and so will be the grid inertia embedded to them, which will lead to a much faster dynamic behaviour. Consequently, the requirements of the EPS in practice will be broader and multidimensional in both the scope and response timeframe [38]. Supporting the network to prevent a voltage collapse following a major network failure requires a rapid reactive current injection. On the other hand, responding to slow changes (tracking of the setpoint) in the load flow requires a corresponding slow response that affects a wider geographic area within the electricity grid. [17], [18], [19], [21].

Yet, for coping with these different needs, PEI come with significantly enhanced control features that traditional power system devices do not possess. They are able to smoothly transit between successive steady-state operating points and also between steady-state and dynamic operating modes in a contingency situation and vice versa. Therefore, a must-try approach that potentially would help in a fluid transition of the changing EPS is to design solutions that draw upon these new control capabilities to the fullest extent [17], [19]. The challenges above mentioned regarding voltage, reactive power and frequency regulation can be attended by control features available in VSC-based converters. This technology has appropriate applications and can be used successfully in HVDC transmission and for connection of wind and PV power plants to the grid [20].

Voltage-Source Converters (VSC) are a type of converter based on Insulated-Gate Bipolar Transistor (IGBT) that possess turn-off/turn-on control capability. It is because of this feature that they can be used as self-commutated converters [30]. With VSC, the polarity of the DC voltage is usually fixed and the DC voltage then is smoothed by a large capacitor, which makes the voltage come across to nearly constant (hence its name).

The additional turn-off control gives many advantages. This can improve the harmonic performance and draw an output signal that resembles a sinusoidal AC wave with Pulse-Width Modulation (PWM) techniques, triggering the

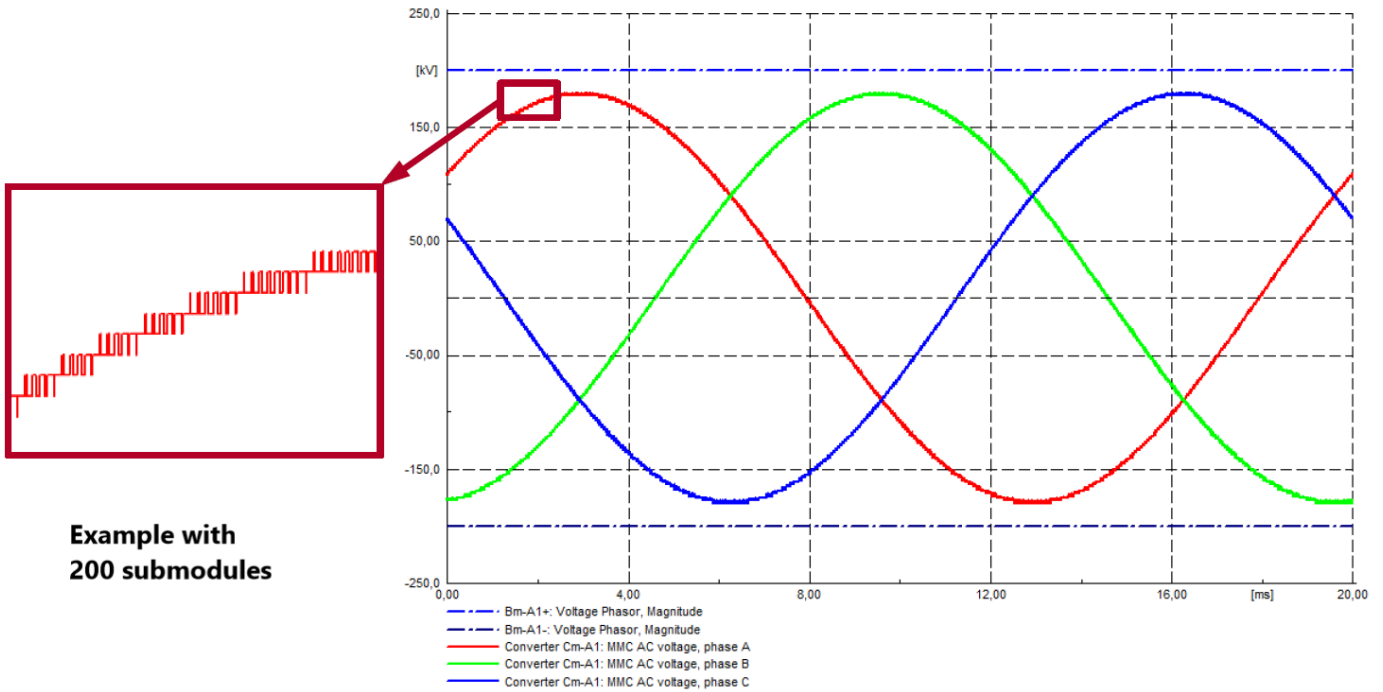


Figure 3.5.: Sinusoidal waveforms depicted by a MMC with 200 submodules [8].

switches of the converters in a suitable time to draw such sinusoidal, as shown in Figure 3.5. VSC maintain a constant polarity of DC voltage and power reversal is reached instead by reversing the direction of current. This makes VSC much easier to connect into a multi-terminal HVDC system. Because of its increased controllability, VSC do not have the necessity of rely on synchronous machines for their operation; further, they can feed power to an AC network consisting only of passive loads, something which is impossible with LCC [30]. Some **major advantages** (and some **areas of improvement**) of VSC are enlisted below [8]:

- **Very good controllability of active and reactive power**
- **Low harmonic content** (with high-switching frequency, MMC depicts almost perfect sinusoidal waveforms)
- **Reactive power can be controlled by the converters**
- **They can be perfectly used regardless of how strong/weak the AC grid they are connected to is**
- **They present *grid-forming* capability** (if their controllers are designed for this objective)
- **High no-load losses** (and increases with higher-switching frequencies)
- **New technology**
- **Efficiency for Ultra-High Voltage (UHV) Transmission** needs to be improved for transmission above 1000 MW

The simplest type of three-phase VSC is composed of six-pulse bridges with IGBT connected with inverse-parallel diodes, but for having a higher definition in the signals (smoother sinusoidal waveform), MMC are nowadays the main type of converter utilised (Figure 3.6). Here, each valve of the two-level converter consists of a large number of IGBT connected in series, and each valve is a separately controllable voltage source. Each valve consists of a number of independent converter submodules, each containing its own storage capacitor [8].

Depending on the type of application and on the time frame of phenomena being analysed on the DC grid, modelling software packages define the detail and complexity level of different computational models for VSC converters [30]. The type of computational models useful for EMT simulations is the Type-5 [8], [30]. The equations that exemplify this model include IGBT and uses small time-steps as integration to represent the fast switching events accurately. These relatively simplified models replicate the average response of switching devices, converters and controls by using controlled sources and switching averaged functions. The controlled sources include the harmonic content from the modulation control (switching functions) on the AC waveforms. Equations 3.5 to 3.8 represent the output reference voltages of the AC-side of these average-value models [30]. For each phase (j) and each upper/lower voltage level (x):

$$v_{xj} = -v_j + \frac{V_{DC}}{2} \quad (3.5)$$

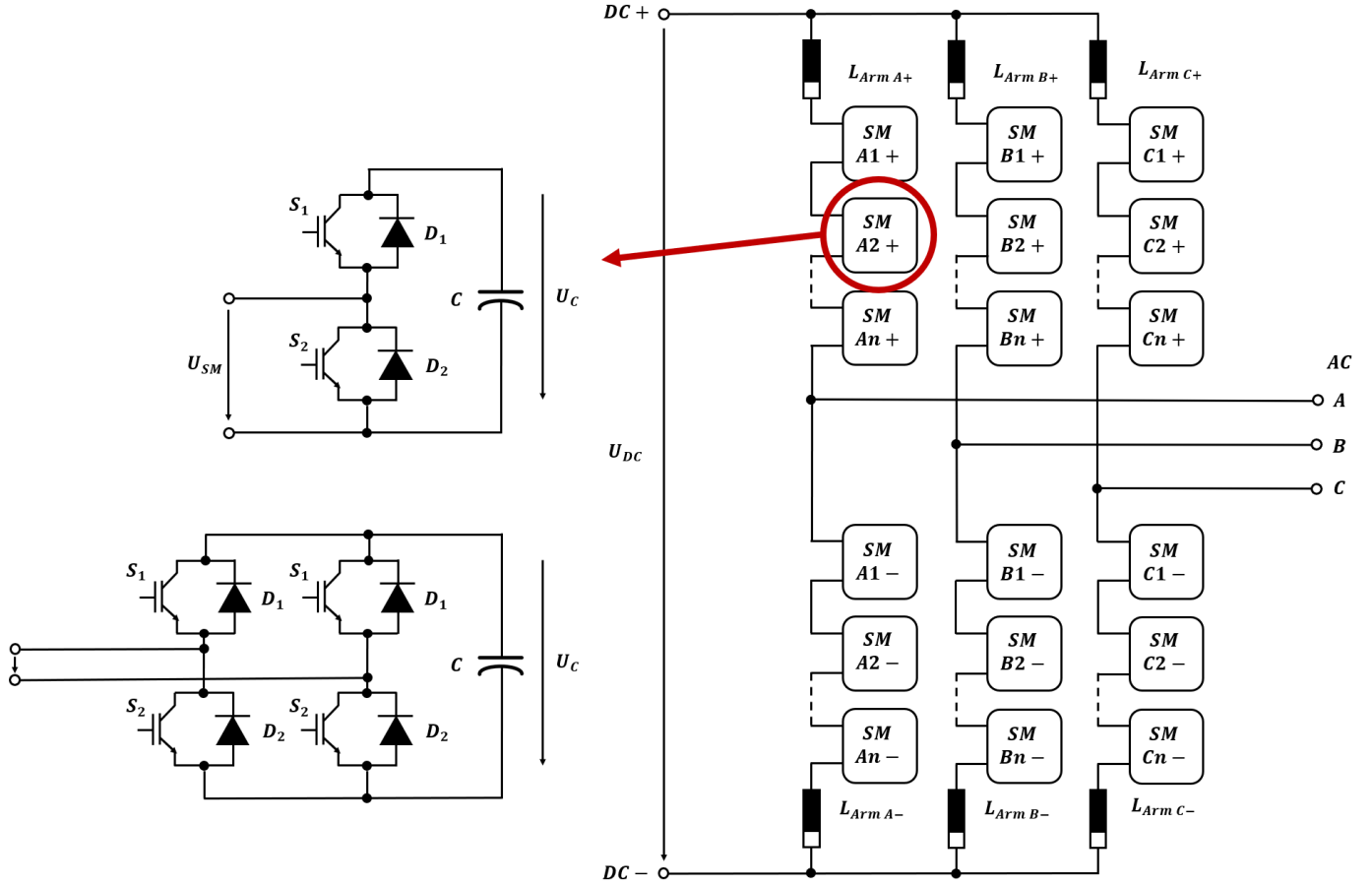


Figure 3.6.: Modular Multi-Level Converter [8].

$$v_{xj} = v_{uj}^{SM} - L_S \frac{di_{xj}}{dt} \quad (3.6)$$

$$v_{xj} = \sum_{i=1}^{N_{xp}} (S_{xji} v_{c_{xji}}) v_{uj}^{SM} = \sum_{i=1}^{N_{xp}} (S_{xji} v_{c_{xji}}) \quad (3.7)$$

$$v_{xj}^{SM} = -v_j + L_S \frac{di_{xj}}{dt} + \frac{V_{DC}}{2} v_{xj} = v_j + L_S \frac{di_{xj}}{dt} + \frac{V_{DC}}{2} \quad (3.8)$$

where the voltage $v_{c_{xji}}$ represents the upper/lower capacitor voltage at each submodule (SM) while the voltage v_{xj} is the total upper/lower voltage at each arm. v_{xj} is a function of the number of switches (S_{xji}) turned on [30].

For the DC side of the average-value converters, formulas 3.9 to 3.12 are derived from the principle of power balance, which states that the power on the AC side must be equal to the power of the DC side plus the converter losses [30]:

$$P_{AC} = P_{DC} + P_{Loss} \quad (3.9)$$

$$\sum_{i=a,b,c} e_j i_j = V_{DC} I_{DC} + P_{Loss} \quad (3.10)$$

$$m_j = 2 \frac{|e_j|}{V_{DC}} \quad (3.11)$$

$$\frac{P_{AC}}{V_{DC}} = \frac{1}{2} \sum_{i=a,b,c} m_j i_j = I_{DC} + \frac{P_{Loss}}{V_{DC}} \quad (3.12)$$

where the power balance is rewritten as a function of modulation index m_j . These formulas represent only some few parameters of the rather complex design of a VSC MMC converter. Moreover, VSC converters are omnipresent elements that take part of structure of all power system elements (generation (REI), storage (BESS) and HVDC) set

in this research. Therefore, these equations may apply for all of the converters embedded in the above mentioned models.

The definition of these formulas was obtained with aid of the advanced technique of Space-Vector Modulation (SVM), briefly explained in [Section 3.5](#).

3.5 VOLTAGE-SOURCE CONVERTERS AS GRID-FORMING ELEMENTS

If sudden increments of active power consumption by the load centres occur while the mechanical power supplied to the generator remains constant, the electrical output power decreases. When a decelerating power arises it means that the rotation of the generator slows down and the frequency of the electric power output drops [57]. In traditional EPS, is the Centrifugal Governor System that controls the speed of a synchronous machine by regulating the amount of fuel that is supplied to it. Accordingly, then the active power balance is restored by the speed governor [57], [58]. With RES, the way of controlling the voltage and frequency cannot be done with CGU speed governors. And, if the EPSF will have a high participation of RES (which are not controllable), this poses new challenges to the system.

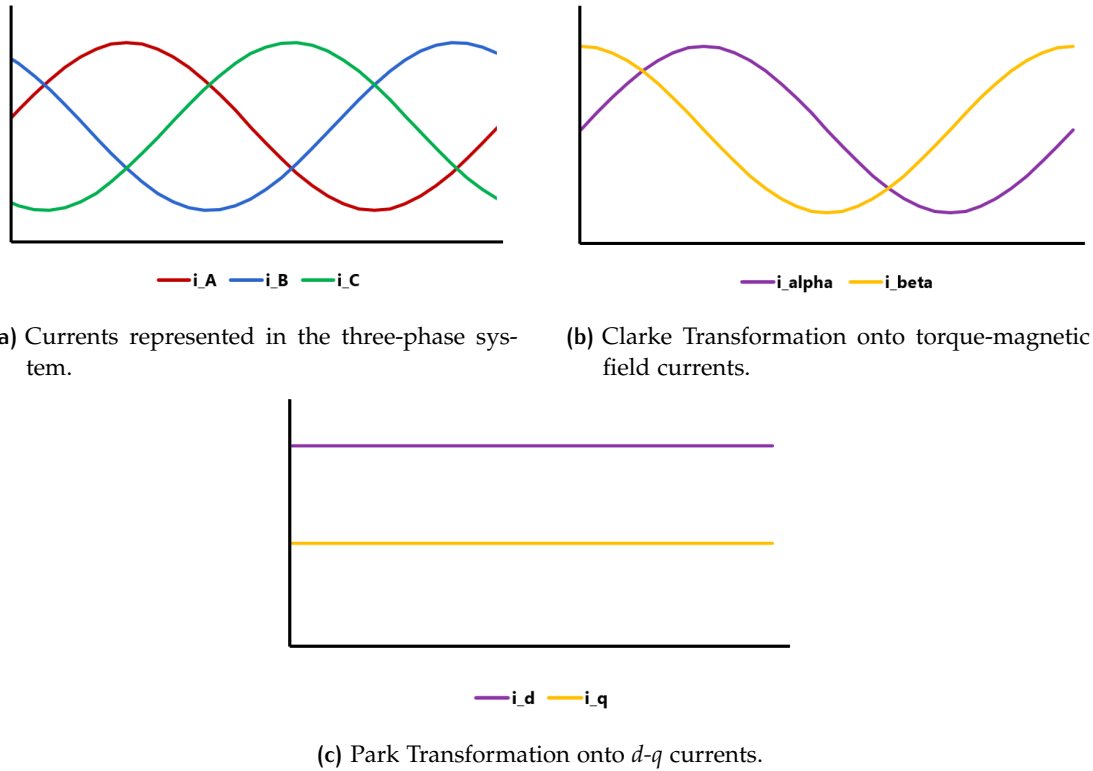
For WT, the VSC manage their power reference (along with atmospheric data, [Section 3.6](#)) the same way governor systems do for the power plants ruled by CGU. The way they control voltage and frequency is with an algorithm known as Space Vector Modulation (SVM) [59]. The idea of SVM methodology is to strip down the VSC controllers, rotating the reference frames of the AC waveforms such that they become DC signals. Straightforward calculations can then be carried out on these DC quantities before performing the inverse transform to recover the actual three-phase AC sinusoidal waveforms ([Figure 3.7a](#)). Therefore, this methodology is used in order to simplify the analysis for the control of VSC the same way it has been utilised for almost a century for the calculations of currents, powers and torques in the synchronous machines of conventional EPS (and thus it can also be utilised for the PMSG calculations) [58], [60]. This technique is known as the **Direct-Quadrature-Zero Transformation (d-q-0)**, also known as the **Clarke-Park Transformation** ([Figure 3.7](#)). For a Type-4 WT, the reference used is the position of the magnetic field in the PMSG rotor. When the magnetic field in the rotor has been determined, SVM aids to define where to apply the magnetic field in order to further move the rotor in the desired direction, with the final goal of producing a torque for placing the stator field in the direction where the largest torque application on the rotor can be reached. And it turns out that the highest torque per current is reachable when the magnetic field of the stator is oriented in a perpendicular position with respect to the rotor [60]. Knowing this, the transformation converts the three-phase stator/rotor quantities into a single rotating reference frame to eliminate the effect of the time-varying inductances. This is done by regulating **torque** and **magnetic field (flux)** in terms of **active** and **reactive current**, respectively, in a way that the three currents in the three-phase system of the WT can be decomposed into two different orthogonal currents, in the exact same structure as **complex power** is divided into **active** and **reactive power**. This transformation of three-phased currents into torque/flux currents is known as the **Clarke Transformation** [61] ([Figure 3.7b](#)), which is represented in a simplified way by the Formulas [3.13](#) and [3.14](#)

$$i_\alpha = \frac{3}{2} i_A \quad (3.13)$$

$$i_\beta = \frac{\sqrt{3}}{2} i_B - \frac{\sqrt{3}}{2} i_C \quad (3.14)$$

where i_A , i_B and i_C represent the three-phase currents, while i_α and i_β represent the decomposed torque and flux currents. In this manner, by controlling the torque and flux the converters automatically control the three currents. However, as these currents are still sinusoidal, the controllers would still struggle to control these values, as they are constantly changing. The controllers further need a steady-state input to work with. For that, the sinusoidal waves can turn out constant by knowing in real time the position of the magnetic field in the rotor. As this information can be derived, the sinusoidal movement of the currents can be straighten-up utilising trigonometric functions. This trick is known as **Park Transformation** [62] ([Figure 3.7c](#)), and essentially lets the controller experience the rotor point of view from a steady state instead of watching it rotating from the point of view of the stator [60]. Matrices [3.15](#) and [3.16](#) describe the complete transformation and its reverse, the former representing the matrix that determines the **d-q-0** transformation while the latter depicts its contra.

$$\begin{bmatrix} i_d \\ i_q \end{bmatrix} = \begin{bmatrix} \cos(\phi) & \sin(\phi) \\ -\sin(\phi) & \cos(\phi) \end{bmatrix} \begin{bmatrix} i_\alpha \\ i_\beta \end{bmatrix} = \frac{3}{2} \begin{bmatrix} \cos(\phi) & \cos(\phi - \frac{2\pi}{3}) & \cos(\phi - \frac{4\pi}{3}) \\ -\sin(\phi) & -\sin(\phi - \frac{2\pi}{3}) & -\sin(\phi - \frac{4\pi}{3}) \end{bmatrix} \begin{bmatrix} i_A \\ i_B \\ i_C \end{bmatrix} \quad (3.15)$$

Figure 3.7.: d - q - o Transformation.

$$\begin{bmatrix} i_A \\ i_B \\ i_C \end{bmatrix} = \begin{bmatrix} 1 & 0 \\ -\frac{1}{2} & \frac{\sqrt{3}}{2} \\ -\frac{1}{2} & -\frac{\sqrt{3}}{2} \end{bmatrix} \begin{bmatrix} i_{\alpha} \\ i_{\beta} \end{bmatrix} = \begin{bmatrix} \cos(\phi) & -\sin(\phi) \\ \cos(\phi - \frac{2\pi}{3}) & -\sin(\phi - \frac{2\pi}{3}) \\ \cos(\phi - \frac{4\pi}{3}) & -\sin(\phi - \frac{4\pi}{3}) \end{bmatrix} \begin{bmatrix} i_d \\ i_q \end{bmatrix} \quad (3.16)$$

With this transformation the reference system is now rotating coordinately along with the vectors; is because of this effect that the reference appears as steady [59], [60], [61], [62]. In other words, the concept of three-phase power, composed of four dimensions (phases A , B , C and time t) was decomposed and simplified to just two dimensions, represented by two differential-mode vector components, the **direct d** and **quadrature q** frame. The third vector represents the time t , which now is in *direct alignment* with the vector of rotation. Hence, it is known as the vector **zero (o)**, name that implies its apparent nullity. The concept of three-phase systems in electrical engineering is sometimes difficult to explain, especially in reports, as it can normally only be represented in a two-dimensional perspective. As this transformation implies a *three-dimensional perspective*, the **zero** vector is projected into the plane of this *three-dimensional* reality.

This transformation breeds many advantages in the control of the VSC converters [8]:

- Because the d - q currents are in DC state, simple controllers can be employed to regulate these quantities
- Direct control of reactive and active power
- Easy tuning of control bandwidths and dynamic performance

3.6 WIND ENERGY SYSTEMS AND HVDC TRANSMISSION

The concept of wind energy embodies interdisciplinary subjects and sciences (mechanical/electrical technologies, control theory, modelling and integration of power systems) [63]. A diagram that displays the function of a WT system is shown in Figure 3.8. In detail are summarised all the elements that make work a WECS:

1. **Wind Power**- WT work because they are designed to collect the kinetic energy from the wind and then convert it into electrical energy that then is fed into the EPS. How much of this energy from can be utilised depends

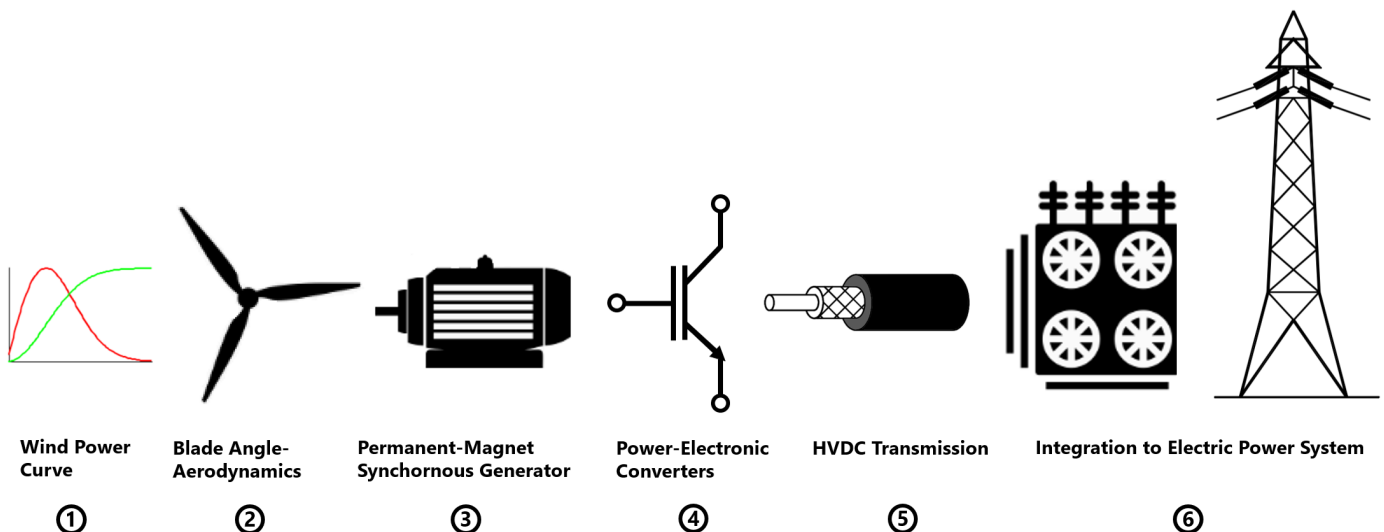


Figure 3.8.: Structure of a Wind Turbine Generator System [9].

on how the wind resource is characterised and on the rotor speed of the machine according to various wind speeds, where it can be defined the locus of maximum power output (**Power Curve**). Across a wide range of wind speeds, the power produced by a WT varies with the cube of the wind speed. This is shown on Figure 3.9, which illustrates the power as a function of the cube of the wind speed. The mechanical power extracted by the WT can be calculated as

$$P_w = \frac{1}{2} \rho A_{\text{rot}} c_p (\lambda, \beta) v_w^3 \quad (3.17)$$

where ρ is the density of the air, A_{rot} is the area swept by the rotor blades, v_w^3 is the cubed wind speed, λ is the tip speed ratio, β is the blade (or pitch) angle, and c_p is the coefficient of power [39], [63]. Further, WT manufacturers provide the specific value of c_p as a set of curves relating the coefficient of power with respect to a set of different combinations of λ and β values, which are stored in a matrix [64]. The tip speed ratio λ is defined as

$$\lambda = \frac{\omega_T R}{v_w} \quad (3.18)$$

where R is the radius of rotor blade and ω_T is the speed of the turbine. However, this holds only for a certain range of wind speeds. At very small speeds, there is not enough wind for the turbine to actually rotate. The wind speed at which the rotor starts to rotate is called the *cut-in speed*. Below this value, no power is produced. The *cut-in speed* is typically about 3-to-4 Metre per Second (m/s) [10]. On the other hand, if the wind is very strong, the loads on the rotor can become too large. Therefore, the so-called *cut-out speed* is the maximum wind speed at which power can be safely produced. This lies typically around 25 m/s [63].

2. **Pitch Angle Control and Power Reference**- Beyond a certain wind speed, the power is limited to a constant value. This value is the *rated power* and typically occurs for wind speeds between 12-to-17 m/s [10]. The angle control of the turbine blades is the means for adjusting the aerodynamic torque of the WT when wind speed is above rated speed in order to maintain the turbine shaft torque within its design limits. When rated power is attained, the power is kept constant by turning the blades along their axis, that is by pitching them [10]. Therefore, if the wind speed is running at ideal conditions for the turbine, β remains in a constant-zero value. If the wind speed grows higher (sudden gust of wind), the power (or the torque) can be limited to its rated value by rotating the blades of the turbine nonlinear servo actuator of the controller, thus adjusting the β angle. The **Aerodynamic Design** of the Blades, as well as the **Pitch Angle Control** and the **Wind Power Characteristics** of the turbine maximise the maximum quantity of energy possible to collect, according to the varying wind speed, thus acting as a **MPPT**. The MPPT works with a power measurement that gives the **Power Reference** to the generator to adapt to the required speed according to the power measurement tracking [39], [64]. This ensures that the rotor can extract the maximum power possible according to the available resources in real time. Figure 3.10 shows the MPPT line for different variable speeds.
3. **Generator and Shaft**- WT can be composed of different **Generator Systems**, which are mainly differentiated between Geared-Drive Systems, Direct-Drive systems, Fixed Speed, Variable Speed, Doubly-Fed Induction Generator (DFIG) and Fully-Rated Converter. Gearing on turbines is getting less frequent now due to the main-

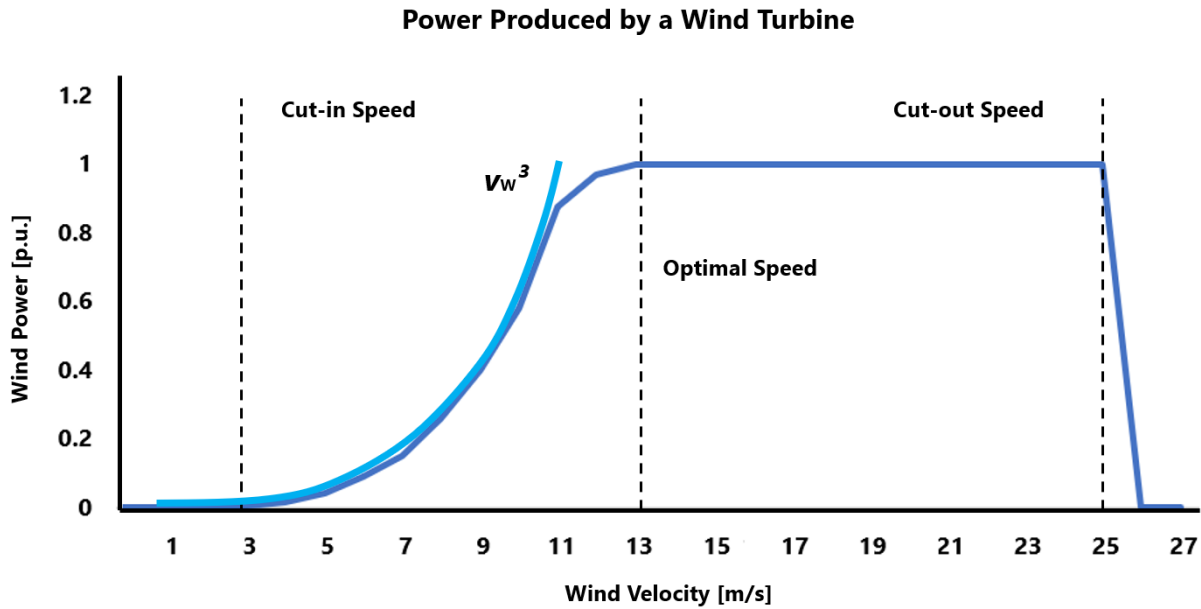


Figure 3.9.: Structure of a Wind Power as a function of Wind Speed [10], [10].

tenance of the gearbox, the noise and inefficiency it creates; instead, direct-drive systems are the main type utilised. With direct-drive systems, the generator is directly driven by the main shaft of the turbine, thus running the generator at low speeds of 30-60 Rotations per Minute (rpm) [9]. As the trend is that direct-drive fully-rated WT generators will be the leading type of system, this research works with this type of design only, specifically the PMSG type. This concept utilises permanent magnets as a mains of electrical excitation; thus additional coils, slip rings and/or brushes are not required, thereby a simpler design [63]. Their functionality is more adaptable with the strict grid codes held in Europe [65], [66], which currently require WT to have high immunity against grid faults and control active and reactive power independently. Besides, the most recent PMSG designs are rated at 10 MW and it is expected that by 2020, WT with nominal power of 15-to-20 MW will be available in the market [63]. Further, with PMSG is assumed that the flux is sinusoidally distributed along the air gap and therefore, no damping winding is considered. This advantage can significantly reduce the excitation losses as well as the torque density of the generator [63], [64]. For PMSG, the magnetic field is given by the rotor magnets and stays constant most of the time. The actual direction of the magnetic field is given by the Electro-Motive Force (emf) of the generator, which is induced in the stator by the rotor field. This emf behaves as a voltage source connected in series with the rotor resistance/leakage inductance and in parallel to the magnetising inductance. If the generator parameters (stator/rotor resistance and magnetising inductance) are known, it is possible to project the magnitude and direction of the emf vector, which would point in the same way as the net magnetic field of its rotor [60]. This direction is used when the controller is going to plot the magnetic field in the stator. Here the field in the stator attracts the rotor in the same way that common magnets attract each other. The mathematical equations can be made by aligning the *d*-component of machine vectors to the rotor flux. Therefore, voltage equations of the machine will be as follows [17]:

$$v^r_{sd} = R_s i^r_{sd} - \omega_r \psi^r_{sq} + \frac{d\psi^r_{sd}}{dt} \quad (3.19)$$

$$v^r_{sq} = R_s i^r_{sq} - \omega_r \psi^r_{sd} + \frac{d\psi^r_{sq}}{dt} \quad (3.20)$$

where R_s is the stator resistance, v^r_{sd} and v^r_{sq} are the *d*-*q* components of the terminal voltage vector, while i^r_{sd} and i^r_{sq} are the *d*-*q* components of the stator currents, respectively. The stator flux components, represented by the greek letter ψ , come from

$$\psi^r_{sd} = X_{sd} i^r_{sd} + \psi^r_{pm} \quad (3.21)$$

$$\psi^r_{sq} = X_{sq} i^r_{sq} \quad (3.22)$$

where X_{sd} and X_{sq} are the *d*-*q* components of the stator reactances, while ψ^r_{pm} is the permanent-magnet flux linkage [17]. All variables with the superscript *r* are associated with the rotor-flux reference frame [17]. For a

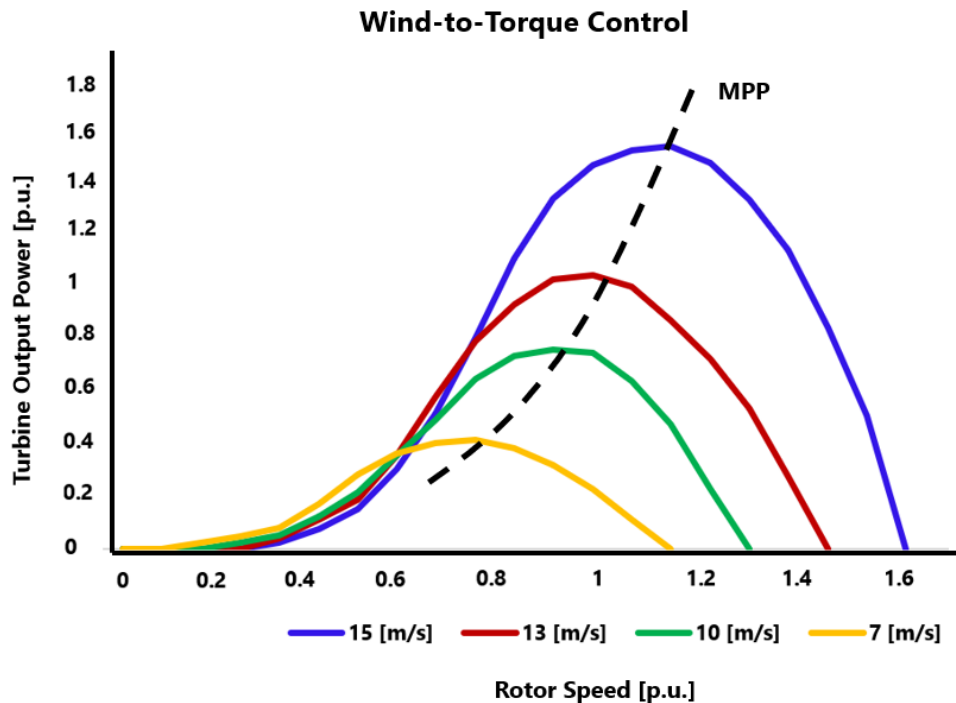


Figure 3.10.: Wind-to-Torque Control Plot [10].

round-rotor type, the stator reactances can be assumed to be equal; as a consequence, i^r_{sd} does not influence the electromagnetic torque. The electromagnetic torque of the PMSG is expressed as [17]:

$$T_e = i^r_{sq} (i^r_{sd} (X_{sd} - X_{sq})) + \psi^r_{pm} \quad (3.23)$$

Under regular conditions, the impact of the wind fluctuations on the shaft is irrelevant. However, during severe disturbances, heavy oscillations in the shaft may surge. For consider these disturbances, two-mass shafts are often modelled by Grid Planning Engineers, where one mass represents the turbine inertia H_w , while the other represents the generator inertia H_R . This is done in order to be able to represent the turbine and generator acceleration responses with acceptable accuracy. K_{tg} is the stiffness of the shaft and D_{tg} is the torsional damping of the shaft. ϕ (identified as $dphi12$ in the model) is the angular displacement between the two ends of the shaft [64]. Moreover, t_R and t_{el} are the mechanical and electrical torques of the generator, while t_w is the torque of the turbine. Lastly, P_w is the collected power from the wind. The arrange of equations for the Shaft Model are defined in this fashion in Equations 3.24 - to - 3.28 [17], [64]:

$$H_w \frac{d\omega_w}{dt} = t_w - t_{mec} \quad (3.24)$$

$$H_R \frac{d\omega_R}{dt} = t_R + t_{el} \quad (3.25)$$

$$\frac{d\phi}{dt} = \omega_w - \omega_R \quad (3.26)$$

$$t_R = K_{tg} \phi + D_{tg} (\omega_w - \omega_R) \quad (3.27)$$

$$t_w = \frac{P_w}{\omega_w} \quad (3.28)$$

4. **Power Electronic Interfaces (PEI)**- The mechanical power generated by the turbines is then converted into electrical power. It has to be supplied to the EPS at the voltage and frequency of that network, always minding that the system of the turbine must work at variable speed, such as the wind itself. Here is when the **Power-Electronic Converters** appear. They convert the varying voltage and frequency into constant voltage and frequency, thus, making the rotational speed of the generator no-longer required from a generator in order to export to the grid [24]. When the power converters connect the intermittent sources to the AC power network,

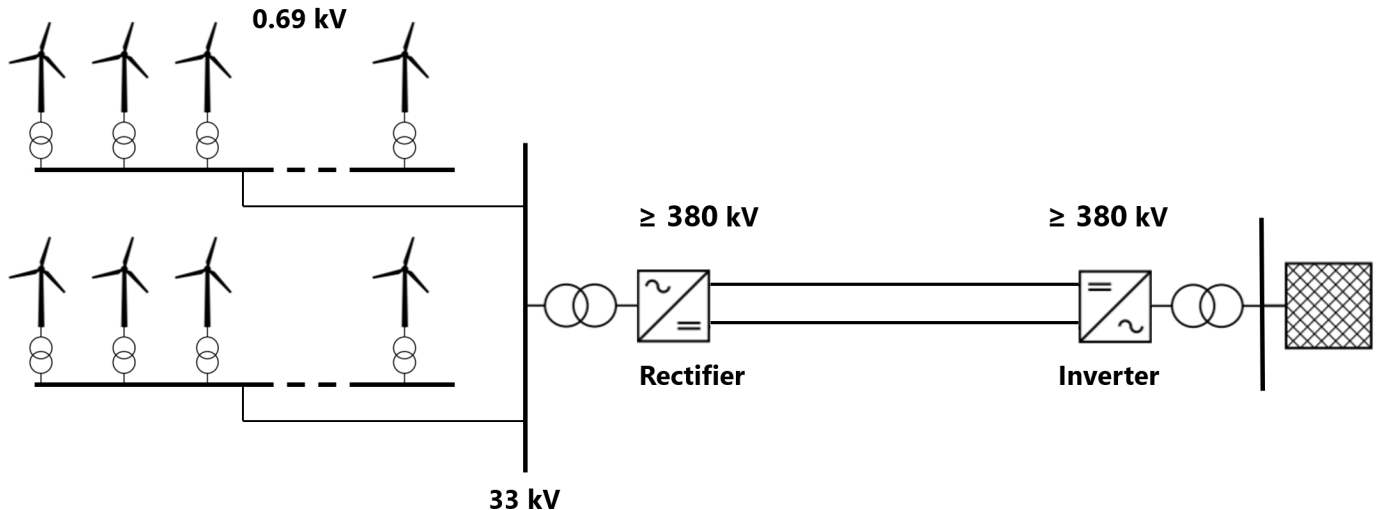


Figure 3.11.: Typical Offshore Wind Farm Diagram very far from Shore [9].

they do it by decoupling one to the other, and neglecting the irregular effects of these sources to the grid, as explained in [Section 3.5](#). In the case of the WT this means that the uncertainty in wind and their mechanical drivetrains are compensated in exchange for the control of these power converters. This can be very helpful in situations where a multi-area grid has lost the links that interconnect one area from the rest, isolating the former. In such case, power converters are capable of adapting the voltage and frequency of the power supply into the voltage and frequency required by the load and maintaining a constant phase angle, therefore *forming the grid* and keep it operating [17], [19], [21].

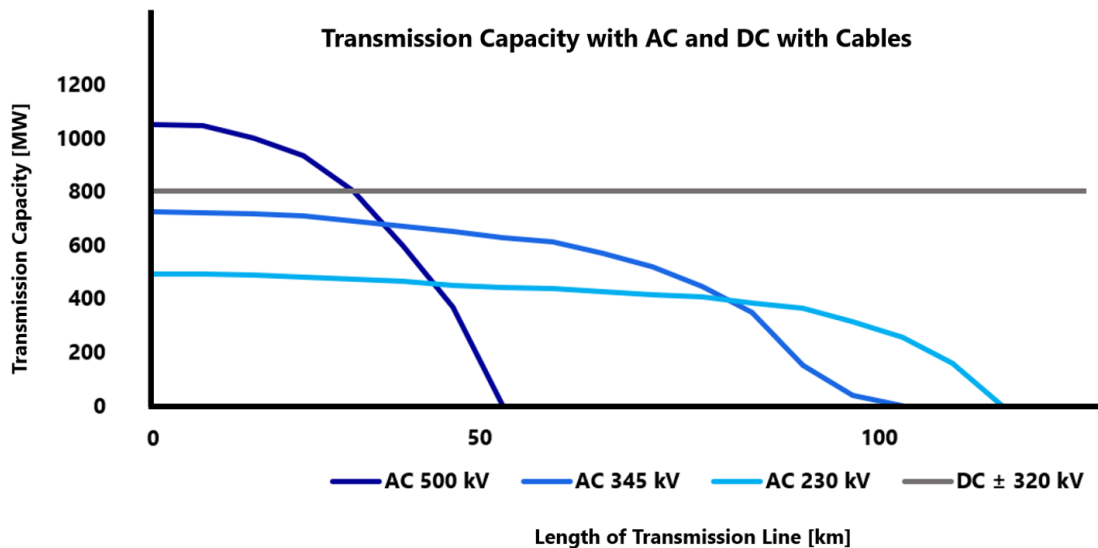
The control strategy for the grid integration of the energy collected by the WF consists on using VSC power converters in a *back-to-back* philosophy. This is, having the two converters in the same location. In this architecture, the **rectifier**, also known as the **remote-end offshore converter**, is in charge of setting the reference of the power to be dispatched based on the speed of the wind and the velocity of its generator. The **inverter**, also known as the **onshore converter**, is in charge of control the reference DC voltage (and during emergencies, both this voltage and the reactive power), in addition to energising the grid the control actions towards the power system [17], [20], [21]. A diagram that displays the topology of an OffWF system is shown in [Figure 3.11](#).

5. **HVDC Transmission**- The complexity of the **Transmission System** depends on the type of installation (onshore or offshore). In case the power plant is offshore, PEC are widely exploited too, particularly if the facility goes beyond 50 km, which is the break-even distance for submarine/underground HVDC cables [9], [11]. HVDC transmission technology becomes especially relevant in EPS with remote generating plants, such as many hydro plants or OffWF.

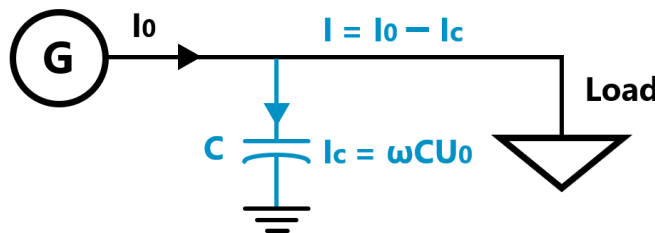
The growing number of wind power plants combined with the increasing distance between offshore power generation and land consumption are two of the main factors driving the adoption of HVDC transmission. One of the main attractions to bet on the high seas is the frequency of very strong winds, which in turn can produce up to 70% more energy than Onshore Wind Farms (OnWF).

When far offshore, the voltage level for transmission is not only increased to a very high level but also converted from AC to DC by the rectifier station and transmits it to the receiving point by submarine cables, where it is turned back into AC utilising the inverter [9]. The reason to use DC voltage for the power transmission is because AC voltages at long distances are not feasible because of the large reactive power consumption of the cables [11], [27], [54], as can be seen in [Figure 3.12](#). This is also why the AC-DC break-even distance for cables is far shorter than with overhead lines [11].

Even though OffWF are costlier to construct, this increase in performance combined with the fact that many renewable energy technologies have advanced substantially in terms of performance and cost could offset these long-term costs. But for reaching those powerful winds, these power plants need to be located farther from the coasts [63]. Yet, even that is not an argument against offshore anymore. For each wind power plant, which would be typically in range of a few hundred MW up to several GW, only one HVDC cable circuit is enough for transmitting power levels of between 100 to 1200 MW [11], [67]. It offers support to meet onerous grid access requirements and helps to improve power quality issues at the connection points. Therefore, this technology provides superior control and quick *Power Restoration* during and after disturbances and contingencies including blackouts. HVDC transmission can support weak grids with BS capability, fine-



(a) Transmission Capacity with AC and DC Cables.



(b) Capacitive Characteristic of Underground Cables.

Figure 3.12.: Comparison of AC and DC Transmission [11].

tuning of AC voltage and reactive power and the ability to energise Wind Power Parks at zero or low wind conditions [11]. Last, but not least, this transmission system is ideal for stabilising irregular electricity flows by quickly compensating for energy fluctuations. Contrary AC, in DC the electrons flow through the circuit unidirectionally, and as a consequence, they do not generate reactive power. In contrast, utilising very long AC cables for the same purpose breeds a quite poor performance because, the larger they are, they generate more reactive power than they consume and require more reactive current to charge and discharge the cable as the network voltage changes polarity 50 times per second. This current is added to the active current needed to transport the energy from one end of the cable to the other [67] (Figure 3.12a). Further, both active and reactive current use the thermal capacity of the cable. Due to the generation of reactive power, AC cable transmission links have a maximum practical length of about 50 to 100 km (more than 50 is possible if using compensation, but would require greater financial expenses). In underground cables longer than 50 km, most of the AC current is required to charge and discharge the capacitance of the cable [11], as shown in Figure 3.12b.

6. **Integration to Electric Power System-** As the demand for energy grows, and therefore the level of complexity of controlling the grid, more intelligent power networks are required. If RES are used, AC power grids get more constrained and vulnerable, with some of the following challenges to cope with [11], [17], [19], [21]:

- Interconnected grids must maintain power balances between production and consumption, including losses.
- Prevention of thermal overloading in all the links of the EPS.
- Generation units must be synchronised at all times. Otherwise, the integrity of the system is in danger; it would be quite difficult to maintain the AC network in a healthy status after a fault, and generator oscillations may be unavoidable.
- Effective reactive power control is mandatory. Without this control, the system will inevitably suffer voltage instability, which potentially widespread, causing chaos in the whole network.

If VSC technology is used for interconnecting inter-area AC power grids, the latter would become reinforced, because the former addresses several support functions to fulfil the abovementioned challenges. A combination

of interconnected DC/AC grids in parallel could alleviate power imbalances because the DC grid can act as a **firewall** between different AC grids [11], [28]. In this manner, the bottleneck problem on one side does not spread to the other anymore. With some further control, the converters can borrow *spinning reserve* from neighbouring AC grids. The *spinning reserve* service can be possible if at least one of the DC converters is connected to a separate AC grid with availability of extra resources. Then, the stressed zone of the network can be automatically supported to restore the **frequency stability** [8], [24].

Another feature is the emulation of **(artificial) inertia**, for mitigating the low ratio of rotating mass (inertia) that usually renewable-based grids do not hold [24]. The converter controllers have the ability to provide additional inertia to strengthening the local stability. It could be the case that a renewable-based grid, with a low Short-Circuit Ratio (SCR) and with few links between the neighbouring zone, loses such links. The artificial inertia feature can support this grid if an involuntary *islanded* scenario surges, as VSC converters hold the characteristic of behaving similar to an infinite AC source [8], [11]. Then, this HVDC link can not only maintain the power balance of that part of the system, but also convert the reactive power needed to keep the AC and DC voltages at expected levels. This will reduce the risk of falling out of step and losing synchronisation in the *island*.

Furthermore, if heavy disturbances arise in several zones, is likely that the EPS faces electromechanical oscillations in the rotors of its synchronous machines. The more severe these oscillations are, the governor systems of the generation units will get closer to their design limits of operation, thus wearing down their mechanical structures. Depending on the specific characteristic of these oscillations, the controllers of the VSC can modulate the signal of the converters for inducing a damping effect that alleviates the undesirable oscillations. This mode of operation is known as **power oscillation damping** [8], [11], [24].

With all the previous advantages that VSC transmission technology presents, BS and NR is particularly doable. The converters can lead the (cold) load pick-up and the reconnection of the generation units with the aforementioned voltage/reactive power controllers. Besides, as in such scenarios power grids would be rather weak and have their SCR low, European regulations have compulsorily set that all the wind power plants to be constructed in the future will comply with the European Network of Transmission System Operators for Electricity (ENTSOE)'s new standards for Requirements for Generators (RfG) [24], [65], [66]. This grid code demands that in such cases the reactive power controllers maintain voltages under specific limits.

3.7 WIND ENERGY AS A LEADING SOURCE

One of the reasons to investigate the potential of renewables to perform a *Black-Start* operation is because of the unavoidable use of these sources in the upcoming years. There has been an increment of electricity production of 140% from 2015, and will continue to go up until 2050 [12]. The share of each type of generating technology in the global electricity production and generation capacity will be greater for REI, as shown in [Figure 3.13](#). Although efforts to study the potential of all types of renewables to perform BS and NR exist and are on current development (that includes solar-PV energy), this research focuses primarily on wind energy. One of the reasons is because wind energy will be the most used means of electricity generation, if offshore and onshore wind (depicted in gray colour) are combined [12], [19], [63]. Other main motives that are causing the wind energy industry to go mainstream are:

- The governments' incentive programs mentioned in [Chapter 1](#).
- These same governments' policies have bounded TSO to tighten up the Grid Code Requirements for RES-based power stations. This means that in the future, WF and large-scale PV systems will have to actively manage frequency, voltage/reactive power, support against voltage excursions, flickers, and harmonics. In other words, for a valid power system integration, renewable power plants will have to meet a *Grid-Forming* Characteristic [65], [66].
- Unlike PV systems, WT can power a network 24 hours a day, as long as there are suitable wind conditions. Additionally, due to its geographical location, strong winds predominate in the Netherlands, especially in the North Sea; thus, the probability of energy resources per year is high. Similarly, the sun is a renewable source which is not reliable to take for granted for the same reason of the geographical location [68].
- At a large-utility scale, wind energy is a better option than solar, as for 2018 [69]. In terms of CO₂ emitted, WT is cleaner than a solar panel, and can produce about forty-eight thousand times the amount of energy per kilo-Watt-hour (kWh) than a solar panel can. In 2016, wind energy supplied 4% of the world's electricity needs, whereas solar energy provided just 0.5% [68], [69]. This is because offshore installations can generate huge amounts of power thanks to the strong and constant supply of wind. Solar panels, on the other hand, have a very limited time frame in which they can produce energy.

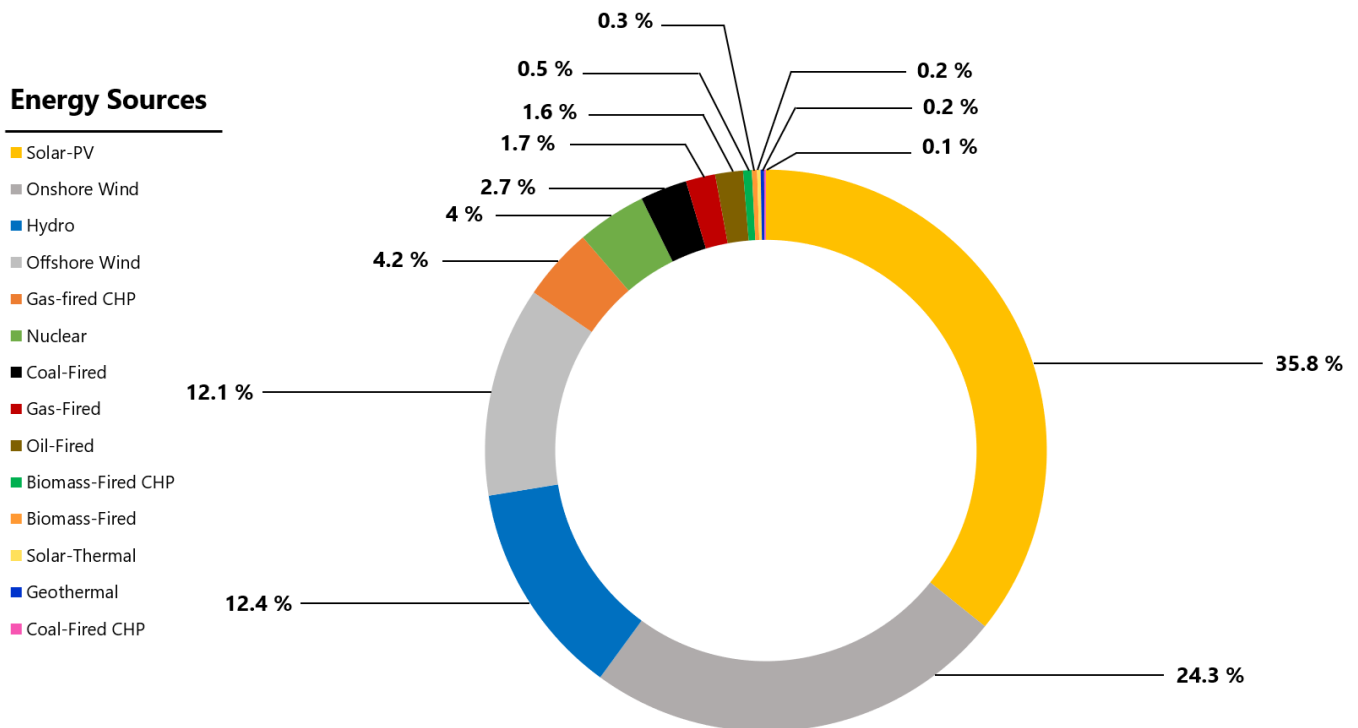


Figure 3.13.: Global electricity production in year 2050 [12].

- Great technological advancements in WECS. The concept of wind energy embodies interdisciplinary subjects and sciences, and all of them have increased in quality [11], [63], [70] :
 - Evolution of the materials utilised for the WT. For the power levels beyond 10 MW, there are restrictions to manufacturers to assemble the turbines with stronger, yet light-weight materials. This applies to all the elements that build the system (blades, tower, nacelle, hub, new foundation concepts, etc.). Rare-earth permanent-magnet materials that excite electrically the generator without the need of coils, and delivering higher power density. Likewise, the newer generation of semiconductor devices are built with materials capable of operate at higher temperatures with higher switching frequencies while also presenting a smaller size than their silicon-based IGBT.
 - Improvements in the overall design of a WT structure, in both the mechanical and electrical aspects of the generation unit. Aerodynamic design of blades. Some of the newer design present lighter, longer and more flexible blades [63]. Similarly, direct-drive electric generators that allow full control of variable-speed winds, capable of boost the power ratings further.
 - The evolution and technological improvements in semiconductor devices that provide the benefits mentioned in Section 3.4. More boundary conditions that can be controlled, cost, reliability, modulation techniques that improve the power conversion efficiency, power density, operating voltage levels, power limits, cooling systems, improved grid current quality, etc.
 - Smart systems for control the WT as well as the intelligent management of WF. Enhanced control capabilities for renewable generation systems/integration to the power network with high flexibility. These innovative control systems are designed to meet the stringent Grid Code Requirements for frequency and voltage/reactive power support, using different Control Theory Concepts, like *Model-Predictive Control* and *SVM Theory*, just for naming some. The reference control variables such as generator speed, torque or power for these schemes are usually provided by a MPPT algorithm that takes part of the Generator-Converter Controls. As for the Grid-Side Converters, they are controlled by a decoupled control that manages direct voltage/reactive power injection. With this innovative scheme, the d - q currents are implicitly controlled as well, as a consequence of regulating the voltage/reactive power. At a large scale, the control systems for the optimum performance of WF have been also developed, in a fashion that allow each WT to work synchronised with the rest, for avoiding negative aerodynamic interaction between the WT. Coordination of Protection Systems is also comprised here, in order to assure the integrity of the system in case of dangerous disturbances.

- The mentioned technological improvements have yielded in enhanced reduction of purchasing and installation costs/competitive prices; this, in turn, has made that the installation rates of wind power plants increase.
- The fact that large turbines can capture higher wind power, has made that manufacturers increase their size, diameter and power ratings. This is the case of WT in OffWF projects, as it is known that air blows stronger and more constant in the sea, at higher heights, and in open spaces. If that trend keeps going, 10–20 MW turbines could be operational in near future with rotor diameters exceeding 150 metres [63].
- For the necessity of a *Black-Start* Strategy, wind power can supply a faster start-up time than CGU after a blackout has occurred in their zone, WT can have start-up times from 40 seconds to 2 minutes, while an hydro-type CGU needs 5 minutes and a coal-type 20 minutes; even multiple start-up capabilities in a short period can be performed, owing to the full-converter-based structure and fast controllers. Similarly, they take less time to be ready to start the load pick-up process, power pick-up from WT 30 seconds to work, while with CGU it takes 40 seconds to 1 minute [55], [70], [71]. And with these properly designed control systems, WT can provide the desired reactive power/voltage and frequency regulation capability that differentiates *grid-forming* elements. A double reinforcement is possible if integrating similar control systems designs in the VSC converters of the HVDC stations.

3.8 BATTERY-ENERGY STORAGE SYSTEMS FOR ENHANCED SUPPORT

Electrochemical energy storage technologies make use of reversible reactions to convert or store electricity. Common Batteries in the industry are often Lead-Acid type. But there are also a lot of other types like Nickel-Cadmium (*NiCd*), Nickel-Metal Hybrid (*NiMH*) and several Lithium-Ion types (*Li-Ion*). Each type has its own assets and drawbacks [13].

With the increasing share of renewable generation, especially the ones with intermittent nature, functions with additional flexibility are needed to permit EPS to operate stably and in a secure way. Although wind energy comprises many advantages, its massive integration into ageing power grids implies technical challenges and potential problems regarding power quality, fluctuations, reliability, interconnection between EPS, control, generation dispatch, among other issues. The real-life performance of the power output provided by a WF may have very steep Δ (severe rises and drops during a day). Besides, if it is intended to have renewables at high penetration levels, is still mandatory for renewable generation to meet SOS and the guaranteed dispatch of power with the minimum requirement in terms of quality leastwise. And, as the penetration levels of RES increase, it is of considerable concern that therefore larger variations in the power output from PV or wind will affect the operation of interconnected grids [13]. Consequently, measures to smooth the output fluctuation to have a reliable power system are mandatory, since generation curtailment must be avoided by any means; otherwise SO may face severe economic penalties, which are steeper on plants with low-to-zero fuel-operating costs [27], [28].

For that, BESS can be an effective tool to ensure flexibility and balancing at all grid levels, in particular with high fractions of PV and wind. Large battery-storage units are being increasingly used in Flexible AC Transmission Systems (FACTS) applications to improve the voltage, frequency, oscillatory and/or transient stability of the system (typical AS), enhancing so the reliability of power supply [29].

Battery systems aid to not only provide start-up power but convert it, so as to allow a reset generator to achieve synchronisation. BESS can be a very useful tool to secure supply and demand balancing when there is a shortage of generation resources [29].

Besides, they can be deployed for improving the efficiency of restarted thermal generators, while also boost decarbonisation and make power networks cleaner [72]. As the entire Globe is embracing RES, storage systems could be a magnificent asset for the clean energy and sustainability concept as they do not possess any source of energy. Instead, they work by absorbing the surplus of energy from the grid and discharging only if they detect network imbalances. In fact, another positive influence of storage systems is that they can limit the excessive output power of WF by absorbing the excessive power injection themselves instead of the grid, thus avoiding imbalances in the network. Under normal operation, these units would not supply power unless their frequency measurement units read a decrease. Similarly, if these frequency-sense units read a frequency increase, then the BESS sink energy, charging themselves. However, if after some time the frequency does not decrease to standard values, the frequency controller must limit the amount of energy that the battery drains in case the battery is already fully loaded [13], [29]. Its way of functioning makes it a kind of archetype of what an Emergency Plant should be [27].

Application	Description	Maximum Power Requirement	Duration Requirement	Response
Governor response.	Automatic dynamic response of the generator after frequency changes. BESS can compensate the lack of governor response of RES.	10% of generator ranking.	Seconds to few minutes.	Fast (milliseconds).
Frequency regulation.	Second by second adjustment of power to match load and regulate system frequency. BESS can free up generation capacity for energy production.	Around 5% of the peak demand (large systems); it can be higher in small <i>islanded</i> systems.	15 to 30 minutes.	Fast (milliseconds).
Reliability enhancement.	Reduce non-supplied energy and supply interruptions due to outages.	1 to 10 MW (depending on the feeder size).	Hours.	Fast (alternative to switching.)
Congestion relief.	Storage RES during grid congestion; then deliver when capacity is available (hence increase the capacity factor of RES and reduce curtailment).	Varies according to application.	Hours.	Slow.
Voltage support.	BESS can attend local demand or reduced curtailment of distributed generation due to voltage regulation problems.	Varies according to application.	Hours.	Slow.
Grid reinforcement deferral.	BESS can defer transmission reinforcements or distribution substations upgrades (transformers) due to peak load growth.	Varies according to application.	Hours.	Slow.
Balancing/real-time dispatch.	Adjustment of production market based on minute by minute basis to match demand. BESS can mitigate price spikes due to volatility of RES.	Does not apply.	1 hour or more.	Slow.

Table 3.3.: Advantages of utilising BESS for AS [29].

Storage systems also possess *Fault-Ride Through* Capability for ensuring that they will keep connected to the network during heavy voltage dips caused by heavy faults of the likes of loss of main generation resources or involuntary *Islanded Operation*. This means BESS can also be actively used for *Restoring a Network* after a blackout. Coupling a WF with storage should be able to allow the wind power plant to act as a *Black-Start Resource*. The BESS can smooth the plant output, provided that the wind plant is never loaded near 100% [73]. One example of just one application can be found in [74], where a work on using solar farms as a Static Synchronous Compensation (STATCOM) at night. This assembly coupled with a WF and BESS, can be capable to stabilise a local *island*. Table 3.3 presents some of the benefits that the integration of BESS could bring [29].

Further, BESS systems include the storehouse part that stores/restores energy in an electrochemical process. Secondly, the storage devices are interfaced with the power system through series-connected VSC, connected to the system at the Point of Common Coupling (PCC) and are charged/discharged through the VSC to smooth the net power injected to the system. Battery-storing systems based on PEC have the ability of deploy very rapidly (scale of few mili-second (ms)), but also, the controller that regulates the system embedded to the PEC permits that the shape of the frequency response can be moulded/shaped in different ways [13], [29]. Several shapes of frequency response could be used, for instance, maximum inertial response, beneficial Rate of Change of Frequency (ROCOF), disturbance following functions, among other benefits.

Important variables to determine the health and performance of this device are the terminal voltage and the internal resistance of the electrochemical battery, which are functions of the battery's State of Charge (SOC), another crucial parameter. The SOC corresponds to the current loading state of the storage device, depicting how much power has been dispatched to the network; thus, the SOC is fully loaded if its magnitude is at one and zero if it is fully depleted. Therefore, a decreased SOC would also draw a more-discharged battery voltage. A diagram representing a Simple Battery Circuit is shown in Figure 3.14. The circuit can be extended with a parasitic reaction path. An equation known as *Peukert's Law* determines the capacity of a battery in terms of the SOC. It is a common reference for most lead-acid batteries. It is described in Equation 3.29 [13]:

$$C_p = I_t^k \quad (3.29)$$

where C_p is the capacity at Ampère-hour (Ah), I is the discharge current in Ampère (A), k is the Peukert constant (dimensionless) and t is the time of discharge. With a detailed datasheet or look-up table from a manufacturer, the

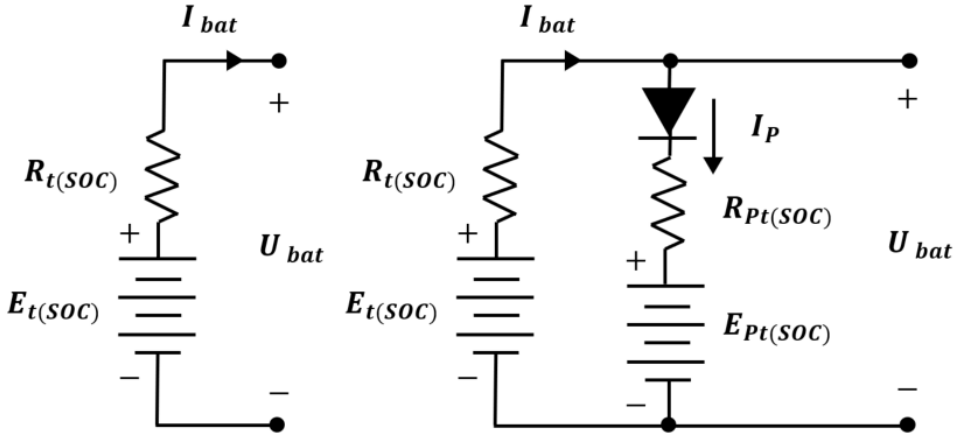


Figure 3.14.: Circuit of a Battery without and with Parasitic Reaction Path [13], [14].

arbitrariness and realistic behaviour of a battery can be described; however, usually this information is difficult to obtain. For that, usually assumptions are made for modelling the terminal voltage as a function of the SOC. However, since the concept of a battery can be defined as an *electric dipole*, a linear assumption can be made [14]. Due to the high-current application of this device, the internal resistance of the battery is considered constant and small. The DC voltage with respect of the SOC is described in Equation 3.30 [13], [14]:

$$U_{DC} = U_{MAX} \text{SOC} + U_{min} (1 - \text{SOC}) - I_{bat} Z_i \quad (3.30)$$

where U_{min} and U_{MAX} are the voltages of the discharged and fully-charged battery cell, in Volt (V), I_{bat} is the current of the battery, where an integrator is used for its calculation, and Z_i is the inner resistance of the battery, in Ohm (Ω) [13], [14]. The formulas for the VSC of the batteries however, are a little simplified compared to the equations shown in Section 3.4 [30]. This is because one of the main functions of a BESS is to act against the EPS frequency response. Thus, the priority is to control the behaviour of the PWM converter at a fundamental frequency converter level instead of a high-switching frequency level. And in that order, the equations that describe the model of the Battery can be based on the RMS-phasor-fundamental-frequency reference for PEC equation modelling according to [30]. Consequently, the equations that describe the VSC are [13], [14]:

$$U_{ACr} = K_o Pm_r U_{DC} \quad (3.31)$$

$$U_{ACi} = K_o Pm_i U_{DC} \quad (3.32)$$

$$K_o = \frac{\sqrt{3}}{2\sqrt{3}} \quad (3.33)$$

where Pm is the modulation factor (or the switching signal), which comes from the control system of the PWM converter. U_{ACr} and U_{ACi} are the real and imaginary parts of the AC voltage, while U_{DC} is the DC voltage of the battery. K_o is a constant factor used in sinusoidal modulation to determine whether or not the amplification factor Pm is smaller than one. If so, the converter is working under normal operating conditions. Then, if Pm is bigger than one, the BESS may have problems with harmonics. Therefore, for a proper operation

$$U_{DC} \geq \frac{\sqrt{3}}{2\sqrt{3}} |U_{AC}| \quad (3.34)$$

it has to be guaranteed that the voltages are within their permissible limits [13], [14].

4

STUDY CASE FOR BLACK-START/NETWORK RESTORATION STRATEGIES

4.1 BLACK-START STRATEGY WITH WIND POWER PLANTS, BESS AND HVDC TRANSMISSION

WF are capable to actively manage a Grid, if their control systems enhance them to do so. Therefore, considering the advanced features that power energy converters installed in utility-scale WF can provide (as stated from [Section 3.4](#) to [Section 3.6](#)), it is possible to exploit these features to perform a BS and NR. By developing and exploiting these advanced control capabilities of utility-scale WF, it is possible to include them in the BS and NR processes, for example, for the control of the high reactive power produced by the long high voltage transmission lines without load, followed by a rapid increase of WF when the load is increasing. This coordinated approach will represent a significant improvement with respect to the reduction of restoration times, which will lead to lower economic and social costs [55], [70], [71].

A coordinated approach between WF, storage (BESS), VSC-HVDC and also conventional generation (CGU) was modelled and tested in this research. Such prototypes have been applied in a coordinated way to reach the target group to simulate a NR in the *PST 16 Benchmark System* (see [Section 4.3](#)), and answer the Research Questions defined in [Section 2.3](#). A large set of different **sciences and disciplines** have been applied to this research:

1. **Grid Protection Analysis and Schemes** for preserving the integrity of the grid after a fault. A model that emulates the coordinated action of protection relays and circuit breakers was part of this work, based on the theoretical analysis found in [7], [27] and [56]. During this stage, algorithms for determining the ideal time for reconnecting the lost generation units, the elements of the transmission network and the loads were designed. This step contributes to answer the [Research Question 1](#).
2. **Electrical and Mechanical Engineering** for extend the built-in WT models with the mechanical drivetrain (pitch angle control, turbine, shaft and aerodynamic models), for adding seven BESS-storage stations, as done in [13] and [29], and for extend two of the three transmission lines the interconnect the areas of the study case for two HVDC links with submarine cables, as it was done in [8] (see [Section 4.3](#)). This step contributes to answer the [Research Question 2](#).
3. **Power System Dynamics, Power Electronics and Control Theory** for modifying the control systems of the VSC converters, (all of which are core elements in the WT, storage and HVDC transmission), in order to endow *grid Forming* and *Black-Start* capabilities to them, as it was done in [17], [20] and [21]. In this stage, necessary modifications in the elements' and controls' systems and tuning had to be executed for the guarantee that all the above mentioned models and their replicas could successfully work together in the simulations during both steady-state and transient-emergency conditions. This step contributes to answer the [Research Question 2](#).
4. **Power Systems Analysis, Transients and Stability** for analyse the obtained results and prove that PEI-elements (inherent in renewables, storage and HVDC transmission) can successfully manage a BS and NR process. This step contributes to answer the [Research Question 3](#).

In this chapter, the implementation of the additional characteristics applied to the general system that gives it the ability to self-heal after major failures is described in detail together with its theoretical control concept that determines the converter reference voltage directly without the need for an underlying current controller. This control concept can be universally applied to all PEI that serve as interface for RES-based generation and VSC-HVDC transmission.

4.2 DYNAMIC SIMULATIONS IN DIGSILENT POWERFACTORY

This section was included so that any reader not familiar with the DIgSILENT PowerFactory 2018 (DPF) working philosophy, language and technicalities can follow the implementation of the control systems in the further chapters.

4.2.1 RMS-EMT SIMULATION DIFFERENCES

DPF contains power system analysis tools capable of evaluating the behaviour of EPS at a small or large-scale in the time domain. These functions, therefore, allow modelling complex systems such as large transmission networks and industrial grids in detail, minding the electrical and mechanical parameters [15].

Stability, control and transients problems are important concerns during the planning, design and operation of modern power and energy systems. Studies engaging electromechanical and electromagnetic transients are performed using time-domain simulations for different periods of time [15].

As shown in [Table 4.1](#), time-domain transient simulations in EPS are classified according to the time frames of the simulations to-be performed and the level of detail that the study analysis requires. For a relatively simple analysis, RMS simulations are usually enough, but if the detail level of the research embodies more information and accuracy, EMT is a better choice [30].

	<i>Time Frame</i>	<i>Network Equations</i>	<i>Machine Equations</i>
RMS	Mid-term to long-term (mili-seconds to seconds)	$V = \left(R + j\omega L + \frac{1}{j\omega C} \right) I$ Algebraic Equations	Slow dynamics included (mechanical equations, power/frequency controllers, turbines, etc.). Stator flux changes instantly after a perturbation.
EMT	Short-term to mid-term (micro- to mili-seconds)	$v(t) = R_i(t) + L \frac{di(t)}{dt} + \frac{1}{C} \int i(t) dt$ Differential Equations	Stator flux dynamics and harmonics are included. High-frequency ranges.

Table 4.1.: Different characteristics between RMS and EMT time-domain simulations [15], [30].

4.2.2 SIMULATION SETUP AND PROCEDURE

Before any time-domain simulation can be successfully executed, first a procedure that serves as a setup has to be properly accomplished. First, a **Load Flow Analysis** has to be performed. Load Flow calculations are used to analyse power systems under steady-state non-faulted conditions. In this manner is assured that the topology of the designed network has the right voltage levels in all its buses, transformers and connected elements, and the right power balance between generation installed capacity and loads. Load Flow analysis defines too the active and reactive power flows for all branches, with their voltage magnitudes and phases for all nodes. With all this information, the user can evaluate the system's strength and/or detect its weaknesses. Likewise, the behaviour analysis is useful for evaluating the performance in existing zones or for future extensions in the EPS [15].

After a successful Load Flow Analysis (power flows and bus voltages at 1 p. u.), **Initial Conditions** of the time-domain simulation have to be defined. Numerical values of the time constants and gains that compose a control block as well as the signals that serve as links between the different control loops that comprise a control system of any of the power components need to be declared for the overall control system to act as expected. In addition to that, the **Network** representation has to be defined (to-work in a balanced/unbalanced system), the integration control options, the time-step size, etc. [15].

If a particular signal or variable of the system is of special interest, its behaviour can be visually analysed by declaring it as a selection variable to be plotted (**Definition of Variables**). Finally, if the user just wants to run a simulation without any special events and just make sure that its designed System runs steadily under normal operating conditions, no event defining a disturbance need to be stressed. Otherwise, events can be defined (**Event Definition** options are available). There is a broad type of events that can be defined (sudden change of load profile, lost of a Network link, the increment of mechanical torque of a prime mover, short-circuit fault, etc.). [Figure 4.1](#) shows a flowchart of the standard procedure for running a time-domain simulation in DPF.

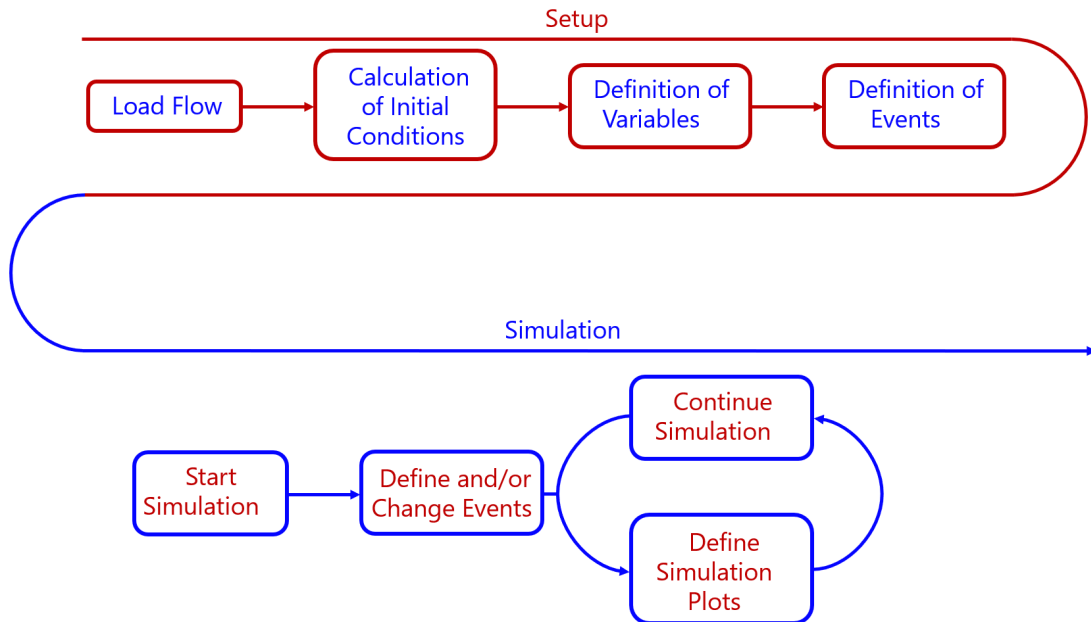


Figure 4.1.: Flowchart describing the Simulation Procedure in DPF. [15].

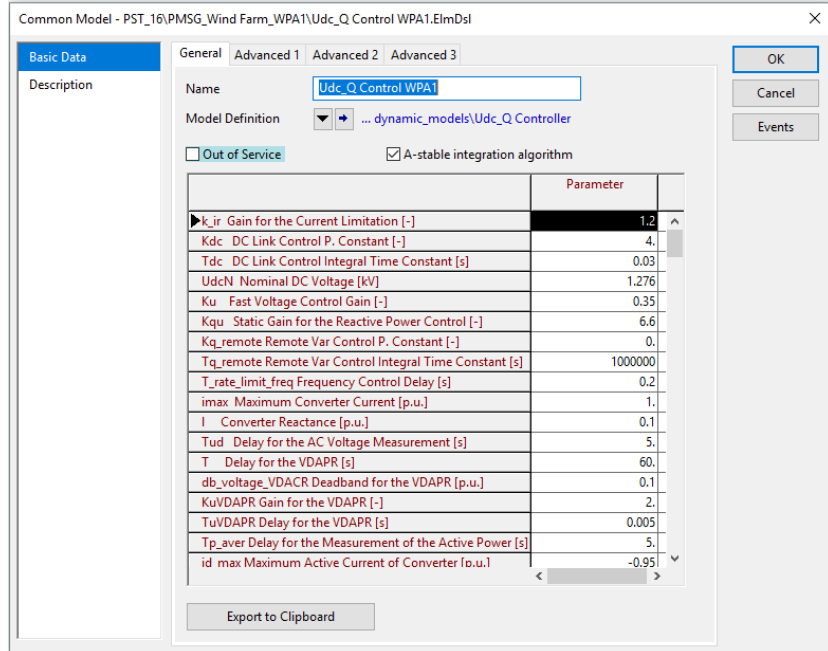
4.2.3 PROGRAMMING AND BUILT-IN MODEL DESIGN

In DPF there is a vast quantity of electrical elements, systems and subsystems already designed and ready to just be connected and work. Normally they are based on international standards (International Electrotechnical Commission (IEC), Institute of Electrical and Electronics Engineers (IEEE), International Council on Large Electric Systems (CIGRÉ), etc.), or manufacturers (after previous confidentiality agreement).

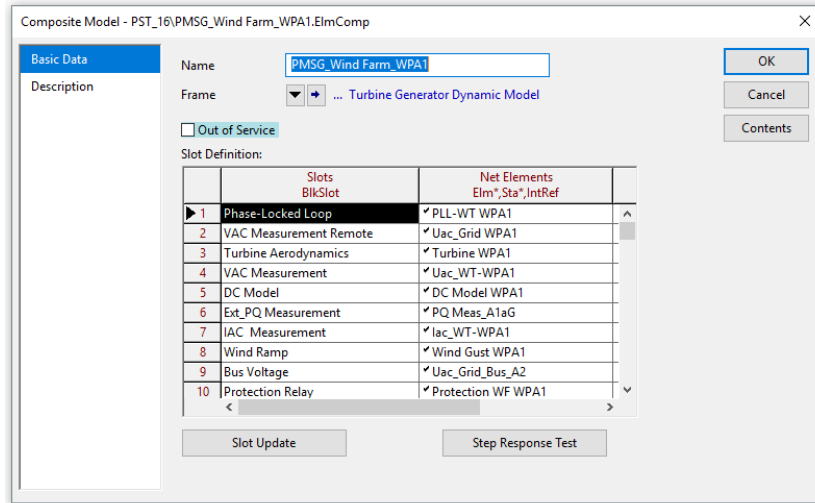
However, it is impossible to represent all types of EPS elements and store this information in the Software package. If a user needs to work with a specific element (controller, relay, PV system, etc.) that is not found in any of the DPF libraries, user-defined models can be designed to represent a customised element or behaviour. The programming language to design user-defined models in DPF is known as DSL.

For example, Figure B.1 represents the **Composite Frame** for the WF-PMSG Model developed for this MSc Thesis. The lines seen in Figure B.1 are external input-output wired signals that inter-connect/communicate each block. The blocks presented in Figure B.1 are **Slots** associated with a specific control loop, algorithm, or equation set that describes specific physical phenomena (mechanical, electrical, magnetic, etc.), or a mathematical pattern. The biggest Slot in this same Figure has been named as **Udc_Q Controller**. It can be inferred by its name that this Slot is associated with the DC voltage/reactive power controller of the WECS overall system. Figure B.8 displays the architecture of this same **Udc_Q Controller**. In DPF terminology, a control loop designed in this software is known as **Block Definition** (or **Model Definition**). A Block Definition can contain the equations that described the physical phenomena above mentioned via a script, or it can contain the information graphically programmed, as seen in Figure B.8 and all the figures of Appendices A - to - D. If any user favours the graphic option, inside each block of all control loops a script that defines a mathematical function (of further physical phenomena) usually has at least still to be written, though. Therefore, even with the graphic-programming option chosen, is almost unlikely to skip coding at least a bit.

Further, it is standardised that some of the defined parameters in each Model Definition can be modified or tuned easily, according to the study objectives and/or circumstances. Perhaps the **Udc_Q Controller**-Block Definition will be the reference of more than one WT installed in the Network during a simulation. Figure 4.6 contains seventeen WF, which means that seventeen DC voltage/reactive power controllers are active in that study case scenario. The location where any of them are located can also be a considerable factor for the assessment of their behaviour. For instance, one of them may be installed next to a shunt compensator, or not. Or it may be too close to a sending-end HVDC station. High-harmonic content may interfere in the overall behaviour of that wind power plant. Considering that, **Common Models** are the front-end interface of the user-defined Block Definitions. Table 4.2a shows an example of a Common Model, where each signal containing information has its name declared with a brief description, and editable blanks where the values of such signal can be modified or tuned, according to the study objectives and/or circumstances.



(a) Common Model of the WT DC Voltage/Reactive Power Controller.



(b) Composite Model of the WT DC Voltage/Reactive Power Controller.

Table 4.2.: Structure of built-in Dynamic Models in DPF.

Lastly, the way each Common Model is linked to one Slot that is part of an Overall Control System Frame is by **Composite Models** (Table 4.2b). Composite Models are based on Composite Frames and they are employed to merge and link several elements (built-in models) and/or Common Models. The Composite Frames enable the reutilise of the basic architecture of the different Composite Models worn on an EPS modelling [15].

Use of DPF Template Power Systems

Licenced users of DPF Software, and/or users who assist to official technical seminars taught by DPF personnel have granted access for downloading Templates of proper **Power Equipment Models** regarding a vast number of applications. These can be generation, transmission or distribution systems, REI, storage, railway systems, protection, etc. The author of this MSc Thesis Research relied on this source to gain reference and to learn more about control systems design for EPS by playing with these numerous templates, working in a self-taught atmosphere. Indeed, as this tool can be considered like an open source for registered users, some of these templates were copied and applied to the *PST 16 Benchmark System* study case.

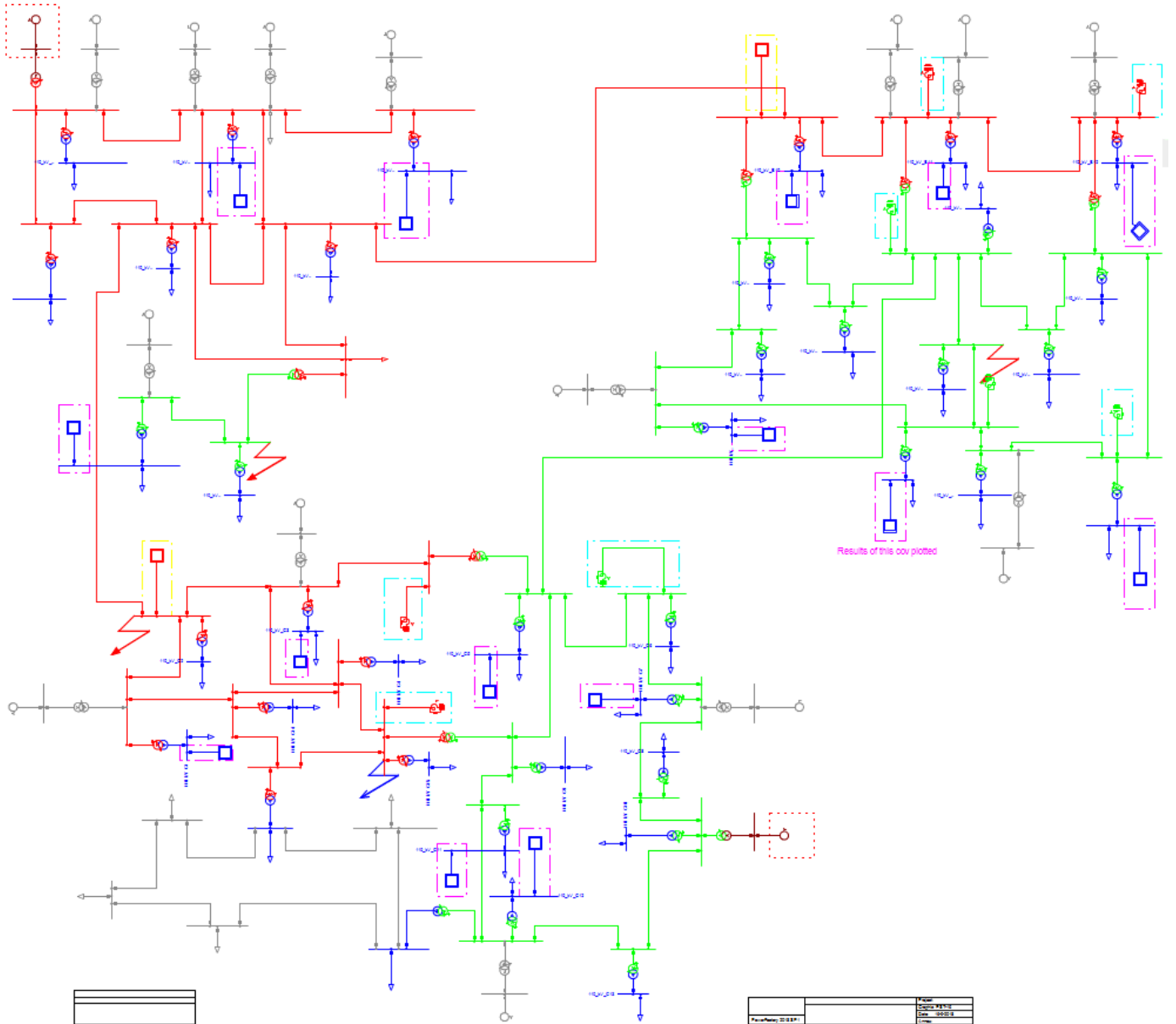


Figure 4.2.: *PST 16 Benchmark System* original case designed in DPF. [16].

4.3 THE ORIGINAL PST 16 BENCHMARK POWER SYSTEM

The study case used for the power system analysis that is the topic of this MSc Thesis Report is the *PST 16 Benchmark System* [16], [38], [39], and it was provided by academic researchers from the Institute of Electrical Power Systems at the *Universität Duisburg-Essen*. This DPF-modelled case depicts a large-scale interconnected EPS with different voltage levels and contains sixteen synchronous generators (CGU) widespread in three strongly-meshed areas, connected by long-distance HVAC transmission lines. In detail, all the elements that conform this network are [16], [38], [39]:

- **Sixteen synchronous machines.** Of which five of them are considered to be hydro-source, four of them nuclear-source, and the other seven work with (hard) coal as source of energy. Most of them have around four-to-five parallel units connected to them, while each single unit is rated at 220 Mega-Volt-Ampère (MVA) (hydro), 259 MVA (nuclear) and 247 MVA (thermal). All of them have a Y-type connection. The total installed capacity is about 15.93 GW.
- **A hundred and fifty one busbars.** Voltage ratings vary from 0.55 to 110, 220 and 380 kV.
- **Sixty four transformers.** Their power ratings are very broad and vary from 130 to 2760 MVA and most of them have a YN (High-Voltage) - Δ (Low-Voltage) vector group connection.

- **Fifty eight load centres.** Their classifications vary from agricultural, domestic, commercial and industrial applications. Their power ratings vary from 20 to 800 MW and from -50 to 100 Reactive Mega-Volt-Ampère (Mvar). The total load demand in GW is 15.9. To put it in context, data from year 2012 states that the annual electricity consumption in Greater London back then was close to 40000 Giga-Watt-hour (GWh). This is, on average, 4.5 GW [75]. So, this model could roughly power a little more than three metropolises like London (including their greater areas).
- **Eight shunt C-type high-pass filters.** Rated at 380 kV. They are employed in order to furnish reactive power and avert resonances in parallel. They also allow the filtering of high and low-order harmonics (like the 3rd), maintaining zero losses in the fundamental frequency [76].
- **Fifty one transmission lines.** Voltage ratings vary from 110, to 380 kV. Distances vary from 0.1 up to 220 km, and the current ratings go from 3320 to 4080 A.

The *mint-condition* model (as it was delivered and without modifications from this author), was originally designed to assess stability problems related to LFO as it has a large size, with its transmission lines interconnecting the three meshed areas very weak due to their large lengths. Further, it was designed based on characteristic parameters and aspects usually found in the European EPS [66]. The modelling of the majority of the components that integrate it was done utilising DPF built-in models [15], whereas DSL was used to model the controllers attached to each generator and the VSC-PEI interfaces in the network. Because of the high complexity, the vast and inclusive quantity of power and control elements contained and the large size of the network, this Benchmark is an excellent canvas to assess an BS and NR as, if the *grid-forming* controllers work successfully there, it is likely that they would perform outstandingly too in other EPS models.

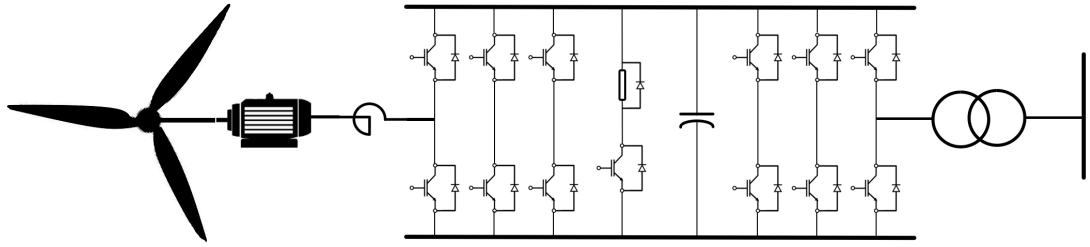
In [Figure 4.2](#) is exhibited a picture of the *mint-condition* model case. The three areas are *Area A*, in the upper-left side, *Area B*, in the upper-right side and *Area C*, in the lower-left side. The main power flow direction is from *Area A* and *Area B* to *Area C* where the majority of the loads are located [39]. *Area A* is the main power exporter area, dispatching also to *Area B*.

In [Figure 4.2](#) it also can be seen seventeen squares. The squares are hierarchical blocks that, if double-ticked, each shows a composite built-in model that emulates a WT or a Grid-Side Converter Station (GSC), depending on the voltage levels ([Figure 4.3b](#)). As stated in [Section 3.6](#), the most powerful WT in year 2020 are expected to have a capacity of up to 20 MW. The DPF-built model, however, has a rated power of 900 MW. So, in fact it represents a scaled WF and the output power is just the sum of all the virtual units that compose it. Moreover, in [Figure 4.3b](#) can be seen that there is no symbol related to any turbine, as there is in [Figure 4.3a](#). This is because this model runs with a controlled-current source, as this is a simplified built-in model that does not consider the mechanical drivetrain neither the aerodynamic components of the WECS. Consequently, it only regards the GSC (it can be seen that [Figure 4.3b](#) only has the inverter but the rectifier is missing). This level of detail for most power system studies is alright because the frequency VSC converter decouples the rotor/generator from the grid, as explained in [Sections 3.5, 3.4](#) and [3.6](#).

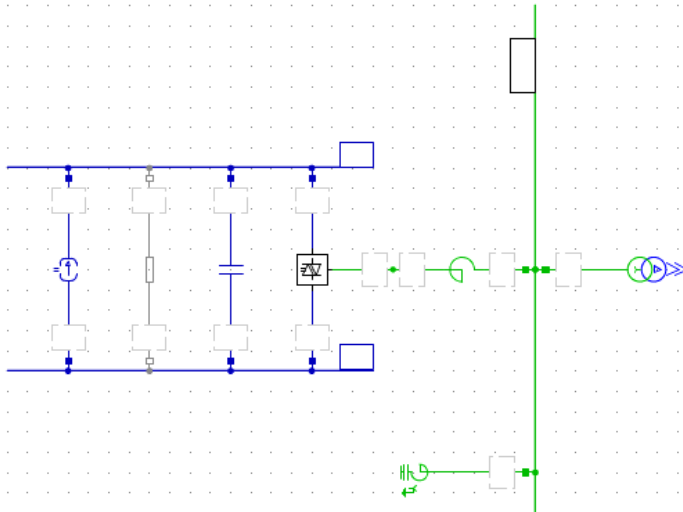
The colours in diagrams [Figure 4.2](#) and [Figure 4.3b](#) represent the voltage levels of the Network. Blue for 0.55 kV and green for 0.69 kV for the simplified current-source models ([Figure 4.3b](#)). For the main grid ([Figure 4.2](#)), brown for 15.75 kV, blue for 110 kV, green for 220 kV and red for 380 kV. In total, the model case has not only sixteen synchronous generators but also seventeen build-in models that represent additional generation, while the number of loads was not increased. Is important to notice that also some elements in [Figure 4.2](#) are sketched in gray. Gray colour defines elements that are out of service for that case scenario.

As mentioned in [Section 2.1](#), the *PST 16 Benchmark System* case study works for two different scenarios, one with zero wind penetration and another with 90% wind power share. [Figure 4.2](#) depicts the latter case, as it can be seen that only two CGU are still active while the rest are off. Therefore, both cases are designed to have approximately the same installed capacity.

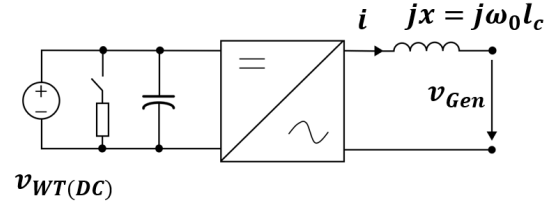
With the nomenclature of the colours/voltage levels, it can then be noticed that the two built-in models with their grid-interface transformers rated at 380 kV (the only two square symbols drawn in red in [Figure 4.2](#)) are in fact simplified HVDC-GSC, although their transmission paths were actually defined as AC overhead lines. This was an intended simplification, which was effected because the original model case was previously used for grid stability analysis in the system only, while the DC dynamics of the transmission links was not part of that previous research. Then, for that inquiry, the transmission lines that interconnect *Area A* from the rest were assumed to employ HVDC transmission. Indeed, the investigation carried out with the *mint-condition PST 16 Benchmark System* was rather not involved in the development of a converter-dominated grid with BS-NR capability. Consequently, neither the controllers attached to each generator and the VSC-PEI interfaces in the model had *grid-forming* characteristics.



(a) Structure of a WECS with a back-to-back VSC.



(b) Current-source aggregated WF model.



(c) Thévenin equivalent circuit of Figure 4.3b.

Figure 4.3.: Wind Energy Conversion Systems [17].

4.4 WIND TURBINE CONTROL SYSTEM TO-BE MODIFIED

As seen in [Figure 3.11](#) and in [Figure 4.3a](#), the structure of a WECS comprises many different voltage levels and their respective transformers, *back-to-back* converters, long-distance submarine cables and shunt compensation. Due to their particular structure, WECS are prone to multiple resonance frequencies of a wide range [\[19\]](#). With the upcoming increase future Wind Power Plant installations, and the relative little practical experience in commissioning and erection of Offshore Projects embodying VSC stations, transient phenomena is always a potential risk [\[18\]](#), [\[63\]](#).

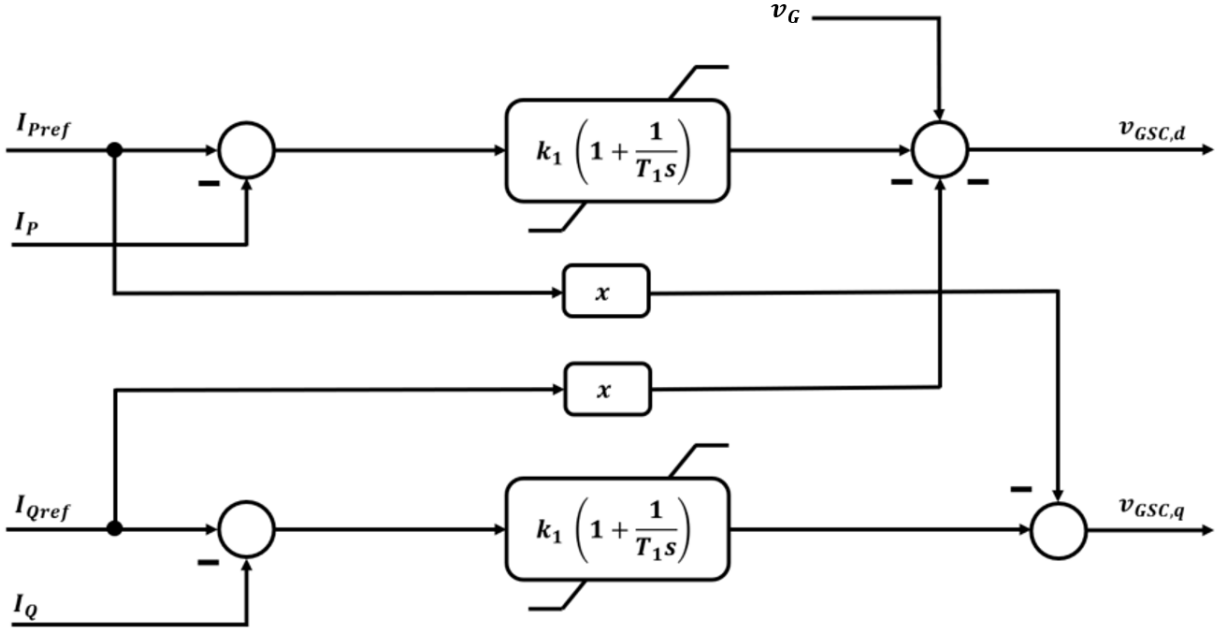
A potential consequence of such fault may be the blocking of the converter stations, which then would change the condition operation of the Offshore zone to an *Islanded Mode*, then with very low-to-nearly zero local load. In response of such event, the contemporary Current-Control Schemes are not equipped with frequency-control capabilities, so, during an *Island*, there would neither be any frequency reference to follow [\[19\]](#). Hence, without any frequency reference neither a real-time grid voltage requirement, the WT cannot rehabilitate the faulted network. [Figure 4.3c](#) is a simplified Thévenin equivalent circuit of the current-source scaled-WT model ([Figure 4.3b](#)). For simplicity, as its name implies the voltage source $v_{WT(DC)}$ provides a DC voltage, assuming constant and sound wind availability. v_{Gen} is the local measured voltage read at the node where the scaled-WT model is connected, and serves as a reference for the following equations, if using the *d-q* frame:

$$v_{WT(DC)} = v_{Gen} - jix_c \quad (4.1)$$

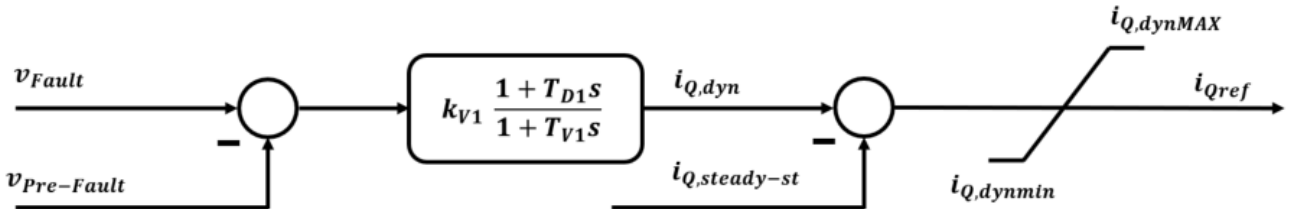
By using the real and imaginary currents analogically as active and reactive currents (i_P and i_Q), they can be rewritten as $i_P = i_d$ and $i_Q = i_q$. Consequently, [Equation 4.1](#) can be decomposed as

$$v_{WT(DC),d} = v_{Gen} - i_q x_c ; \quad v_{WT(DC),q} = -i_d x_c \quad (4.2)$$

Because, in the past, RES were considered to be secondary or complementary generation units, their control schemes were designed for such limited objective ([Figure 4.4](#)), then simply following a neighbouring Slack-Bus reference from Synchronous Machine Generation, and limiting WF installations to areas were the EPS was guaranteed to be



(a) Classical Current Control Method [18].



(b) Reactive Current Setpoint Calculation [18].

Figure 4.4.: Classical Current Control Method with Current Setpoint reference [17], [18].

stiff and stable. Thus, the power reference to the WF being nearly constant. As can be noticed in Figure 4.4a, the reference parameter that serves to set the terminal voltages $v_{GSC,d-q}$ to be related to the grid connection is given by the d - q (active-reactive) current components, which in turn are the outcome of a prior reactive current setpoint calculation (Figure 4.4b), where a steady-state reference is superimposed on a dynamic reference. This control system is successful as long as there is always a load to be dispatched, located in a robust Network. In that context, the feedforward terms work as long as the v_{GSC} signal is known, correcting the error by calculating the Δ -voltage. However, the use of feedforward terms may cause disturbances due to uncertainties in parameters, measurements, frequency, etc., but if especially combined with the currently-used WT control method, the feedforward control is not effective for *grid-forming* operation [17], [19], [21], [38]. The voltage correction ruled by this method is ineffective because the Δ -voltage is not large enough for the overall control system to detect and mitigate the error properly [19]. On that logic, it then assumes that the current reference can be injected into the Network at any time, which is not the case in *Islanded Operation* mode neither with PEI-based generation that aims to have *Black-Start* capability.

Figure 4.5 displays the DC voltage results of all WF in the *PST 16 Benchmark System* after a massive fault followed by *Islanding of Area A*. The effect of the blackout in the three power plants within the affected area is easy to notice compared to the rest of the plots. A sudden increase in voltage arose. The key element is the Integral part of the Proportional-Integral Control (PI) that takes part in the current-control method (Figure 4.4). This plot illustrates that the current reference i_{Pref} does not change despite the sudden fault, and the consequence is a big mismatch between the current reference and the actual current. After the blackout, the actual current i_P drops to nearly zero, but because the current reference did not change, the Integral part of the PI controller winds up (increases the mismatch error), forcing the VSC converter to inject current regardless the fact that a loss-of-load scenario has happened [19]. Meanwhile, surrounding electrical equipment, like transformers, shunt compensators, overhead lines, etc., reach their

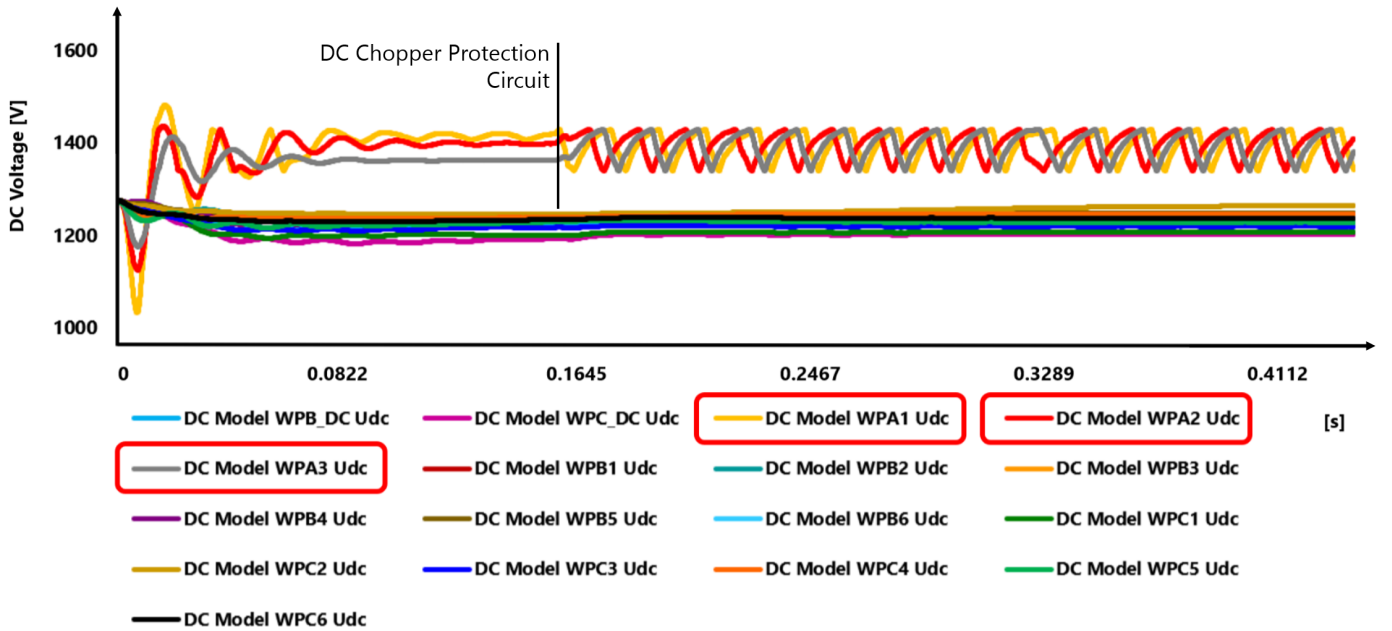


Figure 4.5.: DC Voltage of the WF in *PST 16 Benchmark System* after a blackout in *Zone A*.

saturation threshold several times, and that is also reflected in the DC voltage waveforms, presenting also resonance frequencies [19]. The chopper/capacitor combination at least prevents that the voltage does not further increase to abnormal values that would result in the full destruction of the damaged system. However, if later is intended to start a load-pick up process, the WT would not be able to restore any EPS.

In contrast, the advantage of utilising voltage/phase angle as the reference parameters to power the Grid is that in consequence the active power is influenced by them. Compared to voltage/frequency control, current current control performs poorly as it is incapable of influence in neither way the active power to be dispatched [8], [17], [19].

4.5 POWER AND CONTROL SYSTEM MODELS MODIFICATIONS

As it was stated in [Section 4.1](#), there were major modifications in all the converter-based units aggregated in the original *PST 16 Benchmark System*, and also seven BESS storage systems were added to the model. It is nonetheless important to state that during the DSL programming/modification and test stages, the models were subject to frequent change. These changes were the consequence of continuously-reproduced theoretical analysis and literature review, trial and error approaches during the Load Flow and EMT simulations, numerous failed results, the discovery of valuable information turned into knowledge during the simulation stages due to the unceasing process of knowledge acquirement and the analysis of the failed attempts, and the feedback from supervisors and engineers/scientist expert in the state-of-the-art, etc.

The last version of the *PST 16 Benchmark System* case study has several modifications, which are explained in detail in Subsections [4.5.1](#) - to - [4.5.5](#), and whose classifications are defined according to the power equipment embedded to each control system. Most control loop and algorithm models that exemplify such main changes are illustrated in Appendices [A](#), [B](#), [C](#), [D](#) and [E](#).

If a comparison between [Figure 4.2](#) and [Figure 4.6](#) is done, the following changes can be noticed in the *PST 16 Benchmark System* overview:

- **Seventeen utility-scaled Wind Farms (WF).** Designed to represent PMSG-Type-4 generators, all of them have a Δ -type connection, rated at 1000 MVA, with a Power Factor of 0.98, ready to deliver 910 MW of active power in their neighbouring terminals, and each one with an *External Station Controller* that forces the wind power plants to dispatch specific values of reactive power in Mvar for ensuring a balanced Load Flow, according to the network topology and components. Each WF also comes with a two-quadrant reactive power *Capability Curve* that defines their capacity limits at 1.1 p. u. ([Table 4.4](#)). Besides, they too have Wind/Power reference curves similar to the ones depicted in Figures [3.9](#) and [3.10](#). According to all these factors, all the WECS are designed

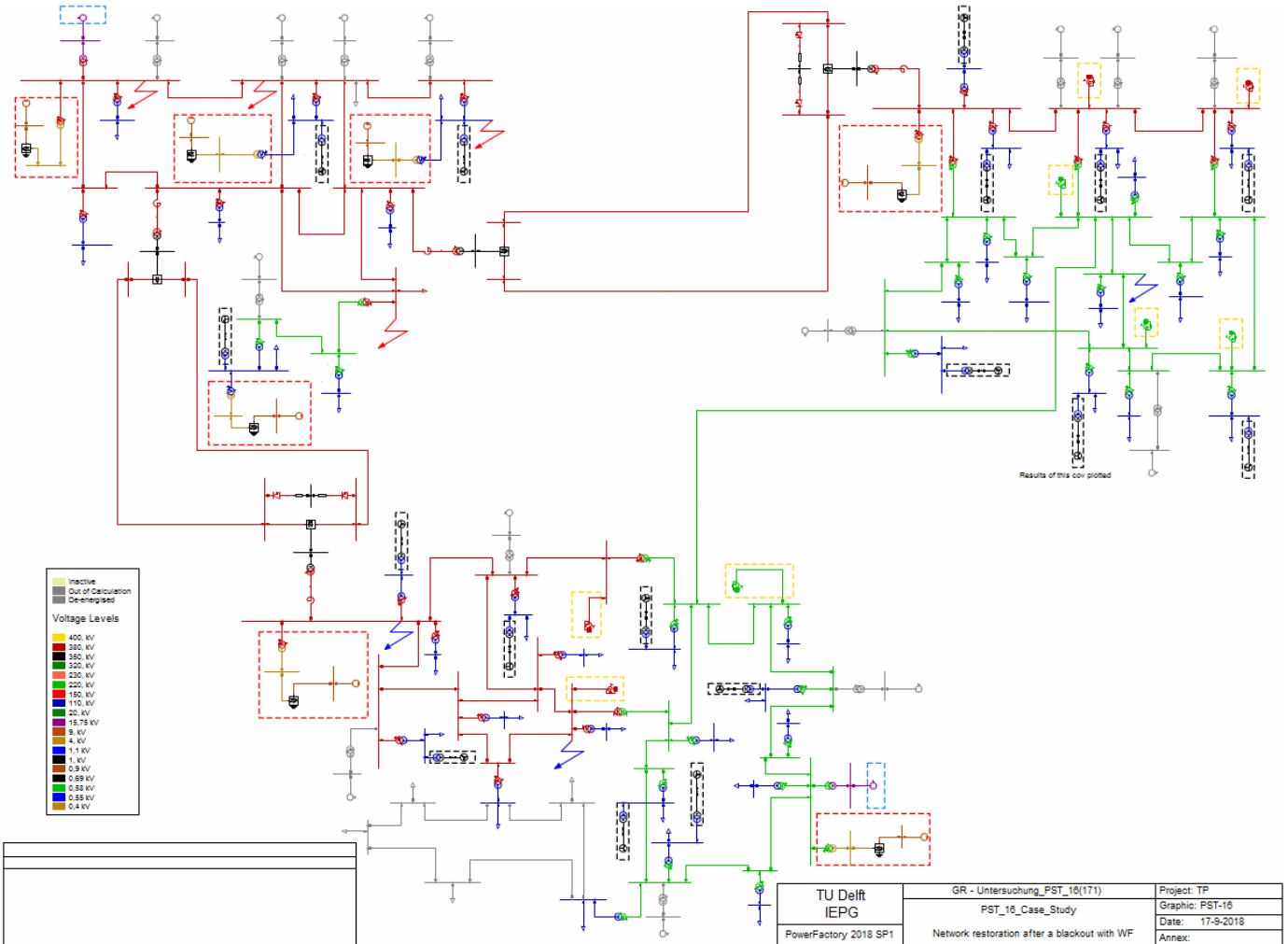


Figure 4.6.: The modified *PST 16* Benchmark System overview.

to deliver a maximum stressed demand of up to 980 MW in a rather tough scenario. All the Wind Power Plants are marked with dash-line rectangles in black.

- The two **Conventional Synchronous Generators** that are active during all operation scenarios (*A1aG* in *Area A* and *C12G* in *Area C*) are marked with dash-line rectangles in **blue**. All CGU voltage levels are still at 15.75 kV but they are now sketched in **purple**.
- **Seven Battery-Energy Storage Systems (BESS)**. They can be identified enclosed in dash-line rectangles in **red**. Each is composed by a 9 kVDC battery connected to a monopolar controlled-voltage source PWM inverter. Their power rating is 45 MVA with an AC voltage at 4 kV. Two of them are installed as emergency plants next to synchronous generators *A1aG* and *C12G* in order to provide excitation voltage and become them *Black-Start* units. Other three are disposed to do the same duty for the three WF located in *Area A*. The remaining two provide frequency support to the sending-end HVDC converter stations. The transformer units of the storing systems are connected to different voltage levels, according to their location and application. Therefore, their secondary windings differ between each other.
- **A hundred and sixty eight busbars**. Seventeen busbar/terminals were added to connect the seventeen new WF to their step-up transformers. As in real-life standards, the voltage level of the WT is 0.69 kV and so it is for the terminals too.
- **Eighty one transformers**. Similar case as the increased amount of busbars. Seventeen step-up transformers were added to connect the electric power from the WF to the grid, and that is done to transform their voltages to a transmission level of 110 kV. In real-life facilities, two transformers are used to step-up from 0.69 kV to an intermediate medium-voltage level of 33 kV and then from it to transmission levels. For simplifying the multiple step-up levels, seventeen equivalent transformers rated at 1000 MVA-0.69/110 kV, with a reactance of 6.65% are used [21]. Their saturation parameters are also active. The newly-added units have a Δ (High-Voltage) - Y (Low-Voltage) vector group connection.

- **Two VSC-HVDC transmission links.** *Area A* is communicated with the rest of the network with DC transmission. Each transmission system is composed of two bipolar half-bridge MMC converters. The *sending-end* rectifiers operate in *P-Q Mode*, while the *receiving-end* inverters do so in *Vdc-Q Mode*. Depending on the operation mode, their neighbouring terminals have specific *Vdc*, *P* or *Q* setpoint values for ensuring a smooth Load Flow. Like the WF, each VSC contains a voltage-dependent reactive power *Capability Curve* (Table 4.12); however, as this HVDC system is designed to allow power to flow bidirectionally, these capability curves are four-quadrant-type. The ratings of the converter stations are 350 kVAC, 760 kVDC and 2000 MVA. Instead of AC overhead lines, this system works with DC cables rated at ± 380 kV and 4080 A.

The modifications that cannot be noticed by just comparing Figures 4.2 and 4.6 are described in the coming subsections.

4.5.1 SYNCHRONOUS MACHINES AND TRANSFORMERS

CGU Governor Systems

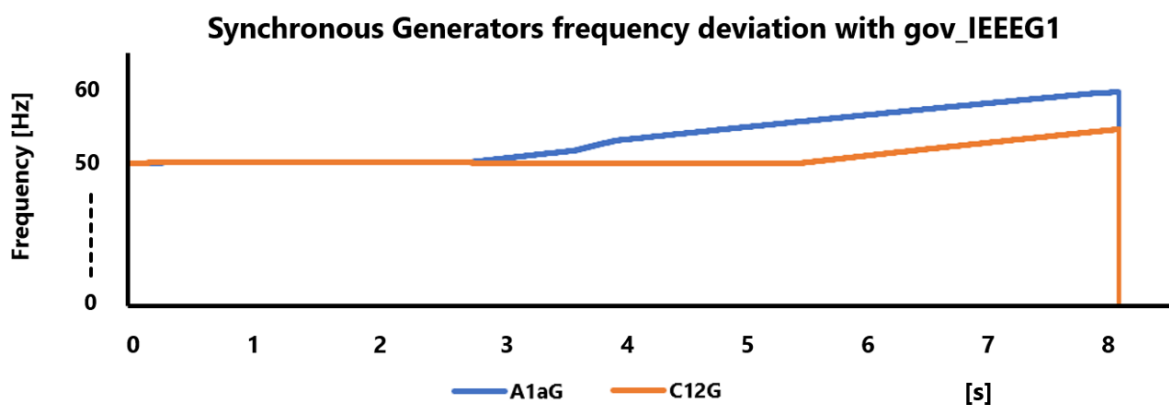
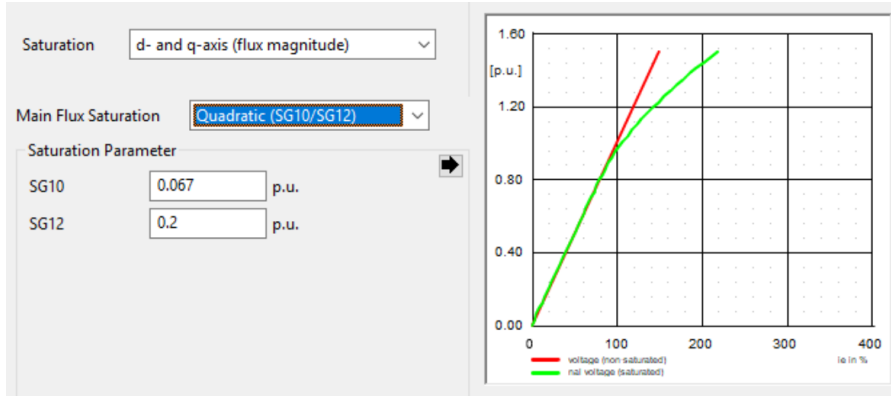


Figure 4.7.: Deep frequency excursion with *gov_IIEEEG1* after applying a Short-Circuit and disconnection of loads.

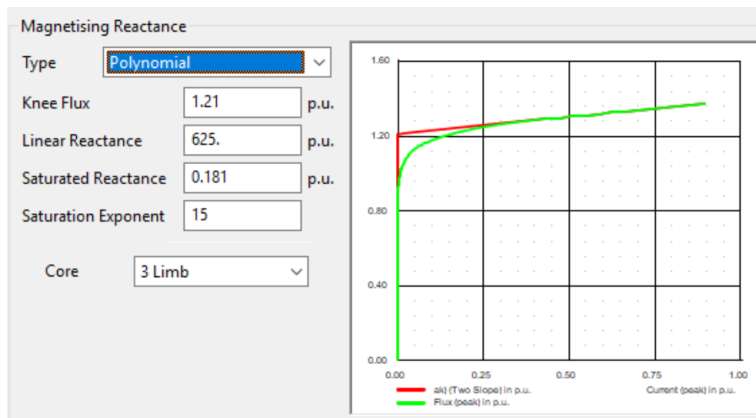
A major modification in the CGU were the replacement of the original Governor System for a built-in Governor Model that includes a SFC with Power Measurement Unit that allows to set the Mechanical Power Reference with frequency regulation with respect to the real-time conditions and necessities of the grid (Frequency Droop Characteristic) [25], [58].

The standard exciter (*EMAC1T*) and governor (*gov_IIEEEG1*) models from the IEEE have been widely used for the voltage and speed regulation of synchronous generators, respectively. When applied to the case study, *gov_IIEEEG1* works optimally during normal operating conditions [58]. Nevertheless, after a first test of the *mint-condition* case study including partial blackouts in *Areas A* and *C*, with loss of both generation and loads, it was detected that the frequency responses of the most-affected Synchronous Machines were not coming back to their nominal 50 Hz value after the oscillations caused by the fault stimulus. Not only that but they neither did stabilise within an upper/lower offset value. Instead, the frequency increased nonstop until the EMT system-matrix inversion failed. Figure 4.7 plots the results of that quick test, showing the frequency deviations of units *A1aG* and *C12G*.

Knowing that result, a test with another governor model was carried out to see if the performance of the 3-Area system could improve, based on [25]. Figure A.4 exhibits the Governor Model with the SFC. Composed by PI controllers with *speed droop-capability* function, which increases/decreases the mechanical power output depending on the frequency deviation. The blocks *Trb* and *Servo* speak for the dynamics of the turbine and servomechanism related to each synchronous generator, and their values in the DSL Common Model depend on the type of source used (hydro, nuclear or coal). The PI parameters of the Governors were increased for coping the high-speed response of the converter-dominated generation units in the 90%-wind scenario. This was done by modifying the values in each Governor System Common Model, similar to the one displayed in Table 4.2a. The SFC is composed of a filter *Tfilter* and a PI (slow) control, which brings the frequency of the grid to its nominal range for quasi-dynamic events. For that, it is necessary to include a power measurement station, whose output signal is denoted by *p* in Figure A.4. A limiter is included just before the output signal of the model; this block ensures that the mechanical power out-



(a) Synchronous Generator Saturation Parameters.



(b) Transformer Magnetising Parameters.

Table 4.3.: Saturation/Magnetisation Parameters.

put is maintained within acceptable values, which can also turned-out to be dynamic during a simulation with an additional algorithm if desired.

Automatic Voltage Regulator (AVR)

The utility-scale generation systems are in part comprised of AVR. The main purpose of AVR-exciter systems is to balance their voltages as the load on the EPS, detected by these generators, changes. An AVR is a voltage controller that keeps the output voltage of the alternator whenever voltage fluctuations occur, as a consequence of the effect of the variable loads. AVR-excitation systems are a kind of feedback control system that senses the output voltage of the synchronous machines, comparing that output to a setpoint, and then generating an error signal that is used to accommodate/readjust the excitation of the CGU [58], [77]. While the excitation current in the field winding of the generator is getting boosted, its terminal voltage so increases too (and vice versa).

The first excitation systems for generators were fabricated with electromechanical systems, but modern AVR use Power Electronic Devices (PED), like thyristors; usually, a small part of the CGU output is used to provide current for the field winding. When multiple generators are connected in parallel, the excitation system has circuits that assure all the generators are working with the same power factor. Similarly, when just one generator is connected in parallel with other sources, such as an external electrical network, changing the excitation has more effect on the reactive power produced by the generator than on the voltage of its terminal, which is established mainly by the connected EPS. The AVR embedded in generators of power stations connected to the network may have additional control functions to help stabilise the EPS against disturbances due to the sudden loss of load or faults [58], [77].

There are the following main functions of an AVR:

1. AVR control the voltage of the system and the operation of the machine closer to stability in a balanced state.
2. AVR divide the reactive load between the synchronous generators operating in parallel. The AVR reduce the overvoltages that occur when a sudden loss of load on the system takes place.

3. AVR are able to increment the excitation of the system under fault conditions so that the maximum synchronising power exists at the time of clearance of the fault.

In the *PST 16 Benchmark System* case study (in *Mint-Condition*) the standard IEEE *EMAC1T* AVR System was employed for the excitation voltage regulation of the CGU. This model, designed by DPF personnel and found as the available templates in the software, has been typically used for the voltage control due to its favourable performance. The AVR Systems in the study case were therefore not subject to any change and this template was replicated for all the synchronous machine units. [Figure A.2](#) presents the Block Definition of this excitation system.

Saturation/Magnetising parameters in Power Transformers and Synchronous Machines

The variety of components and high voltages and currents involved makes EPS *Restoration* technically complex. In real reconnection attempts, simply switching the supply to a transformer back-on can cause high transient voltages that are difficult to control, leading to oscillation effects that can damage or fully-destroy equipment or trip the *Black-Start* generator and such effect can be worse if the equipment has been outaged for a longer time. This causes the supply to shut down again and System *Restoration* to relapse in failure.

With that circumstance known, the DPF (quadratic) electromagnetic saturation parameters of the machines were enabled for consider these phenomena during the reconnection stage of the NR Plans ([Table 4.3a](#)). The electromagnetic saturation data of the generators are found with a quadratic function by declaring the excitation current i_e required to obtain 1 p. u. and 1.2 p. u. of the nominal generator voltage under no-load conditions. The saturation parameters are also defined according to each type of generator (hydro, nuclear or coal). Similarly, the magnetising parameters of all the transformers of the grid were also activated, (polynomial characteristic-type), with the knee flux at around 1.2 p. u. and the linear reactance value dependent on the no-load current losses ([Table 4.3b](#)).

Power System Stabiliser (PSS)

Generators need some kind of feedback in order to regulate their outputs; that is normally accomplished by the AVR, but this system is not fast enough when a line has a power glitch or sudden fault and regulator will make oscillations. For that, a PSS is added to the feedback taking in account generator inertia and so for which final result is a faster damping of the output frequency and voltage [\[25\]](#), [\[58\]](#).

PSS is a supplementary excitation controller used to damp generator electromechanical oscillations in order to protect the shaft line and stabilise the grid. It also damps generator rotor-angle swings, which are of greater range in frequencies in power system analysis. A PSS uses auxiliary stabilising signals to control the excitation system so as to improve power system dynamic performance. Commonly used input signals for the PSS are:

- **Shaft speed**
- **Terminal frequency**
- **Power**

Power system dynamic performance is improved by the damping of system oscillations. It is a very effective method of enhancing small-signal stability performance [\[25\]](#).

In the *PST 16 Benchmark System* case study (in *Mint-Condition*), the PSS shown in [Figure A.3](#) was utilised for the performance improvement of all CGU units. This element in the study case was not subject of any change either and this template was replicated for all the synchronous machine units.

4.5.2 WIND ENERGY CONVERSION SYSTEMS

[Figure B.1](#) displays the Control System Frame of all the seventeen WECS installed in the Network. The Controlled-Current Source WT model was replaced for a DPF Static Generator Element (*ElmGenstat**) defined as an scaled PMSG-WF. In DPF, a Static Generator Element is an user-friendly model to portrait any type of non-rotating generation system [\[15\]](#). These generators are commonly connected to the network through a static converter, hence their name. Even though wind power generation uses rotary generation, they are connected to the grid by means of full-size converters and the behaviour of the power plant, as seen by the network, is determined by the VSC.

[Figure 4.8](#) shows one of the new symbols that represent the scaled WF in the *PST 16 Benchmark System* Network. Each WF are characterised with a two-quadrant reactive power *Capability Curve* that defines their capacity limits at 1.1 p. u., as shown in [Table 4.4](#).

The *ElmGenstat** WT elements do not have a blank where the different reactive power setpoint can be defined. In

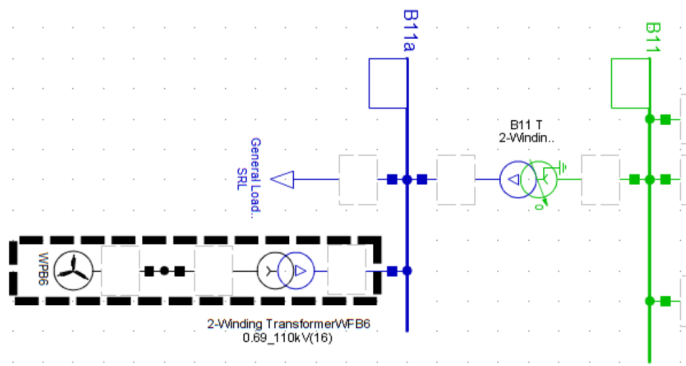


Figure 4.8.: DPF Static Generator (ElmGenstat*) depicted as an scaled Wind Power Plant.

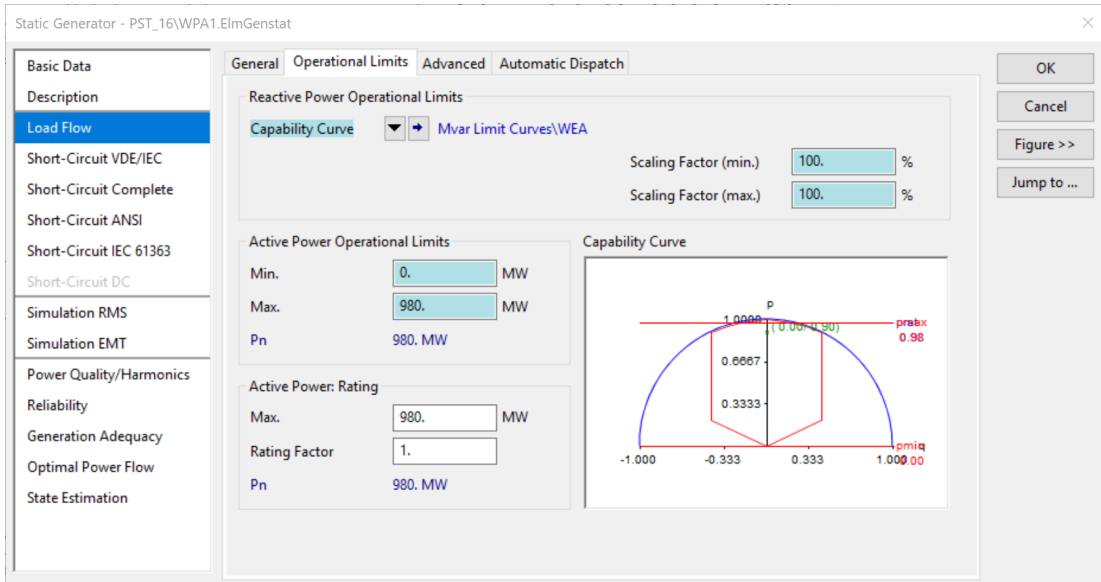


Table 4.4.: Two-Quadrant Capability Curve for all the WECS.

order to force the WECS to deliver specific values or reactive power, an **External Station Control** is required. These controllers can be tuned to have different operation modes; they can control voltage, reactive power, power factor or $\tan \phi$. In this case, the option Q - *Reactive Power* is selected. Table 4.5 gives an example of this additional controller for the wind power plant *WPC5*.

Voltage/Power/Frequency Control with Current Damping

The control system discussed in Section 4.4 was replaced by a new scheme that provides *grid-forming* capability to converter-based generation units. Unlike the former configuration, this newer concept can adapt its current injection depending on the fast-tracking of the grid status and conditions. Despite the enhanced control capabilities, in fact, the newer control concept is based on the older one, with only the Integral component of the PI current controller discarded, and the Proportional component merely shifted towards the output terminal of the controller [19]. One of the main goals of this scheme is to guarantee the damping of transient processes, and this controller is designed in such a way that emulates a resistor in the circuit that causes a voltage drop, thus creating a damping effect. The *emulation* characteristic means that the voltage drop effect is done with a Proportional term of a PI control instead of a resistor; while a resistor could also breed the same effect, it would work with the undesirable power losses that inherently go along with a resistor. For limiting the effect of the resistance emulation to work only during transient current periods, the controller was extended with a washout filter [17], [19], [20]. This first set of modifications are illustrated in Figure 4.9.

The *Grid-Forming* control scheme is named as **Voltage/Power/Frequency Control**. In DPF the Block Definition representing this concept was named as **Udc_Q Controller**. Figures B.8 and B.9 illustrate the two main control systems where the direct voltage/reactive power control theory has been applied. By analysing both illustrations

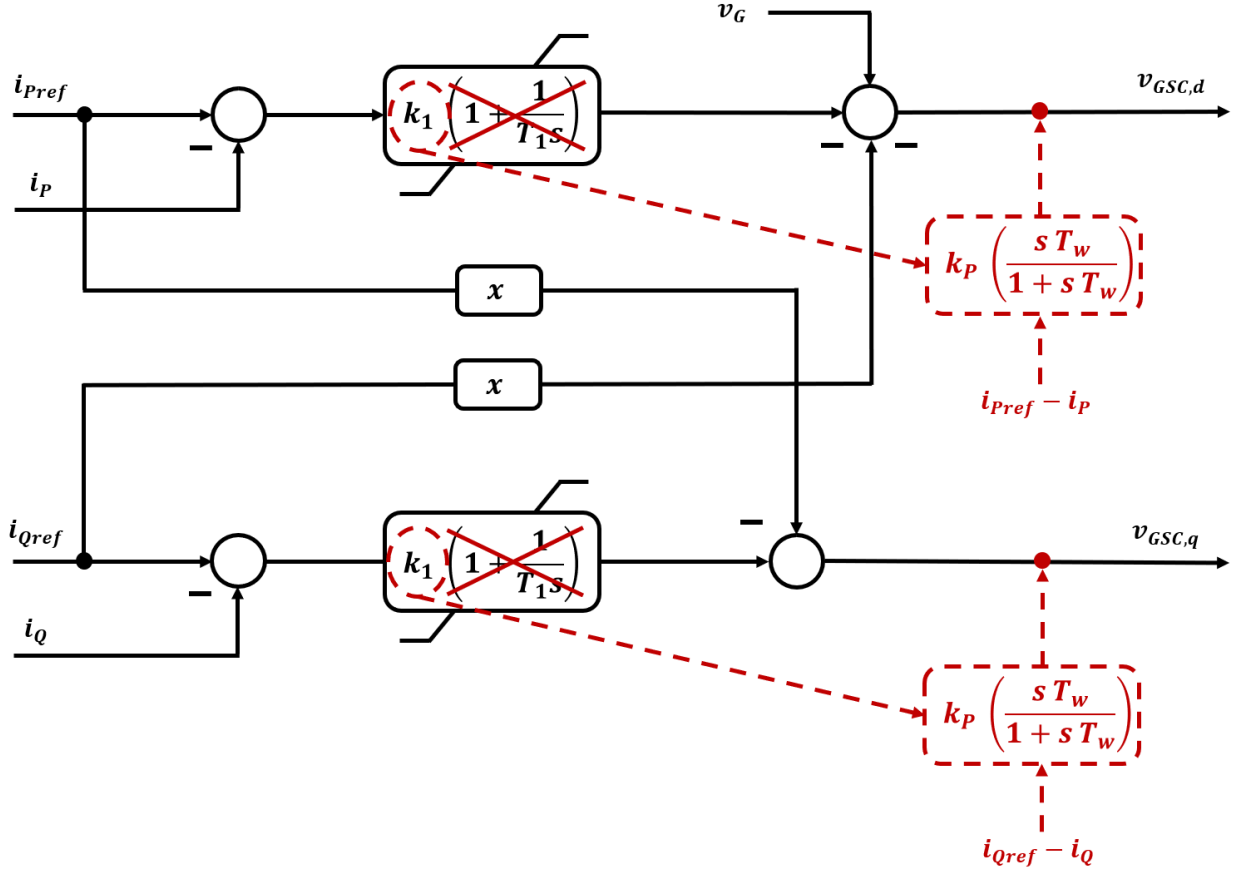


Figure 4.9.: Modifications to the current control method [19].

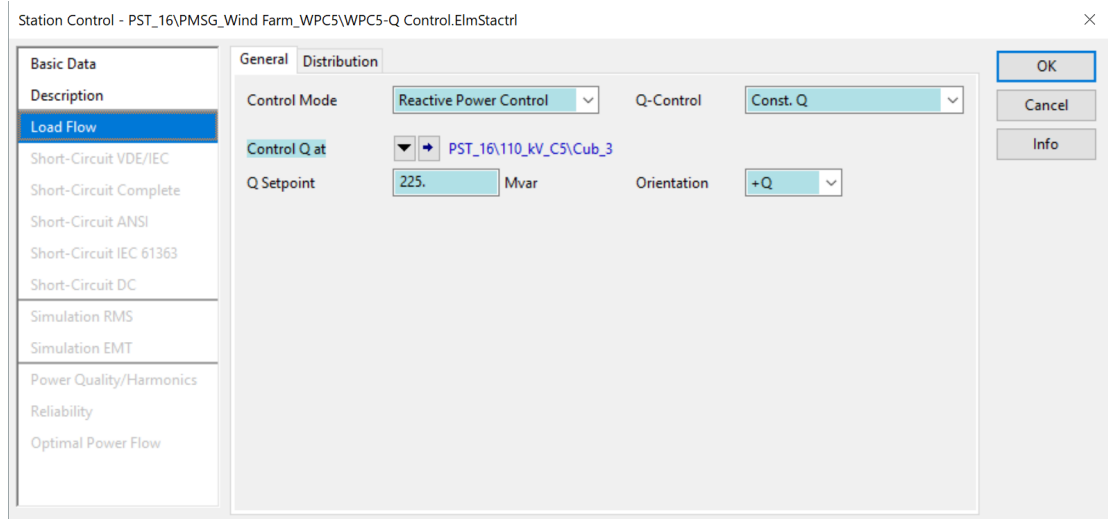


Table 4.5.: External Station Control with Q-Operation Mode.

can be noticed that the new control scheme is still working with feedforward terms and that these control systems are composed by many PI controllers, and not all of them have removed their integral components. In fact, the feedforward regulators remained because, as explained in [Section 4.4](#), they work fine as long as their *d-q* components of the inverter voltage v_{GSC} signals are correct.

The information that serves as the reference for the active current (power) and reactive current (power) to the feedforward regulators are given by PI controllers located in the **DC voltage control** (which gives the signal P_{set_pi} for active power reference) and the **slow-remote reactive power/AC voltage control** (which gives the signal $qref$ for reactive power reference). The control loops can be identified in [Figure B.8](#), where the DC voltage control loop is

enclosed in a yellow rectangle, and the reactive power/AC voltage control loop in a blue rectangle. Figures 4.11 and 4.12 can be seen as detailed illustrations of what can be seen in Figure 4.9. These two Figures show only one output signal each, which are the terminal voltages $v_{GSC,d-q}$ related to the Grid connection. The **Current Limiter Control Blocks** located in both Figures 4.11 and 4.12 represent a current limitation scheme that forbids excessive current injection and prevents to surpass preset maximum allowable current limits [17]. The converter current is limited through the voltage thresholds $v_{GSCd,MAX}$ and $v_{GSCq,MAX}$. Figure 4.10 unveils a phasor/circle diagram that explains the method for the current limitation in the converter [17], [21].

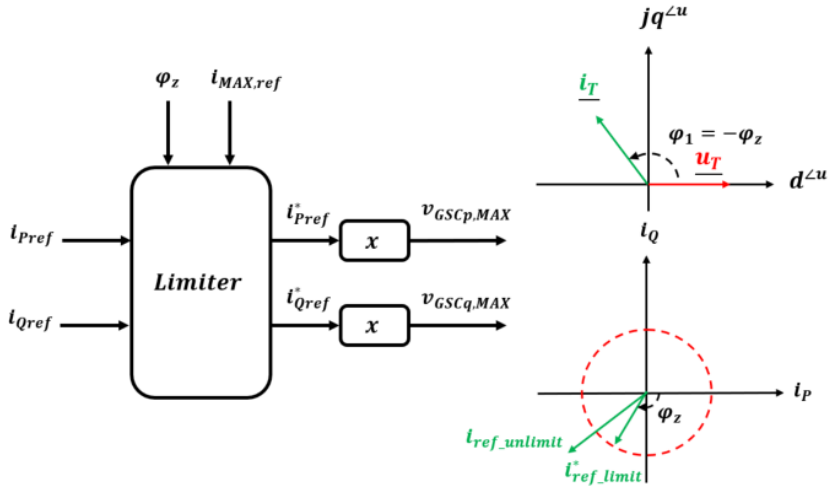


Figure 4.10.: Converter Current Limitation Control [17], [19], [20].

For limiting the real current, if

$$(|i_d + ji_q| - i_{MAXo_ref}) > 0 \rightarrow i_{MAX_ref} = i_{MAXo_ref} - k_{red}(|i_d + ji_q| - i_{MAXo_ref}) \quad (4.3)$$

otherwise

$$i_{MAX_ref} = i_{MAXo_ref} \quad (4.4)$$

For limiting the current reference, in case it is not bounded

$$v_{GSCd,MAX} = v_{GSCq,MAX} = xi_{MAX_ref} \quad (4.5)$$

otherwise

$$v_{GSCd,MAX} = xi_{Q,ref}^*; v_{GSCq,MAX} = xi_{P,ref}^* \quad (4.6)$$

When the actual converter current exceeds the maximum current of the converter, a new maximum current value is calculated [21]. The new calculated maximum current value is used in the limiter block along with the angle of the grid impedance seen by the converter. The reference current limits of the d - q converter control voltages are limited based on the impedance of the grid and the new calculated maximum current value. This means that the converter adjusts the reference currents based on the impedance seen by it and thus it provides the best possible voltage support [21].

It is important to clarify that the **Current Limiter Control Blocks** are actually implemented in DPF between both **Udc_Q Controller** and **Current Limitation and Damping Model Definitions**, evinced in Figures B.8 and B.9. If the Composite Frame of the WT models is analysed (Figure B.1), it can be seen that the Slots linked to the **Udc_Q Controller** and the **Current Limitation and Damping Model Definitions** are next to each other.

In the **Udc_Q Controller**, the main control loops are the **reactive power/voltage** and the **active power/frequency** channels. The outputs of each control loop provide the inverter voltage signals $v_{GSC,d}$ and $v_{GSC,q}$.

- **Reactive Power/Voltage Control Loop.** Figure 4.11 exhibits the control loop that calculates the d -component of the voltage injected to the grid. This channel can be operated in voltage or reactive power mode. In case it is run by the first choice, it then is controlled by the first section of the system, known as the **Slow-Remote/Global Regulator**. This first approach is based on a hierarchical control concept, in which this upper-level slow-acting controller tracks setpoint changes dictated by systemwide exigencies [38]. A droop characteristic (predefined and adjustable voltage/reactive power ratio) calculates the reactive power reference q_{ref} , followed by a PI controller. The u_{ref} input signal is fixed to the initial-condition values of the measured reactive current, the voltage

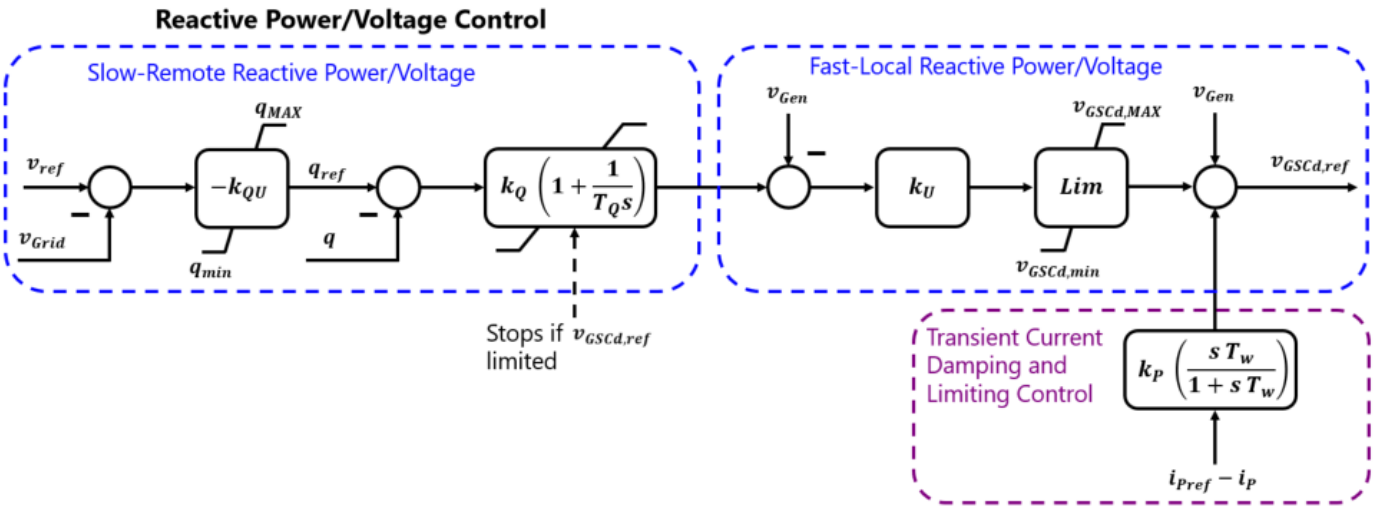


Figure 4.11.: Reactive Power/AC Voltage Control Loop [17], [19], [20].

u_{Grid} and the values of the value of the k_{QU} proportional gain of the droop characteristic, defined in each Common Model. The voltage u_{Grid} is considered as a global (or remote) signal, as it is measured in a node located in the global network. This first part is designed to stabilise the system when relatively lethargic transients take place, acting with a response time of 5-to-30 seconds. This time constant, whose signal is named as T_{dc} in the DPF study case, can be defined and tuned in the Common Model and its value should be selected in order to be large enough to avoid significant control action during network short-circuit but yet small enough to prevent from unnecessary tap movement in On-Load Tap Changer (OLTC)-transformers [17]. The k_{QU} proportional gain of the droop characteristic is defined with Equation 4.7:

$$k_{\text{QU}} = \frac{\Delta q}{\Delta v_{\text{Grid}}} \quad (4.7)$$

From there, q_{ref} is calculated, and then the signal named $v_{\text{GSCd},\text{ref}}$ can be further known. The latter signal is determined for cases where reactive power injection is not necessary, and thus it may be updated at regular intervals [38]. Signal $v_{\text{GSCd},\text{ref}}$ is computed as shown in Equation 4.8:

$$v_{\text{GSCd},\text{ref}} = -\frac{q}{k_{\text{QU}}} + v_{\text{Grid}} \quad (4.8)$$

Similarly, in case this control loop detect major voltage dips or the current limit is reached, the controller automatically changes its mode of operation to the reactive-power choice. Then, its reference input signals is directly passed to the downstream part of this main control loop, known as the **Fast-Local Regulator**. The **Fast-Local** regulator was designed for sudden events demanding faster responses. It presents a proportional behaviour in steady-state operation, but can be increased with a lead-lag block to acquire a dynamically varying gain in order to respond accordingly to the major voltage dips and/or excessive currents [19]. A fast-voltage static gain K_u is the first addition of this primary-action downstream part. Its input signal comes directly from the output of the secondary-action upstream part, where the voltage signal used here is u_{Gen} (from the scaled WT Generators), which means it is a local signal. For boosting-voltage response, it is better to work with a local signal, as it is in an immediate neighbouring zone. The response time must be fast enough to cope with network faults (for instance, less than 30 ms [38]), and it also must have a compelling influence in relay-protection scheme operations [38]. The output signal after the K_u multiplication enters a voltage limiter, with limits $v_{\text{GSCd},\text{MAX}}$ and $-v_{\text{GSCd},\text{MAX}}$, which are previously calculated with help of the signal $i_{q,\text{ref}}$, which comes from the **Current Limiter Control Block**, and it does so depending on the selected active or reactive current priority mode of operation [17]. The limited output is then added to the measured generator voltage u_{Gen} , and this last output is in fact the output of this main control loop ($v_{\text{GSCd},\text{ref}}$).

- **Active Power/Frequency Control Loop.** Figure 4.12 exhibits the control loop that calculates the q -component of the voltage injected to the EPS. The output of the DC voltage controller is the active power injected to the network, and the reference comes from the DC link PI controller. Considering equations 4.1 and 4.2, the active

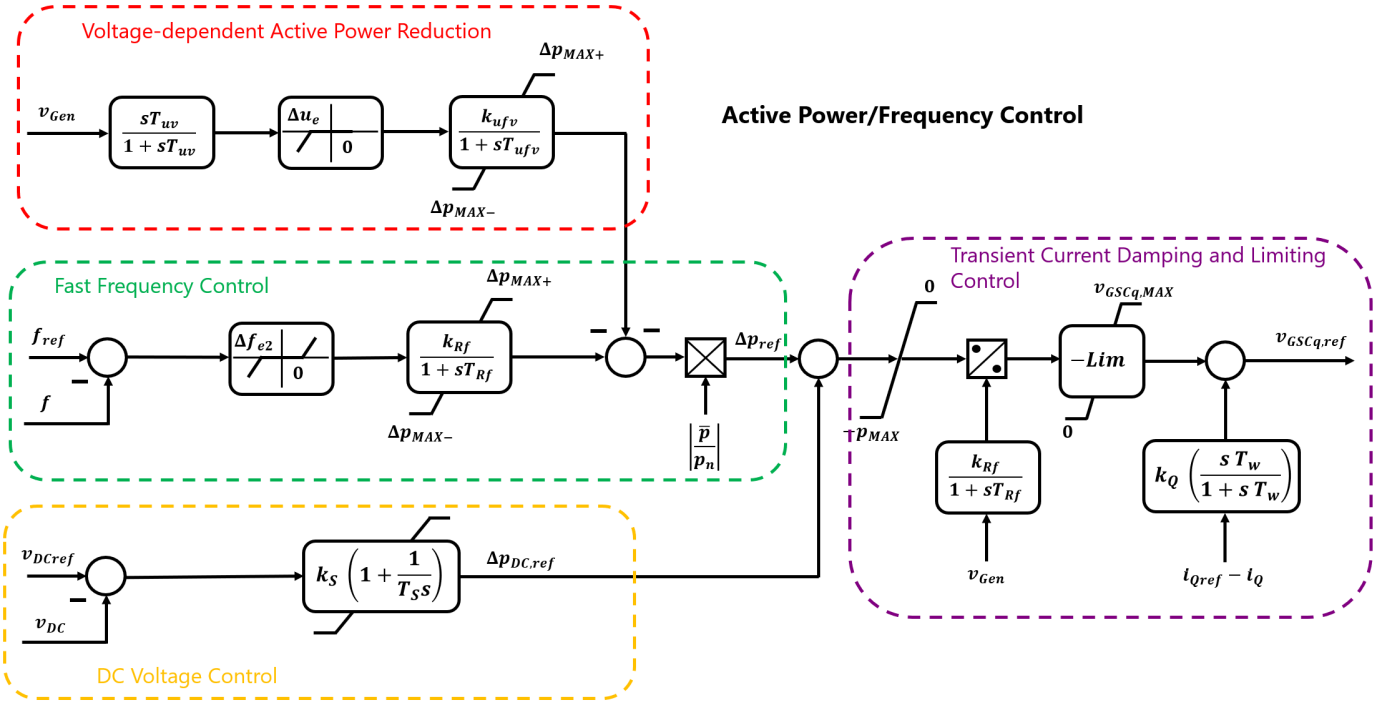


Figure 4.12.: Active Power/Frequency Control Loop [17], [19], [20].

power can be controlled by using the q -component of the converter voltage, which can also be used to limit excessive currents [17]:

$$p = v_{\text{Gen}} i_P = -v_{\text{Gen}} \frac{v_{\text{WT(DC),q}}}{x_c} \quad (4.9)$$

With Equation 4.9 can be seen that reactive current injection requirement is no required in this theoretical concept and instead direct voltage control can be implemented to regulate the active power [17], [18], [20]. In case of an *Island* or a blackout, or any event that derive in transients or faults, there is no risk of integrator wind-up, because direct reactive power/voltage/frequency control can make the dispatched current to adjust itself for the objective of grid stability in response to the changing converter voltage [38]. Therefore, the scheme is more like the conventional voltage control in synchronous generators.

The DC voltage control works nonstop in this control loop channel. But this loop also has additional modes of operation and the system automatically changes it according to the present situation and needs of the EPS [17], [21], [38]. This can be translated into emergency situations:

1. **Fast Frequency Control.** In case the control systems detect a frequency deviation, this option is activated.

When the frequency of the system rises above a preset threshold, the block named *OverfrequPowerReduction* performs, thus limiting the power injection to the grid. This output is, in turn, the input of a PI control block with the time constant $T_{\text{rate_limit_freq}}$ and the default value of this signal in all Common Models is of 0.2 seconds. This number is selected to deal with the fast response time of the converters [17]. In Section 3.5 was briefly discussed the Governor Systems in CGU. Remembering the main function of a Governor, this part of the overall **Udc_Q_Controller** can emulate similar functions. Despite the name of the *OverfrequPowerReduction* block, this mode of operation also works to mitigating underfrequency deviation errors. Therefore, in the case of underfrequency scenarios, power can also be increased when required. However, in real EPS the surplus generation of power must be controlled with further effort than when the power is reduced. For that, the *Gradient Limiter* control block is used in case a limitation of the rate-of-change is desired [21]. Hence, if a certain power reserve is expected to be maintained, WT can contribute to this control.

2. **Voltage-Dependent Active Power Reduction (VDAPR).** The philosophy of this control branch is similar to a feedforward control. Its main purpose is similar to the previous mode of operation, but it complies its functions by means of adjusting the power injection capability of the converter based on the terminal voltage of the inverter that makes contact with the external power network. Therefore, if a major fault occurs, this loop completely prevents the converter from injecting current to the grid. In this manner, the VDAPR reduces the setpoint reference power of the converter immediately and so improving the transient

stability of the entire EPS [21]. The VDAPR section alleviates situations when sudden *islands* or blackout events arise.

By analysing the **Udc_Q_Controller** concept, turns out that it can be interpreted as a kind of an AVR. According to Subsection **AVR**, AVR excitation systems are used in standard Synchronous Generators. The **Voltage/Power/Frequency Controller** presented in this section has the same objectives for the control of *grid-forming* converter-based generation/transmission systems that an AVR has for the control of CGU. And the way both control systems work also has some parallelisms. AVR excitation systems measure the output voltages of the Synchronous Machines and compare those outputs to a setpoint, then generating an error signal that is used to adjust the excitation of the CGU. As a consequence, the excitation currents in the field winding of the Generators will be regulated accordingly; it is maintained steady if no prior actions were executed, otherwise, if measuring an error, then it will adapt the excitation currents to maintain stability, either increasing it or decreasing it [77].

Phase-Locked Loop (PLL)

In [Section 3.5](#) the SVM control theory was briefly explained with the reasons why it needs to be applied for the ease of the EMT study case models operation. Due to dynamic performance issues, for rotating the reference frame of the current controllers, voltage synchronisation has to be applied because without it, stable control is difficult to grasp [8].

This can only be done with voltage-tracking algorithms, such as PLL. PLL provide the voltage-angle reference to their linked controllers. They can be described as a natural application of the SVM control theory because they provide the reference that the VSC converters need for controlling the currents in the *Clarke-Park* reference frame system. This is implemented by controlling the angles in such fashion that their *q*-components rotate to equal zero and their *d*-components match to the synchronising voltage [8]. [Figure B.7](#) shows a built-in Model Definition of a PLL.

DC Circuit Model

As the ElmGenstat* element ([Figure 4.8](#)) does not have any DC bus, unlike real WT, a DSL model had to be designed to include the DC busbar, chopper and capacitor, as done in [21] and [26]. [Figure 4.13](#) presents the Block Definition of the **DC Model**. The actual implementation in DPF as a Model Definition is unveiled in [Figure B.6](#).

Because of the previous *Clarke-Park Transformation*, the input power signals revealed in [Figure 4.13](#) are actually already DC signals. However, the input signals that enter the to the Capacitor block in [Figure B.6](#) are in fact currents, as the input power signals were previously transformed into currents. The DC voltage therefore is calculated with its current component divided by 20 Farad (F) (default value in most Common Models) of capacitance. An integrator adds up to the resulting voltage for having the DC voltage output. If required, the DC Chopper can dissipate excessive currents, acting as a mains of protection. The protection logic, unveiled in [Table 4.6](#), represents the trigger conditions for the protection circuit, in this case, chopper circuit [21]. The chopper activates when the measured DC voltage surpasses the upper-threshold hysteresis limit and deactivates itself if it goes back to non-damaging voltage levels. The hysteresis threshold limits are defined in the **DC Model** Common Model tab, represented by the parameters *uDC_Chon* and *uDC_Choff*.

<i>Protection Circuit</i>	<i>Trigger Condition</i>
DC Chopper	Activated if $u_{DC} > u_{DC_Chon}$ Deactivated if $u_{DC} < u_{DC_Choff}$

Table 4.6.: Protection Circuits and Trigger Conditions of the scaled-WT [21].

WT Aerodynamics and Mechanical Drivetrain

WT are connected to the electric grid with VSC that decouple the electrical and mechanical systems. As WT are idled by the network, Power System Analysts often consider the mechanical dynamics effects as close to negligible

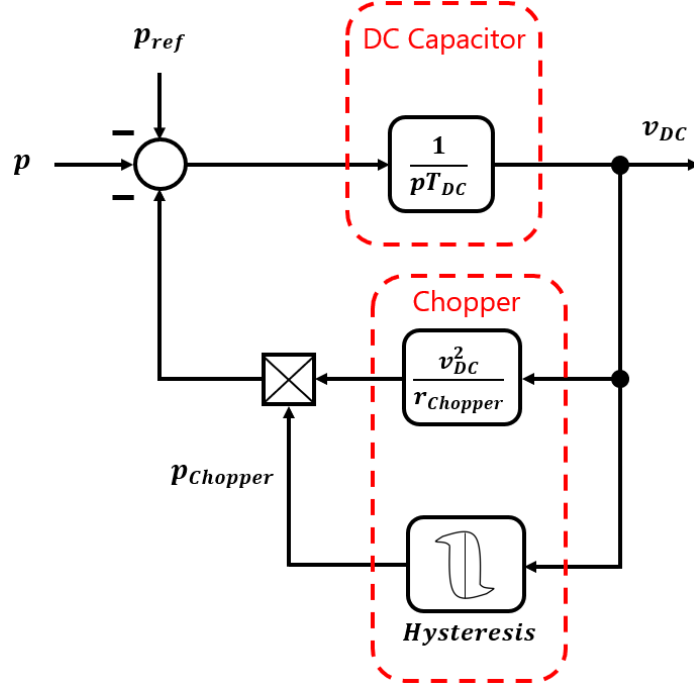


Figure 4.13.: Control Loop of the DC Circuit encompassing the Capacitor and the Chopper [21].

for the evaluation of EPS stability and robustness, while the uncertainty in wind is compensated with the control of these converters or it is simply assumed that the hypothetical location where the WF is installed has guaranteed steady/strong environmental conditions [17], [21]. Another practice is to study steady-state conditions or transient events considering time series for these turbines, which are taken based on average climatic conditions, including wind flow, aerodynamics, and variability. Further, the mechanical dynamics systems are continuously improving and therefore, potentially negative effects can be acceptably be neglected for most steady-state and even transient simulations.

Despite the former arguments, regardless of how efficient and marvellous the technology improvements are, wind is still the energy source. Therefore, if the availability of wind source and electricity consumption do not match, the control systems to make WT *Black-Start* capable do not matter. Moreover, for companies that sell or buy WECS, the mechanical dynamics can make a difference between selecting or discarding different manufacturer options [63]. Because of the latter arguments in favour, it was decided to extend the WF Models developed in this MSc Thesis Project and hold a more-complete System. For the assessment of different atmospheric conditions, the mechanical drivetrain, the aerodynamic equations and an electromechanical conversion block were also added to the overall composite model.

If looking at the WT Model Frame in Figure B.1, Slots for the aerodynamics/mechanical systems are there too. Figures B.2 - to - B.5 exhibit the Block Definitions of the **Pitch Angle Controller**, **Turbine/Aerodynamics**, **Shaft**, and the **MPPT Tracker**, which gives the power reference to the **DSL DC Model**. Additionally, a variable **Wind Velocity Block** and a **Swing-Equation Block** were also developed by coding formulas in DSL. In order to match with the theoretical description of the aerodynamic/mechanical systems that compose a WECS system, these Model Definitions were designed to match what was described in Section 3.6.

-Pitch Angle Controller

Figure B.2 unveils the Block Definition of the **Pitch Angle Controller** that each of the seventeen WECS hold. Its function is to limit the generator speed to its rated value for wind speeds above rated wind speed [39]. The control loop contains a PI controller whose proportional gain K_p_{pitch} generates a blade angle setpoint derived from the difference between the reference speed of the WT generator ($wref_{wt}$) and the actual speed ($speed_{gen}$) signals [78]. The integral part of the PI controller includes the time constant T_i_{pitch} and two max/min limits with the finality of imposing an anti-wind-up loop. The anti-wind-up prevents from integrating mismatch errors between the reference and measured signals while the power control is not active or while the pitch angle is held constant by the pitch logic [39], [78]. The philosophy of the SFC implemented in the Governor System selected to work with the sixteen CGU

units in the study case was mimicked to be an extra element in the **Pitch Angle Controller** [25]. It also includes an active power measurement instrument that is installed in a busbar next to the point of connection with the WT and it can detect over-excessive electrical power or lack of it and accordingly influence the WT frequency to go back to their nominal values with help of another (slow) PI controller. The output of the blade angle PI block is compared to a feedback signal to calculate a difference error in order to determine at all times if it is necessary to operate the pitch system or not use it if otherwise. The feedback signal comes from an inverted gain with rate limiters and another Integral element. The rate of change of the pitch angle, and their limits and time constants can be custom-tuned in the Common Model of each Block Definition for defining the maximum/minimum rate of change in the pitch angle. This section also includes other limiters that set the maximum and minimum β angle that the WT can pitch. In the last block of the **Pitch Angle Controller**, another parallelism with respect to the CGU Governor Systems is found with the time constant T_{servo} . This block is a representation of the pitch actuator system.

-Wind Speed (Wind Ramp)

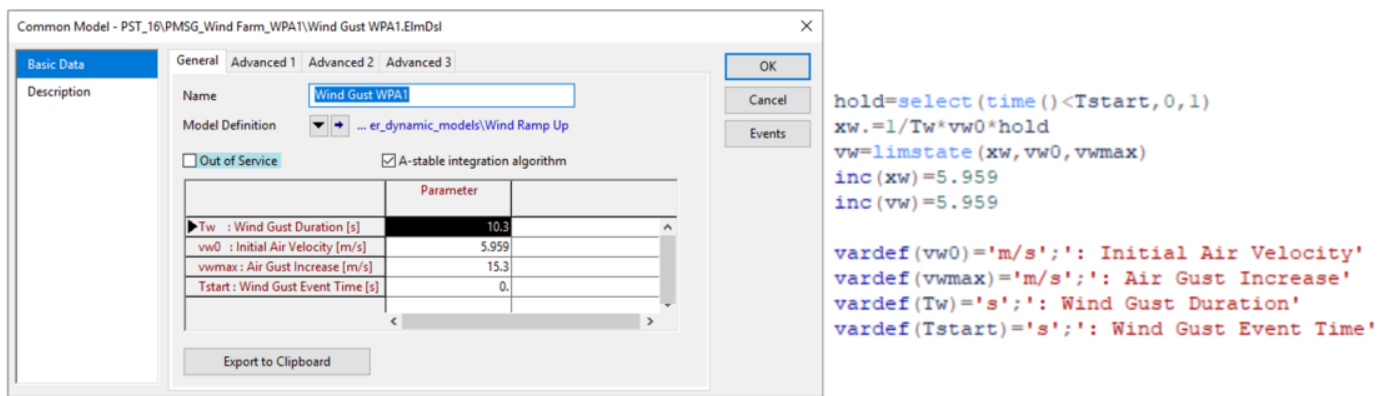


Table 4.7.: Wind Gust DSL Common Model and Block Definition [22].

A DSL Block was designed to create an effect that follows suit the variable behaviour of wind (wind gusts) [22]. Table 4.7 unveils the Block Definition with the equations that describe sudden acceleration in the wind located where the *PST 16 Benchmark System* power grid is located. As initial parameters it includes the aforementioned *cut-in* and *cut-out* speed limits that an usual WT would take in account for operational success [57]. By definition, the Derivative term of an augmented Proportional-Integral-Derivative Control (PID) represents the rate of change between the setpoint and the process variable error. It determines the slope of the error over time and multiplies this rate of change by a derivative gain [22]. Applied to this Block, it is designed to migrate an initial wind speed set in the Common Model to a final speed larger or smaller than the initial speed, with a non-linear effect. Usually, Derivative terms are not widely used in control systems given its variable impact on system stability applications, but in this case is a good approach for emulating random changes in wind speed [22].

If it is, however, not necessary to aggregate these effects in an analysis simulation, this block can be put out of service and instead just indicate a constant wind speed (usual values coinciding with the rated speeds of 12-to-15 m/s).

-Turbine/Aerodynamic Model

Figure B.3 displays the Model Definition where the Equations 3.17 and 3.18 (representing the **Wind Power** and the λ **Tip Speed Ratio**) are modelled. The only changeable parameters found in its Common Model window are the density of the air ρ (in the study case defined as rho) and the rotor blade area A_{rot} (in the study case defined as R).

Outside the inner block displayed in Figure B.3 these formulas are predefined with initial-condition signals for a smooth initialisation of the model, but once that stage is passed, that inner block calculates the wind power output based on the c_p characteristic matrix, the λ tip-speed ratio (calculated in this same block too) and also as a function of the input signals β pitch angle, the available wind speed, and the speed of the turbine, which is calculated in the next Block and therefore works as a feedback signal.

Variable-speed WT can modify their locus of maximum power available, that is, whatever wind circumstance is available at the moment (low / high-speed winds). Exempli gratia (e. g.), at lower wind speeds they adjust the rotor

speed at changing wind speeds so that $c_p(\beta, \lambda)$ always is maintained at the maximum value possible [78]. c_p has a maximum for any particular λ and β . Hence, for extracting the maximum power for any peculiar wind speed, the control strategy of this Model Definition is to change the rotor speed in order to always reach the most-convenient tip speed ratio λ possible. As it was explained in [Section 3.6](#), WT manufacturers provide the specific value of c_p with

Common Model - PST_16\PMSG_Wind Farm_WPA1\Turbine WPA1.ElmDsl

```

Pwind=lim(rho/2*pi()*sqr(R)*Cp*pow(vw,3)/1E6,0,1.2)
Cp=sapprox2(beta,lambda,matrix_i)
lambda=speed_tur*R/vw
Pwind_max=lim(Pwind,0.1,1.5)
Pwind_min=0.1

```

Table 4.8.: 66×49 Wind Power Matrix Array.

respect to a set of different combinations of λ and β , which are stored in a matrix. The matrix used in the DPF model is characterised by a two-dimensional look-up table with 66×49 characters, which are translated into the different curves that describe the possible combinations of speed/power that the WT can wander around. Along with the variable parameters described above, the parameter *matrix_i* encompasses the 66×49 array, as shown in [Table 4.8](#). This array is designed in such a way that, when operating at rated speed, the WT have a Coefficient of Power c_p of 0.45, and, in case the wind blows at speeds above 18 m/s this number however would not increase anymore. The values in the matrix were defined according to template references found in the DPF libraries.

-Shaft

As described in the **Generator and Shaft** Subsection in [Section 3.6](#), oscillations in the WT shaft should be considered in the simulations in order to exemplify cases with strong/heavy faults and evaluate the turbine and generator acceleration response after the faults with acceptable accuracy, because this part of the WT has the most significant influence on the power fluctuations, in terms of mechanics [39], [78]. On that order, the DSL Model Definition of the Shaft ([Figure B.4](#)) was designed to include mechanical inertia with the two-mass model concept representing the two-dominant masses, according to what was expound in [Section 3.6](#) [39], [78]. The WT rotor mass with a larger inertia H_w and the mass of the Generator with a relatively lower inertia H_R . H_R is a changeable parameter in the DSL Common Model of this built-in Block Definition (represented by the variable definition *H*) [39]. The low-speed

side of the shaft is depicted by the stiffness K_{tg} and the torsional damping coefficient D_{tg} . The model is a direct-drive design, as there is no high-speed gearbox included [39].

ϕ (identified as *dphi12* in the model) is the angular displacement between the two ends of the shaft [64]. t_R and t_{el} are the mechanical and electrical torques of the generator, while t_w is the torque of the turbine. Lastly, P_w is the collected power from the wind.

The output signals from this control loop are the turbine speed *speed_tur* and the mechanical power *pt*. *speed_tur* is part of a feedback loop between the **Shaft** and **Turbine** Model Definitions while *pt* becomes an input signal for the calculation of the generator speed.

-Swing Equation of Motion

The Static Generator Element (ElmGenstat*) that represents all the scaled-WT in the study case (Figure 4.8) does not accept input signals regarding speed references, given the fact that this default-DPF Model is designed to represent non-rotating generation [15]. Therefore, wiring up the mechanical power signal *pt* coming from the **Shaft** Model Definition to the ElmGenstat* element as an input signal with the objective to obtain an output speed from the Static Generator would be completely futile because this element is not arranged to interpret any input in terms of mechanical parameters or speed. This would be otherwise possible if instead of using an Static Generator Model, a DPF Synchronous Machine Element (ElmSym*) would be used for the PMSG representation, as it was the case in Subsection **WT Back-to-Back Philosophy in DPF** [15].

For illustrating this issue, a comparison between Figures A.1 and B.1 can be made. The Slot block that links the **Synchronous Machine Dynamic Frame** with its ElmSym* Model has both input/output wired signals, according to Figure A.1. One of these output signals, whose name is *w* or *xspeed*, is the calculated speed of the generator, which feedbacks the Centrifugal Governor and the PSS. On the other hand, the Slot block that links the **Wind Turbine Generator Dynamic Frame** (Figure B.1) with its ElmGenstat* Model only has two inputs as signals, but no output signal whatsoever. Therefore, the reference denoting the generator speed is missing.

The **Swing Equation of Motion** built-in DSL Model Definition was designed to overcome this issue [22].

```

xp. = (pt - (-1*p)) / Td
speed_gen=lim(xp, 0, 1.2)
inc(xp)=1
inc(speed_gen) =xp
inc(p)=-1
inc(pt)=0

vardef(Td)='p.u.;"Damping Torque Coefficient Based on Power'

```

Figure 4.14.: DSL Model Definition with the Formulas describing the Equation of Motion for the PMSG [22].

Figure 4.14 unveils the equations coded in DSL for obtaining the generator speed. From there it can be seen that if there is a difference between the mechanical power *pt* and the electrical power *p*, the PMSG rotor as a consequence has to accelerate or decelerate [79]. Therefore, the speed derivative *xp.* is the result of this difference. This Block mimicks the behaviour of real rotating synchronous machines, whose rotor decelerates or accelerates with respect to the synchronously rotating air gap Magneto-Motive Force (mmf), when they detect disturbances in the system frequency, thus deriving in relative motion [79].

$$\frac{2H}{\omega_s} \frac{d^2\delta}{dt^2} = P_a = P_m - P_e \quad (4.10)$$

Equation 4.10 shows the **Swing Equation of Motion** [79]. It is a non-linear differential equation of the second order that characterises the rotation of the rotor of any synchronous machine. The exchange of power between the mechanical rotor and the electrical network due to the rotation of the rotor (acceleration and deceleration) is called **Inertial Response** [79].

The mechanical power *pt* input signals was computed from the previous **Shaft** Black Definition, while the electrical power *p* input comes from the measurement instrument stations used in DPF for metering voltage (StaVmea) and current (StaImea) [15], followed by the **d-q Transformation** and the **PQ-Calculator** Block Definitions, whose Slots are indicated in B.1. The parameter T_d is a damping torque coefficient based on power. The name of the output signal that thus serves as reference for the **Shaft**, **Pitch Angle Controller** and **Power Reference (MPPT)** Block Definitions is *speed_gen*. A brief description of the measurement units can be found in the Subsection **Measurement Instruments**.

Size	Pomega_x	Pomega_y
1	0.	0.
2	0.05	0.5
3	0.1	0.6
4	0.18	0.68
5	0.3	0.75
6	0.4	0.79
7	0.5	0.81
8	0.6	0.83
9	0.7	0.9
10	0.8	0.95
11	0.9	1.
12	1.	1.
13	1.	1.1
14	1.	1.2
15	1.	1.3

Table 4.9.: Look-up Table for determining the Maximum Speed based on measured Active Power [22].

-Power Reference (MPPT)

This control loop does a coordinated work with the **Aerodynamic** and the **Pitch Angle Controller** Model Definitions to make sure that the WT operates at its locus of maximum power [39]. The generator speed input signal *speed_gen* is adapted according to the tracking characteristic featured in this loop, which, in turn, is based on frequency, DC voltage and active power measurements located in different locations regarding the WT and the power grid. At the same time, it guarantees that the generator speed limits are not crossed. Further, although it is expected that the generator speed would operate normally at its nominal value, the **MPPT** also has the capability of allow dynamic variations as a response of counteracting disturbances detected in the system, within the preset speed range limits, so that, in any circumstance the turbine/generator speeds do not become too large [78].

Figure B.5 shows the Model Definition of the **MPPT Power Reference**. Because it is desired that the DC voltage is maintained stiff and constant, the measured signal *Udc* is compared to a preset reference *u_pu* based on the nominal DC voltage of the Turbine-Side Converter Station (TSC). Meanwhile, the measured active power *p* input is filtered and its outcome is linked to a look-up table that determines different power reference values linked to a corresponding speed value, represented by the Figures 3.9 and 3.10. Table 4.9 illustrates the two-dimensional look-up table with the characteristics *array_Pomega* in *p*. *u*. The array is based on Figure 3.9 where it can be seen that after going further than the nominal values, there is no more data. The real-time power measurement, therefore, will have a corresponding speed value, which becomes the speed reference of the system (*wref*). Then, the calculated generator speed *speed_gen* is compared to the *wref* reference.

The compared DC voltage and active power output signals enter to different PI controllers with external non-wind up limiters [22]. Both contain the same proportional gain *Kp* parameter but different integral time constants for the DC voltage (*Tp*) and the active power (*Tpp*), the former having a faster parameter than the latter by default. Is in these two PI blocks when an instruction to pick up reactive power is activated in case there is a major disturbance detected in the overall EPS. Figure 4.15 unveils the code behind the reactive power pick-up instruction, for both PI blocks referent to DC voltage and active power. This feature can be considered as an AS for the Second and Third Stages of the BS and NR Processes, when there is a priority of reactive power demand, as clarified in Section 3.3 [22]. Lastly, in this Block Definition there are three additional blocks whose duty is to select the type of operation this controller may adopt for its functions, either DC voltage reference or active power reference/look-up table. The latter option is set by default, along with an active power priority; but if a major disturbance in the system arises, the mode of operation changes to DC voltage with reactive power priority. Before the output signal of the **MPPT** Block Definition is computed, an additional selector sensing frequency further aids to activate the previous logic, otherwise,

```

limits(T)=[0, )
x.=K/T*yi
yo=lim(K*yi+limstate(x,y_min,y_max),y_min,y_max)
inc(gg)=0
gg = select(time()>61,1,0) !200 ! For Reactive Power Pick-Up
!gg = select(time()>30,1,0) ! For Active Power Pick-Up
event (1,gg-0.5, 'name=this variable=xpdc')

x.=(K/T*yi)*fff
yo=lim(K*yi+limstate(x,y_min,y_max),y_min,y_max)

inc(ff)=0
ff = select(time ()>61,1,0) ! For Reactive Power Pick-up
gf = select(time ()>50,1,0)
jj = select(gf,0,1)
fff = select(ff,0,1)
!ff = select((time()>30. and. abs(p)>= p_switch_nor),1,0)
!For No-Grid Connected
!ff = select(time ()>30,1,0) ! For Grid Connected
event (1,ff-0.5, 'name=this dtime=1 variable=xpdc value=0')

```

Figure 4.15.: Look-up Table for determining the Maximum Speed based on measured Active Power [22].

it discards any changes if unnecessary. As a result, the output signal *pref* is obtained [22].

In the last seven Subsections was described the **Aerodynamic/Mechanical Drivetrain** features that extended the WT Model to also consider mechanical and atmospheric factors in the EMT simulations. The signal *pref* now serves as an additional factor that the **DC Model Circuit** Block Definition must consider, because with this extension *pref* now is the speed/power reference value that otherwise the **DC Model Circuit** Block Definition considers static [17], [21].

Clarke-Park (*d-q*) Transformation

Also used in WECS, BESS and HVDC Transmission System Models. In Figure B.1 a Slot with the legend *Park Transformation* can be seen. The Block Definition related to this Slot is a set of equations that apply the SVM Theory described in Section 3.5. The output signals are the result of the transformation of the *d-q* Transformation of the three-phased voltages and currents metered for each WECS unit in the *PST 16 Benchmark System* study case.

Modulation Limitation

Also used in WECS and HVDC Transmission System Models. In the case of uncontrolled behaviour of the current or direct voltage control, the reference voltage of the GSC must be maintained within the maximum allowed modulation level. [18]. The **Modulation Limitation** Block Definition is in charge of that duty. Figure B.10 shows this DSL-modelled control system. The limitation level minds the magnitude of the entire Space Vector *d-q* of the reference voltage and decreases each element individually in accordance with predefined nominal values set in their own Common Model windows [18]. The modulation index is based on the AC/DC converter voltage relationship, shown in Equation 4.11.

$$m_{\text{Nom}} = \frac{2\sqrt{2} V_{\text{AC,Nom}}}{\sqrt{3} V_{\text{DC,Nom}}} \quad (4.11)$$

The limitation is only active when the maximum modulation level is exceeded. In the study case, the modulation index is limited to 1 p. u. to avoid additional nonlinear effects, but up to 1.15 p. u. still performs acceptable [19].

WT Back-to-Back Philosophy in DPF

In earlier stages the topology of the aggregated WF was composed of a *Back-to-Back* philosophy, with each side connected to a series inductor compensator, and the instrument carrying the generation duty was a regular DPF Synchronous Machine Element (ElmSym*). In the configuration of this element, the type of rotor was defined as salient-pole rotor and with a low inertia constant *H*. During most of this research, this topology was the selected standard with which works were done and where the different control systems in the simulations were developed, applied and tested. One of the main arguments to adopt this system was that it totally mimicked the theoretical standard of a *back-to-back* WECS, like the one shown in Figure 4.3a. In turn, the application of that reference can be seen in Figure 4.16. This topology presented both **advantages** and **disadvantages**, which are following enlisted:

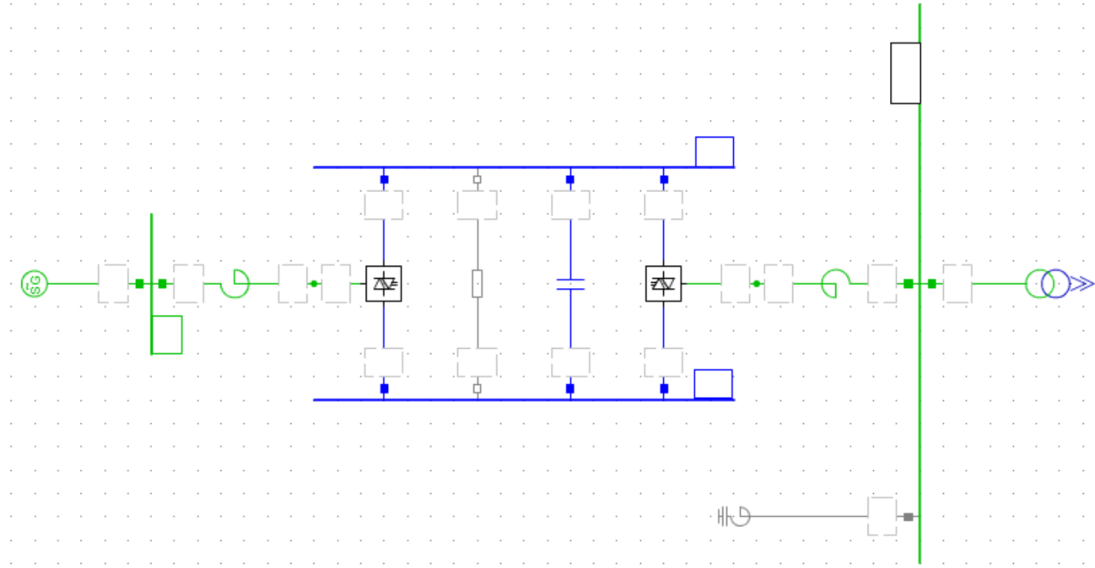


Figure 4.16.: Back-to-Back philosophy with a Salient-Pole Machine as the PMSG.

- Full representation of all the components and control systems that a standard WECS system would be comprised of.
- Accurate Model that does not neglect or assume phenomena.
- Detailed parameter data of a salient-pole Synchronous Machine.
- Because of the (ElmSym*) extension, there is no need of develop a built-in DSL Model for represent the Swing Equation of Motion.
- After several trial-error tests, very good results for steady-state operation.
- Extending the WF model with a *Back-to-Back* topology to the seventeen units in the study case made it extremely inefficient.
- Including more elements to the study case makes it more difficult to control and to mitigate errors.
- Ineffective and slow trial-and-error process during the simulation stages.
- The *back-to-back* architecture required too much computational effort, exceeding the Giga-Byte (GB) capacity of calculation and data storing of the Laptop used for the simulations.
- EMT simulations took too much time to finish an entire run, this is in terms of days.
- After the blackout events during EMT simulations, the study case became even slower.
- A conjoint BS-NR strategy under the extended model turned out to be excessively difficult to achieve with acceptable results.

Having a *back-to-back* philosophy seemed to be an excellent approach to the analysis of this research. However, the *PST 16 Benchmark System* is already a too-large and complex model; extending it implied **consequences** that could not have been detected were it not for running a simulation. The system characteristics of the Laptop Computer where the DPF software licence was installed include an Intel(R) Core(TM) I7-4770HQ CPU processor with 2.20 Giga-Hz (GHz)/2.20 Mega-Hz (MHz) of frequency and a disk with 46 GB available for data storing. A major problem enlisted in the itemised **disadvantages** was that identifying a cause of error in the system became an extremely slow process due to the huge computational effort and time scale required to perform a complete NR with the EMT time-domain option. The time scale of completing a run with all the events required for a NR strategy was in terms of approximately five days, assuming that the laptop computer used for running DPF had enough GB-storing capacity. In Sections 3.1 and 3.3 were discussed major blackouts in recent times, common causes and usual approaches to *restore* outaged EPS. There can be known it usually takes at least one hour to *restore* a seriously outaged large-scale power grid. Therefore, running an EMT simulation in the extended study case with realistic time frames between events, as explained in Section 3.3, in a laptop with the characteristics described was indeed hardly possible.

Yet, despite these results, initially was decided to keep the fully-detailed model and try to improve the study case. Some of the attempts of improvement were speeding up the simulations by tuning the DPF study case and time-domain settings, increasing the time steps, sacrificing accuracy definition, considering smaller matrices during com-

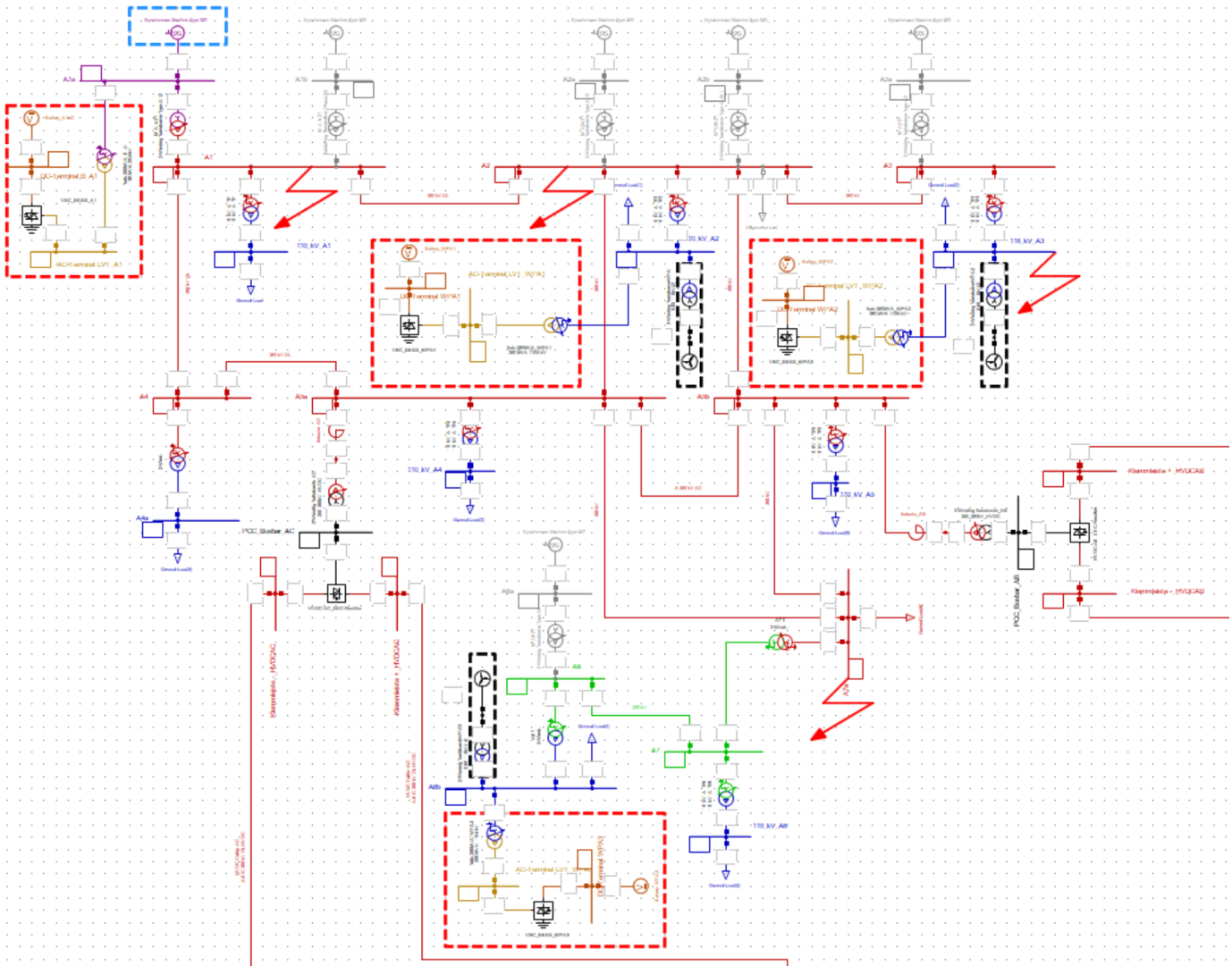


Figure 4.17.: Zoom-in of Zone A.

putation and the avoidance of matrix recalculation after manifested events. Likewise, many DSL Model Definitions were subjects of scrutinised changes. However, the enhanced simulation debugging attempts did not improve the simulation time and in some cases the performance and results went worse. Another approach was to simply move the DPF software licence to a Personal Computer (PC) connected in parallel with other PC to multiply the computation capacity and thus speed up the simulation time. Unfortunately, the DPF software cannot be run in several PC at the same time and if it could, multi-core processors would not have any influence on the performance of the simulations. In this case, the performance of the simulations could only be improved by having a faster core in the processor. Therefore, the last attempt to still use the *back-to-back* configuration onto the *PST 16 Benchmark System* was to just move the DPF software licence to a PC with a large disk for storing massive data and a faster processor. This was successfully done in a PC with 200 GB extra for storing data and with a Intel(R) Core(TM) I7-7700 4-core processor with 3.60 GHz/3600 MHz of frequency. Indeed, when initialising an EMT simulation the speed performance got significantly improved. However, the same effect of the study case becoming slower after the blackout events during EMT simulations ensued as well, but then with a magnified effect. Thereby, simulation tests became even slower than when running in the laptop. On account of these results, the *back-to-back* WT topology was replaced by the ElmGenstat* configuration (Figure 4.8) and all the following tests were carried out with the latter system.

4.5.3 MEASUREMENT, PROTECTION AND RESTORATION LOGIC-RELAYS

Four massive Short-Circuit Faults are predefined to take place in *Area A* (Figure 4.17), located by the red-bolt symbols. Each of the shorts are three-phase-type with $Z_{Fault} = 0 \Omega$. For the protection of the outaged area, a Logic based on

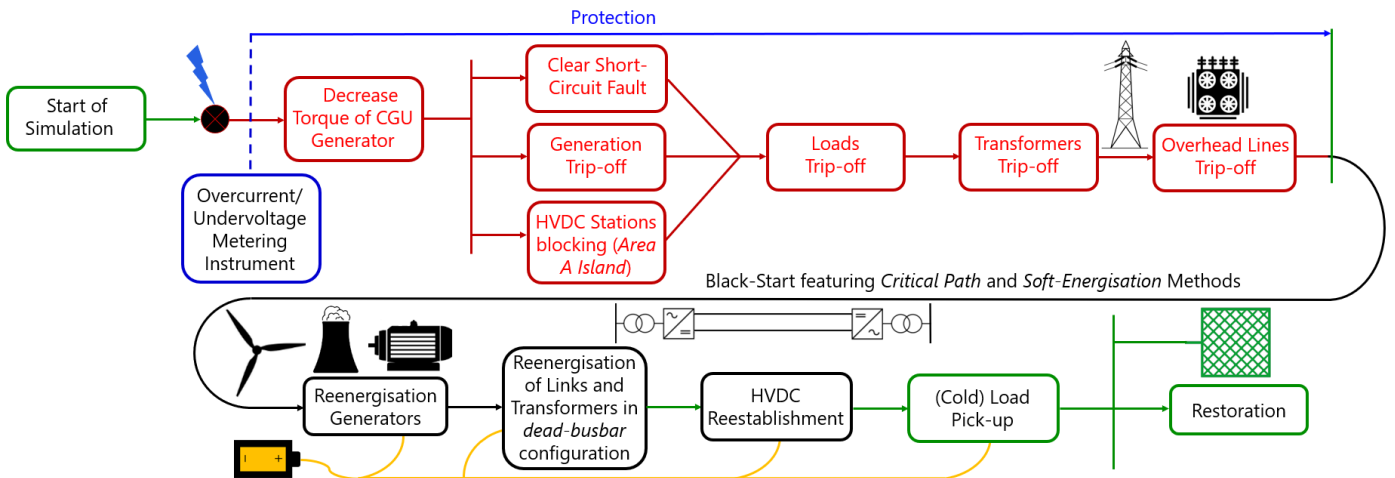


Figure 4.18.: Flowchart describing the Protection and Restoration Scheme [7], [23].

Short-Circuit/Overcurrent Relay Scheme was elaborated. The elements that detect the fault, however, are not the relays themselves. They need a voltage/current measurement station located on the buses where the faults take place (Subsection [Measurement Instruments](#)). These elements are a simplified version of what Potential and Current Transformers do in Electrical Substations, and instantly alert the relay system about the fault. They are the messengers the actuators need for execution.

Once detected, the logic acts with a set of different time delays. Given the magnitude and severity of the faults, not only *Area A*, but in fact, other zones within the whole System could collapse, as it indeed happened during several simulation tests. Therefore, an *isolation* of *Area A* is programmed to prevent damage to spread, blocking the HVDC stations and opening the contacts of their AC-side circuit breakers. The protection of all the power elements in that area was also protected by the same protection scheme, disconnecting all generation units, loads and transmission lines and transformers.

This DSL Model is not only in charge of protecting the network, but also to perform the re-building of the damaged grid, thus performing the conjunct BS-NR according to what was found in [7], [27] and [56]. The starting moment of the BS Plans can be user-modified.

Simulations were executed to assess different *Restoration* paths and times. [Appendix E](#) reveals the logic code that was implemented in the five protection units designed to preserve the integrity of the whole *PST 16 Benchmark System* Network. As stated in [Section 3.3](#), a disclaimer is advocated for discarding external factors and events out of the scope of the software simulations for the *Restoration* time calculation. The external factors embody switching interlocks and circuit breakers manually, energisation of the internal circuitry that reignites non-BS units, SO/utilities manager meetings, the additional time it has to be taken for the coal generation units to heat themselves and further communication between the different parties relevant to the *Black-Start* plans that may increase the duration of this stage [40].

The philosophy behind these protection units is based on the CPM Method described in [Section 3.3](#) [7]. From that logic, an Excel sheet algorithm was created to apply the theoretical steps regarding a BS-NR Associated Strategy. [Table 4.10a](#) exhibits a part of that sheet, paying attention in considering realistic inter-event Δ -times in terms of protection and grid re-structuring. The left-hand side sheet is composed of cells containing different tripping times. Several options were sorted to find the best tripping-time option. The left-hand-side table is, in fact, larger than it appears to be in [Table 4.10a](#); its whole vertical palette is not shown for layout reasons. The right-hand side sheet contains the calculation of the time differences between events; thus the origin where the numbers in the left-hand-side cells come from. Events here could mean tripping on/off circuit breakers, clearing the short-circuit faults, or activate controls for emergency regulation of Governor Systems or their generic equivalents for the RES-based generation units.

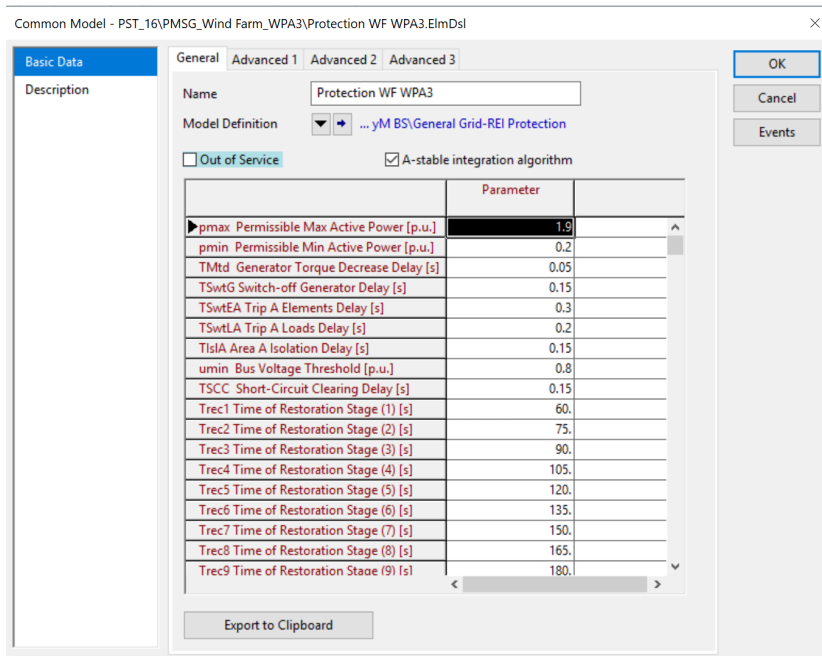
In turn, [Table 4.10b](#) shows a Common Model based on the DSL Protection/Restoration Block Definition. If looking closely, the parameters in that table coincide with the so-called **Option 4**-cell column shown in [Table 4.10a](#). That option of time-event commands were implemented in [Table 4.10b](#).

The **Measurement, Protection and Restoration** DSL Model has two main tasks:

- **Protection.** To safeguard damaged electric circuits after heavy faults, clearing short-circuits and tripping elements for prevent them to damage and/or tripping off zones that otherwise would spread-out imbalance the

Relay Action Times [s]				Adibi CPM		
Option 1	Option 2	Option 3	Option 4		[m]	[s]
1.9	1.9	1.9	1.9	Optimistic Time	0.15	9
0.2	0.2	0.2	0.2	Most Likely Time	1	60
0.05	0.05	0.05	0.05	Pessimistic Time	2	120
0.15	0.15	0.15	0.15	Short-Circuit Fault	1.506667	90.4
0.3	0.3	0.3	0.3			
0.2	0.2	0.2	0.2	Multiplication Factor	4	
0.15	0.15	0.15	0.15	Division Factor	6	
0.8	0.8	0.8	0.8	Time Conversion	60	
0.1	0.1	0.1	0.15	Time Per Event (tc)	1.025	61.5
0.5	60	60.0	60	Time Difference ($\sigma(\pm)$)	0.308333	18.5
1	165	121.5	75.0			
1.5	247.5	183.0	90.0			
2	330	244.5	105.0			
2.5	412.5	306.0	120.0			
3	495	367.5	135.0			
3.5	577.5	429.0	150.0			

(a) CPM Criterion applied to Restoration duration times [7].



(b) Common Model of one Protection/Restoration Block Definition.

Table 4.10.: Protection and Restoration System Model based on CPM [7], [27].

system. In case it is intended to resemble a full-blackout, the circuit breakers of all elements in *Area A* can be tripped off; this includes all generation units, transmission lines, transformers, in addition to the loss-of loads. The tripping delay times used for the circuit breakers action were based on standards according to [27], [40] and [7].

Initially, only four protection systems for the outaged *Area A* were implemented but during the simulation stages it was learnt that the effect of the *Area A* shutdown derived in further havoc in the other two areas, just as it was analysed in Section 3.3 [7], [27], [40], [56]. As a consequence, another fifth relay had to be designed to protect circuits of both *Area B* and *Area C*, fragmenting these areas because they suffered as well dangerous load imbalances. The code of the first four relays is shown in Section E.1, and the one for the fifth relay in Section E.2. These units work in a cross-coordinated way and they do not interfere with each other's activities.

- **Black-Start and Network Restoration.** After the faults are cleared, *Area A* and some zones inside *Area B* and *Area C* are shut down. The second part of this DSL-modelled Block Definition is to *Restore* power as quickly, reliably and safely as possible while minimising the stress on network components. In this stage, several methods were tested based on the order of reconnected paths and elements.

By trial and error, it was discovered that the approach that achieves full grid reconstruction while at the same time preserves the integrity of the system is to first energise transmission lines, cables and transformers, on that

specific order (unless a transformer was a crucial path to continue the reenergisation). Knowing this diagnosis, all involved non-energised network components (overhead lines, cables, and transformers) are first connected to each other via their substations (a so-called dead busbar network configuration) and to a power plant without activated voltage excitation. Once the network is partially *restored*, then the terminal voltages of the BSU are slowly increased from zero to nominal kV according to how many elements are yet to be restored [23]. The slow voltage increment is thought to avoid transformer saturation, and, as a result, all grid components are brought back to gradual energisation and so preventing from transient oscillations, reduction in stress in the network elements and substations [23].

It is remarkable to state that this approach, discovered by experimenting, is, in fact, one successful methodology tested and used in by energy companies; this technique even has a name, which is *Soft Energisation* [23].

Soft Energisation has proven to be reliable, safe and easy to control, because it does not bring stress or high risks of damaging equipment during live tests as the network voltage is recovered slowly. It does not have restrictions in regard to any EPS size, type, location and it works regardless of the involvement of any kind of components. This makes it very suitable if it is desired to do a conjoint BS-NR with a high participation of converter-based generation units; the effect of volatility and fast responses of PEI-based elements can be reduced with this method that, as its name implies, *restore* the grid very softly. For the *Restoration*, small generators can be used to energise a network of any size, while performing *soft energisation* to step-up transformers makes possible to start additional power plants and increase the fault level, thus increasing boundary conditions and hardening the EPS. Further, *soft energisation* is especially suitable for situations with low generation capacity availability [23].

The aforementioned characteristics make it typically successful in the first-time try out (very low chance to follow-up blackouts). This high flexibility and assurance of success are seen as a very competitive advantage in tendering for project managers in charge of the purchase of new equipment because of limited feasibility studies are needed [23].

Of course, this scheme also comes with some points of consideration. In order to implement it successfully, the controls of the circuit breakers involved must allow connection to dead busbars; this means that during the BS and NR stages, UV relays must be deactivated. The *Soft Energisation* Method has a rather slow nature, this means that perhaps more time will be required for *restoring* a large-scale grid. The excitation control of the generation units involved must be capable of slowly and gradually increase the generators terminal voltages from 0 to 100%. All these requirements imply that the generators protection settings probably would have to be reviewed and modified and that special operational actions from the SO (as well as training) would have to be required [23].

Soft Energisation also requires to have independent power supplies for the generator excitation; interestingly, during the simulation stages it was discovered that the WF could not perform the BS stage completely by themselves. This was the main reason to include more storage units that initially considered to the *PST 16 Benchmark System* Network. An illustrative Flowchart describing **Measurement, Protection and Restoration** DSL Model is displayed in **Figure 4.18**.

4.5.4 BESS-STORAGE SYSTEMS

Figure 4.19 shows a diagram that explains the BESS archetype, while **Figure 4.20** depicts the storage units installed in the DPF study grid; all the storage units are enclosed in the **red-dashed** rectangle. Seven BESS models were included in the case study, three of them supply AS to the three outaged WF in the *Area A*, while other two support in a similar fashion the only two CGU machines that are active during all study cases. Lastly, the remaining two give frequency support to the receiving-end converters of the two HVDC transmission systems. The model is based on [13] and has a simplified electrochemical battery model, a charge controller, a reactive power/voltage controller, and a frequency deviation model. The voltage level was modified and stepped-up from 0.9 to 9 kV by connecting more cells in series, according to the electrochemical battery parameters. The frequency deviation controller presents also changes, an additional selector block to prevent the battery from discharge during unnecessary circumstances was added, setting a threshold of ± 0.5 Hz.

Before starting the simulations, these elements were believed to be relatively secondary because, as their contribution for grid stability is remarkably important, they certainly cannot do the BS and NR Strategies themselves, as it otherwise was believed to be possible for the DSL-modified WECS Power Stations. Despite BESS obviously cannot do an EPS *Black-Start* alone, it came to be that neither WF can do that solely; after running a simulation in DPF with the BESS units out of service, it turned out to be that the wind power plants could not crank-up any line, cable,

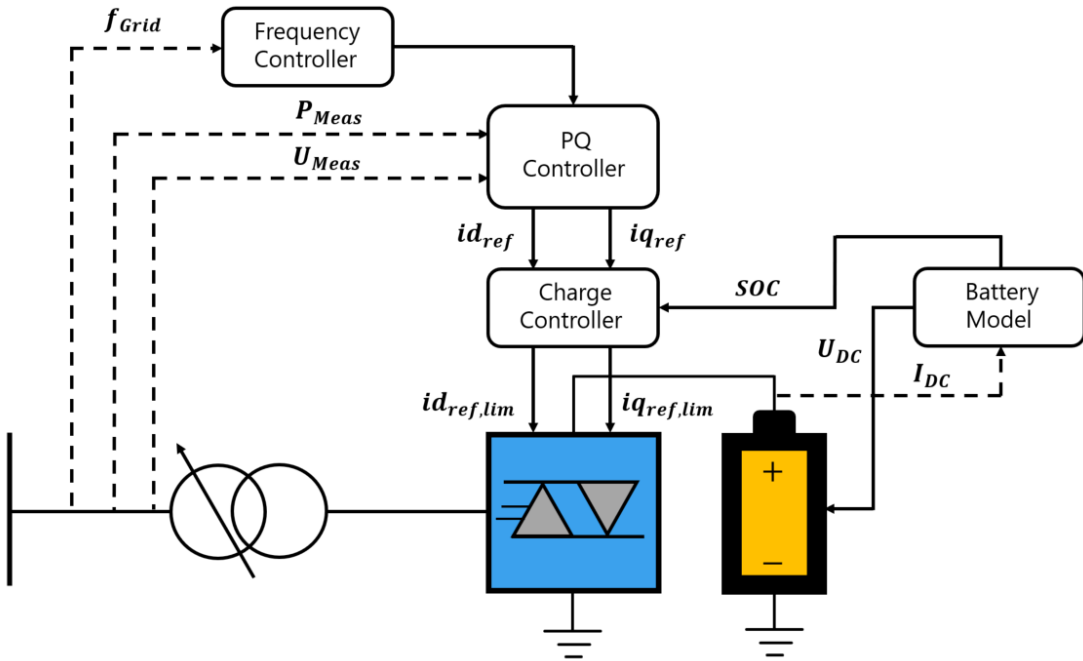


Figure 4.19.: BESS-Storage System Concept [13].

transformer and, even less, any load on their own. It was just after the BESS were activated, and connected in a PCC with the WF busbars, that the WECS could be considered to be BS Units. The result of this simulation was somewhat surprising because it is supposed that PMSG do not require of an external DC source to supply their excitation circuits; yet, in the simulations, only with the auxiliary implementation of the BESS they could *Black-Start*.

The use of open-source DPF templates was done for replicating the BESS Models, as it was stated in Subsection [Use of DPF Template Power Systems](#). The structure and design of these BESS-Battery Units were based on the DPF BESS Application Example Technical Report, whose reference is [13]. Before any modifications to the *Mint-Condition PST 16 Benchmark System* case study were applied, there were no emergency/storage units in the grid. However, compared to the previous model modifications, the author of this MSc Thesis Report did few modifications on the BESS-Battery Models, and most of their Block Definition and Common Models remain without changes with respect from [13]. Therefore, the main contributions from this MSc Thesis Project with regard to the storage units was the successful functional installation of these storage unit templates, which then went through modifications in their following elements:

- **Frequency Controller** Model Definition ([Figure D.4](#)). A selector block was added just before the output signal of this Model Definition in order to prevent the storage units to work under unnecessary situations that did not really required emergency support.
- **Battery** Common Model. Additional battery cells were connected in series in order to increase the battery voltages from 0.9 to 9 kV.
- **BESS** Composite Frame ([Figure D.1](#)). Two additional wired signals were added to the original BESS Composite Frame; the sine and cosine of the angle reference of the BESS PWM converter (signals *sinphi* and *cosphi*).

Battery System

[Figure 4.20](#) shows that the battery appears in DPF in the single line diagram as a DC voltage source. In order to apply the voltage output of the voltage-source battery model ([Figure D.3](#)) to the DC voltage source, a control system for the voltage regulation of the source is required. Therefore, the BESS systems are composed of two Composite Frames. One for the VSC converter interface and another for the voltage control of the battery. [Figure D.2](#) shows the Composite Frame of the battery.

[Figure D.2](#) shows a Block Definition based on the theory discussed in [Section 3.8](#). The Model Definition of the Electrochemical *Li-Ion* Battery just needs the DC current of the Battery; in turn, the Model Definition gives out the outer DC voltage, the SOC and also the DC-voltage cell required for the charge controller [13]. The extension of cells connected in series was done in order in order to make the storage units more bulky in case their non-BS

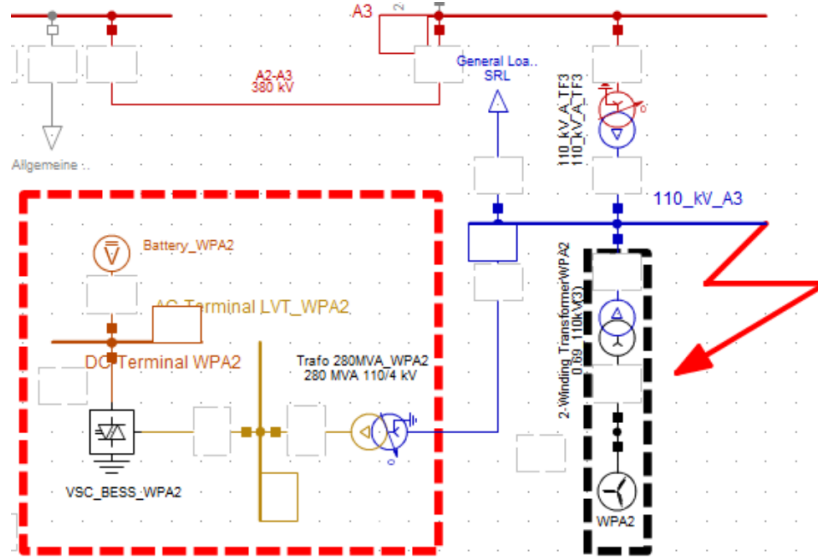


Figure 4.20.: BESS-Storage System.

counterparts may require more energy after an emergency situation (Table 4.11). The Integrator ($1/sT$) that counts the input/output of the battery needs an initial condition (SOC_0). This value is part of the parameters of the Common Model shown in Table 4.11. During the initialisation process, it is assumed that the battery is not being charged or discharged. So, the active power exchange of the BESS is zero for the load flow.

BESS Controller

The IGBT-based controller administers the current dispatch with respect of its d - q components, which could be seen as controlling the BESS in terms of active and reactive power [13], [29]. With the active power output, it is possible to control the frequency of the grid. Similarly, with the reactive power, the voltage can be controlled. The reactive power output of the BESS is not bound to the battery capacity, so the AC voltage could be controlled continuously [13].

For the success of the operation of the BESS, some boundary conditions have to be imposed [13]:

- The storage systems only can consume active power if their battery is not fully loaded ($SOC < 1$).
- The storage systems only can always supply active power unless its battery is fully depleted ($SOC > 1$).
- The battery should be automatically recharged if its SOC has reached a certain lower limit. With this characteristic, the BESS has always the ability to control the active power in both ways.
- The total output of active and reactive power must not be greater than the complex rated power. Therefore, a priority is needed for active or reactive power.

The structure that conforms the BESS Composite Frame includes a **Frequency Controller** (Figure 4.7), **Voltage/Power Controller** (Figure D.6) and a **Charge Controller** (Figure D.5); with these Model Definitions the former conditions can be fulfilled. In real applications, the SOC has to be calculated from the battery current and voltage. With the DSL Model, this can be mimicked along with help of the adequate measurement instruments.

-Charge Controller

The **Charge Controller** Block Definition (Figure D.5) consist of a charging logic that fulfils the SOC boundary conditions $SOC_{min} \leq SOC \leq SOC_{MAX}$ and a current limiter that limits the absolute value of the current order according to the limits $I_{min} \leq i \leq I_{MAX}$ [14]. The signal Δi is the difference of the reference d -axis current from the **Voltage/Power Controller** ($i_{d,p}^*$) and the modified d -current from the charging logic ($i_{d,s}^*$) [13], [14]. The d -axis current has always a higher priority than the q -axis current. The feedback of that signal to the **Voltage/Power Controller** prevents a wind-up of the PI controller.

-Voltage/Power Controller

The **Voltage/Power Controller** (Figure D.5) Block Definition has a slow current controller for setpoint tracking and a slope with a deadband for proportional voltage support [13], [14]. Their input signals are compared with references

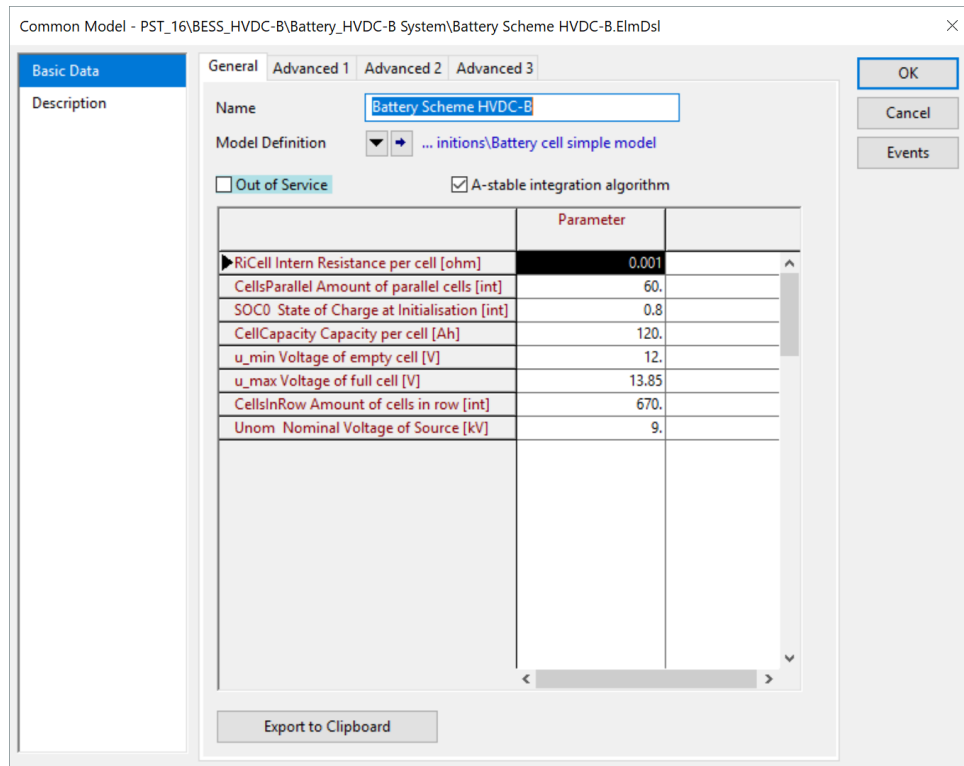


Table 4.11.: BESS-Storage System Common Model.

and their resulting deviations are filtered with a First-Order Polynomial Delay Filter (PT1) that serves as a low-pass filter. Then, PI controllers are used to regulate the d - q elements [13].

-Frequency Deviation Controller

The **Frequency Deviation Controller** is shown in Figure D.4. During a system frequency disturbance is read by a PLL, a correspondent change in active power from the BESS is activated. This is done with an Integrator consisting of a droop characteristic that defines how much active power is released (or sucked). If, for instance, the droop gain K is set to be $K=0.04$, then the BESS active power is activated if the frequency deviation is greater than 2 Hz (for a 50 Hz system) [13].

The command variable fo is fixed to the variable frq with the command $inc(fo)=frq$. The block named as *Offset* is used to compensate the Block Definition output $dpref$ if that value does not equal to zero after a load flow; this is done because the previous signal p_order_frequ is always zero after initialisation [13].

During the simulations it was found that this controller was more sensitive to the frequency deviations than expected (and that desired), to the extent that underfrequencies of 49.9 Hz were enough for the controller to be activated and start dispatching active power, when in reality was not necessary and the BESS had been discharged worthlessly. To mitigate that effect, a block was added working as a selector that limits a predefined frequency threshold that, if not overcrossed, then it prevents the **Frequency Deviation Controller** to dispatch (or sink) active power when there is no real emergency need to be discharged, or to absorb power when it is already fully charged.

4.5.5 HVDC TRANSMISSION

Two rather sophisticated HVDC transmission systems with VSC-MMC models and ± 380 kV submarine cables were included in the case study as a replacement of the simplified sending-end converter models. The HVDC station control model includes the following blocks: p - q , v , i and ϕ measurement stations for both AC and DC (Subsection **Measurement Instruments**), a voltage/frequency controller that enables the station to operate in *Islanded Mode*, an active power controller, a reactive power controller, a synthetic inertia emulator, an active-power output control depending on frequency (frequency sensitive mode), a power oscillation damper, standardised current limiters and controllers, a fault-ride through scheme, a modulation calculator, and a local-remote signal calculator and protection

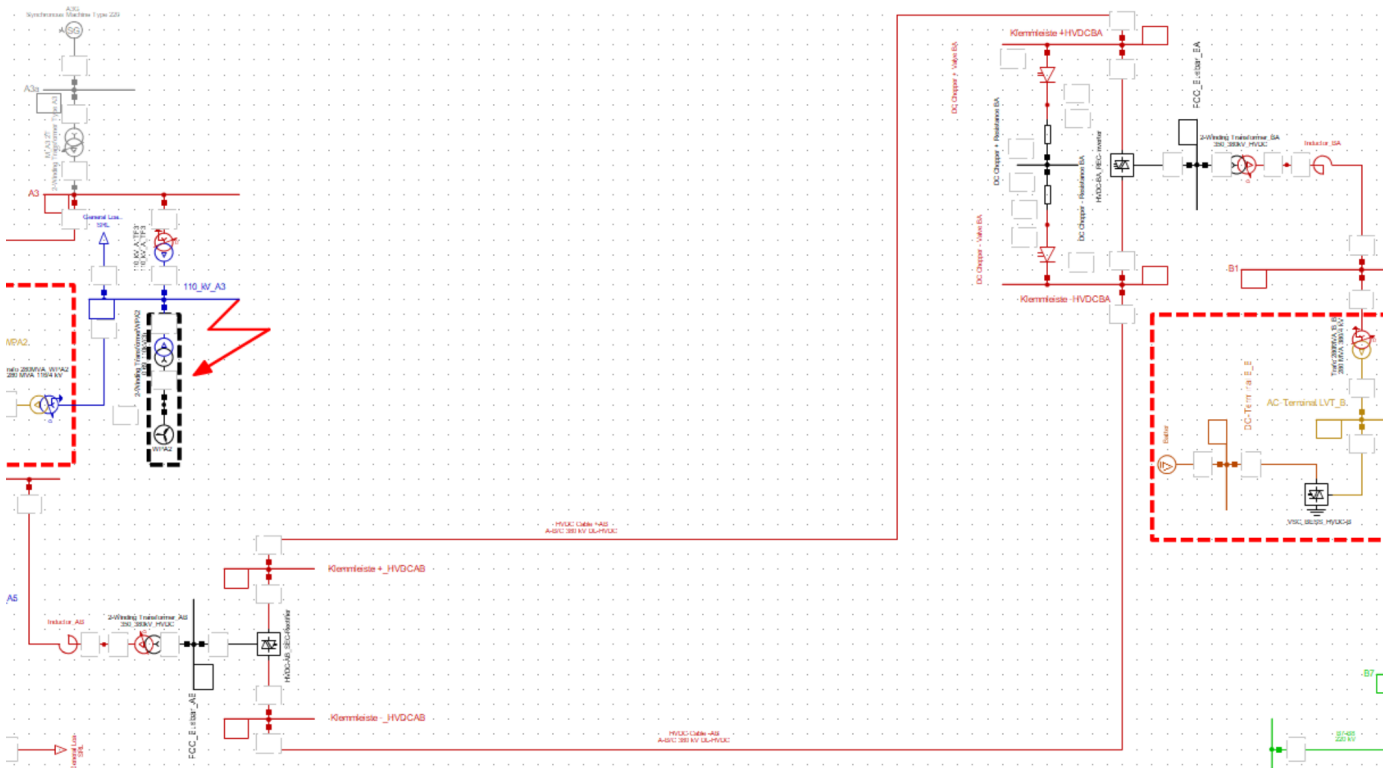


Figure 4.21.: MMC-HVDC Transmission System that interconnects *Zone A* with *Zone B* [8].

block, all of which correspond to the offshore and onshore converter stations. It also includes available slots to declare the circuit breakers that could be employed for the protection of the HVDC system. Further, the *receiving-end* inverters have a protection scheme for network faults containing overcurrents and/or overvoltages. In such a scenario, all IGBT are blocked but the current can still flow through anti-parallel diodes, while the excessive power can be dissipated with chopper inductances.

An MMC-HVDC Transmission System can be seen in Figure 4.21. This Illustration depicts the HVDC Link that interconnects *Area A* with *Area B* in the *PST 16 Benchmark System*. VSC does not impose restrictions on the direction of the current, so the direction of the power flow can be changed without the necessity to reverse the polarity of the voltage. The equivalent circuit shows that when the VSC technology is employed, the magnitude of the controllable voltage source can be changed. It is also necessary that the polarity of the voltage is constant [24].

In two terminal schemes, it is common for one drive converter to operate in DC voltage regulation mode (slack bus) and for another drive to operate in power control mode, as shown in [Figure 4.22](#), represented by the constant voltage line, in black, and the two different constant power modes, in red. Unlike LCC, there is no restriction on which terminal supplies voltage or power control. Therefore, the system can be designed to fit the AC systems (power control at the drive on the weaker side of the AC system).

However, the DC voltage controlling station (slack bus) is preferably connected to the strongest AC system side, to limit the impact on the AC system.

The use of open-source DPF templates was done for replicating the HVDC Transmission Models, as it was stated in Subsection [Use of DPF Template Power Systems](#). The design of this complex control system was based on the CIGRÉ Technical Report No. 604 [30]. In turn, the MMC-HVDC model was provided by DIgSILENT GmbH during a seminar on HVDC and FACTS [8]. The two HVDC Systems installed in the *PST 16 Benchmark System* Network are therefore replicas based entirely on the former reference. The models were only installed in the case study without going through exhaustive modifications in any of their control systems. The inclusion of these sophisticated HVDC Transmission Systems has the sole objective of assessing the dynamic performance of the grid considering components of this kind that will inevitably take part of the EPSF.

Just like the WECS, the VSC-HVDC Stations are also characterised with a reactive power *Capability Curve*, defining their capacity limits. However, as these converter stations possess the modality to let flow power bidirec-

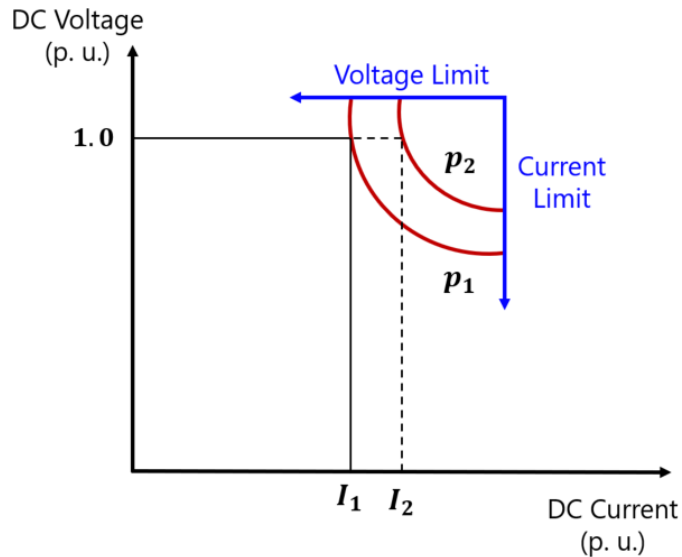


Figure 4.22.: V - I Characteristic for a VSC operating in active power control mode [24].

tionally, they use a four-quadrant curve that allows them to do so. The four-quadrant capability curve is shown in Table 4.12.

Compulsory use of Frequency Measurement

The system frequency is one of the most important parameters that this Composite Frame needs in order to work; this is because all the Control Model Definitions that belong to this Composite Frame depend on the real-time measurement of frequency. e. g., in case of excessive power transportation (because some transmission lines went disconnected), then the excessive power has nowhere to go. Consequently, this will bring both overfrequencies and underfrequencies in different areas of the damaged grid, and fragmentation. In turn, this system can quickly reduce the production of power, mitigating undesirable effects.

The entire VSC-HVDC System is based on inquiry in the frequency domain for analysis of harmonics and small-signal stability. Figure 4.23 presents a Norton-Equivalent Circuit representing the VSC controller forming a closed-loop with the EPS impedance with other controllers [8]. According to the unit circle shown, instability occurs if **Nyquist Criterion** is not met. Moreover, if stability is given, but with small (insufficient) margin, harmonics at the near to frequency intersection with the unit circle can become too high.

However, in order for the MMC-HVDC Stations to have BS capability, not only a reference of frequency has to be at all times maintained but also the offshore rectifier station at all times needs to preserve a constant DC voltage in its DC \pm terminals; and, as was explained in Section 4.5.2, this can be achieved by stop injecting current if there is no reciprocal demanding loads connected to the grid anymore [24].

Figure C.1 shows the Composite Model behind the two HVDC-MMC Transmission Systems installed in the *PST 16 Benchmark System*. Its main control loops described in the following Subsections work principally according to Δ -frequency deviation measurements. Further, in Section 3.6 can be found a theoretical explanation of the use and functions of these HVDC control systems.

-Active/Reactive Power Controllers

VSC converters can control the power injected in the DC lines through voltage magnitude and the control of the voltage angle in EPS. The parameters of the EPS are established by the configuration of the external network, while the AC voltage magnitude and phase of the drive can be completely controlled [24]. The control of the converter in relation to the grid permits a controlled voltage drop in the total reactance (reactance of the valve plus the leakage reactance of the converter transformer) to define the reactive current through the converter. The controller provides current reference commands to accomplish the appropriate control modes; the measured currents are controlled to match these orders.

The **Active Power Control** Model Definition (Figure C.2) has as a main objective to transmit power through the DC link. Figure C.3 shows the Model Definition of the **Reactive Power Control**. The reactive power control is achieved

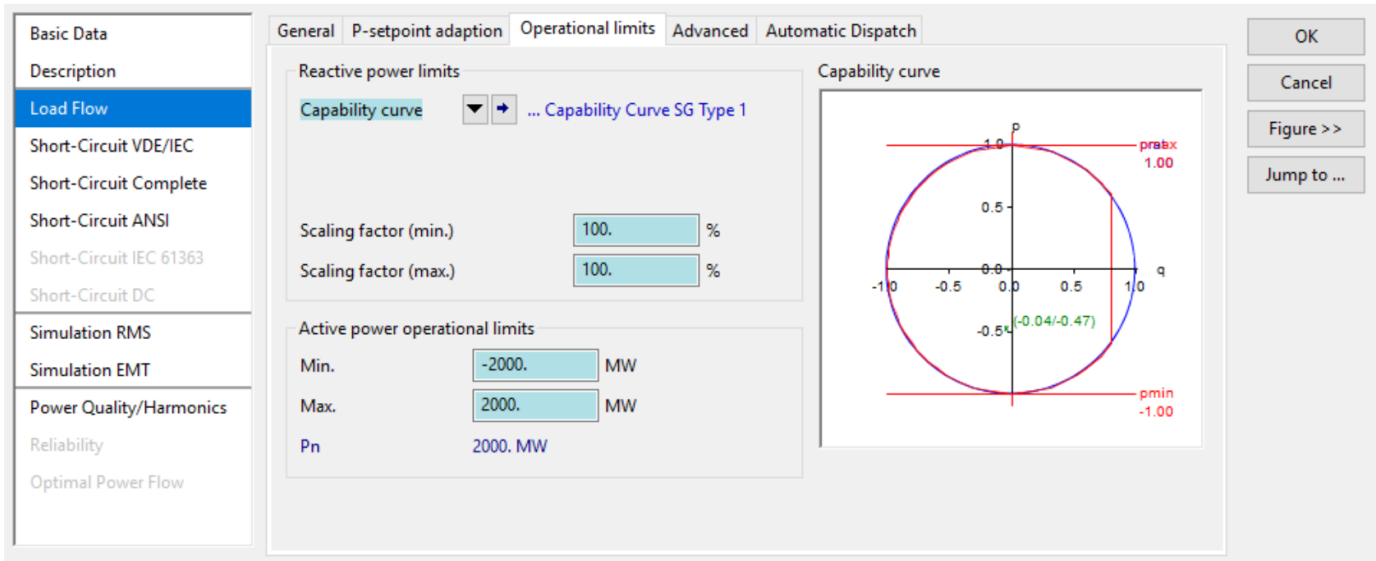


Table 4.12.: Four-Quadrant Capability Curve for all the HVDC Stations.

via the control output reactive power on each station. The $d-q$ reference currents $i_{d,1}$ and $i_{q,1}$ are produced by these two control loops, respectively. The active power loop can be configured to control either the DC voltage or the active power, provided that the grid is sufficiently strong. The reactive power loop, in turn, can be selected to regulate either the AC voltage or the reactive power at the PCC. These controllers are the default priority mode of operation; that is, under normal operating conditions.

The **Reactive Power Control** Model Definition has an additional mode of operation, which is with power factor control. In case this option is to be selected, a desired power factor setpoint can be specified. The relation between the measured active power and its relation with the trigonometric function $\tan \phi$ results in the desired reactive power, which fulfils the desired power factor [30].

-Emergency Power Control (EPC)

The code of the **Emergency Power Control** Block Definition is disclosed in Figure C.8. This model quickly restores control power by the TSO. EPC provides with a fast rate of change possible to respond to fast power deviations on the EPS. A higher degree of accuracy is needed in these situations; then it cannot be assumed that the entire system is operating within its limits.

The HVDC Links can assist the *PST 16 Benchmark System* to recover from a critical perturbation by rapidly increasing or decreasing the power transferred through it, or even to change the power flow direction by means of the power signal Δ_{EPC} . In case there is an emergency caused by a severe disturbance, which could be a loss of a transmission line, loss of a generator or loss of a major load, an appropriate power adjustment signal is sent to HVDC power control to compensate the loss.

The HVDC interconnection can be programmed to respond in a predefined manner and the mode of operation changes to EPC-Mode. This could be an increase or decrease in power through the HVDC link and/or a change of control modes following a generator or transmission line outage [8], [24]. This function helps maintaining the EPS stability and limit the disturbance to spread over a wider area.

-Synthetic Inertia

During a system frequency disturbance, the balance in the generation/demand relationship is lost, and so the system frequency would change at a rate initially determined by the total system inertia H_T [14]. For counteracting that situation, converter-based generation connected to the EPS utilising fully-rated power converters can provide with very-fast frequency response. In industry, this is known as *Artificial or Synthetic Inertia Emulation*. This concept can be applied to RES-based generation, BESS, HVDC transmission and all systems that use VSC as PEI to connect to the grid. In the case of the HVDC transmission, this control loop allows dispatching power bidirectionally producing an additional power in the form of inertial power [14].

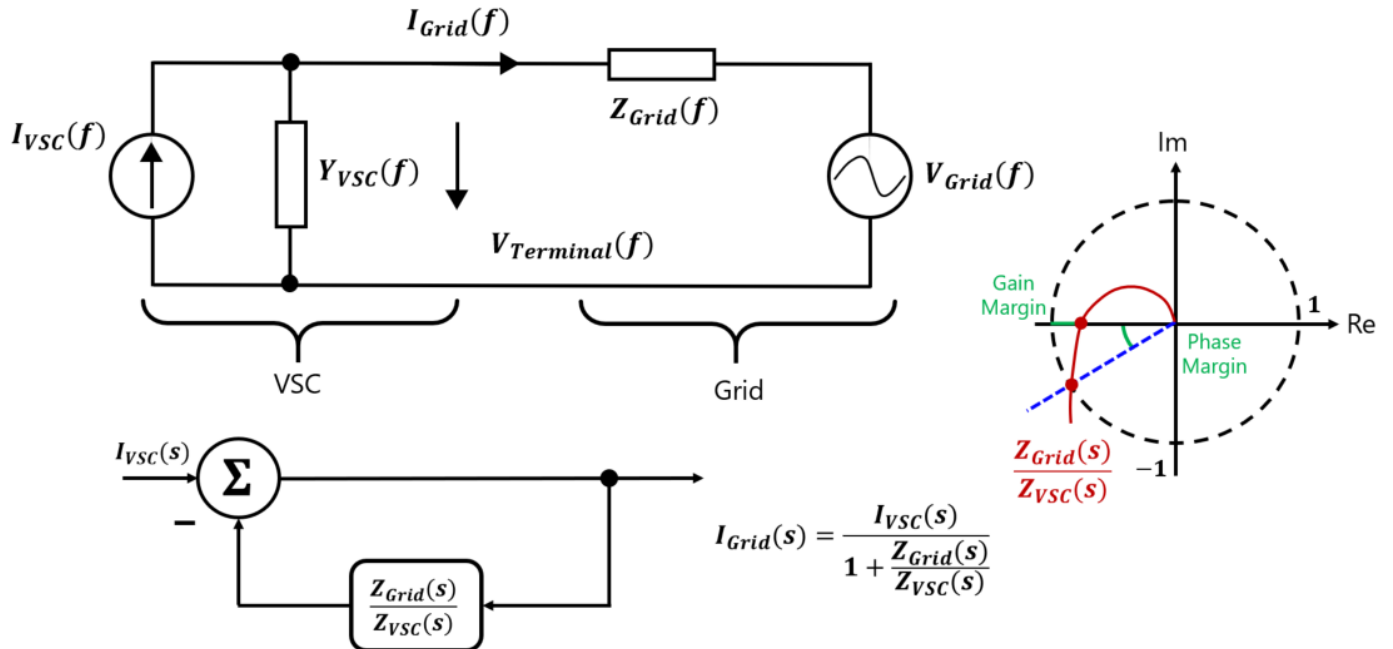


Figure 4.23.: Frequency Analysis according to Nyquist Criterion [8].

The **Synthetic Inertia** Model Definition can be seen as a simple loop that increases the electric power output of the PEI during the initial stages of a significant downward frequency event [14]. It can be calculated as an equivalent of the Swing Equation, as seen in [Section 4.5.2](#)

$$\Delta P = 2fH_{\text{syn}} = \frac{df}{dt} \quad (4.12)$$

[Equation 4.12](#) shows the Equation behind the **Synthetic Inertia** Model Definition, where H_{syn} is the value of the synthetic inertia in seconds, and f the frequency in p. u. [14]. The **Synthetic Inertia** Model Definition works according to the active power output. A frequency derivative signal determines if this block is required to perform in case significant loss-of-load detection occurs.

-Frequency Sensitive Mode (FSM)

The **Frequency Sensitive Mode** Block Definition is unveiled in [Figure C.5](#). **FSM** is the operating mode of a power-generating module or HVDC system in which the active power output changes in response to a change in system frequency, in such a way that it assists with the recovery to target frequency [80]. In the event of a frequency step response, the MMC converters should carefully manage overshoot and damping of the response aiming at avoiding unnecessary active power oscillations.

If the **FSM** Block Definition is active, the HVDC system can be capable of responding to frequency deviations in each connected AC network by adjusting the active power transmission in accordance with the parameters specified by each TSO. Further, the adjustment of active power frequency response shall be limited by the minimum HVDC active power transmission capacity and maximum HVDC active power transmission capacity of the HVDC system (in each direction).

The **Frequency Sensitive Mode** Block Definition controls the active power output with regard to the power/frequency relation (power up/down). The activation of this control loop allows enhanced low-frequency sensitivity metering.

-Power Oscillation Damping (POD)

This Model Definition performs an active modulation of active/reactive power in order to counteract and damp oscillations. The power transferred through an HVDC link can be automatically modulated in the range of 0.8 to 5 Hz to damp the low-frequency power oscillations within one or both of the interconnected AC systems.

Significant damping of power system oscillations can be attained when the active power at the end of transmission lines is modulated, especially in the situation in which the transmission line is interconnecting two areas that oscillate against each other [81]. The point is that the modulated active power of the converter stations at the end of the HVDC lines could accelerate (or decelerate) local generation, which contributes to a network damping effect on the power

system. Also, the generators on the remote system are only slightly affected [81]. The **Power Oscillation Damping** Block Definition (Figure C.6) was thought to damp the existing oscillations in certain frequency ranges and also damping oscillations in multiplied quantities. The **Active/Reactive Power Control** Loops assist to this element.

-Fault-Ride Through (FRT)

The **Fault-Ride Through** Block Definition is unveiled in Figure C.7. It is important that the system be able to diagnose voltage imbalances and decide on an adequate injection of negative components in the case of asymmetric faults. Similarly, rapid detection of voltage imbalances in the network and subsequent injection of the negative sequence is desirable during asymmetric faults.

The FRT capability of DC interconnectors becomes one of the backbone prerequisites to ensure the safe operation of interconnected *island* systems, especially in cases where the HVDC station is comprised of the primary supply source, which can also operate in parallel with additional sources.

The FRT Block Definition ensures proper control of power exchange (active and reactive), DC voltage regulation and AC (voltage and frequency) characteristics in applications such as OffWF. In addition, TSO demand injection of reactive current in case of voltage deviation. Whenever there are several faults in the EPS, this controller injects reactive current for counteracting the low-voltage condition situation at the VSC terminals. The positive-sequence reactive current is proportional to the voltage drop to support the positive-sequence voltage recovery. On the other hand, the negative-sequence reactive current is proportional to the negative-sequence voltage.

This Model Definition provides dynamic voltage support during faults. It has the ability to provide additional reactive current during low-voltage FRT to support the EPS. Therefore, the control system makes the HVDC stations stay connected to the network in defiance of the faults that result from low voltages. This scheme has been arranged to respond faster than the **Active/Reactive Power Control** Loops.

-Voltage/Frequency Control

An VSC-HVDC scheme can control the frequency of an AC system if it interconnects at least two asynchronous systems by automatically adjusting the power being delivered into or out of that grid experiencing under frequency/overfrequency, in order to balance the load with the supply [8], [24]. This could be particularly applicable for a small EPS such as an *island* which is susceptible to under/over frequencies. However, it should be noted that the frequency control capability is limited by the active power rating of the link [24].

Figure C.4 shows the **Voltage/Frequency Controller** Model Definition with *grid-forming* capability. With this element, the conjoint BS-NR Strategy is possible with the MMC-HVDC Stations. In case of an *island* operation, where part of the grid is completely isolated, this control loop can generate its own frequency reference by means of an oscillator (also with help of the **FSM** Control Loop) that mirrors the frequency in the onshore system to the offshore counterpart.

4.5.6 MEASUREMENT INSTRUMENTS

Used in all System Models. In DPF can be found default instruments that represent metering stations that can be used for RMS or EMT simulations [15]. They can be used as many as desired. In order for the overall **Composite Frame** System to receive their measured signals, they need to be wired up with their correspondent Slots located inside the aforementioned **Composite Frame** Systems. The measurements work for both DC/AC systems. The available types of measurement stations are [15]:

- **Voltage Measurement Instrument (StaVmea).** In order to work, the need to be connected with a busbar.
- **Phase Measurement Instrument (ElmPhi_pll).** DPF has default models that perform the duty of a PLL. In order to work, the need to be connected with a busbar.
- **Current Measurement Instrument (StaImea).** In order to work, the need to be connected with a cubicle that takes part of a busbar.
- **Active/Reactive Power Measurement Instrument (StaPqmea).** In order to work, the need to be connected with a cubicle that takes part of a busbar.

5

RESULTS/PERFORMANCE EVALUATION

A total of six simulation tests were made as much as to verify the correct functioning of the network's load flows, *grid-forming* control, protection and *restoration* systems for both the *base* operational case and the and the operational scenario with 90% wind penetration. The Sections that contain each of the six tests are enumerated below:

1. **PST 16 Benchmark System Network (100% CGU) Load Flow Analysis**
2. **PST 16 Benchmark System Network (100% CGU) EMT Outage followed by Restoration**
3. **Test of Individual Wind Farm with the Grid-Forming Control Systems**
4. **PST 16 Benchmark System Network (90% WF) Load Flow Analysis**
5. **PST 16 Benchmark System Network (90% WF) EMT Outage followed by Restoration with Optimum Wind**
6. **PST 16 Benchmark System Network (90% WF) EMT Outage followed by Restoration with Low Wind**

5.1 PST 16 BENCHMARK SYSTEM NETWORK (100% CGU) LOAD FLOW ANALYSIS

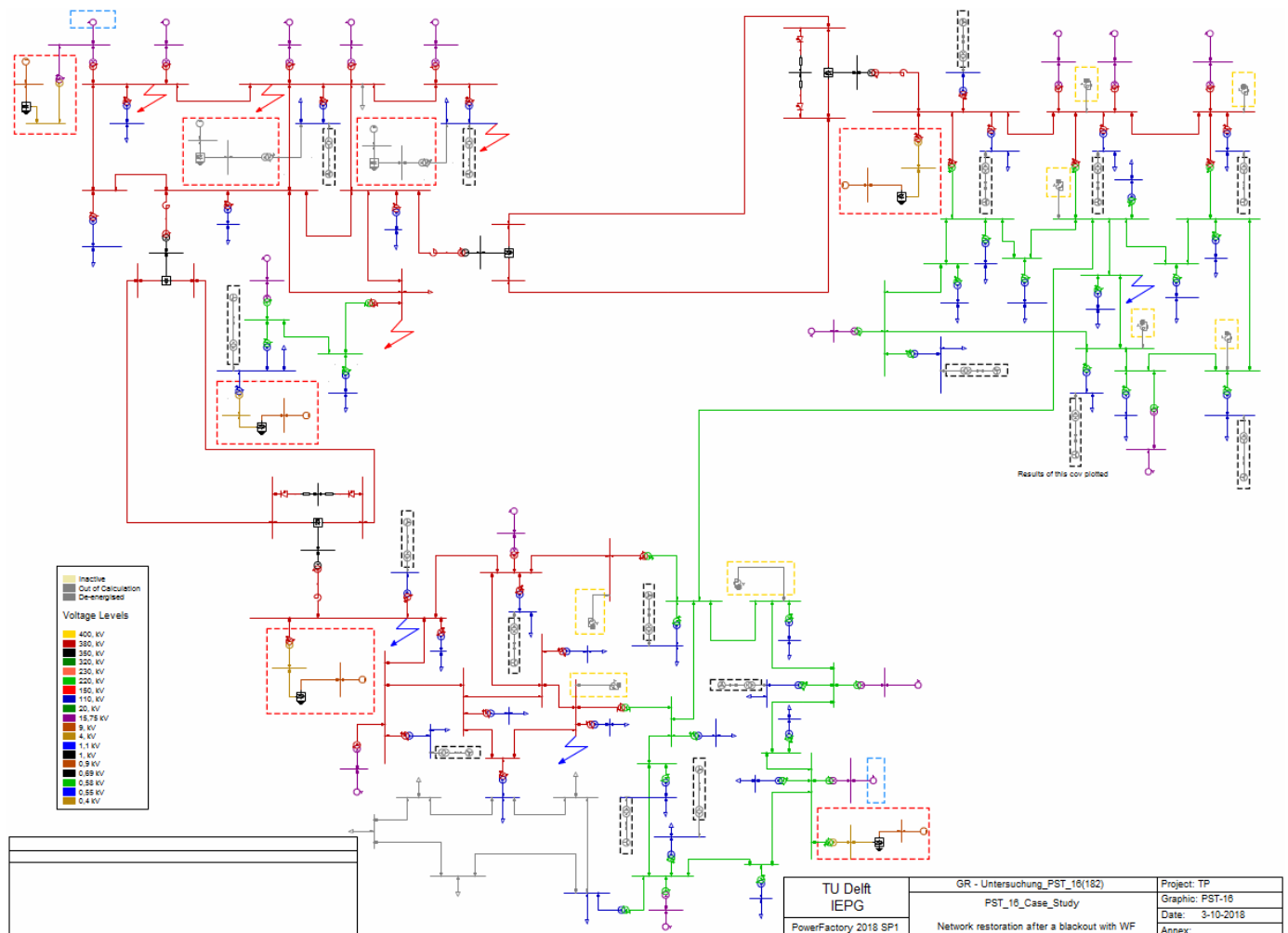


Figure 5.1.: PST 16 Benchmark System case overview with 100% CGU Active.

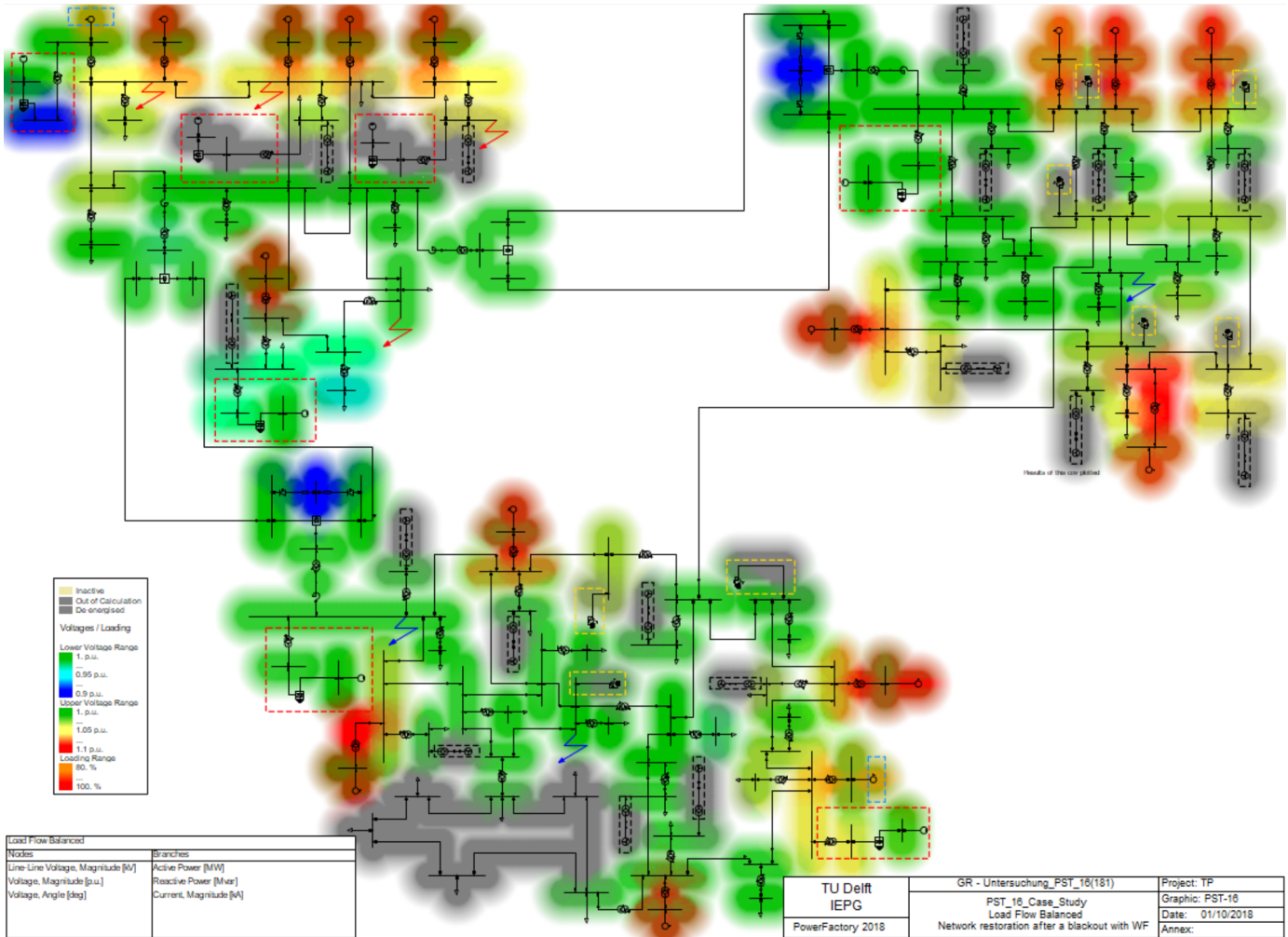


Figure 5.2.: Load Flow Analysis applied to the 100% CGU PST 16 Benchmark System Network.

Load Flow Studies are probably the most common of all power system analysis calculations. They are used in planning studies to determine if and when specific elements will become overloaded. In operating studies, Load Flow Analysis is used to ensure that each generator runs at the optimum operating point; demand will be met without overloading facilities. The information that a Load Flow Analysis provides is:

- **Voltage Magnitude and Phase Angle at each bus.**
- **Active and reactive power flowing in each element.**
- **Reactive power loading on each generator.**

The *PST 16 Benchmark System EPS*, on its *Base Case Scenario (100% CGU)* is presented in [Figure 5.1](#). It can be seen that the all the CGU units are active. In this Load Flow Analysis ([Figure 5.2](#)), busbars are coloured in regard of the voltage level they hold. If their voltage levels are at 1 p. u., the glow around them is **green**. With the same logic, undervoltages are denoted by cold colours and overvoltages by hot colours. The rest of the elements are only coloured if they are operating from 80% loading and onwards, the higher the loading, the **reddish** colour. **Gray** denotes an element out of service or inactive. Otherwise, no colour is assigned.

Usually, in EPS is admissible to measure the generation units loading close to their nominal values, though is not the same case for transformers and busbars to be overloaded, which are recommended to avoid them reach that point. For this case study, the network holds a healthy shape, with their generation units working close to nominal values and all its loads and elements absorbing adequate quantities of active and reactive power.

The executed Load Flow Analysis was a balanced-positive sequence type. Automatic tap adjustments for transformers was disabled, but reactive power limits and the automatic model adaptation for convergences was enabled. There is no real danger or warnings in this EPS; as it can be seen in the DPF Output Window via [Table 5.1](#), there are no warning messages while the Newton-Raphson Program converged relatively fast with nine iterations, despite the large structure of this grid. Further, none of the elements go beyond 100% loading.

Error (0)	Warning (0)	Info (49)	Event (0)	Other (52)	Contained text			
Element 'AlaG' is local reference in separated area of ' Cub_1 ' Element 'B3G' is local reference in separated area of ' B3a ' Element 'HVDC-BA REC-Inverter' is local reference in separated area of ' Klemmleiste +HVDCBA ' Element 'HVDC-CA REC-Inverter' is local reference in separated area of ' Klemmleiste +HVDCCA ' Grid split into 9 isolated areas Calculating load flow...								
<hr/>								
Start Newton-Raphson Algorithm... Step 1 / 3: Scaling total load demand with factor 5.774e-01... Iteration 0: Klemmleiste +_HVDCAC 9.35e+04 HVDC-AC_SEC-Rectifier 8.78e+02 Iteration 1: Klemmleiste +_HVDCAC 5.00e+04 C2G 1.5e+03, Relax factors: (Max. Step: 4.65e-01, Linesearch: 1.00e+00) Iteration 2: Klemmleiste +_HVDCAC 4.82e+04 C7G 2.15e+03, Relax factors: (Max. Step: 3.60e-02, Linesearch: 1.00e+00) Iteration 3: 110_KV_C13 9.46e+01 HVDC-CA REC-Inverter 1.23e+03, Relax factors: (Max. Step: 1.00e+00, Linesearch: 1.00e+00) Iteration 4: 110_KV_C1 9.51e+01 HVDC-CA REC-Inverter 5.55e+02, Relax factors: (Max. Step: 1.00e+00, Linesearch: 1.00e+00) Newton-Raphson converged with 4 iterations. Step 2 / 3: Scaling total load demand with factor 8.165e-01... Iteration 0: 110_KV_B12 1.38e+02 HVDC-CA REC-Inverter 6.12e+02 Iteration 1: 110_KV_B12 1.24e+02 HVDC-CA REC-Inverter 5.46e+02, Relax factors: (Max. Step: 6.97e-01, Linesearch: 1.43e-01) Newton-Raphson converged with 1 iterations. Step 3 / 3: Scaling total load demand with factor 1.000e+00... Iteration 0: 110_KV_B10 2.41e+02 HVDC-AC_SEC-Rectifier 6.07e+02 Iteration 1: 110_KV_B10 2.30e+02 HVDC-AC_SEC-Rectifier 5.86e+02, Relax factors: (Max. Step: 2.61e-01, Linesearch: 1.29e-01) Iteration 2: 110_KV_B12 2.13e+02 HVDC-AC_SEC-Rectifier 5.49e+02, Relax factors: (Max. Step: 4.32e-01, Linesearch: 1.47e-01) Iteration 3: 110_KV_B12 2.08e+02 HVDC-AC_SEC-Rectifier 5.38e+02, Relax factors: (Max. Step: 1.94e-01, Linesearch: 1.00e-01) Iteration 4: 110_KV_C1 1.09e+02 HVDC-CA REC-Inverter 7.33e+02, Relax factors: (Max. Step: 1.00e+00, Linesearch: 1.00e+00) Iteration 5: 110_KV_C1 7.22e+01 HVDC-CA REC-Inverter 5.12e+02, Relax factors: (Max. Step: 1.00e+00, Linesearch: 2.99e-01) Iteration 6: 110_KV_C2 2.06e+01 HVDC-CA REC-Inverter 1.12e+02, Relax factors: (Max. Step: 1.00e+00, Linesearch: 1.00e+00) Iteration 7: 110_KV_C13 1.13e+01 C2G 2.88e+01, Relax factors: (Max. Step: 1.00e+00, Linesearch: 1.00e+00) Iteration 8: 110_KV_C13 4.96e-02 C7G 1.07e-01, Relax factors: (Max. Step: 1.00e+00, Linesearch: 1.00e+00) Iteration 9: 110_KV_C13 2.41e-04 C7G 4.54e-04, Relax factors: (Max. Step: 1.00e+00, Linesearch: 1.00e+00) Newton-Raphson converged with 9 iterations. Load flow calculation successful.								
<hr/>								
Report of Control Condition for Relevant Controllers								
<hr/>								
Control conditions for all controllers of interest are fulfilled.								
<hr/>								
Load Flow Calculation								
<hr/>								
AC Load Flow, balanced, positive sequence Automatic tap adjustment of transformers No Consider reactive power limits Yes Max. Loading of Edge Element 90.00 % Automatic Model Adaptation for Convergence Yes Lower Limit of Allowed Voltage 0.90 p.u. Upper Limit of Allowed Voltage 1.10 p.u.								
<hr/>								
DIGSILENT Project: PowerFactory ----- 2018 Date: 04/10/2018								
<hr/>								
Study Case: PST_16_Case_Study Annex: / 1								
<hr/>								
Name	Type	Loading [%]	Voltage [p.u.]	Voltage [kV]	Station/Branch	Apparent Power [MVA]	Current [kA]	Current [p.u.]
<hr/>								
Overloaded Elements								
M_A2a 2T	Tr2	90.52		A2		1077.08	1.57	0.90
				A2a		1116.78	40.94	0.91
M_A2b 2T	Tr2	90.52		A2		1077.08	1.57	0.90
				A2b		1116.78	40.94	0.91
M_A6 2T	Tr2	99.33		A6		468.62	1.25	0.99
				A6a		476.79	17.48	0.99
M_B10 2T	Tr2	92.78		B10		1027.77	2.50	0.93
				B10a		1070.30	38.09	0.93
M_B2a 2T	Tr2	93.37		B2		1139.43	1.68	0.93
				B2a		1202.14	42.78	0.93
M_B2b 2T	Tr2	98.64		B2		1229.14	1.81	0.99
				B2b		1269.98	45.20	0.99
M_B3 2T	Tr2	96.62		B3		1446.77	2.12	0.97
				B3a		1492.75	53.13	0.97
M_B8 2T	Tr2	95.23		B8		966.49	2.38	0.95
				B8a		1010.20	36.31	0.95
M_C10 2T	Tr2	94.90		C10		951.26	2.40	0.95
				C10a		987.37	35.48	0.95
M_C14 2T	Tr2	94.83		C14		936.63	2.40	0.95
				C14b		976.90	35.46	0.95
M_C2 2T	Tr2	93.80		C2		1448.80	2.14	0.94
				C2a		1506.83	55.24	0.94
M_C7 2T	Tr2	94.50		C7		1468.74	2.15	0.94
				C7a		1536.42	55.65	0.95
A6G	Sym	92.76		A6a		476.79	17.48	0.93
B8G	Sym	98.27		B8a		1010.20	36.31	0.96
C10G	Sym	96.05		C10a		987.37	35.48	0.94
C14G	Sym	95.03		C14b		976.90	35.46	0.94
C2G	Sym	97.72		C2a		1506.83	55.24	0.98
C7G	Sym	99.64		C7a		1536.42	55.65	0.98

Table 5.1.: Load Flow Analysis applied to the 100% CGU PST 16 Benchmark System Network.

5.2 PST 16 BENCHMARK SYSTEM NETWORK (100% CGU) EMT OUTAGE FOLLOWED BY RESTORATION

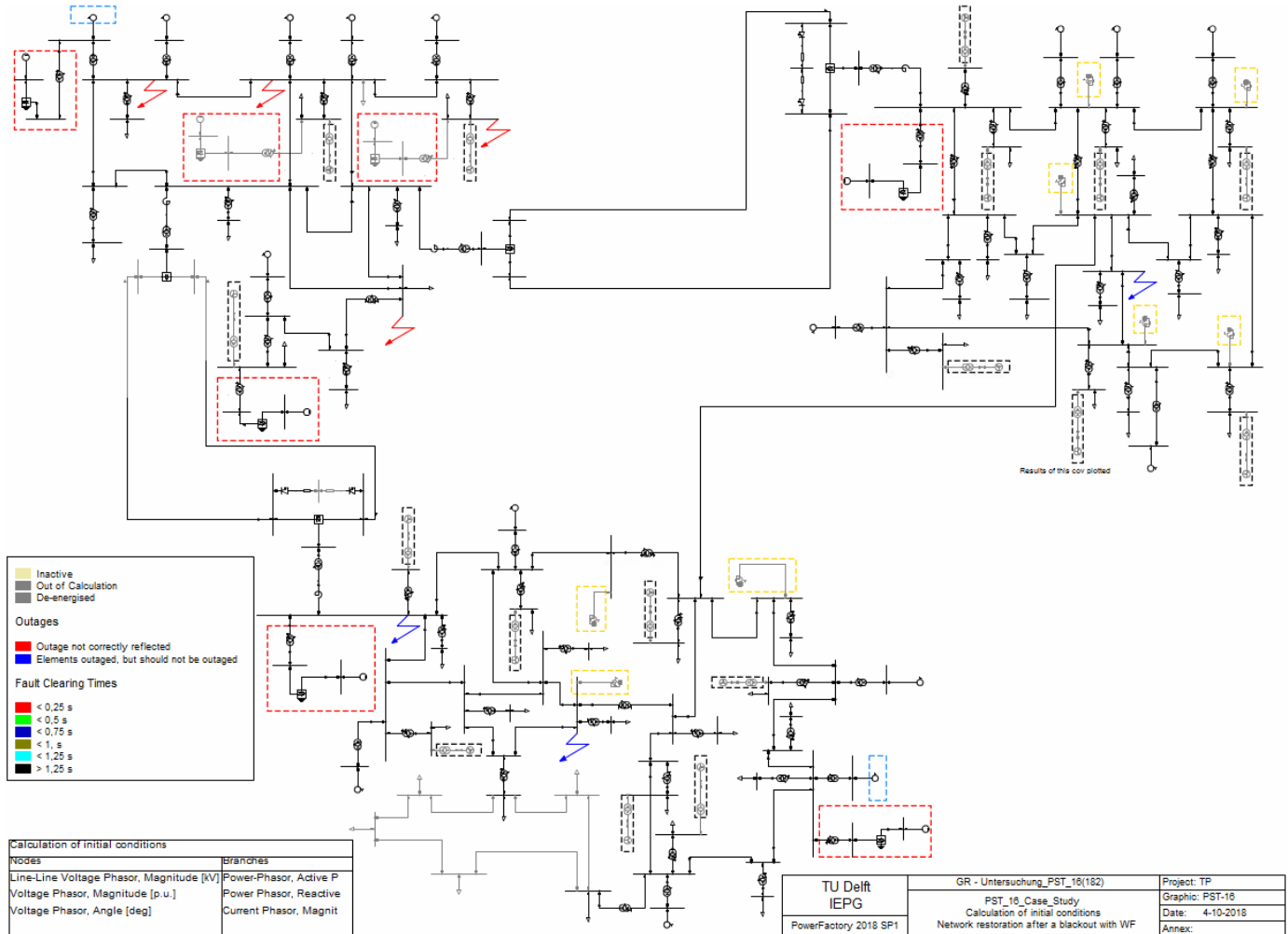


Figure 5.3.: EMT Simulation on the 100% CGU base-case scenario.

In this section, the plotted results of the EMT Simulation carried out in the *base-case* scenario are presented. A blackout in the area communicated by the HVDC Links (*Area A*) undergoes four massive short circuit faults in a defined period of time, which will derive in a quick response from the protection system described in [Section 4.5.3](#). The fault is so hard that the network cannot avoid collapse and hence the area suffers a complete blackout that even this protection system can not avert from it. Consequently, the proper protection scheme of the HVDC transmission system is put to action, which basically trips their circuit breakers and blocks their converter stations to *isolate Area A* from the rest. After some time with no energy supply, the BS-NR Plans start to take place one by one, recomposing the EPS that previously was broken down. The BS-NR Strategy is based on the theoretical review of [Section 3.3](#) and the design of the Protection System explained in [Section 4.5.3](#). So, after a blackout, there are three stages to follow:

1. Preparation: Critical-time actions
2. Black-Start: Critical elements and loads for cranking power
3. Network Restoration: (Cold) pick-up of all remaining elements and loads

The nomenclature/names of most elements in the EPS include letters *A*, *B* or *C* for the easy identifying of the plotted elements.

The time-domain EMT Simulation is led to run without any preprogrammed events during the first ninety seconds. This is so that in the resulting graphs the initial behaviour of the plots can be seen before the severe

Basic Options	
Verify initial conditions	Active
Automatic step size adaptation	Active
Solution of linear equations	Iterative method
Step Size	
EMT Small time step size	0.0001 seconds
Maximum step size	200 seconds
Solver Options	
Solve dynamic model equations at initialisation	Active
Enable partial initialisation in case of deadlock	Active
Fast convergence check	Active
Fast computation of outputs	Active
Maximum number of iterations	200
Integration	
Maximum error for dynamic model equations	1%
Damping factor	0.99
Iteration	
Maximum error for bus equations	1 MVA
Maximum error for model network equations	0.1%
Maximum number of iterations	25
Iteration limit to recompute Jacobian matrix	5
Simulation Times	
Time between initialisation and blackout faults	1.5 minutes (approximately)
Restoration system time taken to begin	1 minute after the fault
Total simulation duration time (absolute)	17 minutes

Table 5.2.: Settings for the EMT Simulation.

disturbances, and thus easier to compare the behaviour of all the systems before and after the faults and the *grid restoration*.

The RAS in case of a massive shutdown is led by the Hydro Generator *A1aG*, accompanied by a BESS. The storage unit excites the voltage terminals of the synchronous machine in case of a full blackout, so, in this manner, this association is a BSU. Table 5.2 presents some of the defined parameter options for the running simulation. In general, these options were selected in order to try to improve the speed of the overall test yet without sacrificing too much definition in the plots. One of these options is the *Automatic step size adaptation*, which allows increasing the step size in moments when the program detects the simulation does not require high detailed curves, e. g., during large periods of steady operation. But if required, this option goes back to a small time step if relentless EMT transients take place; an obvious consequence though is that then the simulation slows down. The standard maximum EMT time step size that is acceptable for the software in order to perform a simulation without errors has to be 0.0001 seconds; any number slightly larger than that brings already non-convergence errors of the type *maximum number of outer-loop iterations for dynamic model equations has been reached*.

The solution of the linear equations works good with both *Direct method* or *Iterative method*. Several simulations were performed with both options and no noticeable effect was distinguished. However, the second option was selected because it is recommended to use it if the case study is large and complex [15]. The total simulation duration time (absolute) was defined after several executed experiments, but also considering the relatively large size of the *PST 16 Benchmark System Network*.

Initially, the total simulation duration time (absolute) was intended to be as large as one hour; decision mainly concluded by the fact of the quite large and convoluted network the *PST 16 Benchmark System* happens to be. Its installed capacity, as reviewed in Section 4.3, probably needs a long time to recover after suffering the shutdown of even just one of their areas. Despite this evident need, the real actual time required to run a 17-minute (absolute)

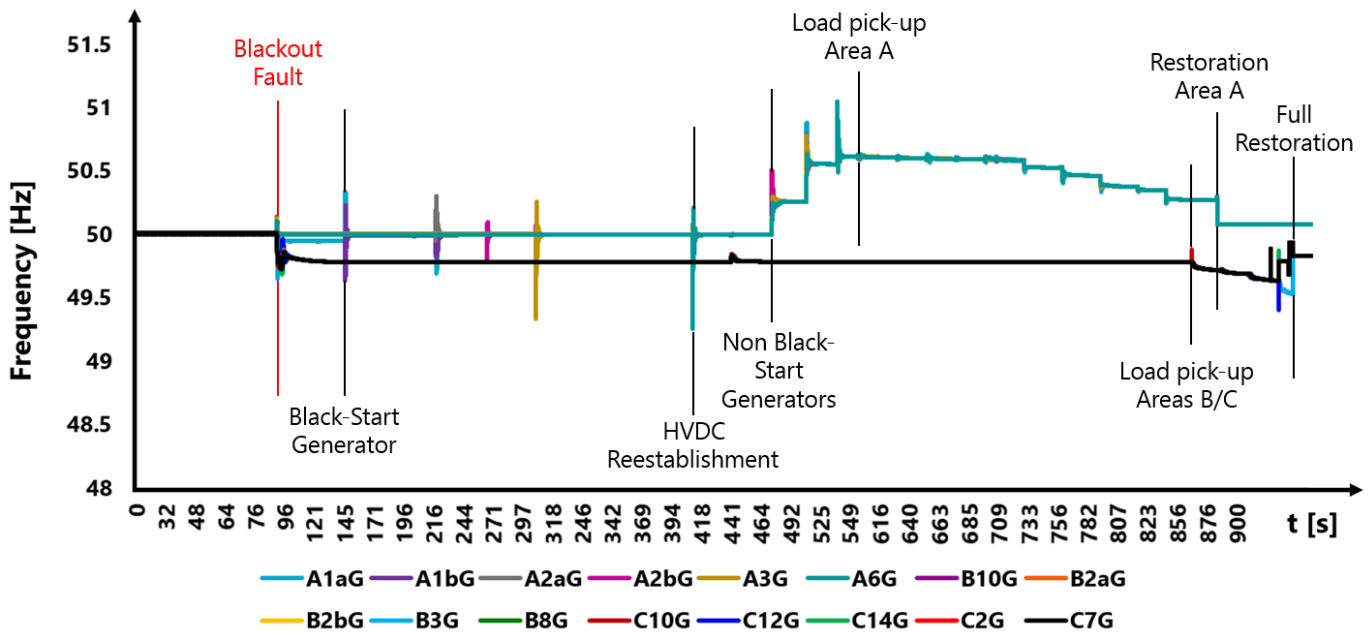


Figure 5.4.: Synchronous Generators Frequency Plots before, during and after the outage and *Restoration* events.

EMT Simulation with a network of the likes of this case scenario is of approximately 24 hours (in great regard, due to the same problems discussed in Subsection [WT Back-to-Back Philosophy in DPF](#)). This means that a 60-minute absolute-time EMT Simulation with blackouts and the RAS schemes on the *PST 16 Benchmark System Model* would take approximately 4 days to finalise. Moreover, the computer equipment would need to have a huge data storage capacity. For the assessment of the dynamic performance of the *Restoration* capabilities of the EMT 100% CGU Case Study after a blackout, the following plots are presented. Figures 5.4 and 5.5 present the results of the **frequency** and **rotor angle** of the sixteen synchronous machines (hydro, nuclear and coal-type) before and after the *Area A* blackout.

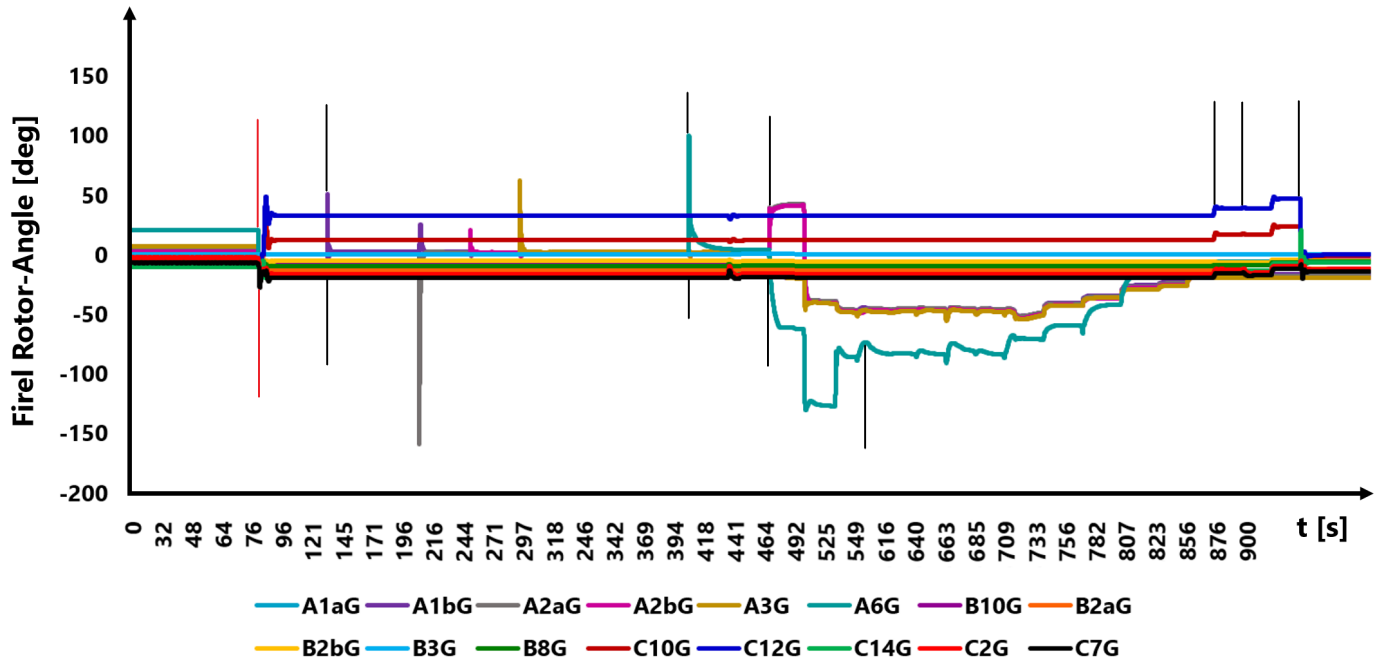


Figure 5.5.: Synchronous Generators Rotor Angle Plots before, during and after the outage and *Restoration* events.

The plots with their nomenclature starting with the letter A are correspondent with the six generators inside *Area A*. In both plots can be noticed a superb initialisation behaviour before the disturbances. After more than one minute

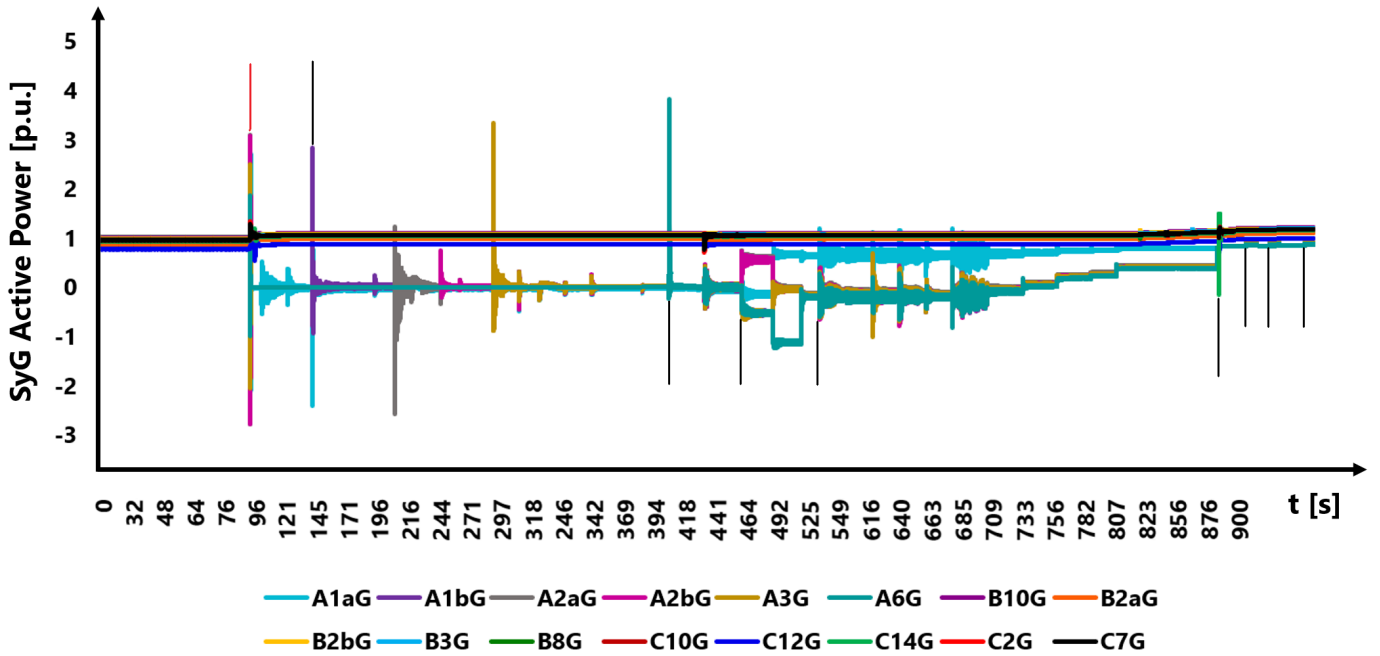


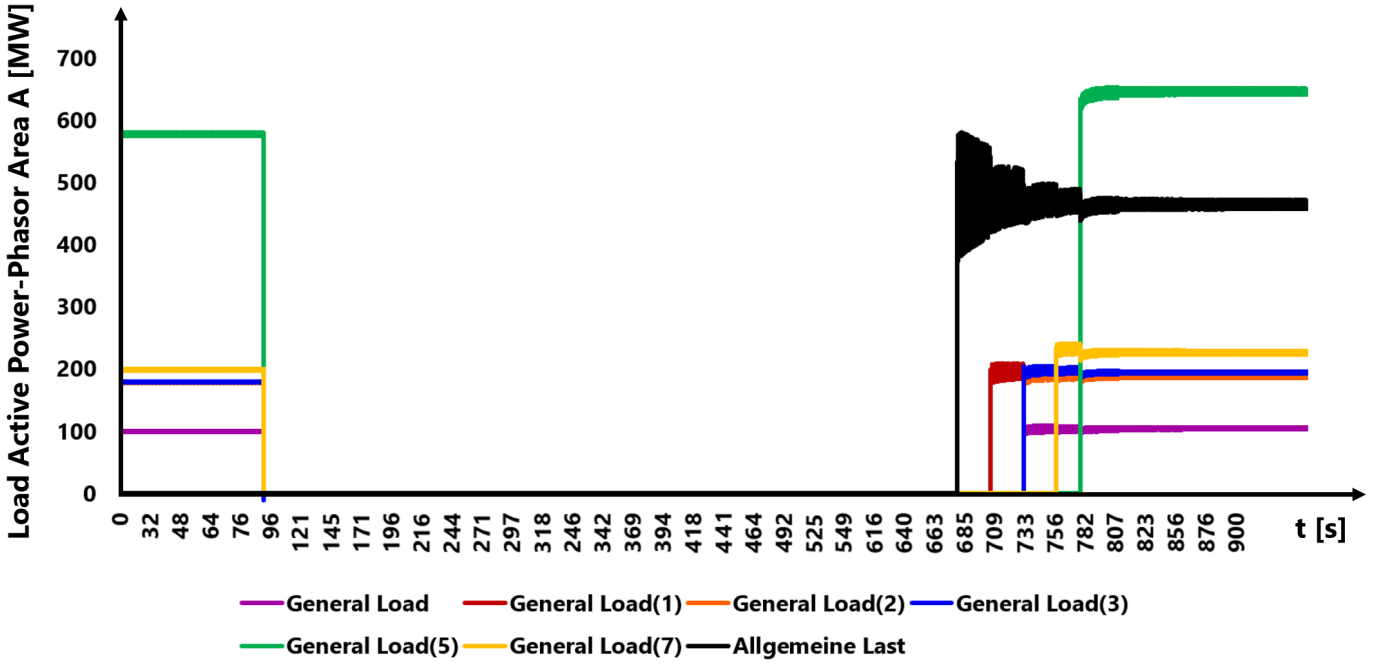
Figure 5.6.: Synchronous Generators Active Power in MW.

running without problems, the massive faults take place, shutting down *Area A* completely. After the blackout and the HVDC system out of service, it takes approximately another minute for the **DSL Protection and Restoration System** to begin the BS Plans. the frequency of the generators in *Areas B* and *C* suffer a slump of approximately -0.2 Hz. This is because the loss of the *Area A* generation share; *Areas B* and *C* contain more generation units, but there are also numerous load centres there, especially in *Area C*. Further, when the simulation is almost finished, it can be seen additional dynamic responses in all the plots. It turned out that, due to the extreme contingency, not only *Area A* but also some zones within *Areas B* and *C* had to be shut down as a *load shedding* protection scheme. Yet, despite the higher number of generation units in the remaining areas, they still cannot make up the loss of *Area A* without the frequency noticing it. However, regardless of the major loss, the rest of the network remains stable.

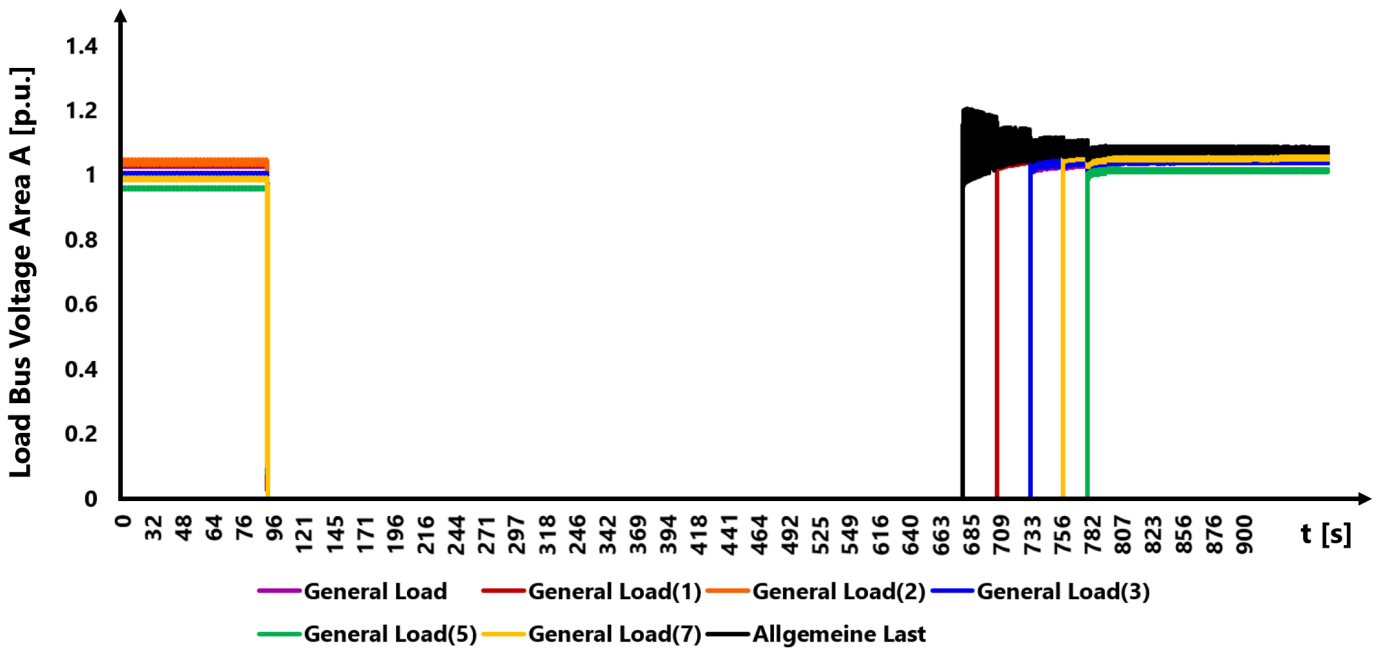
In both plots it can be seen the effect of the outage, besides the drop in the frequency, there are displacements in the rotor angle positions with respect to their originals. Still, after the blackout, the EPS manages to adapt to the change and keeps running. The peaks that are seen in the plots are the consequence of events during the simulation; usually, these events are about reconnections or actions of the governors and controllers. According to the *Control System Stability Theory* [58], if it is not for those peaks previously caused by the faults, the system would continue to present stable results.

The reconnection scheme was designed according to the empirically-discovered *Soft Energisation Method* [23], so, first only AC transmission lines, cables and transformers are reconnected according to a dead-busbar network configuration [23]. Between each stage of reconnection, there is set to have some dead time to let the EPS heal after the unavoidable disturbances that imply reconnecting outaged systems. Then, the utility-rated transformers are reenergised. It is recommended to reconnect first the lines that hold lower voltage levels as they require less reactive power demand. However, this was a quite of a dilemma due to *Area A* having nearly all its system running at 380 kV. There is only one set of overhead lines and a busbar at 220 kV, while the rest is running at the next higher voltage level. Afterwards, during the experimental simulations it was discovered that the system can hold on the reconnection of the AC cables and transmission lines regardless of their voltage levels, as long as only this type of elements is brought back to the grid first.

The first generation unit to be back online is the BSU *A1aG* association composed by a hydro generator and a BESS unit. After the outage, there are no major deviations in the plots until all the six outaged generation units are reconnected. This occurs approximately after the model has been running for approximately nine minutes (around 549 seconds in the plots). The large deviations in the frequency (Δ -upwards) and rotor angle (Δ -downwards) are the consequence of restarting the remaining synchronous machines. Because at that moment only transmission lines, cables and transformers are reconnected but no loads, the frequency of these generators have to go up, as there is virtually no load demand, while the load demanded by the former already-connected elements does not contribute to the frequency to go back to the nominal 50 Hz. In Figure 5.6 can be noticed a correspondent behaviour in the

Figure 5.7.: Active Power Delivered to the Loads of *Area A* in MW.

generators, in terms of the delivered **active power**; the ones in the affected area are delivering very few MW, while a ripple effect in the electric power plot can be seen in the generator in *Area A*. That is because of the **reactive power** and **magnetising parameters** of the generators. The rotor-angle stability of these units is at high risk, as it can be seen in Figure 5.5; the respective value for the *A1aG* unit being the one with the steepest change. This Figure encompasses why it is so complicated to perform a BS Operation. Without a method previously analysed cautiously, the system can fall back dramatically, especially during the first moments of a BS, when the EPS is particularly weak. Despite the visible instability in the rotor angle positions, the network turned out to be robust enough to cope with this stress, to the point that it could reach the **third Restoration stage**, which consists of the (cold) load-pick up.

Figure 5.8.: AC Voltage of the busbars connected with the Loads of *Area A* in p. u.

Figures 5.7 and 5.8 demonstrate the active power delivered to some of the Loads in *Area A* (in MW) and the voltage at the buses where these very Loads are connected (in p. u.), respectively. In analysing these latter plots with the former

ones, it can be seen that from the moment the first Load, appointed as *Allgemeine Last*, is picked up, both frequency and rotor angle parameters start to come close to their initial values before the havoc. Similarly, the delivered active power from the generators in *Area A* (Figure 5.6) starts to increase; this makes sense because that power is the same one injected onto the loads plotted in Figure 5.7. Figures 5.5 - to - 5.8 demonstrate the successful implementation of the **DSL Protection and Restoration System** onto the *PST 16 Benchmark System* Power Grid. It can be concluded that the BS and NR can be done if conventional rotating machines are the main generation units, though this is not a surprise. CGU have been used since the beginning of the XIX Century, so *Restoration Schemes* led by them have been successfully tested and implemented ever since after their industrial standardisation. The major goal of running a simulation with the *base study case*, with no wind penetration but 100% conventional generation, was to have a framework reference to compare them with the results of the case with 90% wind penetration, which is the main study of this MSc Thesis Research.

As for the elements and loads shut down in *Areas B* and *C*, they were restored just before the finalisation of this test. After the last element for these two areas is brought back online, the final reaccommodation of frequency, power and rotor angles takes place, and a similar behaviour like the ones shown in Figures 5.7 and 5.8 but for the pick-up loads in *Areas B* and *C* takes place. However, those plots for this simulation were not included in this Report. Still, the same phenomena was replicated in the operational scenario with 90% wind.

5.3 TEST OF INDIVIDUAL WIND FARM WITH THE GRID-FORMING CONTROL SYSTEMS

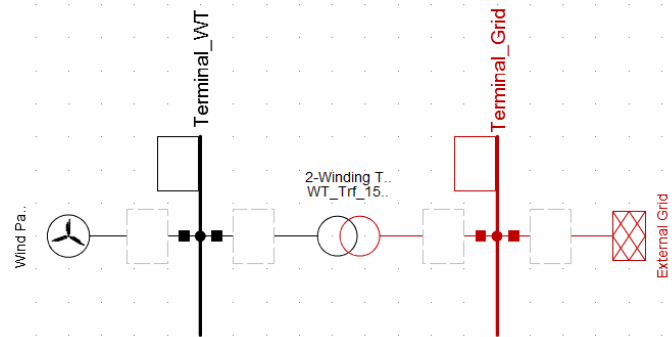


Figure 5.9.: Wind Power Plant with a rating of 900 MW.

Figure 5.9 represents a WF with the equivalent power of ninety PMSG-WT, each one with a rated power of 10 MW. The scaled WF is connected to a **0.69 kV busbar** and, in the PCC, an equivalent transformer representing the multiple step-up transformations from the WT to the HV bus is the link from the generator to the external grid. The transformer has a rating of 1580 MVA, $0.69 \Delta-391 Y$ kV and a reactance of 30%. The external grid is connected to a **380 kV busbar**.

Before modifying the control schemes of all WF in the main case study, first, it has to be guaranteed that one single unit can work acceptably. Therefore, the objective of this test is to demonstrate that the modifications applied to the original current-based WECS (Figure 4.3b) were done appropriately and that the new controls succeed in dispatch electric power to the external grid.

During this simulation no events were included, as testing drastic faults in an external grid model ElmXnet (details in DPF 2018 Manual [15]) is not feasible. Actually, the main purpose of this test was to solely evaluate if the control system models implemented and explained in Chapter 4 could work together in synergy. Naturally, during the implementation of different EPS models and their mutual interconnection, desired results usually do not come out at the first try. So this test was useful to detect inaccuracies and alleviate them.

Moreover, this experiment was useful to detect secondary malfunctions derived from variables wrongly defined in the Common Model windows; e. g., plot results showing an expected behaviour, however, having an odd offset not corresponding with the predicted expected magnitude.

The results show both mechanical and electrical aspects of the system, where their behaviour are described by a bunch of plots with time t in seconds as the omnipresent variable in the x -axis.

5.3.1 WECS MECHANICAL DYNAMIC PERFORMANCE

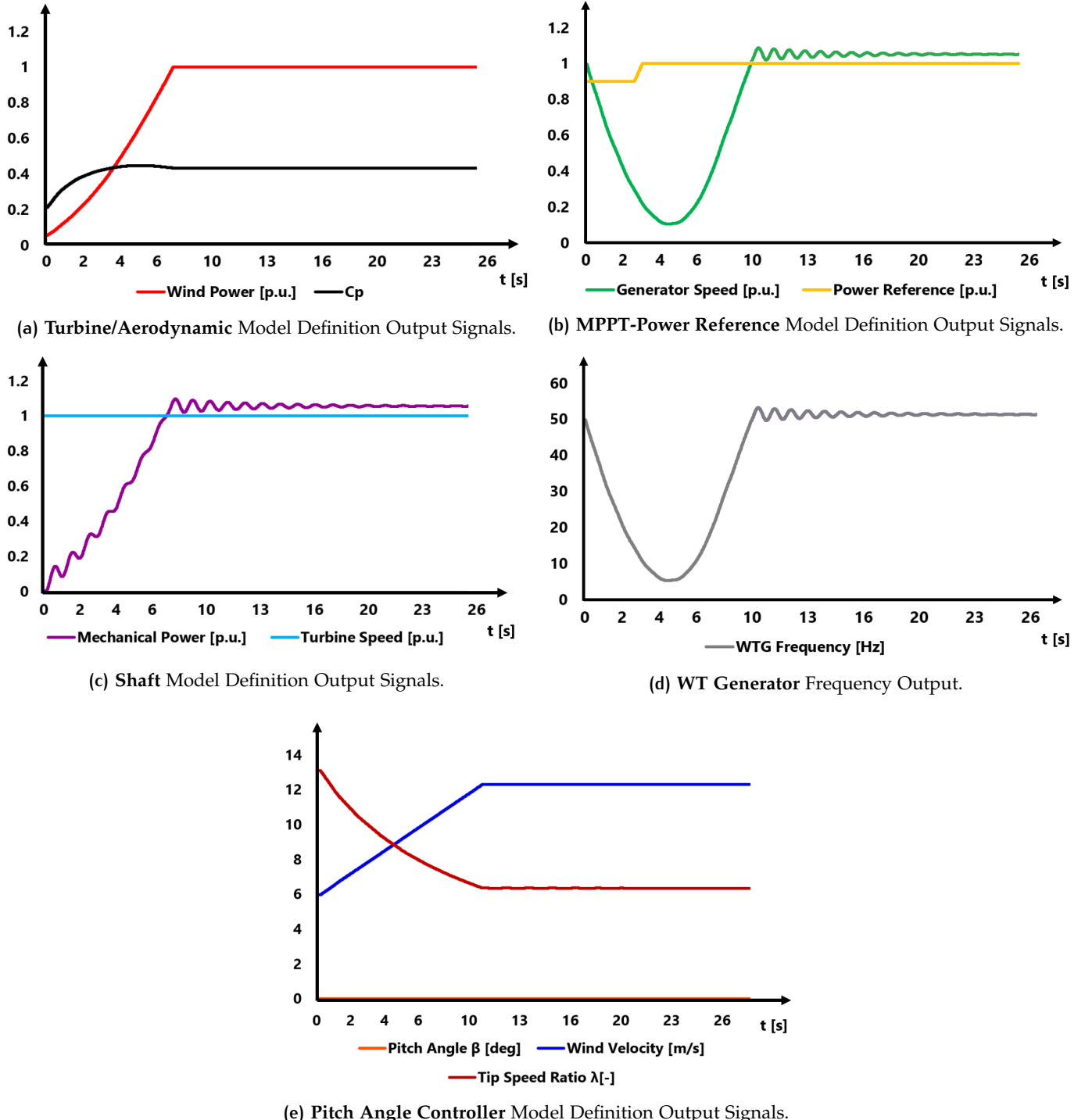


Figure 5.10.: WECS Mechanical Dynamic Performance.

The coefficient of power $C_p(\beta, \lambda)$ in Figure 5.10a behaves as expected with a response value close to 0.4, a magnitude usually derived from a WT running at rated conditions. On that same logic, the Pitch Angle β is nearly zero, according to Figure 5.10e; this means so far the controller has not detected necessary to pitch the blades angles for overcoming excessive wind speeds, so the wind must be running at a speed suitable with the design speed of the WECS. In this same plot can be seen that indeed the wind speed went up from 6 to 12.5 ms. Actually, all the plots for the mechanical/aerodynamic drivetrain perform as expected; in the beginning, the generator speed and so the WF frequency endure a steep decrease of speed that takes ten seconds to come through. This is because the set initial

conditions for the wind speed were chosen not to match with the nominal speed ranges of 12 - to 17 m/s. Indeed, for testing the operation of the **Wind Gust** Block Definition, its initial value was very close to standard WT *cut-in* velocity. However, the derivative controller in the latter Model Definition did its function by increasing gradually the wind speed until reaching the 12.5 m/s. The generator speed and the frequency of the generator acted accordingly and by the time that speed was reached, the generator speed reached 1 p. u. and the frequency 50 Hz. It can also be noticed a parallel behaviour between the mechanical power from the Shaft (Figure 5.10c) and the wind velocity.

5.3.2 WECS ELECTRICAL DYNAMIC PERFORMANCE

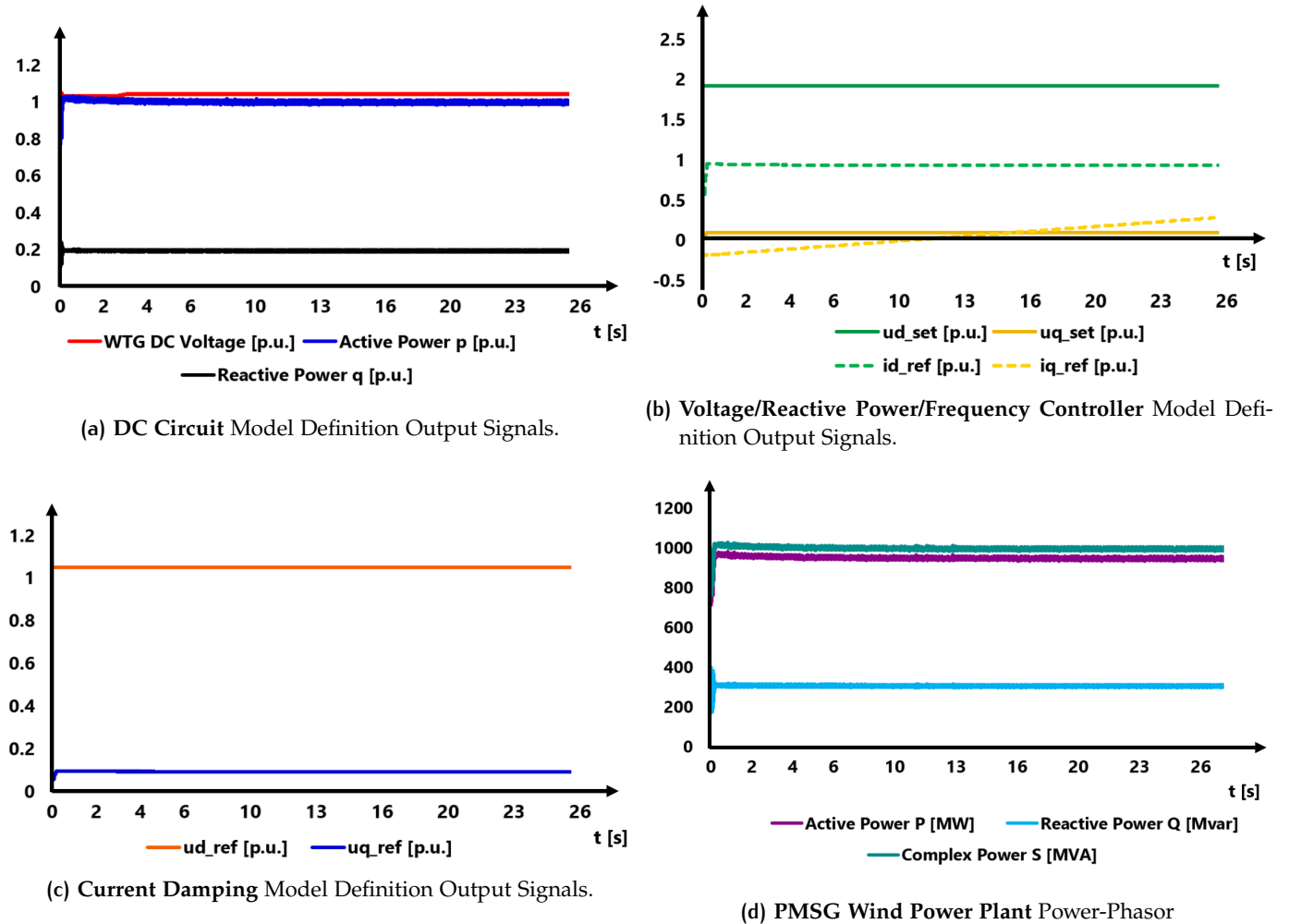


Figure 5.11.: WECS Electrical Dynamic Performance.

The two blocks where the mechanical-to-electrical power conversion occurs is in the MPPT and the DC Circuit Model Definitions, respectively. In Figure 5.11a the DC voltage output, in red, presents a plot close to 1 p. u., or 1.276 kV of nominal voltage. In that same plot, the active and reactive power p and q are the input references for the Voltage/Reactive Power/Frequency Controller explained exhaustively in the Subsection **Voltage/Power/Frequency Control with Current Damping**. The output signals of this very control are displayed in Figure 5.11b. Most plots behave as expected except for the output signal ud _set, which has a magnitude extremely high (its output value is twice a expected); nevertheless the Current Damping Block Definition (Figure 5.11c) does its job by bringing back to 1 p. u. the reference d - q voltages that will be part of the requirements for the Modulation Model calculates the target voltage value according to the external grid conditions. It does it via the PI Proportional term and the washout filters like the ones shown in Figures 4.11 and 4.12.

Finally, Figure 5.11d presents the delivered power-phasor magnitudes of the individual WF to the external grid. As it was described, the WF consist of ninety PMSG-WT, each one rated at 10 MW. In this last plot, the nominal active power is delivering approximately 900 MW.

5.4 PST 16 BENCHMARK SYSTEM NETWORK (90% WF) LOAD FLOW ANALYSIS

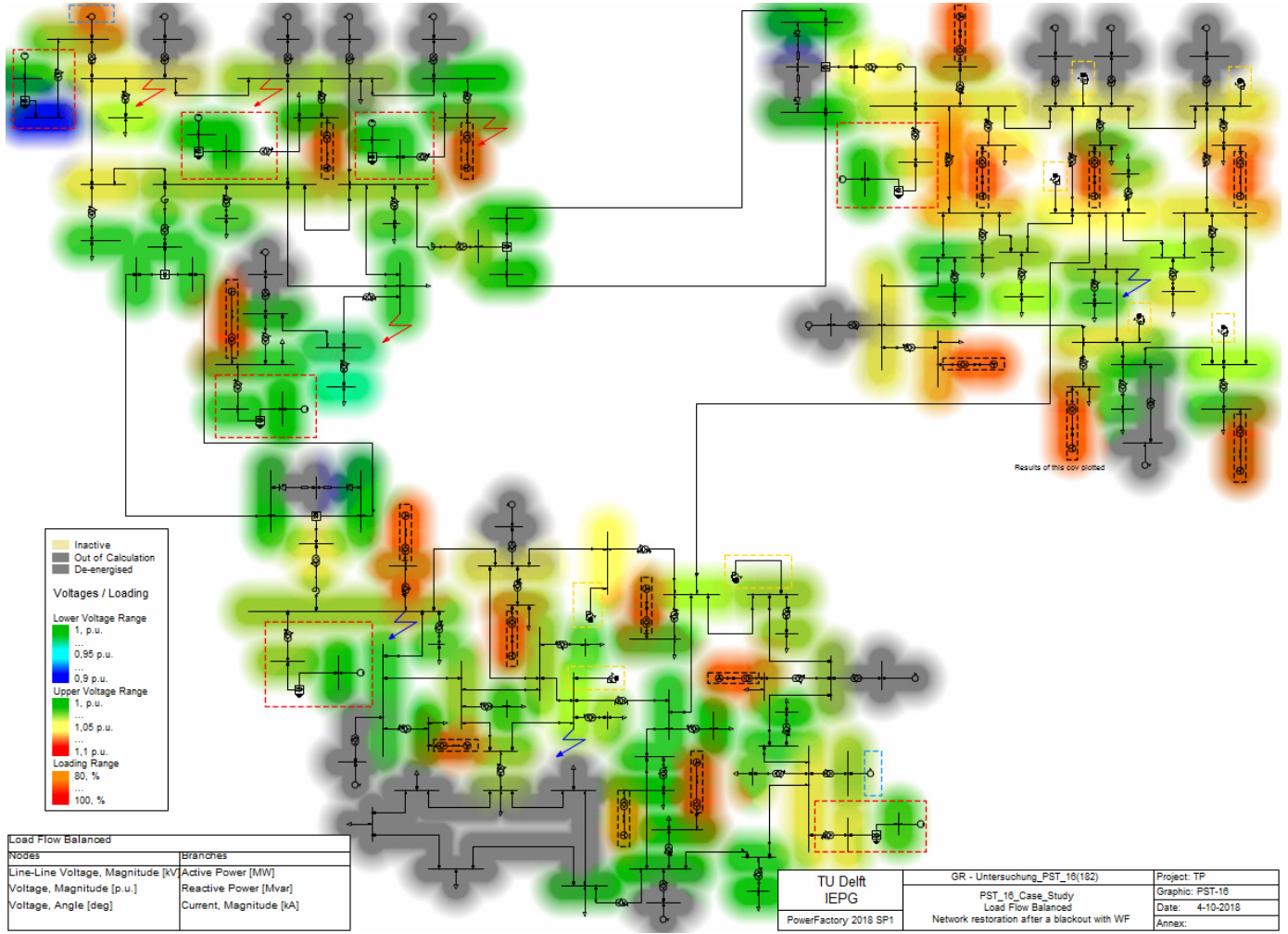


Figure 5.12.: Load Flow Analysis applied to the 90% Wind-Share PST 16 Benchmark System Network.

The scaled WF prototype tested in the previous Section 5.3 was the replica model for all the wind power stations seen in the *PST 16 Benchmark System* EPS. Therefore, seventeen copies of this WECS Model were installed there. These replicas can now be seen active in the Load Flow Study applied to the *PST 16 Benchmark System* Network as shown in Figure 5.12. The *PST 16 Benchmark System* EPS, on its *Base Case Scenario* (100% CGU) is presented in Figure 5.1. The proceeding for this Analysis is the same one that was applied for the *base case* study, including the same Load Flow settings. The real big difference is only the substitution of the CGU for the WF. The Load Flow Study applied to this case study scenario appears in Figure 5.1. In the Load Flow Analysis it can also be said that the grid has as well a healthy condition, with most busbars having around 1 p. u. and all the generation units working closely to their nominal values. The difference now is indicated by the WF, now active as they are accompanied by an red-orange glow and again all its loads and elements absorbing adequate quantities of active and reactive power. Just like the previous Load Flow Study with the CGU, this Load Flow Analysis was a balanced-positive sequence type, automatic tap adjustments for transformers was disabled, but reactive power limits and the automatic model adaptation for convergences was enabled. In a similar fashion, there is no real danger or warnings in this EPS, as it can be seen in the DPF Output Window via Table 5.3; there are no warning messages while the Newton-Raphson Program converged as well rather fast with only seven iterations, despite the large structure of this grid. The successful Load Flow Analysis could be done with decisive help from the **External Station Controllers** installed in each WF (an example of this additional controller is found in Table 4.5). With these regulators, an established reactive power setpoint can be placed in a cubicle inside of the busbar each WECS unit is connected.

Error (0)	Warning (0)	Info (33)	Event (0)	Other (51)	Contained text
Info					
Element 'A1aG' is local reference in separated area of 'Cub_1'					
Element 'C12G' is local reference in separated area of 'C12a'					
Element 'HVDC-BA_REC-Inverter' is local reference in separated area of 'Klemmleiste +HVDCBA'					
Element 'HVDC-CA_REC-Inverter' is local reference in separated area of 'Klemmleiste +HVDCCA'					
Element 'HVDC-BA_REC-Inverter' is local reference in separated area of 'Klemmleiste -HVDCBA'					
Element 'HVDC-CA_REC-Inverter' is local reference in separated area of 'Klemmleiste -HVDCCA'					
Grid split into 17 isolated areas					
Calculating load flow...					
Info					
Start Newton-Raphson Algorithm...					
Step 1 / 3: Scaling total load demand with factor 5,774e-01...					
Iteration 0: Terminal_WT_WPB1 4.22e+02 HVDC-AC_SEC-Rectifier 5.58e+02					
Iteration 1: Terminal_WT_WPB6 4.27e+02 HVDC-AC_SEC-Rectifier 3.03e+02, Relax factors: (Max. Step: 4,57e-01, Linesearch: 1,00e+00)					
Newton-Raphson converged with 1 iterations.					
Step 2 / 3: Scaling total load demand with factor 8,165e-01...					
Iteration 0: Terminal_WT_WPB6 7.75e+02 WPB6 5.50e+02					
Iteration 1: Terminal_WT_WPB6 3.44e+02 WPB6-Q Control 3.54e+02, Relax factors: (Max. Step: 1,00e+00, Linesearch: 1,00e+00)					
Newton-Raphson converged with 1 iterations.					
Step 3 / 3: Scaling total load demand with factor 1,000e+00...					
Iteration 0: Terminal_WT_WPC4 1.86e+02 WPB6-Q Control 3.54e+02					
Iteration 1: 110_kv_B1 6.61e+02 General Load(12) 6.61e+02, Relax factors: (Max. Step: 1,00e+00, Linesearch: 1,00e+00)					
Iteration 2: 110_kv_B1 2.94e+02 HVDC-CA_REC-Inverter 2.44e+02, Relax factors: (Max. Step: 6,47e-01, Linesearch: 1,00e+00)					
Iteration 3: Terminal_WT_WPB6 1.19e+02 WPB6 1.19e+02, Relax factors: (Max. Step: 1,00e+00, Linesearch: 1,00e+00)					
Iteration 4: Terminal_WT_WPB6 4.39e+01 WPB6 4.39e+01, Relax factors: (Max. Step: 1,00e+00, Linesearch: 1,00e+00)					
Iteration 5: Terminal_WT_WPB6 6.36e+00 WPB6 6.36e+00, Relax factors: (Max. Step: 1,00e+00, Linesearch: 1,00e+00)					
Iteration 6: Terminal_WT_WPC1 8.57e-02 WPC1 8.57e-02, Relax factors: (Max. Step: 1,00e+00, Linesearch: 1,00e+00)					
Iteration 7: Terminal_WT_WPC_DC 6.54e-05 WPC_DC 6.54e-05, Relax factors: (Max. Step: 1,00e+00, Linesearch: 1,00e+00)					
Newton-Raphson converged with 7 iterations.					
Load flow calculation successful.					
Info					
Report of Control Condition for Relevant Controllers					
Info					
Control conditions for all controllers of interest are fulfilled.					
Load Flow Calculation					
AC Load Flow, balanced, positive sequence					
Automatic tap adjustment of transformers No					
Consider reactive power limits Yes Max. Loading of Edge Element 90,00 %					
Automatic Model Adaptation for Convergence Yes Lower Limit of Allowed Voltage 0,90 p.u.					
Upper Limit of Allowed Voltage 1,10 p.u.					
DIGSILENT Project:					
PowerFactory -----					
2018 SP1 Date: 4-10-2018					
Study Case: PST_16_Case_Study Annex: / 1					
Name Type Loading [%] Voltage [p.u.] [kV] Station/Branch Apparent Power [MVA] Current [kA] Current [p.u.]					
Overloaded Elements					
AC-Terminal LVT_A1 Term 0.81 3,24 PST_16					
2-Winding TransformerWPA2 90.74 110_kv_A3 895,06 4,76 0,91					
Terminal_WT_WPA2 900,04 759,20 0,91					
2-Winding TransformerWPA3 90.50 A6b 893,79 4,75 0,90					
Terminal_WT_WPA3 901,13 757,27 0,91					
B11a 921,05 4,77 0,91					
Terminal_WT_WPB6 914,88 760,25 0,91					
2-Winding TransformerWPC1 90.07 110_kv_C1 905,20 4,73 0,90					
Terminal_WT_WPC1 910,02 753,54 0,90					
2-Winding TransformerWPC4 90.96 110_kv_C12 904,35 4,77 0,91					
Terminal_WT_WPC4 910,28 761,04 0,91					
2-Winding TransformerWPC5 91.90 110_kv_C5 931,10 4,82 0,92					
Terminal_WT_WPC5 924,87 768,29 0,92					
WPA1 Genstat 90.02 Terminal_WT_WPA1 900,21 745,76 0,89					
WPA2 Genstat 90.00 Terminal_WT_WPA2 900,04 759,20 0,91					
WPA3 Genstat 90.11 Terminal_WT_WPA3 901,13 757,27 0,91					
WPB1 Genstat 92.00 Terminal_WT_WPB1 920,02 742,14 0,89					
WPB2 Genstat 90.23 Terminal_WT_WPB2 902,35 718,15 0,86					
WPB3 Genstat 90.07 Terminal_WT_WPB3 900,70 737,38 0,88					
WPB4 Genstat 90.43 Terminal_WT_WPB4 904,26 715,35 0,85					
WPB5 Genstat 91.47 Terminal_WT_WPB5 914,68 726,32 0,87					
WPB6 Genstat 91.49 Terminal_WT_WPB6 914,88 760,25 0,91					
WPB_DC Genstat 91.01 Terminal_WT_WPB_DC 910,13 734,35 0,88					
WPC1 Genstat 91.00 Terminal_WT_WPC1 910,02 753,54 0,90					
WPC2 Genstat 91.53 Terminal_WT_WPC2 915,31 736,60 0,88					
WPC3 Genstat 92.04 Terminal_WT_WPC3 920,43 748,58 0,89					
WPC4 Genstat 91.03 Terminal_WT_WPC4 910,28 761,04 0,91					
WPC5 Genstat 92.49 Terminal_WT_WPC5 924,87 768,29 0,92					
WPC_DC Genstat 91.72 Terminal_WT_WPC_DC 917,23 735,84 0,88					

Table 5.3.: Output Window Results for the 90% Wind-Share Load Flow Analysis.

5.5 PST 16 BENCHMARK SYSTEM NETWORK (90% WF) EMT OUTAGE FOLLOWED BY RESTORATION WITH OPTIMUM WIND

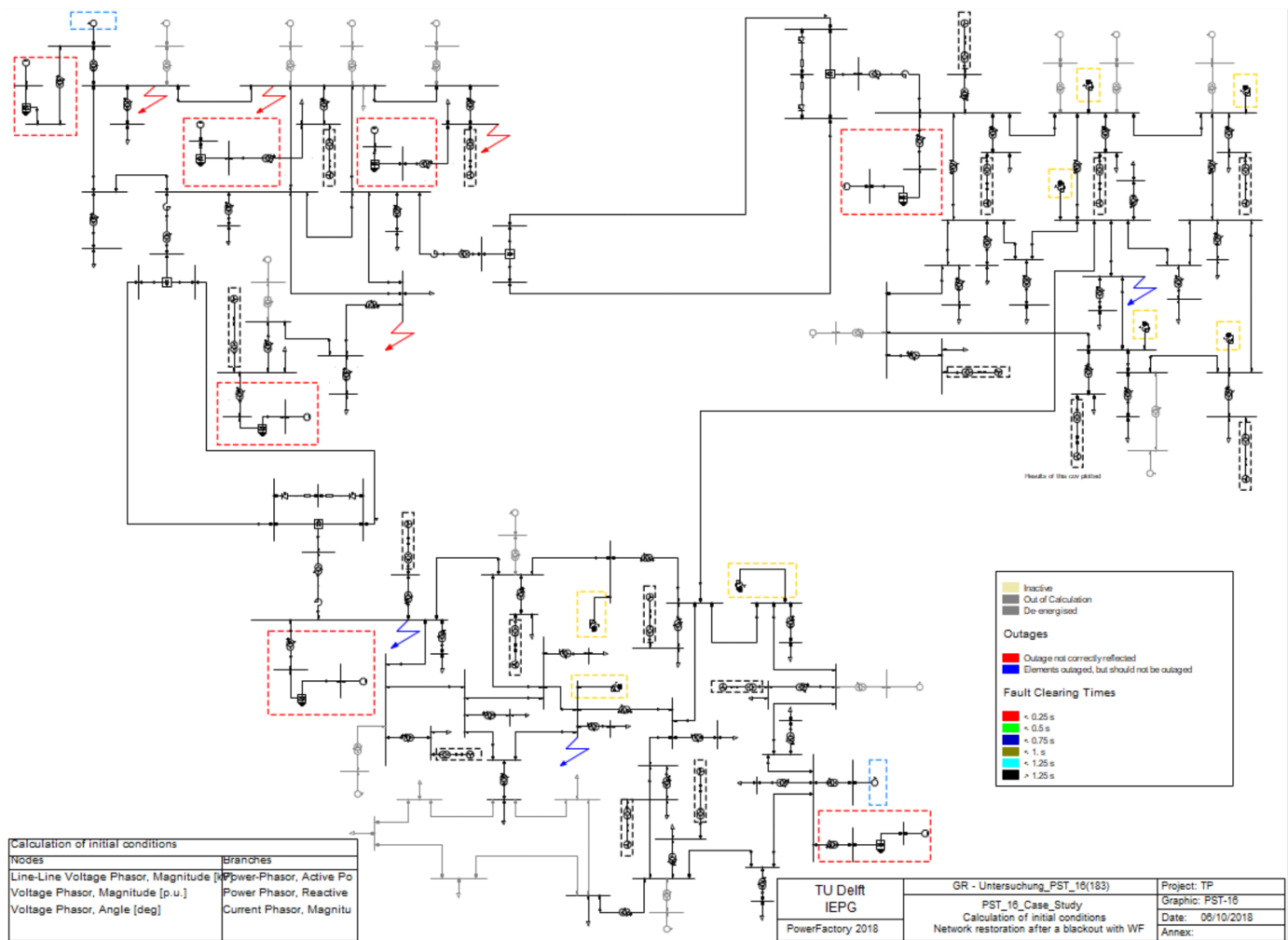


Figure 5.13.: EMT Simulation on the 90% Wind Share study case scenario.

In this Subsection, results of the main study objective of this MSc Thesis Project are plotted and discussed. In this study case, all the WECS power plants are operating in a location with wind speeds that vary from 12 - to - 15.3 m/s, which are very optimal atmospheric conditions of wind speed.

Simulation Events/Fault - Study Cases\PST_16_Case_Study\Simulation Events/Fault :						
	Name	Time	Object	Out of Service	Object modified	Object modified by
►	110_kV_A3_SC	90,4	110_kV_A3	<input type="checkbox"/>	6-10-2018 12:41:47	Inoris
►	A2_SC	90,4	A2	<input type="checkbox"/>	6-10-2018 12:42:28	Inoris
►	A7a_SC	90,4	A7a	<input type="checkbox"/>	6-10-2018 12:42:01	Inoris
►	A1_SC	90,4	A1	<input type="checkbox"/>	6-10-2018 12:42:00	Inoris

Table 5.4.: Table showing defined events at the EMT initialisation.

The proceeding for these EMT Simulations are the same ones that were applied for the *base case* study, including the same *initial-conditions* settings. Comparing Figures 5.13 and 5.3 it can be noticed that now the CGU machines are out of service and instead the seventeen WF are the leading sources of electric power. The case study with 90%

wind penetration still maintains two CGU units active, the hydro synchronous machine *A1aG* located in *Area A* and the thermal synchronous machine *C12G* located in *Area C*. These synchronous generators are marked with dotted blue rectangles. When starting the simulation, one can see the defined events in the *Simulation Events/Faults* Table (Table 5.4). There, it can be selected the place where the fault is intended to take place, time, the name of every event, etc. When the EMT Simulations just started, only the short-circuit faults are preset, but no event clearing the faults and neither any event representing any *Restoration* action. This is because all these subsequent events are programmed in a way that they only appear if the faults previously occur. Otherwise, if no action is triggered, no event in the *Simulation Events/Faults* Table appears, just like with real protection schemes.

5.5.1 EMT 90% WF CASE STUDY DYNAMIC PERFORMANCE DURING INITIALISATION

The following plots demonstrate the dynamic performance of the EPS before any disturbance; this shows that the implementation of the new control systems and power system elements has been done successfully.

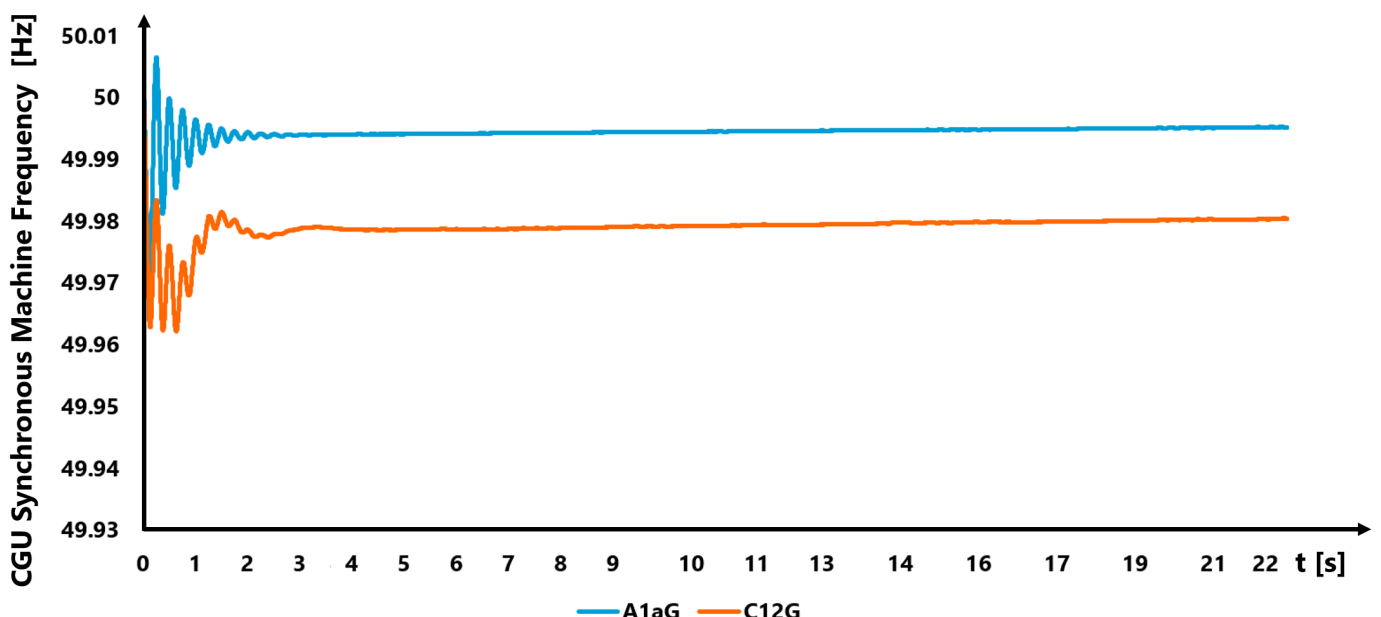


Figure 5.14.: EMT Frequency plots of the Synchronous Machines after 22 seconds of initialisation.

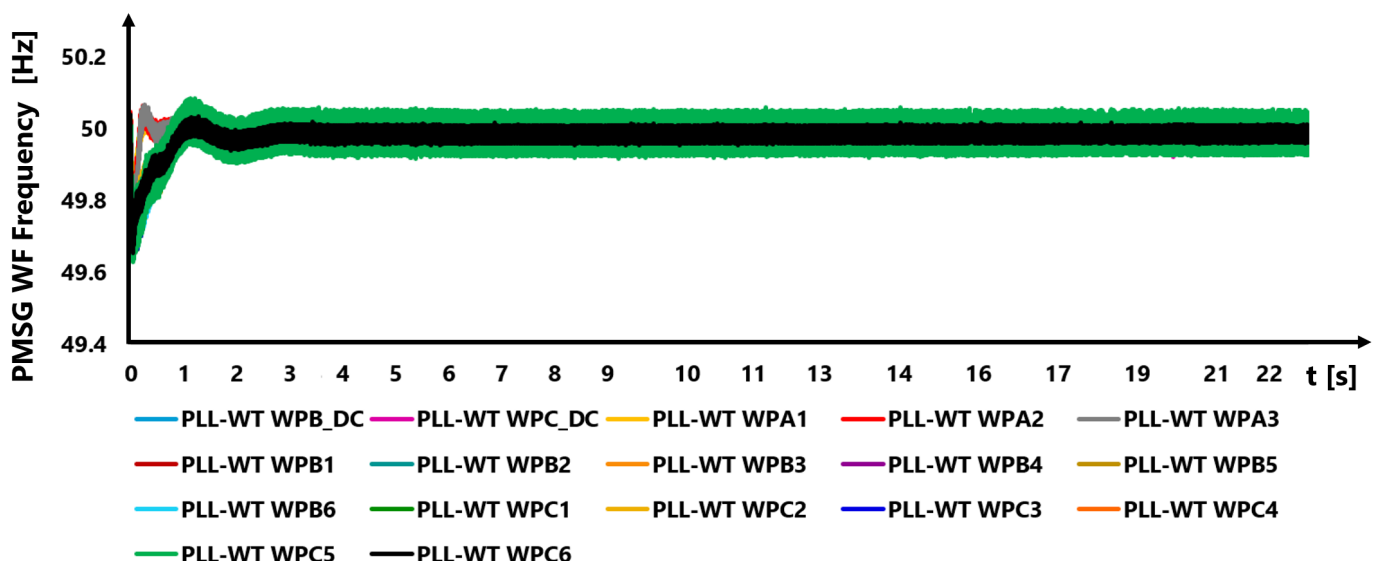


Figure 5.15.: EMT Frequency Plots of the Wind Power Plants after 22 seconds of initialisation.

Figures 5.14 and 5.15 present the first 22 second of EMT simulation results in terms of the frequency for the hydro/-coal synchronous machines and the WF, respectively. If no disturbance is taking place, the plots would continue to behave stably and tending to the nominal value of 50 Hz. The ripple in the frequency plots for the WF shown in Figure 5.15 is caused in part because of the electromagnetic interference of all the converters that compose their own structure but also the Proportional terms of the PI controllers inside the PLL taking part of the wind power plant units. For the WF, these proportional gains are set as 100.

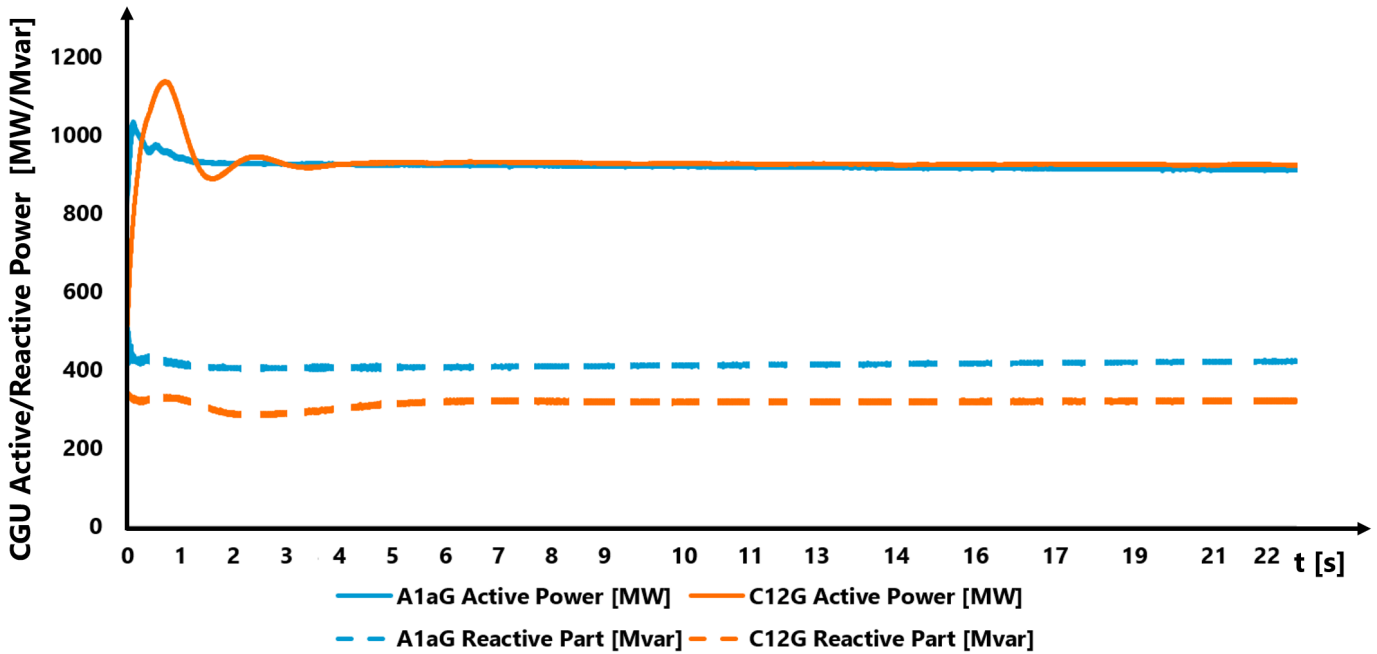


Figure 5.16.: EMT Active/Reactive Power Plots of the Synchronous Machines after 22 seconds of initialisation.

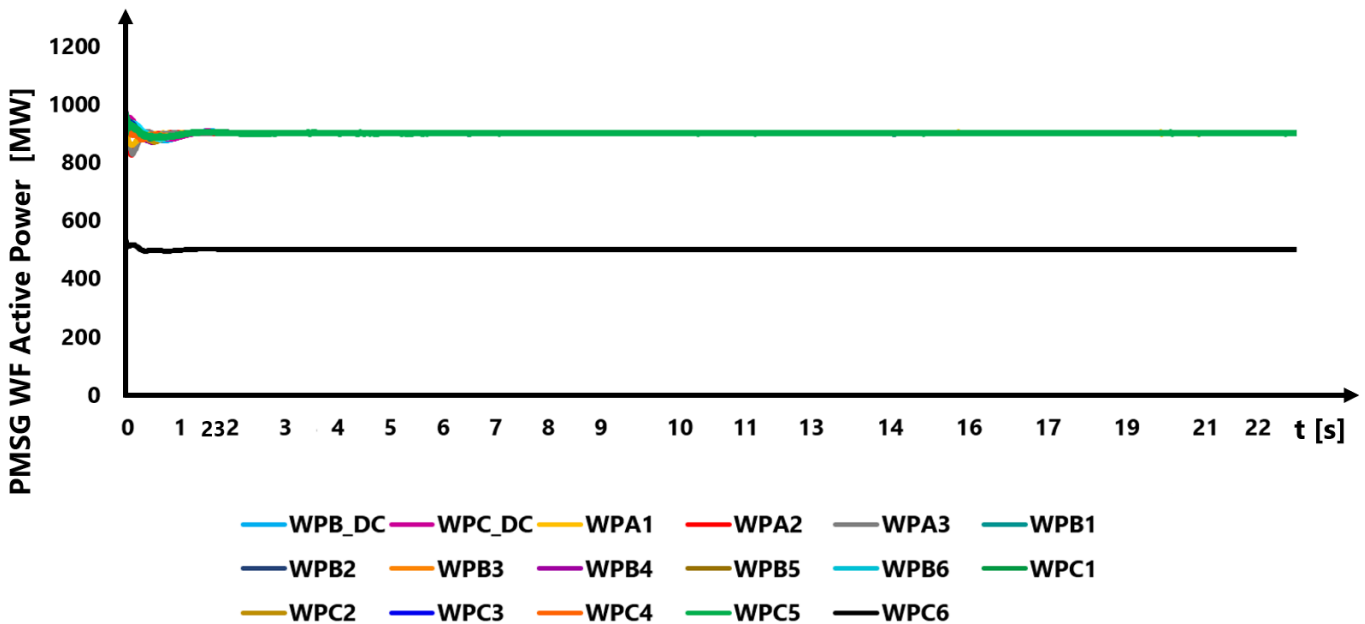


Figure 5.17.: EMT Active Power Plots of the Wind Power Plants after 22 seconds of initialisation.

The Power-Phasor results for all generation units are shown in Figures 5.16, 5.17 and 5.18. The active power operational limits for the hydro-generator $A1aG$ is 1100 MW, while 1235 MW for the coal-generator $C12G$. Both are operating within their safety limits and under their nominal parameters. In turn, the target active power sixteen of the seventeen PMSG-WF are set to deliver to their PCC busbar is 900 MW. Figure 5.17 shows that sixteen of these WECS are indeed generating the desired output real power. The remaining WF, appointed as $WPC6$, only delivers a

target setpoint of 500 MW. This was designed in order to reproduce the same installed capacity that the original *base study case* with no RES holds.

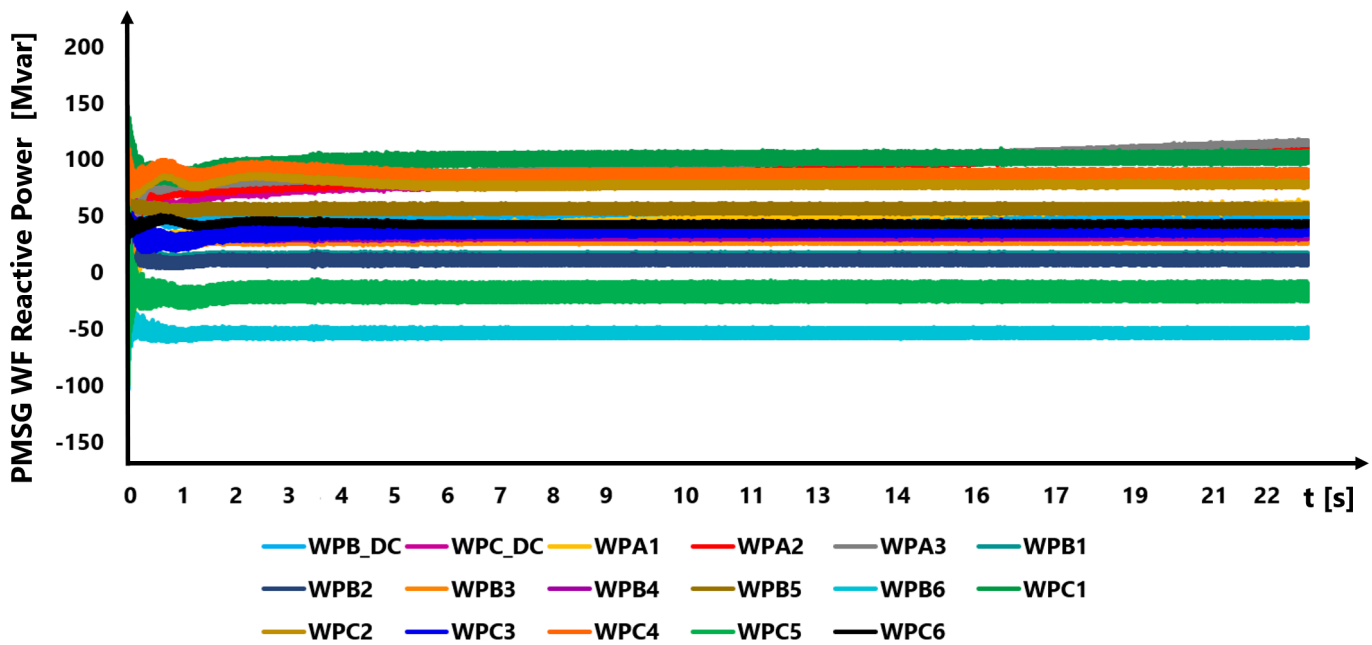


Figure 5.18.: EMT Reactive Power Plots of the Wind Power Plants after 22 seconds of initialisation.

The reactive part of the total power produced by the wind power plants appears in Figure 5.18. Unlike the active power, these parameters were figured out based on several Load Flow Studies. Each different value for their respective wind power unit contributes to have the healthy power network that can be appreciated in Figure 5.12. Different factors affect the different setpoint values for reactive power, the location of the WF, negligible or decisive amount of harmonics produced in that area, proximity with fellow generation units, defined participation factor for each generator, etc. They have their different reactive power parameters according to the *External Station Controller* each WECS has, as shown in Table 4.5.

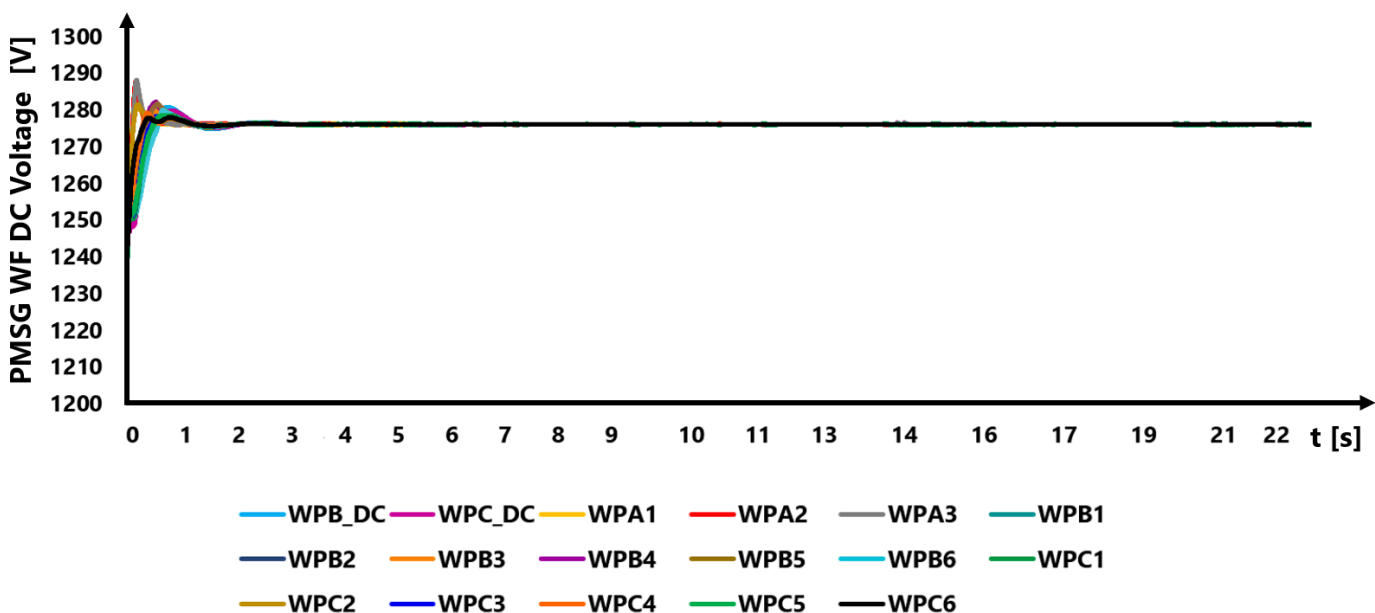


Figure 5.19.: EMT DC Voltage plots of the Wind Power Plants after 22 seconds of initialisation.

The DC voltage per each WF is calculated by means of the **DC Circuit Model**. Each wind power plant has 0.69 kVAC, but when converted to continuous current, they hold approximately 1.2476 kVDC. Figure 5.19 demonstrates that this

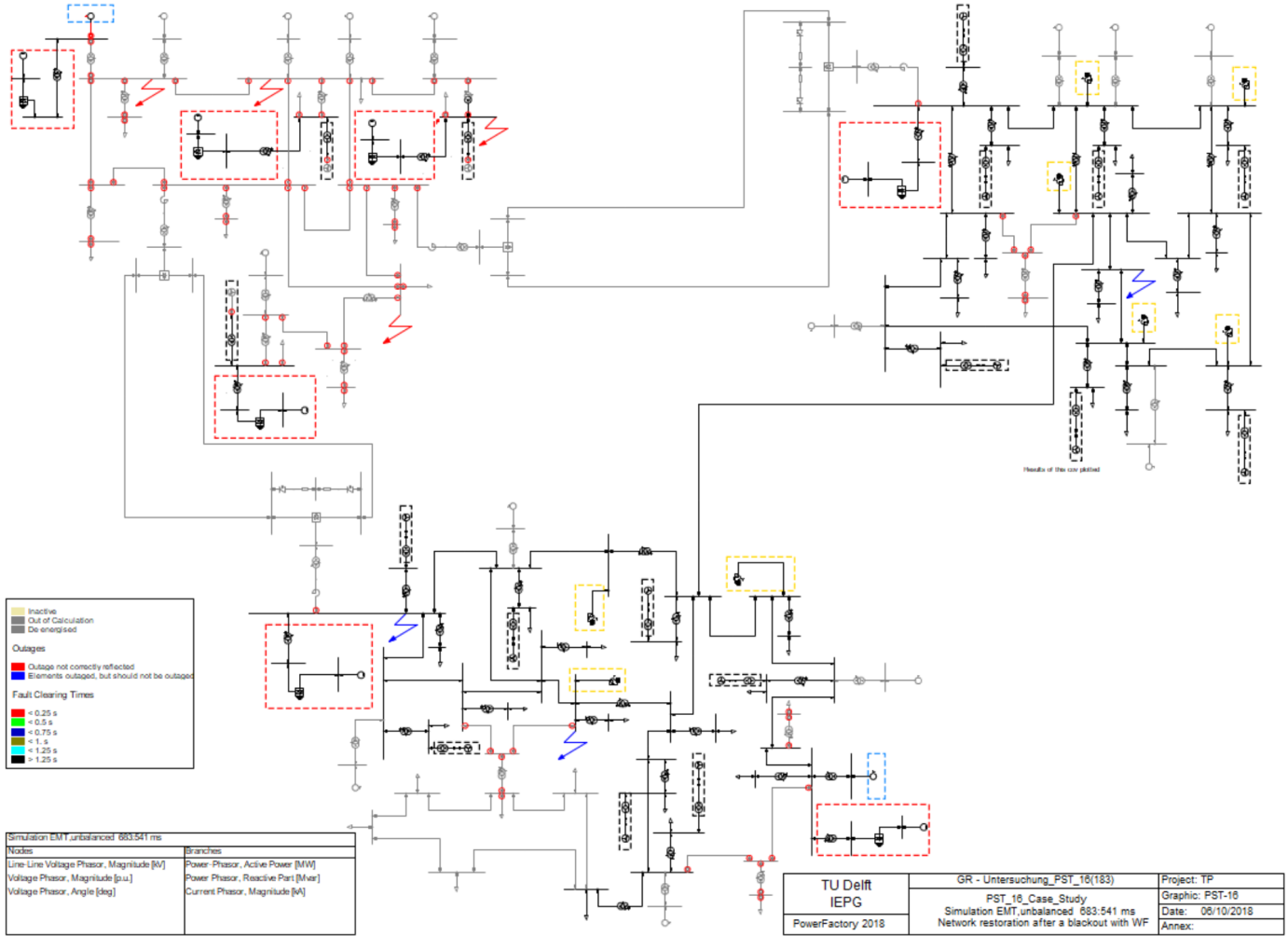


Figure 5.20.: EMT Simulation on the 90% Wind Share study case scenario just after the blackouts.

target value is indeed obtained by the modified control systems, because it can be seen that all the WF converge with this voltage value.

5.5.2 EMT 90% WF CASE STUDY DYNAMIC PERFORMANCE AFTER A BLACKOUT

Comparing Figures 5.20 and 5.13 it can be noticed that in the first Figure there are way more elements in the network sketched in gray. This was a direct consequence of the **DSL Protection and Restoration Scheme** working. After the four short-circuit faults, the *Area A* is fully out of service and isolated from the rest of the grid; as it can be seen, the HVDC Transmission Systems are also out of service. The red dots in 5.20 represent the tripped circuit breakers that have been opened by the protection relays by order of the **Protection and Restoration Scheme**.

Table 5.5 displays a table with numerous events; some of those events already happened (those written in gray) while the ones in black are yet to occur. When this very simulation just started, its *Event Output Table* only displayed the four short-circuit faults user-predefined, but no other event whatsoever, as it can be seen in Table 5.4. As it was formerly explained, this is because this scheme was designed to command their protection events just in case if a prior fault took place, otherwise, no action is ordered, and no further events appear on the Table. So, when a predefined fault has taken place, this protection system is triggered to protect the system, shedding as many circuits as necessary in order to prevent them to burn, damage or exploit. The events shown in Table 5.5 are just some of all the events programmed to first protect the damaged area of the EPS and then, after some time has taken place after the serious disturbances, to perform the BS and NR Plans. As it was described, this DSL protection and *restoration* system was designed according to the theoretical review exposed in Section 3.3 and Subsection **Measurement, Protection and Restoration Logic-Relays**.

Simulation Events/Fault - Study Cases\PST_16_Case_Study\Simulation Events/Fault :						
	Name	Time	Object	Out of Service	Object modified	O
✓	110_kV_B_TF5_Out	0.6403167	110_kV_B_TF5	<input type="checkbox"/>	06/10/2018 07:38:56 p.	▲
✓	GL_Out(20)	0.6403167	General Load(20)	<input type="checkbox"/>	06/10/2018 07:38:56 p.	
✓	C3-C5_Out	0.6403167	C3-C5	<input type="checkbox"/>	06/10/2018 07:38:56 p.	
✓	C5-C6_Out	0.6403167	C5-C6	<input type="checkbox"/>	06/10/2018 07:38:56 p.	
✓	C5T_Out	0.6403167	C5 T	<input type="checkbox"/>	06/10/2018 07:38:57 p.	
✓	GL_Out(41)	0.6403167	General Load(41)	<input type="checkbox"/>	06/10/2018 07:38:57 p.	
✓	GL_Out(34)	0.6403167	General Load(34)	<input type="checkbox"/>	06/10/2018 07:38:57 p.	
✓	110_kV_C_TF13_Out	0.6403167	110_kV_C_TF13	<input type="checkbox"/>	06/10/2018 07:38:57 p.	
✓	C12-C13_Out	0.6403167	C12-C13	<input type="checkbox"/>	06/10/2018 07:38:57 p.	
✓	C13-C14_Out	0.6403167	C13-C14	<input type="checkbox"/>	06/10/2018 07:38:57 p.	
✓	110_kV_C_TF8_Out	0.6403167	110_kV_C_TF8	<input type="checkbox"/>	06/10/2018 07:38:57 p.	
✓	SyM_A1aG_Rec	60.00845	A1aG	<input type="checkbox"/>	06/10/2018 07:35:14 p.	
✓	M_A1a_2T_In	75.00845	M_A1a 2T	<input type="checkbox"/>	06/10/2018 07:35:08 p.	
✓	A1-A2_In	90.00845	A1-A2	<input type="checkbox"/>	06/10/2018 07:35:08 p.	
✓	A_TF2_In	90.00845	110_kV_A_TF2	<input type="checkbox"/>	06/10/2018 07:35:08 p.	
✓	SyM_WPA1_Rec	105.0084	WPA1	<input type="checkbox"/>	06/10/2018 07:35:04 p.	
✓	A2-A3_In	120.0084	A2-A3	<input type="checkbox"/>	06/10/2018 07:35:08 p.	
✓	A_TF3_In	120.0084	110_kV_A_TF3	<input type="checkbox"/>	06/10/2018 07:35:08 p.	
✓	SyM_WPA2_Rec	135.0084	WPA2	<input type="checkbox"/>	06/10/2018 07:35:08 p.	
✓	A1-A4_In	150.0084	A1-A4	<input type="checkbox"/>	06/10/2018 07:35:08 p.	
✓	A2-A5a_In	150.0084	A2-A5a	<input type="checkbox"/>	06/10/2018 07:35:08 p.	
✓	A2-A5b_In	150.0084	A2-A5b	<input type="checkbox"/>	06/10/2018 07:35:08 p.	▼

Table 5.5.: Table showing the DSL Protection and Restoration System defining the RAS for healing the grid after the disturbances.

The procedure of the blackout has been previously explained throughout this MSc Thesis Report; however, in Figure 5.20 it can also be seen that not only *Area A* suffered shutdowns, but also some parts of *Areas B* and *C* suffered from fragmentation (just like the case with 100% CGU).

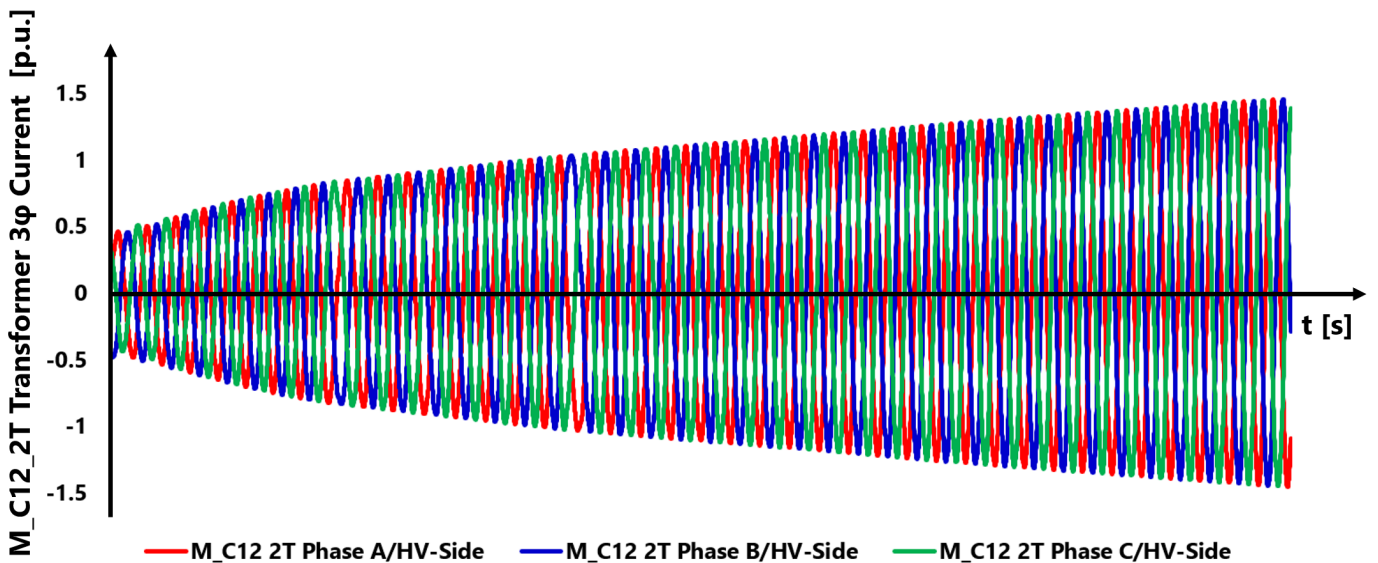


Figure 5.21.: Three-Phase Currents in the HV-side of Transformer *M_C12_2T*.

This was unexpected as this situation could not have been foreseen if not doing an EMT simulation formerly. With the different type of generation systems leading the grid, the latter undergoes different phenomena and so has to respond with different manners.

As RES-based generation embody more control systems and their dynamics are significantly faster than the dynamics of heavy and stiff rotating machines, the stability of a converter-dominated EPS is more difficult to sustain. In this

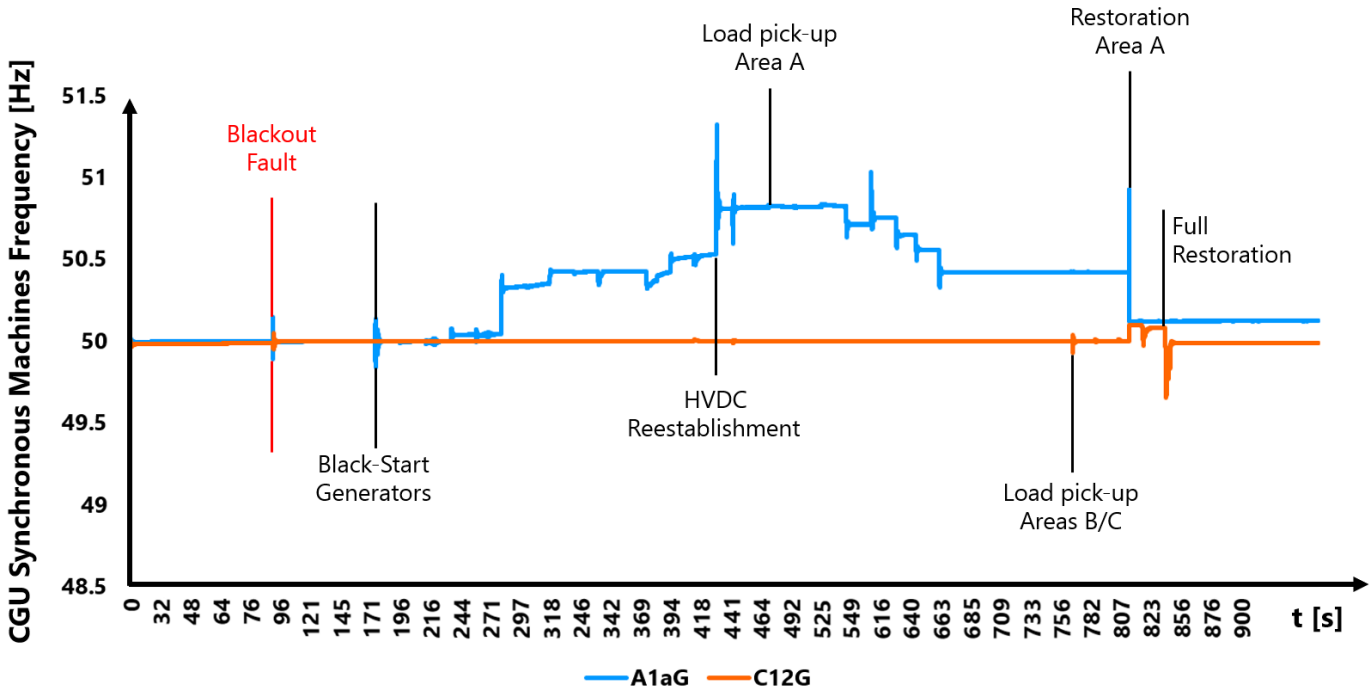


Figure 5.22.: EMT Frequency Plots of the CGU Synchronous Generators before, during and after the outage and *Restoration*.

case, many transformers of *Areas B* and *C* were suffering of an increase of current flowing through their coils. The increment of current was so large that was going beyond 2 p. u. This led to unsustainable conditions for the grid to keep operating. Eventually the grid collapse and the simulation would fail.

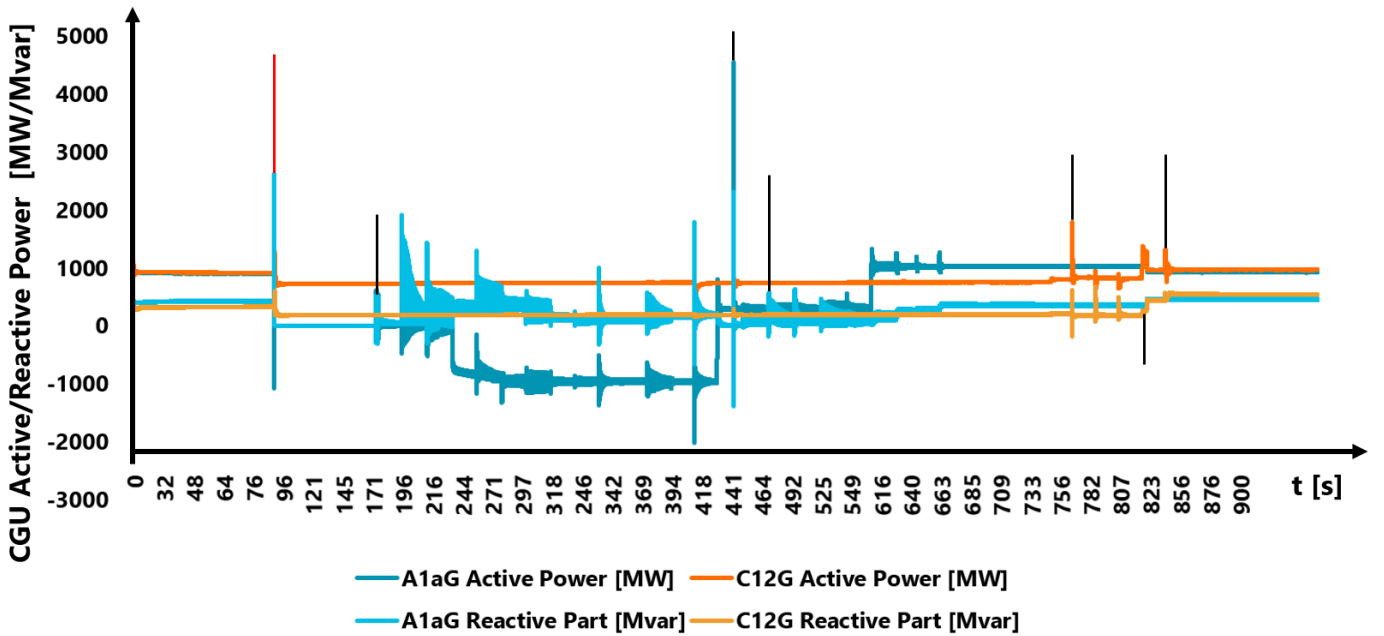


Figure 5.23.: EMT Active/Reactive Power Plots of the Synchronous Machines before, during and after the outage and *Restoration*.

Figure 5.21 exhibits the three-phase currents of the transformer *M_C12_2T*. This transformer is connected in the same busbar the coal-generator *C12G* also is, so it is the link between this generator with the rest of the network. This effect happened in many of the transformers taking part of *Areas B* and *C* after the blackout in *Area A*. Therefore, in order to neutralise this negative effect, a fifth **Protection and Restoration Scheme** had to be designed for especially for *Areas B* and *C*. That is why some additional circuits in these other areas were tripped off as well.

Figures 5.22 and 5.24 present the frequency behaviour of all the nineteen generation units active in this case

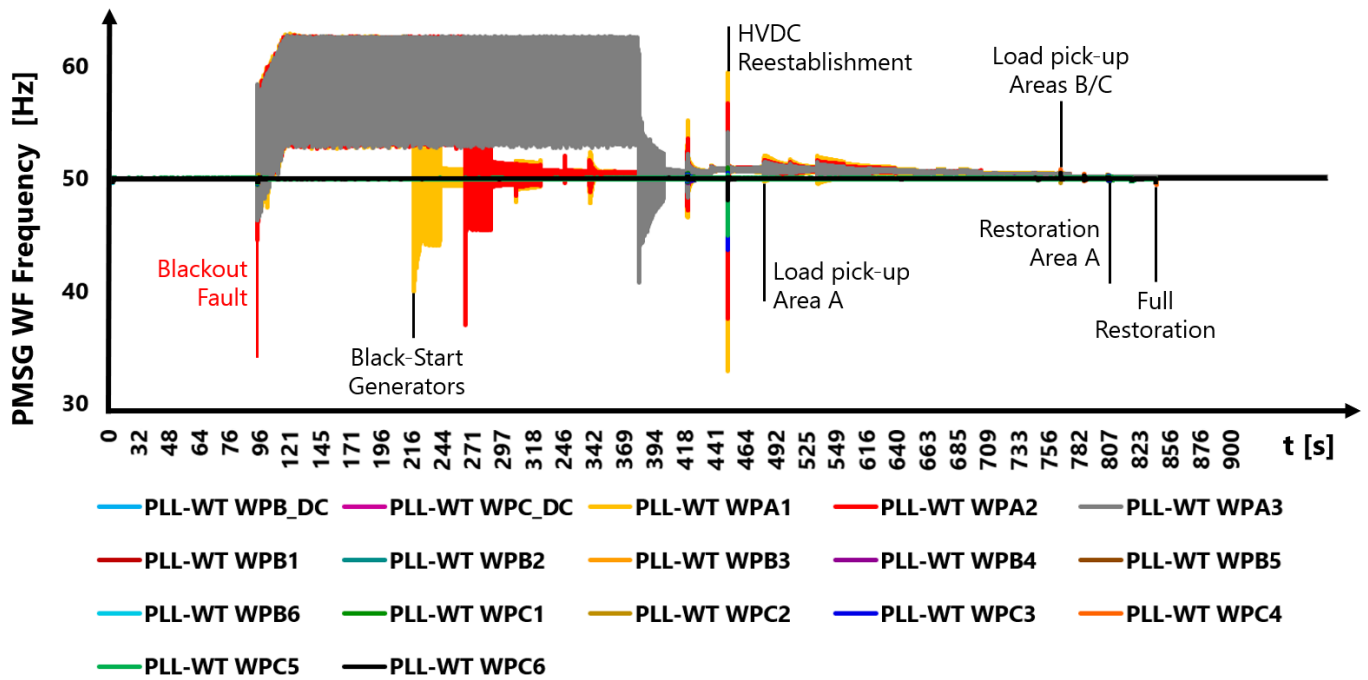


Figure 5.24.: EMT Frequency Plots of the Wind Power Plants before, during and after the outage and *Restoration*.

study. Those generators being part of the affected *Area A* were shut down and not until some minutes taken place afterwards these generators were started up again. The first generation unit to be back online was the hydro generator *A1aG*, approximately a minute and a half after the fault occurred, followed quickly by the WF *WPA₁*, around thirty seconds after the CGU was back online. Around one minute after, *WPA₂* went back online too. Finally, approximately five minutes after the fault, the WF *WPA₃* was reenergised. After analysing Figures 5.22 and 5.24 can be concluded that in the end both types of generation CGU and RES-based generation succeed to back to the nominal 50 Hz system frequency. However Figure 5.24 denotes that the WECS underwent serious disruption from the moment the blackout took place. After the three wind power plants went disconnected, their frequencies started to oscillate in a similar fashion DC voltage does according to Figure 4.5.

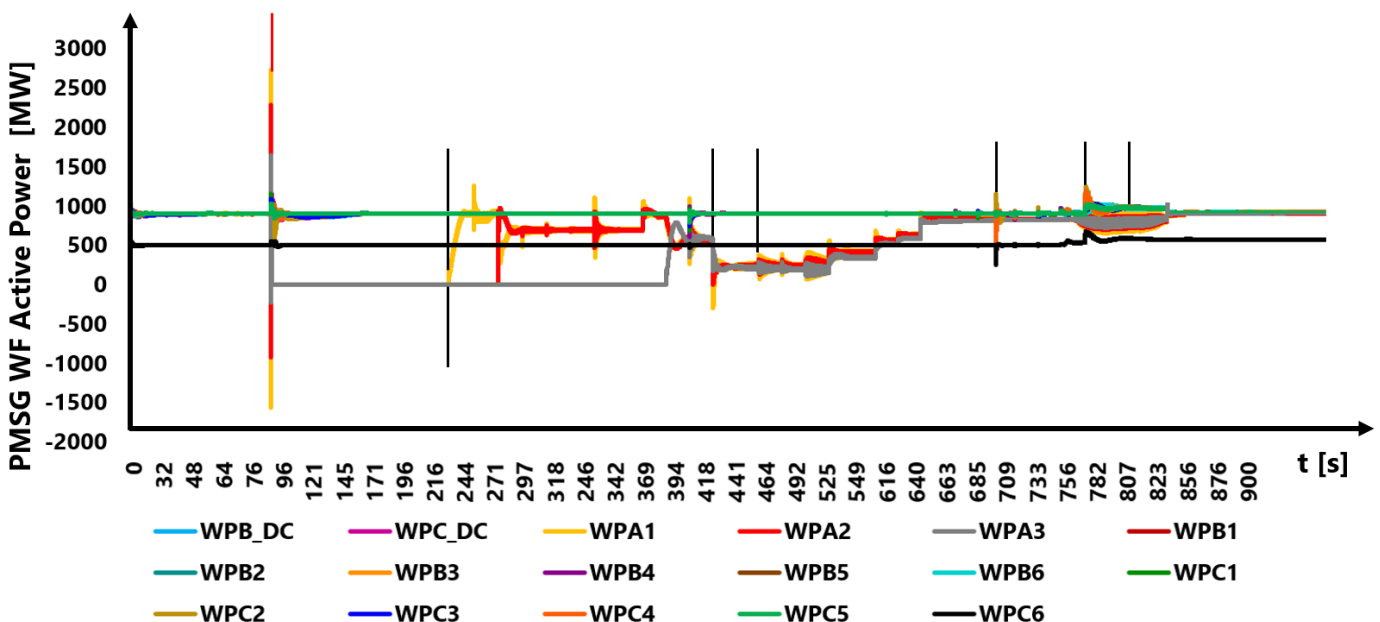


Figure 5.25.: EMT Active Power Plots of the Wind Power Plants before, during and after the outage and *Restoration* events.

This was clearly because the VSC converters of these WF were blocked and, because the *Load Shedding* scheme

compartmentalised the generators from the loads, the power generated did not have anywhere to go. However, the oscillations turned out to be way higher than expected, as they reached 60 Hz. In previous simulations, a similar outcome was developed but the oscillation peak used to top at 51 Hz.

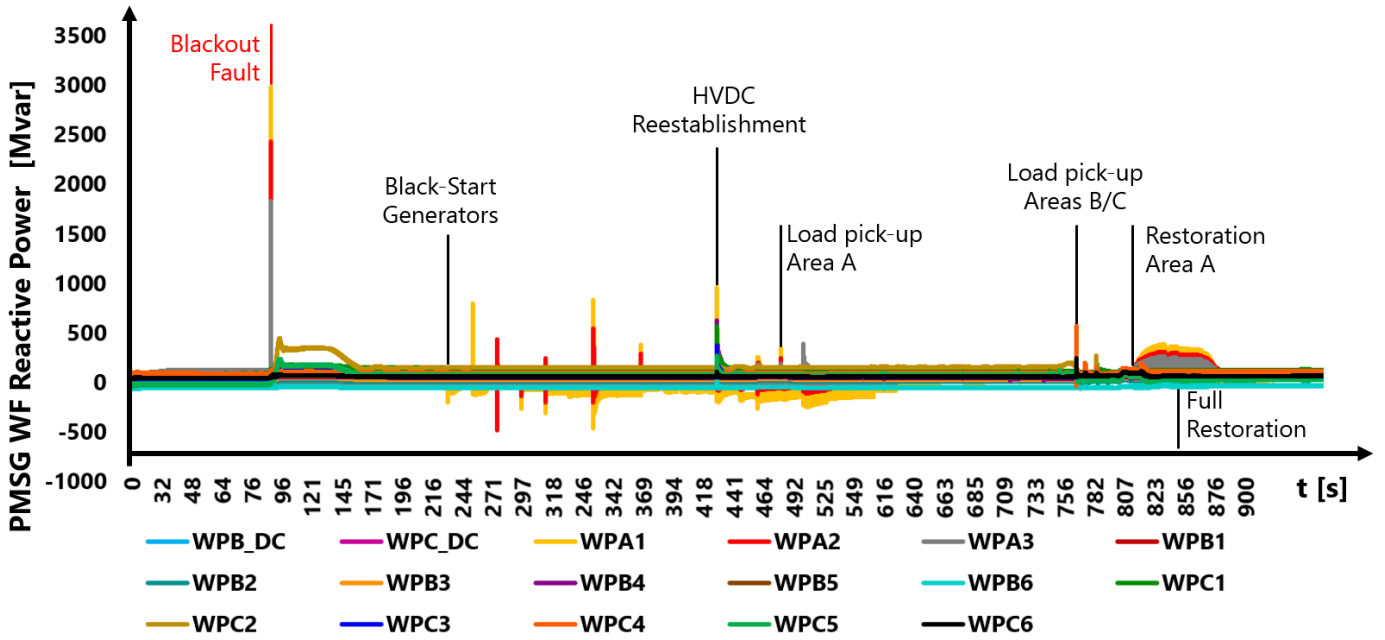


Figure 5.26.: EMT Reactive Power Plots of the Wind Power Plants before, during and after the outage and *Restoration* events.

Despite that initial better performance with just 51 Hz, in those previous simulations the frequency failed to return back to 50 Hz or at least to find a tendency towards there. Therefore, the last simulation results were placed in this Report. A possible solution for decreasing the extremely high peaks in frequency could be decreasing the proportional term values of the PI controllers inside the PLL of each WT. In contrast, this last simulation saw the undesirable ripples in the WF frequency fading after the first elements in the network were reenergised, as it can be seen in the frequency plots for the three WECS.

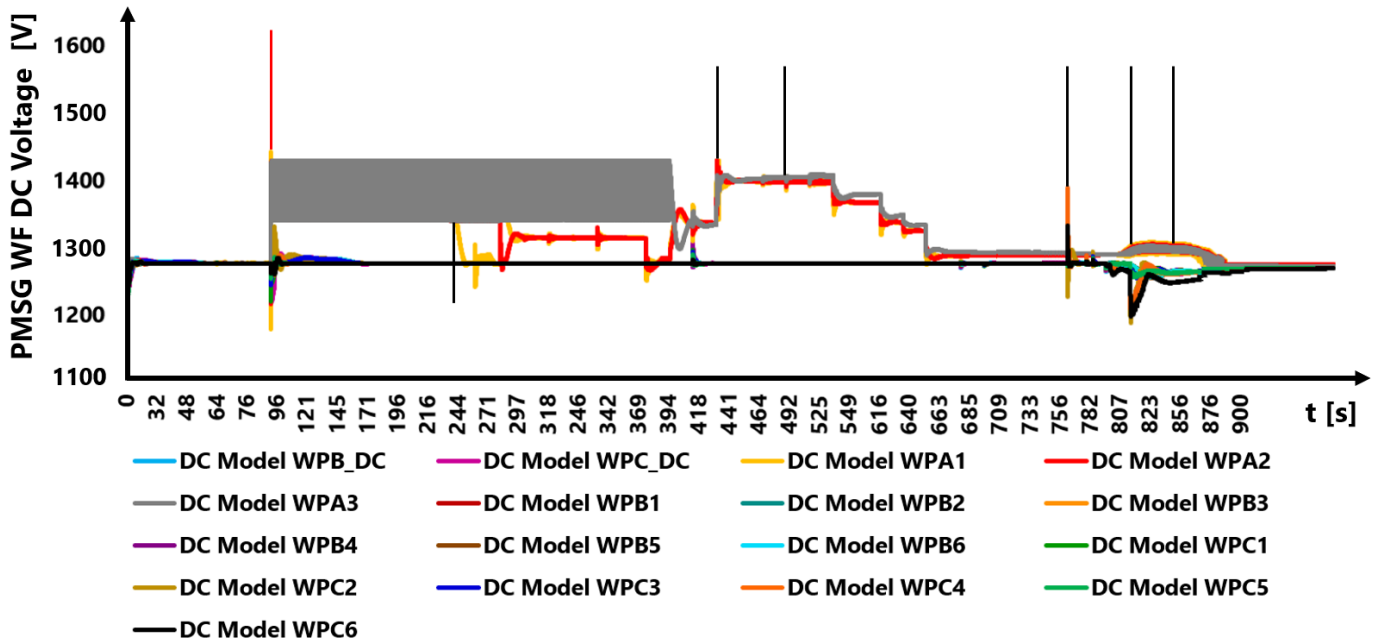


Figure 5.27.: EMT DC Voltage Plots of the Wind Power Plants before, during and after the outage and *Restoration* events.

In defiance of these undesirable effects, these aberrant oscillations in the frequency stopped at the same time

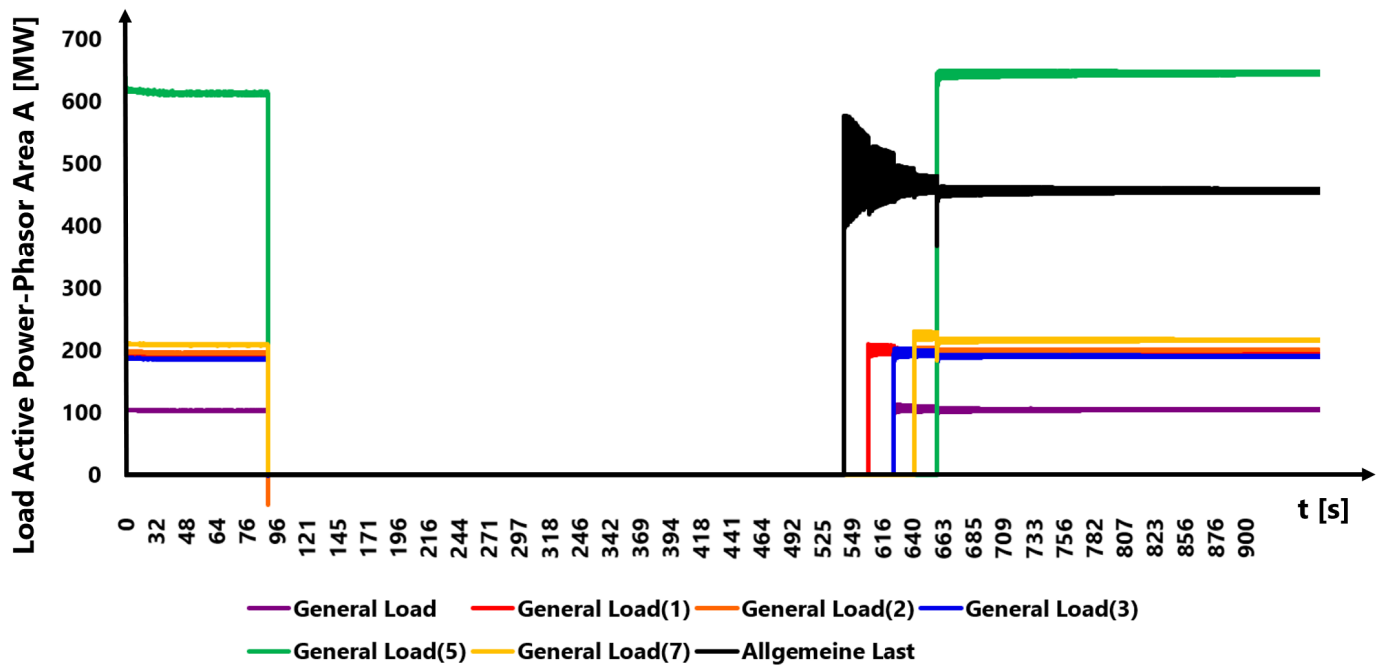


Figure 5.28.: Active Power of the busbars connected with the Loads of Area A in p. u.

the gradual process of rebuilding the grid started. It was because the implementation of the **Voltage/Reactive Power/Frequency Controller** that this successful reestablishment of the nominal delivered active power was possible.

The active and reactive power produced by the nineteen generators are plotted in Figures 5.23, 5.25 and 5.26. After the blackout and subsequent loss of generation, no transients are shown, and all generators are at zero. But when they are reenergised, violent transients arose in the hydro generator A1aG. This unit caused even more problems by going to negative values of active power.

At this moment, the mechanical net output power of this unit was zero, but in electrical terms, rather than provide power, it was sucking it up.

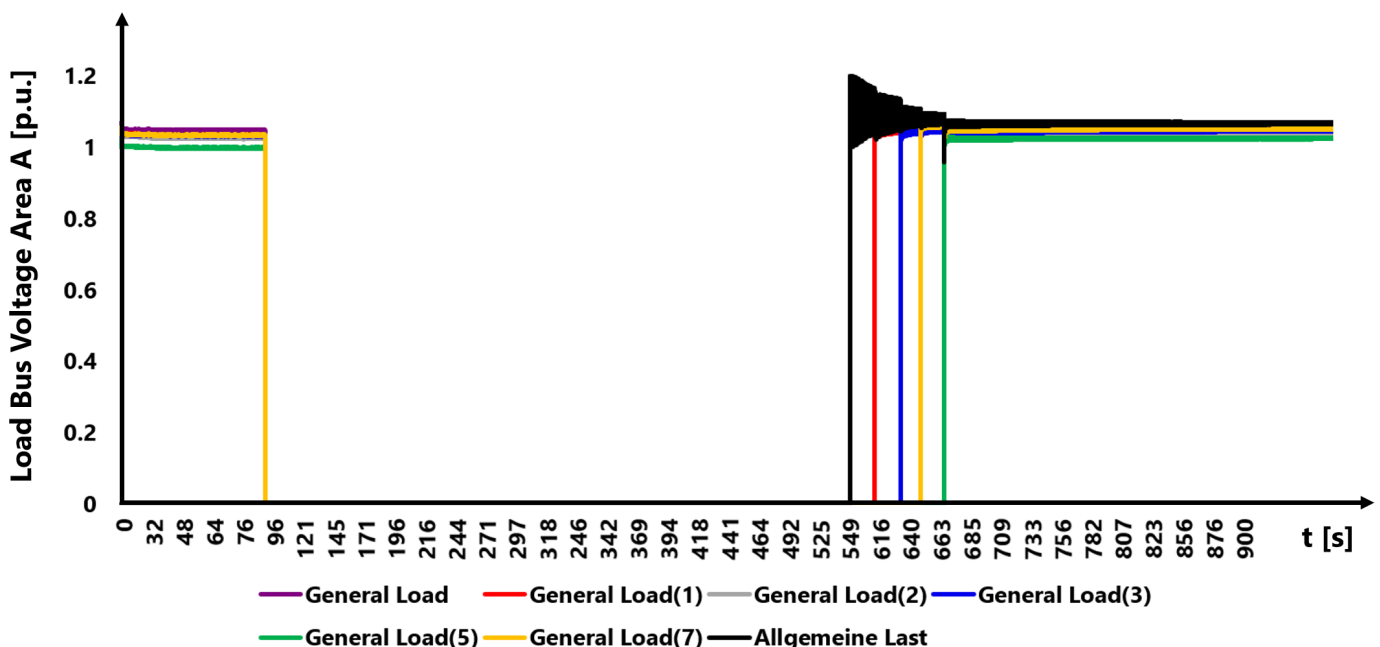


Figure 5.29.: AC Voltage of the busbars connected with the Loads of Area A in p. u.

It was until the reconnection of the transformers and loads when this unit went back to regular operation. In turn, Figure 5.25 demonstrates that the wind power plants did not come up with a similar undesirable effect. When these

units were lost their electrical active power at least remained at 0 MW. Approximately five minutes after the blackout, the load pick-up process started. From that moment, the hydro generator $A1aG$ and the WF WPA_1 , WPA_2 and WPA_3 had their output active power increasing at the same time their frequency going downwards until converging to 50 Hz. The pick-up process in *Area A* is displayed in Figures 5.28 and 5.29. In analysing the time each of the shown loads was cranked up by looking at the responses in the Frequency and Power-Phasor plots previously unveiled, it can be concluded that a converter-dominated EPS can manage any disturbance in the system and that is capable of lead a *Black-Start-Restoration Scheme*.

Although the generation units seem to struggle during the whole process, they get away with the *Restoration Goal*. The system makes sure that the load centres do not notice further disturbances after the power reestablishment, deriving in rather smooth plots for the Power-Phasor and Busbar Voltage for the Loads at *Area A*. The responses noticed in Figures 5.28 and 5.29 are almost identical to the ones from the *Restoration Scheme* led by CGU as displayed in Figures 5.8 and 5.7.

When the converters of the WECS block due to the sudden *island*, the DC voltage plots (Figure 5.27) present similar performance typical of the WT that have the *grid-following Current Injection Control*, as shown in Figure 4.5. However, with that previous control scheme the (cold) load pick-up would have been completely unsuccessful because the load *Restoration* must be slow and gradual, and this method injects an initial setpoint power regardless if the reinstalled load demand matches with this power injection setpoint; leading to an uncontrollable scenario where could derive in subsequent shutdowns [17], [19], [21]. Contrary to that performance, the **Voltage/Reactive Power/Frequency Controller** tracks accurately the demanded load as it is reintegrated to the healing EPS. This is also why the final values of active power, frequency and AC/DC voltage shown from Figures 5.24 - to - 5.29 return to their initial parameters before the blackout, demonstrating that if the new control systems are correctly applied, they can provide the necessary *grid-forming* robustness to the electric network for self-healing after a blackout.

As discussed in Subsection **Saturation/Magnetising parameters in Power Transformers and Synchronous Machines**, the magnetic/saturation factors embedded in all high-power electric elements are a decisive aspect for the success to *Black-Start* successfully an outaged network. After various EMT tests proposing different critical *restoration* paths, the only one that allows a round completion of an entire run considering the magnetising/saturation factors was based on the *Soft Energisation Method* discussed in Subsection **Measurement, Protection and Restoration Logic-Relays**.

For instance, the transformer $M_{A1a} 2T$, that is the link between generator $A1aG$ with the rest of the grid, presented severe aberrations as plot curves instead of the expected sinusoidal three-phase shapes, when another reconnection method was tested. Figure 5.30 presents the three-phase currents in the HV-side of this very transformer throughout the whole EMT simulation.

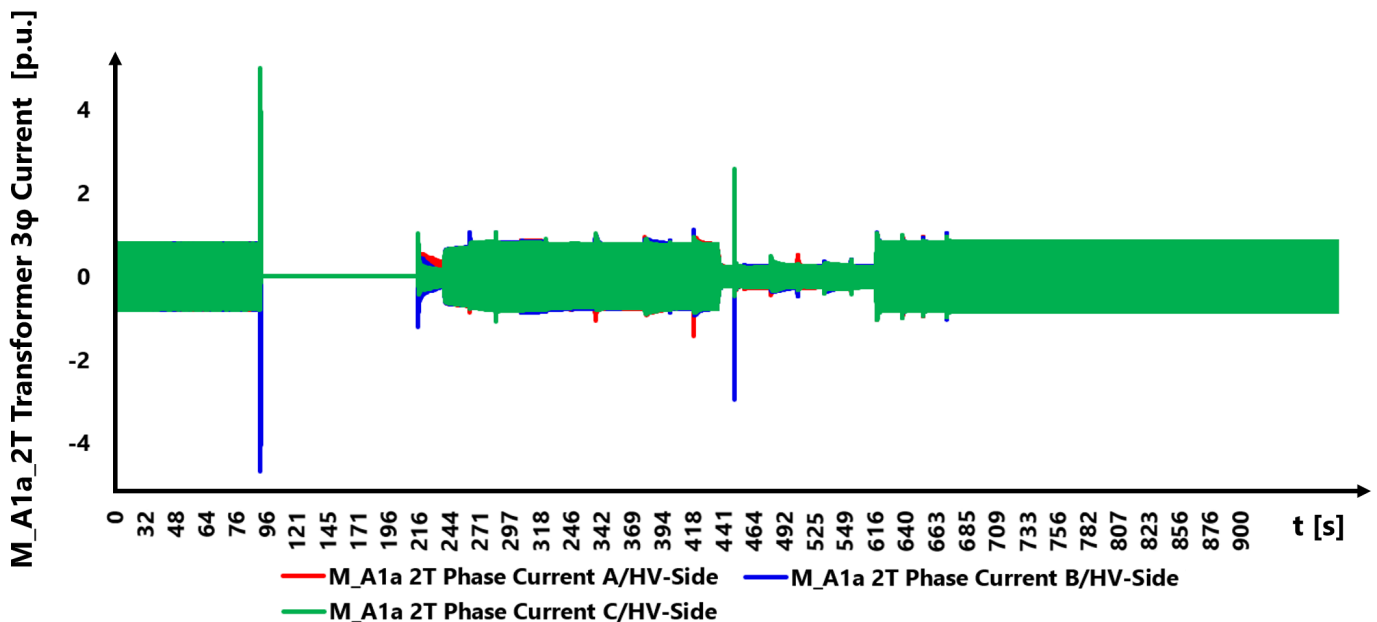


Figure 5.30.: EMT Three-phase Current of the Transformer $M_{A1a} 2T$, connected next to the Generator $A1aG$.

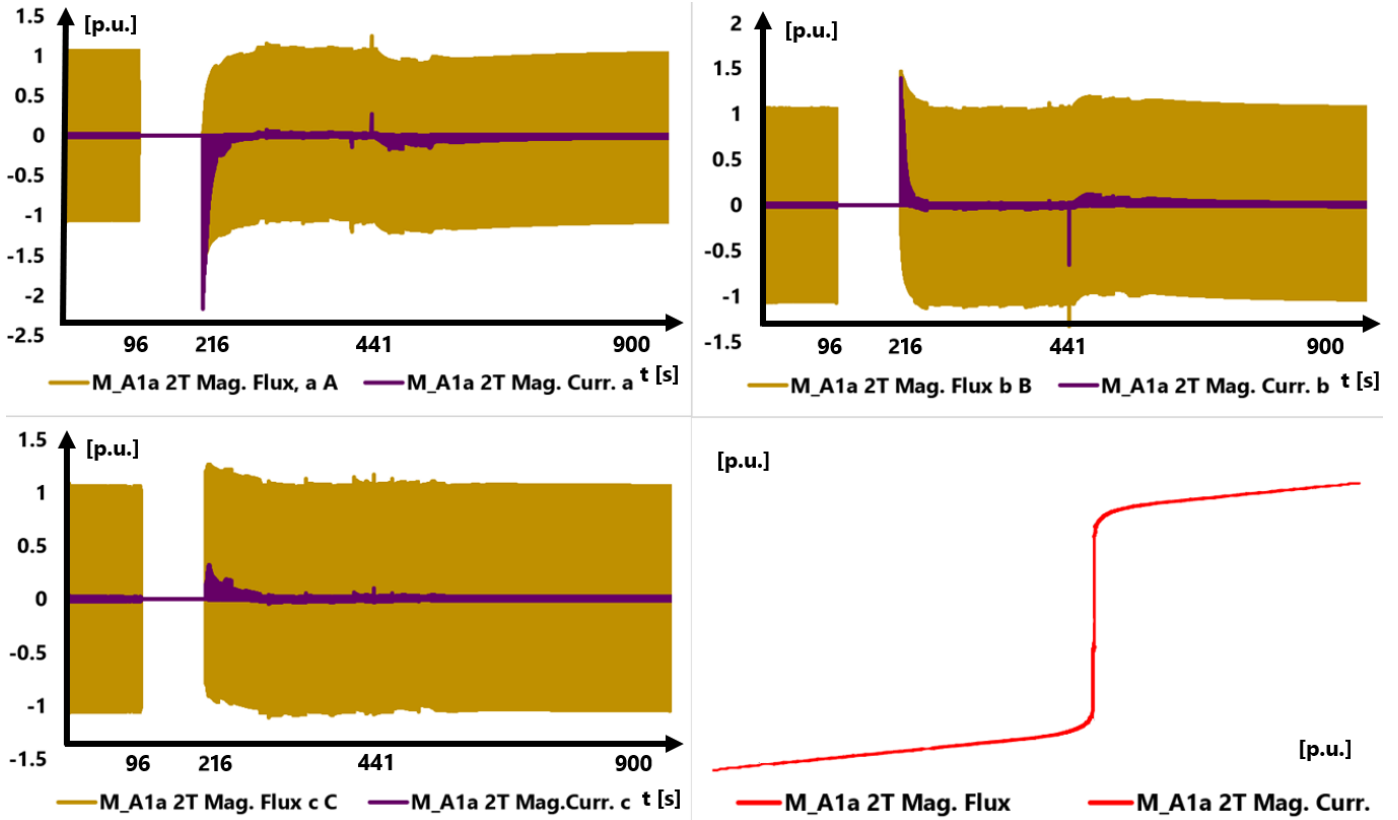


Figure 5.31.: Magnetising Flux (ϕ) vs. Magnetising Current per each phase of the Transformer $M_{A1a} 2T$.

One of the short-circuit faults that derived in the full-outage of *Area A* was located in the busbar where the Low-Voltage (LV)-side of this same transformers was connected. Then is evident why the faulty peak of current at the instant of this fault is so large (reaching 5 p. u.). Regardless the heavy fault, the combination of the *Soft Energisation* applied to the CPM Method, explained in [Section 3.3](#), prevents this transformer, along with the rest, from suffer serious damage after the blackout. In turn, the current peaks when this transformer is reconnected (216 second or 3.6 minutes in [Figure 5.30](#)) does not go far from 1.5 p. u. The next largest current peak occurs after 7.35 minutes of simulation runtime; this was caused by the closing of the HVDC Stations circuit breakers. The No-Load Current parameter of this transformer is set as 0.16 %; this makes its linear reactance to have a magnitude of 625 p. u., according to the automatic adjustments in the DPF 2-Winding Transformer Parameters [\[15\]](#). The rest of the magnetising parameters for this transformer can be observed in [Table 4.3b](#).

Considering these parameters, [Figure 5.31](#) reveals the Magnetising Flux (ϕ) vs. Magnetising Current Plots per each phase of the Transformer $M_{A1a} 2T$. An Hysteresis Loop with respect to the same parameters per each phase can also be observed. Usually, as long as the magnetising current does not go beyond 4 p. u. or does not hold for a significant amount of time (in seconds) values above 1.1 p. u., this transformer should be out of danger [\[7\]](#), [\[27\]](#). On that logic, the maximum peak of magnetising current for the $M_{A1a} 2T$ transformer occurs when this element is reenergised and it barely goes beyond (-)2 p. u. This is the most critical event for this element; as for the remaining restoration events, they only cause small-scale disturbances, and by the time the simulation is about to reach its end, the magnetising plots tend to go back to their initial values.

[Figure 5.21](#) was placed in this Chapter in order to stress the emerging necessity of include additional protection systems in the *PST 16 Benchmark System Grid*. [Figure 5.21](#) showed the effect that occurs on some of the transformers in the *Areas B* and *C*. The strength of an EPS is defined as the ability of the system to maintain its voltage during the injection of reactive power [\[82\]](#). Strong power networks experience less voltage change following an injection of reactive power. SCR, defined as the ratio of the interconnected short circuit MVA in the grid (before connecting the generator) to the MW size of the interconnecting generator [\[82\]](#), has been utilised to quantify the strength of the EPS with respect to the interconnecting generator. The lower the SCR, the weaker the EPS would be [\[82\]](#). Weak systems become more troublesome when they have more RES penetration, due to the fast response of the PEI and the controllers that regulate them. As it was explained in Subsection [Wind Energy Conversion Systems](#), this

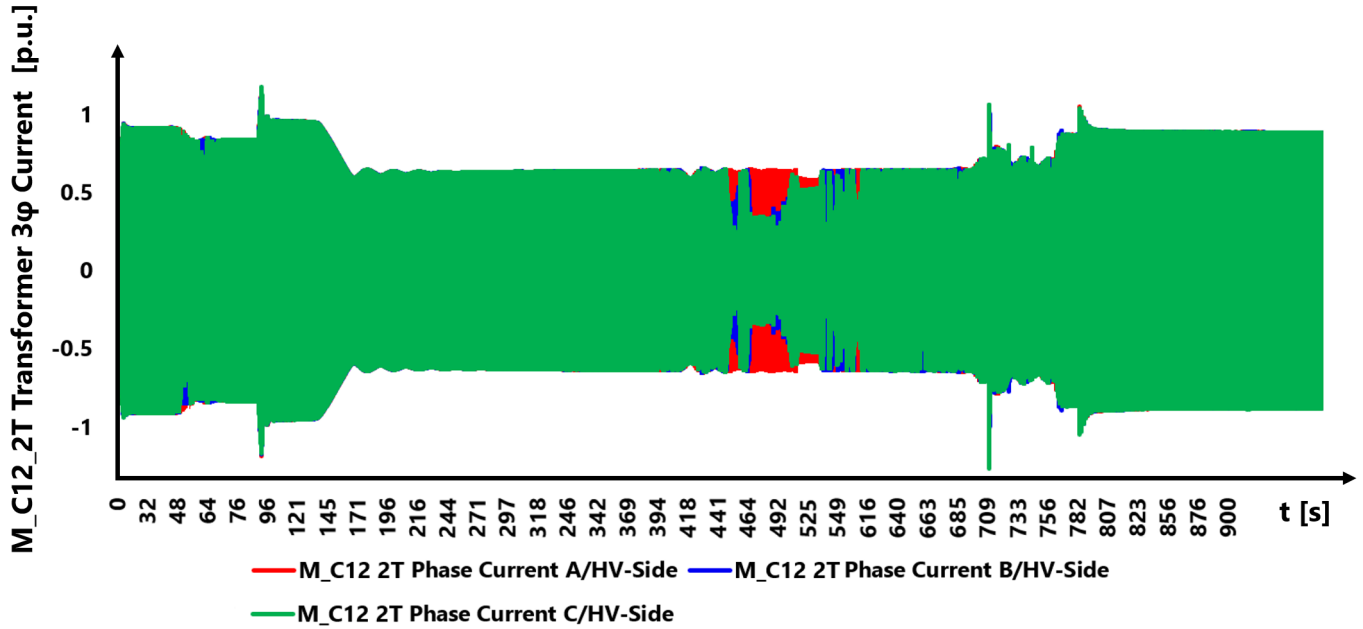


Figure 5.32.: EMT Three-phase Current of the Transformer M_A1a 2T, connected next to the Generator $A1aG$.

is due to the fact that the voltage/reactive power control loops within these electronic-based generation units are capable of almost instantaneous reactive power injection in response to any voltage change at the PCC. Fast reactive power injection/absorption to a weak grid, characterised by high voltage/reactive power sensitivity, sometimes translate to undamped voltage oscillations, and, if the network is very large and composed of many elements, there are more possibilities to have something operating wrongfully. Therefore, apart from the system strength, the speed of the voltage controllers associated with the RES has a substantial impact on the dynamic response of the renewable source and the stability of the interconnected grid [82]. While reducing the voltage controller gain would slow down the voltage controller response associated with the RES and could mitigate the voltage oscillations, it would also slow down the post-contingency voltage recovery.

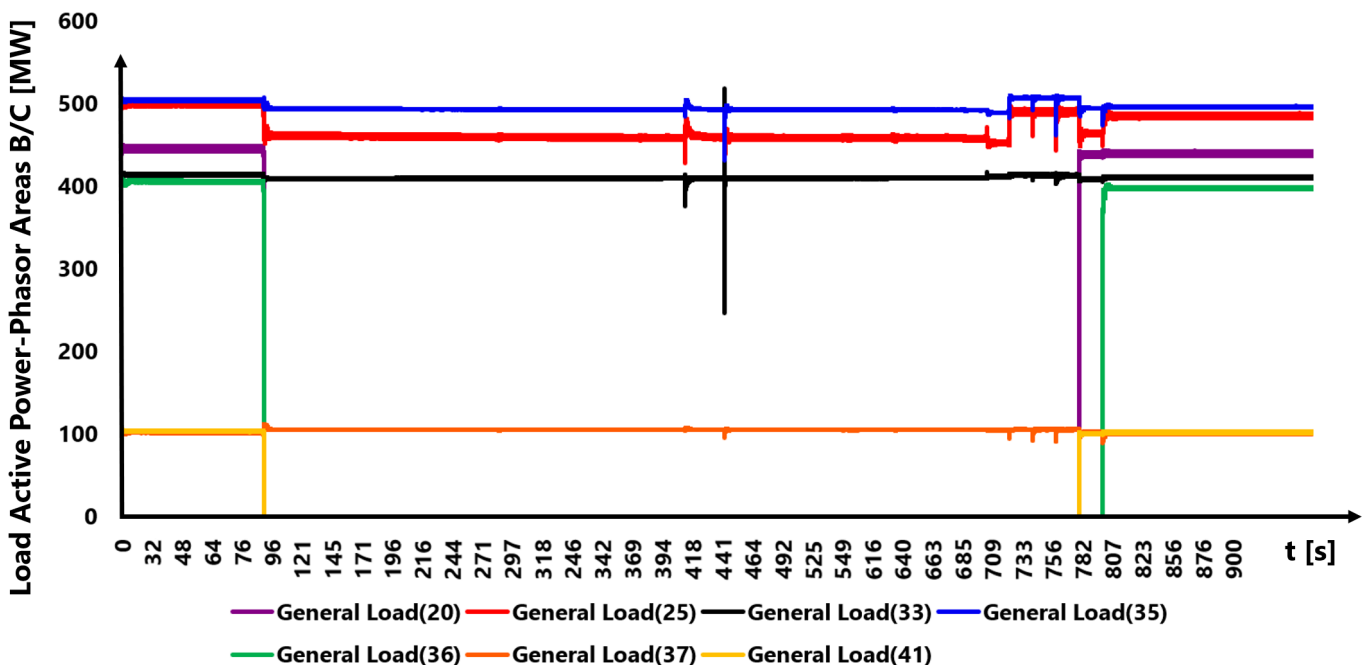


Figure 5.33.: Active Power of the busbars connected with the Loads of Areas B and C in p. u.

The balance between the post-fault transient voltage recovery and a stable response is critical to grid integration

studies for renewable sources connecting to weaker portions of the grid. The simulation results with 90% wind penetration conclude that the faster dynamics of the WECS installed in the grid breeds the consequence of uncontrollable currents if a massive fault takes place, such as a blackout.

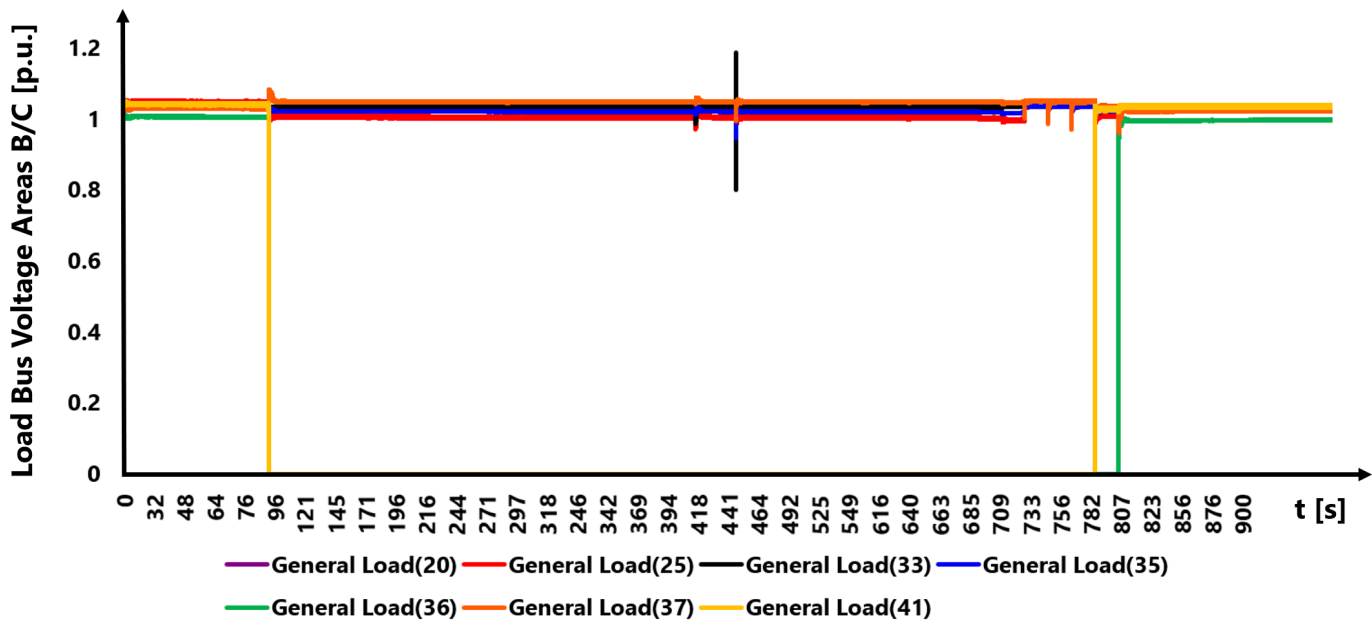


Figure 5.34.: AC Voltage of the busbars connected with the Loads of *Areas B* and *C* in p. u.

Figure 5.32 exhibits once again the three-phase current of on the HV-side of the *M_A1a 2T* transformer, but this time the surge increase of current has been blocked by the **Protection SG C12G** System, as appointed in the DPF Common Model of the *C12G* coal-fired generator.

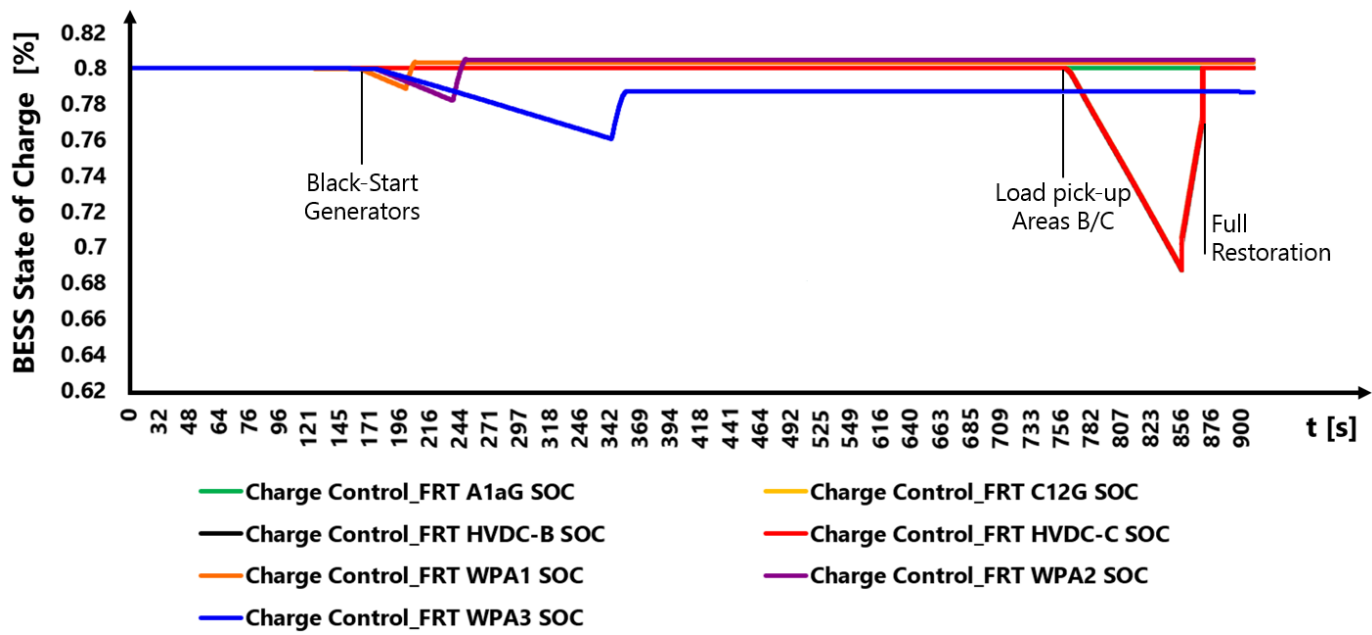


Figure 5.35.: State of Charge of all the BESS-Storage Units before, during and after the outage and Restoration events.

When the fault that derives in the outage takes place at 90.4 seconds, an upper/lower peak can be noticed in Figure 5.32. This behaviour is exactly the same effect displayed in Figure 5.21, but now, the aforementioned Protection System acts as an **Overcurrent Relay**, tripping off elements and loads in order to alleviate the excessive current flowing in this transformer due to the loss of generation in *Area A*, a direct aftereffect from the generator *C12G* operating above its nominal capacity. After the programmed outage has done, this protection system also contains a program that *Black-Starts* the outaged areas. In this same Figure 5.32 can be noticed a sudden decrease of

the HV-phases *B* and *C* in the transformer *M_A1a 2T*. This occurs after the HVDC Stations are brought back online. As this happens before of the load pick-up process in *Area A*, the other areas can now feel the reenergisation stage, exemplified as transients in the HV-phases on this transformer.

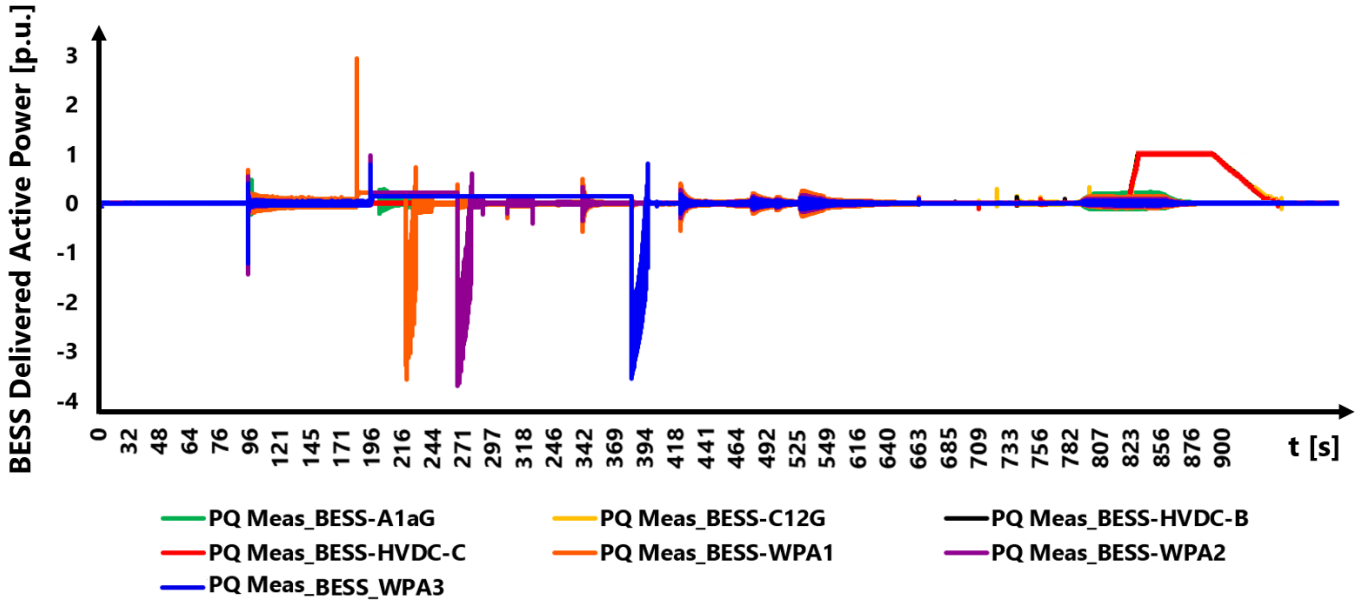


Figure 5.36.: Active Power of all the BESS-Storage Units before, during and after the outage and *Restoration* events.

The additional **Protection and Restoration System** works with a current measurement instrument (StaImea*) that meters the current flow in the transformer that is going to be protected. Whenever this metering instrument detects an overcurrent, it triggers an algorithm that trips off determined circuits in order to alleviate the overload. The code of this **Protection and Restoration System** is unveiled in [Section E.2](#). In this case study, this protection system works coordinately with the other four **Protection and Restoration Systems** in order to not sabotage their collective goal of *restore* the network. This element is the one that manages the reenergisation of the lost circuits in *Areas B* and *C*, as it is seen in Figures [5.33](#) and [5.34](#). These Figures display only some of the total amount of loads that these two areas contain; in this case only the General Loads (20), (41) and (36) went offline to later get energised again. The rest of the loads and elements tripped-off do not appear in these plots but they were successfully reenergised too.

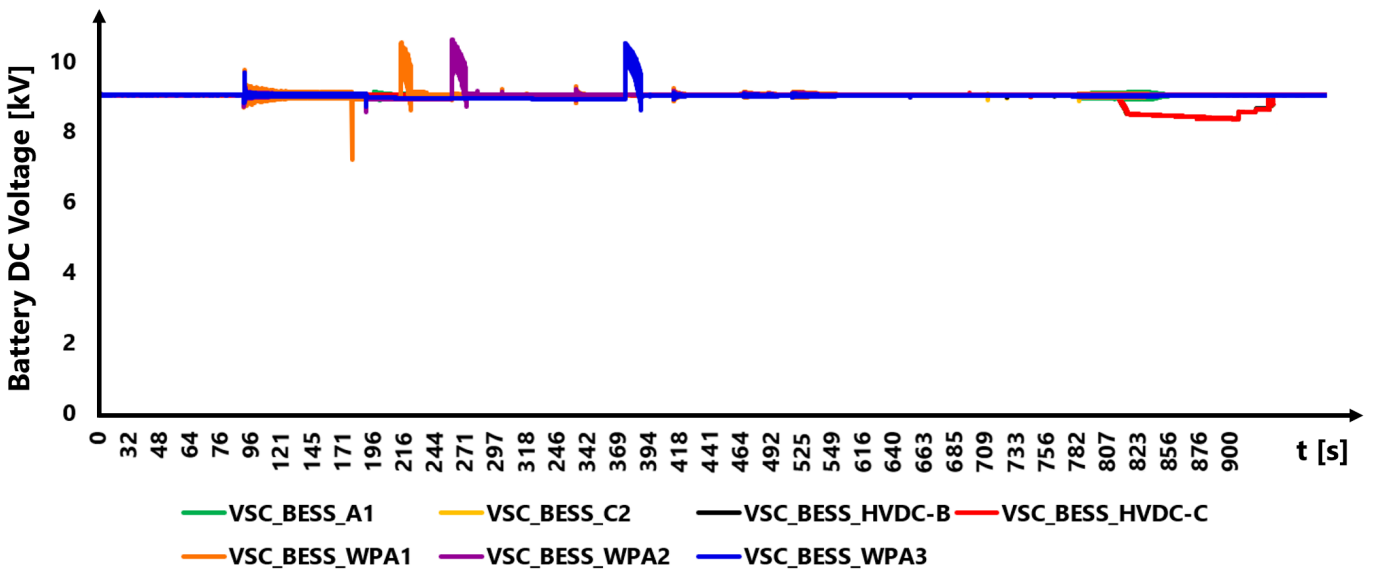


Figure 5.37.: DC Voltage of all the Batteries before, during and after the outage and *Restoration* events.

Figures [5.35](#), [5.36](#) and [5.37](#) represent the performance outcome of the BESS-Storage Units in terms of the State of

Charge (SOC), dispatched active power and DC voltage, respectively. In total, seven battery banks were installed throughout the *PST 16 Benchmark System Network*.

The BESS Units *WPA₁*, *WPA₂* and *WPA₃* were pivotal for the successful *Black-Start* for the WECS that hold the same names, because they provide the essential function of exciting the terminal voltage of the PMSG. Figure 5.35 demonstrates this when the SOC plots suffer steep discharges from the moment each wind power plant was brought back to reconnection. In order to these wind power stations could produce again, first they have to be *Black-Started* themselves. As the BESS units provided with the current necessary to get excitation voltage in their PMSG, the storage units went discharged.

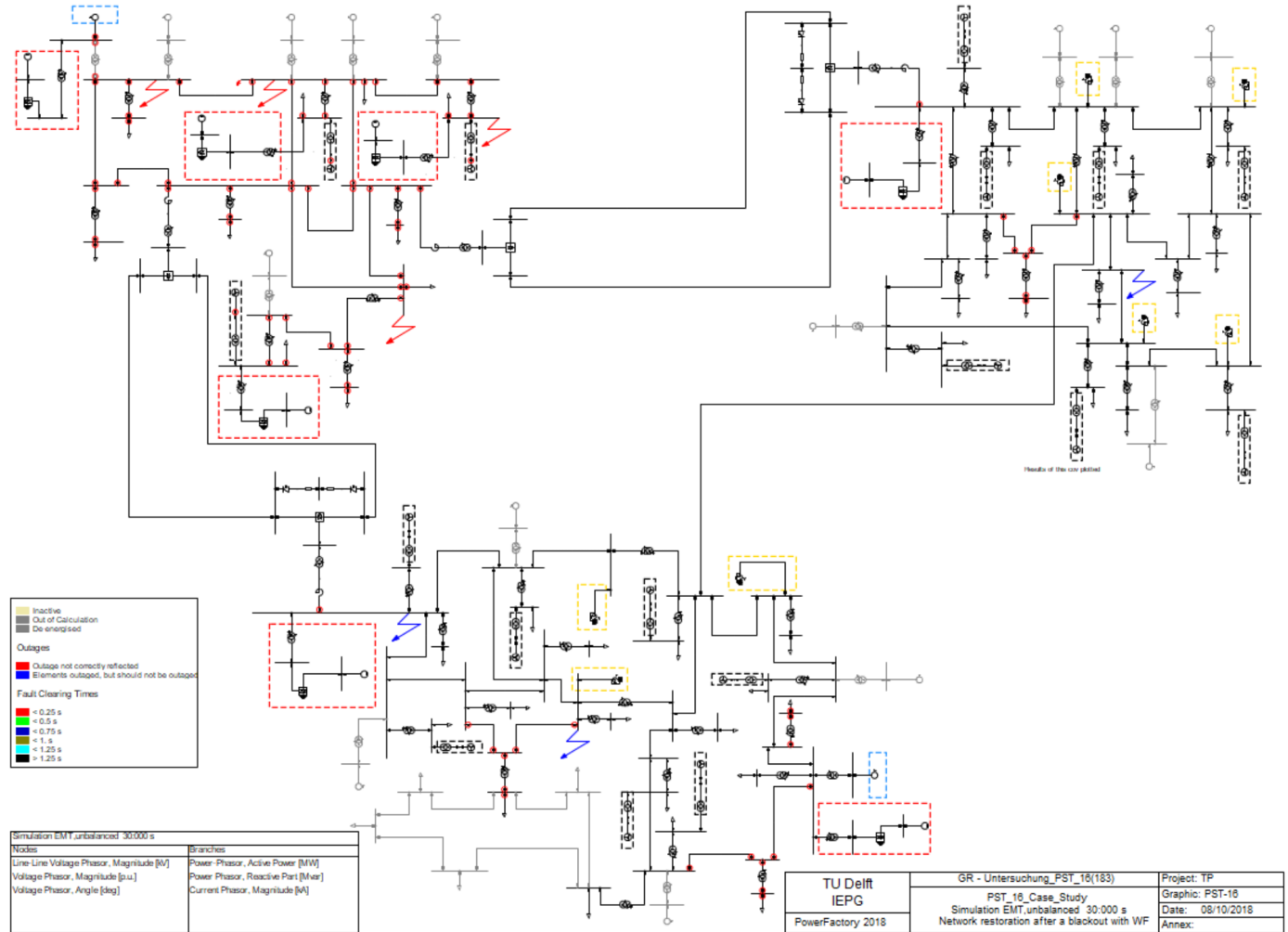


Figure 5.38.: *PST Benchmark System Network* with 90% Wind Power after the finalisation of the EMT Simulation.

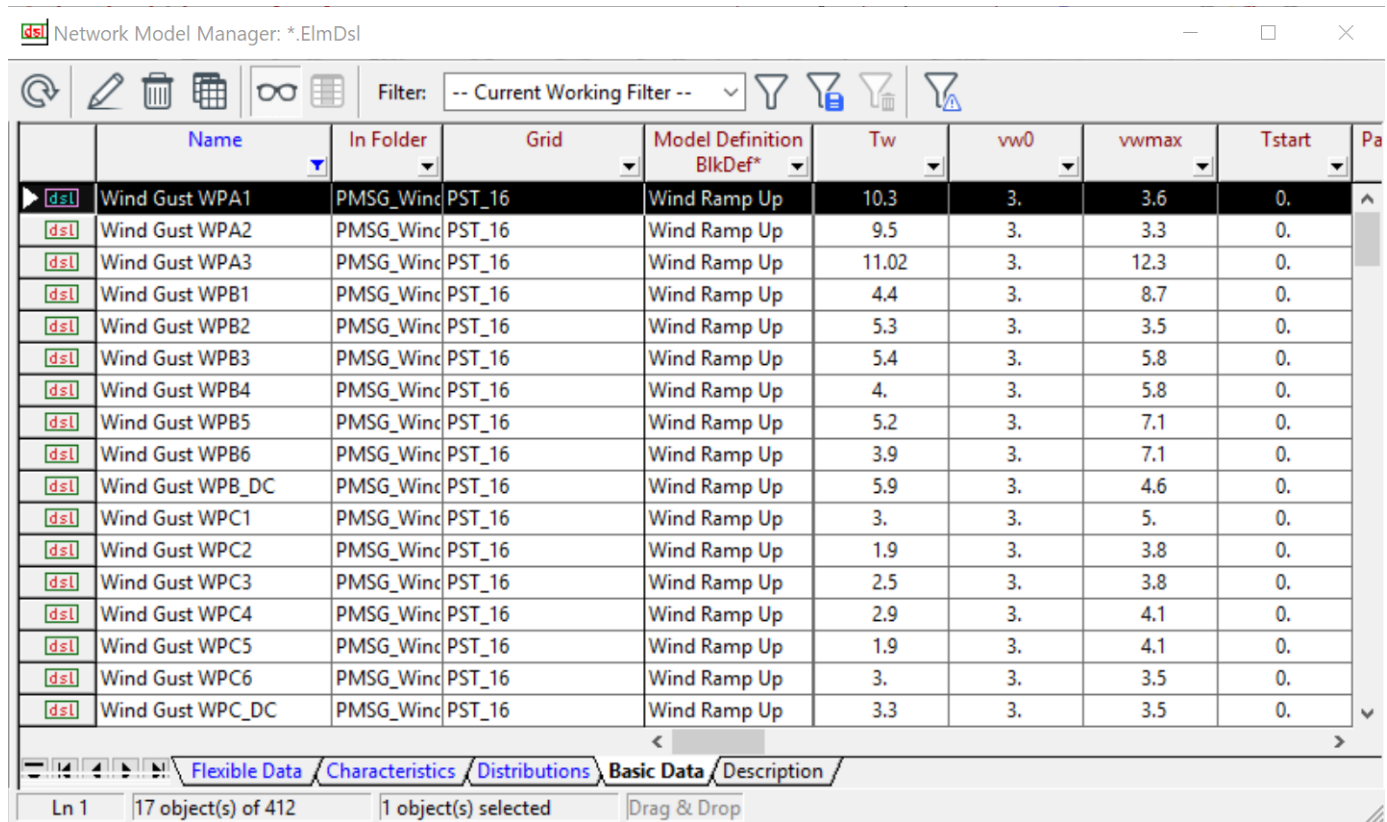
Other two elements provide the same service for the omnipresent CGU units, and the last two provide mainly the AS of frequency support by providing extra-power to the units already passing over their nominal capacities. Comparing Figures 5.35, 5.36 and 5.37 with the rest representing the measured behaviours for the *Restoration* assessment, a performance tendency can be found. Every time an event bringing big consequences onto the grid arises is reflected on each of these plots. The additional support of the storage units helps to ease the strikes that imply reconnecting high-power elements back to the network and damp the consecutive oscillations. For instance, the BESS were crucial as well for the successful completion of the pick-up of the elements and loads unserved in the *Areas B* and *C*, as it can be seen in the last three minutes of the EMT simulation. The curves plotting some of the BESS parameters coincide with the time of the load pick-up in *Areas B* and *C*. During these last minutes, the amount of auxiliary power the BESS provided was considerably big, to the point of decreasing their nominal DC voltage to almost 8 kV, while the battery reached the 70% charging status. Because of the use of PWM converters as the interface to the grid, this AS is conveniently fast. After the EMT Simulation with 90% Wind Penetration has finalised, the *PST Benchmark System Network* now fully restored and all its tripped-off circuits, elements and loads are brought back to the grid. Figure 5.38 exposes the overview of this EPS. The red dots in 5.20 represent the now-closed circuit breakers that have

been opened by the protection relays by order of the **Protection and Restoration Scheme**. Compared to Figure 5.20, Figure 5.38 does not have any previously tripped-off elements sketched in gray colour anymore. This means all the previously lost elements of the grid were taken back to energisation.

5.6 PST 16 BENCHMARK SYSTEM NETWORK (90% WF) EMT OUTAGE FOLLOWED BY RESTORATION WITH LOW WIND

As it was made clear in Subsection **WT Aerodynamics and Mechanical Drivetrain**, regardless of how efficient and marvellous the *grid-forming* **Voltage/Reactive Power/Frequency Controllers** are, wind is still the energy source. Therefore, if the availability of wind source and electricity consumption do not match, the control systems to make WT *Black-Start* capable do not matter.

Because of this inarguable fact, it was decided to extend the WECS with the mechanical and aerodynamic models that will give the DSL **DC Circuit Model** the reference of power that the WF ought to inject to the grid based on the atmospheric conditions and the real-time status of the network.



	Name	In Folder	Grid	Model Definition	Tw	vw0	vwmmax	Tstart	Pa
Wind Gust WPA1	Wind Gust WPA1	PMSG_Wind	PST_16	Wind Ramp Up	10.3	3.	3.6	0.	
Wind Gust WPA2	Wind Gust WPA2	PMSG_Wind	PST_16	Wind Ramp Up	9.5	3.	3.3	0.	
Wind Gust WPA3	Wind Gust WPA3	PMSG_Wind	PST_16	Wind Ramp Up	11.02	3.	12.3	0.	
Wind Gust WPB1	Wind Gust WPB1	PMSG_Wind	PST_16	Wind Ramp Up	4.4	3.	8.7	0.	
Wind Gust WPB2	Wind Gust WPB2	PMSG_Wind	PST_16	Wind Ramp Up	5.3	3.	3.5	0.	
Wind Gust WPB3	Wind Gust WPB3	PMSG_Wind	PST_16	Wind Ramp Up	5.4	3.	5.8	0.	
Wind Gust WPB4	Wind Gust WPB4	PMSG_Wind	PST_16	Wind Ramp Up	4.	3.	5.8	0.	
Wind Gust WPB5	Wind Gust WPB5	PMSG_Wind	PST_16	Wind Ramp Up	5.2	3.	7.1	0.	
Wind Gust WPB6	Wind Gust WPB6	PMSG_Wind	PST_16	Wind Ramp Up	3.9	3.	7.1	0.	
Wind Gust WPB_DC	Wind Gust WPB_DC	PMSG_Wind	PST_16	Wind Ramp Up	5.9	3.	4.6	0.	
Wind Gust WPC1	Wind Gust WPC1	PMSG_Wind	PST_16	Wind Ramp Up	3.	3.	5.	0.	
Wind Gust WPC2	Wind Gust WPC2	PMSG_Wind	PST_16	Wind Ramp Up	1.9	3.	3.8	0.	
Wind Gust WPC3	Wind Gust WPC3	PMSG_Wind	PST_16	Wind Ramp Up	2.5	3.	3.8	0.	
Wind Gust WPC4	Wind Gust WPC4	PMSG_Wind	PST_16	Wind Ramp Up	2.9	3.	4.1	0.	
Wind Gust WPC5	Wind Gust WPC5	PMSG_Wind	PST_16	Wind Ramp Up	1.9	3.	4.1	0.	
Wind Gust WPC6	Wind Gust WPC6	PMSG_Wind	PST_16	Wind Ramp Up	3.	3.	3.5	0.	
Wind Gust WPC_DC	Wind Gust WPC_DC	PMSG_Wind	PST_16	Wind Ramp Up	3.3	3.	3.5	0.	

Table 5.6.: Settings for the different **Wind Gust** Common Models.

One of the fundamental conclusions that can be confirmed with authority after having developed this MSc Thesis Project from the beginning to the end of the writing of this report is that planning, developing and executing a *Black-Start* with CGU is an extremely complicated task already. Then, raising the level of complexity to be able to mould the WF in such a way that their control systems could do the same task was another investigation equally difficult.

The control systems that were developed in this Research Project are quite complex and contain several loops that work together at the same time. If besides all these factors, an extra variable is added that implies unfavourable atmospheric conditions, *a priori*, without the need to do an EMT simulation, it can almost be concluded that it is very unlikely that the conjunct BS-NR Strategy could be done.

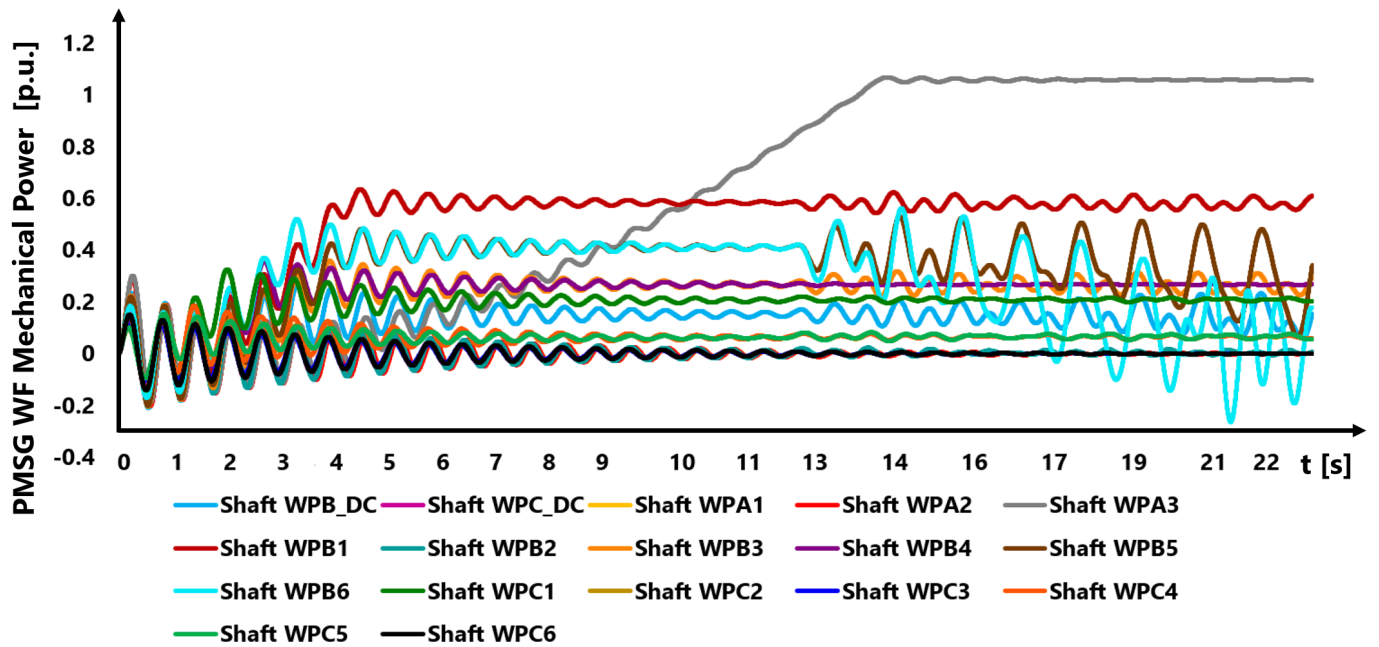


Figure 5.39.: EMT Mechanical Power Plots of the Wind Power Plants considering substandard wind speed conditions.

Nonetheless, to avoid leaving that question unchecked, an EMT simulation was also run considering that scenario. [Table 5.6](#) displays all the DSL **Wind Speed (Wind Gust)** Block Definitions, one per each WF placed in the network. There, T_W stands for the change of the wind speed, in seconds, vw_0 the initial wind speed, in m/s, vw_{MAX} the wind speed increase, in m/s, and T_{Start} is the time when the wind gust start to arise. In the previous case study, with favourable meteorological conditions, the vw_{MAX} column was sorting parameters from 12 - to - 17 m/s. In contrast, [Table 5.6](#) is now sorting lower top wind speeds. The average top wind speed according to these new parameters is just 5.27 m/s; this is barely higher than the standard *cut-in* speed for most manufactured WT.

[Figure 5.39](#) presents the outcome performance of wind power plants in terms of mechanical power, which in turn is a function of the available wind resources. This signal comes from the DSL **Shaft** Block Definition ([Figure B.4](#)). The mechanical power form the WF WPA3 is the only one that delivers as much power as in the previous operational scenario with splendid wind resource. It serves as a reference to what is to be a desired mechanical power output against the results drawn due to poor wind conditions. In turn, the rest of the WF present unacceptable performances, as none of the rest can be considered as a reliable generation source anymore. Some of the units that do not raise enough mechanical power at least see their outputs damped, however, there are several units that not only are not able to provide enough power but also suffer from abnormal oscillations that, far from being damped with the passage of time, they become more aggravated.

As it was demonstrated in Subsection [WECS Mechanical Dynamic Performance](#), there are parallelisms between the behaviour of the mechanical power collected by a WECS and its own generator frequency and speed outcome performances. Therefore, the bad performance in the collected mechanical power does not stop there; similar results would be seen in the plots of generator frequency and speed (these frequency and speed plots for the low-wind operational scenario were not included in this Report). The oscillations that grow in peak can then put in risk the physical integrity of the WT, to the point of completely breaking apart the PMSG.

With this test along with the previous one with good atmospheric conditions, it can be concluded that it is completely realistic and doable to perform a *Restoration plan* with OffWF if there are suitable atmospheric conditions in the location the power stations are installed. For that, it is advocated to go conservative and not to put at risk the integrity of an already outaged network by trying to execute a BS-NR Operation if there are not acceptable climatic conditions. The, it can be considered riskless to perform such a scheme if wind availability with speeds from 11 - to - 17 m/s are available. If the wind resource is available (and even better, abundant) the matter whether a WF-BESS association could restore an outaged EPS depends entirely on the control systems that regulate the wind power plant-storage system.

6 CONCLUSIONS

The results of the EMT Simulations performed in DPF conclude that converter-dominated generation can have *Grid-Forming* and *Black-Start Capability* if their control systems are modified properly. With the Simulations Results it is demonstrated that the proposed **Voltage/Power/Frequency Control** can perfectly regulate large-scale EPS, regardless if that network contains high-share of RES. In case of extremely heavy disturbances that even derive in a blackout and/or unintended *islanding operation* arise, the **Voltage/Power/Frequency Control** can stabilise and, if necessary, *Restore* the entire grid and bring it back to energisation after prolonged periods of outage, even if the large-scaled EPS has 90% of its total generation capacity as RES-type, specifically Wind Power Plants.

Due to the great amount of power that can be generated from the strong and constant supply of wind, large-scale Offshore Wind Farms are the perfect candidate for exploit these promising capabilities for improving the SOS for the EPSF. Yet, converter-interfaced generation, such as Wind Power, results in fundamental changes in EPS

operation, dynamics, control and protection. Therefore, if it is true that the EPS have the goal to continuously integrate converter-based generation in the coming years, then this means that WT manufacturers will have to modify their manufacturing designs and process in order implement these *Grid-Forming* control systems for regulating the new WT installed in the EPSF.

Some of the main findings after the completion of this MSc Thesis Project are itemised below:

- **Voltage/Power/Frequency Control** can be interpreted as the PEI-version of what an AVR is to a CGU synchronous generator. This means that in order to apply the proposed *Grid-Forming* control system onto converter-based generation, the modifications manufacturers ought to execute must resemble up to some extent the control systems that comprise an AVR, but at the same time, it must be also capable to control the faster dynamics that VSC converters involve.
- The proposed **Voltage/Power/Frequency Control** Systems, however, are not the only elements that a network with high penetration of renewables requires if the latter undergoes a massive shutdown. In order to restore an outaged grid, it is also required to calculate the best *Critical Restoration* path that allows the reenergisation of the lost elements (transformers, overhead lines, cables, compensation, loads, generation, etc.), without damaging them during the process.

6.1 ANSWERS FOR RESEARCH QUESTIONS

Once the results of the simulations have been obtained and analysed, it is granted the authority to answer the research questions that were stipulated at the beginning of this very MSc Thesis Report, specifically the questions declared in [Chapter 2](#).

1. **Based on Black Start/Network Restoration TSO sequences, how to model a protection system for restoring an outaged network?**

With the **Protection and Restoration System** developed during the evolution of this Research. One of the decisive problems with WT regarding *Restoration* is the lack of extremely precise control over power output. Any unexpected change in output can blackout a small *island* during the *Black-Start* plans. The key is managing and tightly ensuring the load and generation balance. Reactive power plays a big part in voltage management. The philosophy behind these protection units is based on the CPM ([Section 3.3](#)) and the *Soft-Energisation* Method (Subsection [Measurement, Protection and Restoration Logic-Relays](#)). The CPM is composed of three stages:

- a) **Preparation:** Definition of the immediate critical-time actions after the outage and that defines too the ideal restoration path based on the particular characteristics that composed the faulted network.
- b) **Black-Start:** Critical elements and loads for cranking power. The optimisation algorithm is put to practice here, by reenergising just the vital elements that secure a smooth *Black-Start*. The application of the *Soft Energisation Method* suits perfectly in this stage.

c) **Network Restoration:** (Cold) pick-up of all remaining elements and loads. When the grid-rebuilding operation has reached this point, the grid is now stronger than when the blackout just took place. Now it is possible to reenergise loads with relatively low risk of rolling back to further risks of a blackout.

This method can be summarised as an optimisation problem concerning pathfinding, and selection of key resources and key loads to be picked up. Here it is developed a strategy for *restoring* grid, after a *post-mortem* study. Proper scheduling and coordination between the responsible parties and different actions are fully required, as otherwise further errors would hinder the rebuild strategy. The **Protection and Restoration System** connects all non-energised network components (overhead lines, cables, and transformers) first connected via their substations (a so-called dead bus bar network configuration) and to a power plant without activated voltage excitation. Once the network is partially restored, then the terminal voltage of the BSU are slowly increased according to how many elements are yet to be restored. The slow-voltage increment is thought to avoid transformer saturation. As a result, all grid components are brought back to gradual energisation and so preventing from transient oscillations, reduction in stress in the network elements and substations.

2. What are the necessary modifications to extend the WT and BESS models used in stability studies for Black Start/Network Restoration simulation?

The existing VSC current control scheme can works as the base frame of the new **Voltage/Power/Frequency Control**. The modifications the old control scheme need to go through are the removal of the Integral term of its PI controller, and the shift placement of the Proportional part to the output terminal of the controller to be compared against a current-damping controller composed by washout filters that damp overcurrents that only take place during transient periods. The feedforward terms of the old system are kept, and active power control is performed using DC voltage as the setpoint controller. The **Voltage/Power/Frequency Control** contains two main control loop channels that calculate the inverter voltage signals $v_{GSC,d}$ and $v_{GSC,q}$ which in turn can be interpreted as the active/reactive power that the electrical network demands based on their needs measured in real time. Moreover, the controller contains other control loops for multiple operation modes:

- A hierarchical scheme based on a slow/global reactive power controller with PI characteristic and a fast/local voltage controller with a proportional characteristic. This first approach is based on a hierarchical control concept, in which this upper-level slow-acting controller tracks setpoint changes dictated by systemwide exigencies. The first part is designed to stabilise the system when relatively lethargic transients take place, while the downstream section of this loop was designed for sudden events demanding faster responses.
- An overfrequency emergency controller that decreases the power as fast as necessary in order to stop rapidly-increasing frequencies. This loop also has the capability to adapt to the feed-in power during and following short circuits in line with the variation of the frequency in the EPS. This loop also can operate to mitigate underfrequency deviations by then setting a command to the PMSG for increasing the generated power.
- A voltage-dependent active power reduction (VDAPR) that adjusts the power injection capability of the converter based on the terminal voltage of the inverter that makes contact with the external power network. Therefore, if a major fault occurs, this loop completely prevents the converter from injecting current to the grid.

Additionally, simulations proved that in order to be *Black-Start Capable*, the WF need to have an independent small-scale power plant to trigger their excitation voltage in their terminals. BESS-Storage Units were coupled with the WF located in the outaged area in order to provide them current for the excitation voltage. Coupling a WF with storage allows the associated unit to act as a BSU. The battery can smooth the plant output provided that the WECS is never loaded near 100%.

3. Considering the theoretical analysis and the research results, is it possible for WF BESS and PEC to restore a network during different atmospheric conditions?

Assuming that the WF were already equipped with the new **Voltage/Power/Frequency Controllers**, it is completely realistic and doable to perform a *Restoration* plan if there are suitable atmospheric conditions in the zone the WF are installed. Abundant wind availability with speeds from 11 - to - 17 m/s are enough for the wind power plants to collect the necessary power they need to operate properly. If the wind resource is available (and even better, abundant) the matter whether a WF-BESS association could restore an outaged EPS depends entirely on the control systems that regulate the wind power plant-storage system.

If, however, the wind source is scarce, that is another story. Answering the third research question for regarding the low-wind conditions is quite straightforward. Reason says should be improbable the successful *Restoration* of an outaged network ruled by WF located in a place where at that moment the meteorological conditions

are not favourable. In principle, RES with scarce sources are not useful for a *Black-Start* Operation. In order to successfully complete a *Network Restoration* it is vital to perfectly match generation and load in an unstable *island*. A *Restoration* operation is already a quite difficult issue on its own. Having scarce resources of wind would just magnify the already gargantuan challenges that the grid may face; on the contrary, low resources, or resources that cannot be controlled would lead to *island* collapse, can reverse the *Black-Start* progress. Furthermore, the outcome of the EMT Simulations under poor wind resources gave reason to this argument. It is unlikely that WF with low wind resources could do a *Black-Start*.

It is because this reason that WF installations go far offshore, because it is known that the farther from shore, the stronger and more-constant abundant wind can be found; due to the same logic manufacturers are also designing taller towers for the newer WT designs because at higher heights the wind also blows harder. Construction, erection and commissioning engineers do not decide to install a wind power plant facility without previous research on the candidate locations. Historical data from atmospheric stations aid them to define what place can guarantee them acceptable meteorological conditions to fulfil the stringent load power demand from the Globe's increasing population.

6.2 RELATED AND FUTURE WORK

The massive integration of converter-dominated generation and the robust SOS are two of the most important aspects that the EPSF demand. This MSc Thesis Research focused mainly on wind energy, but solar-PV is also another favourable option to research. The *PST 16 Benchmark System* Network can be extended to assess the interaction of different RES-based generators, their dynamic responses and their performance altogether. The combination of different types of generation sources could derive in a very rich EPS model; it already has hydro, coal-fired, nuclear synchronous machines, plus the wind power plants, VSC-HVDC Transmission and the BESS.

Another work that also could be developed could be the study with less penetration of wind power. The goal of this alternative test would be to have a more-realistic simulation scenario resembling today's EPS. It is true that OffWF are taking a leading role in construction and installation of future facilities, but today there is still no large enough Wind Power Plant to mimic an installation injection 900 MW in the Entire Globe yet.

Another potentially useful future work related to this Research could be the total translation and migration of the *PST Benchmark System* Model from the software packed DIgSILENT PowerFactory to a real-time digital simulation environment, such as the Real-Time Digital System (RTDS), from RTDS Technologies. One of the complications of running a time-domain EMT Simulation is that usually occupies a lot of computational calculations and effort, especially if large-scale models are to be tested. The main argument in favour to change form one simulation tool to the other is that the Hardware-in-the-Loop (HiL) environment is capable of running an EMT Simulation in real time, as its name implies. With that tool, simulations could dramatically streamline. A simulation of a 17-minute *Black-Start* would no longer take 24 hours of real time to round finalise, with the RTDS simulation of a 17-minute *Black-Start* would take the exact same 17 minutes. In fact, if it is desired to do a statistical study of a large-scale system, such as the *PST 16 Benchmark System* Network, RTDS can achieve even faster-than-real-time simulation. In which case, a very large system that would take hours or days to simulate on a PC or Laptop could be achieved in a matter of seconds or minutes. Moreover, with the assistance of an RTDS environment, the reimplementations of the *Back-to-Back* WT structure could be plausible.

Harmonic stability is another essential study necessary to guarantee the stable operation of the offshore EPS. Particularly, harmonic stability is a critical aspect that needs to be further carefully investigated. The high-frequency interactions between the power converters and the rest of the electric power equipment must be properly damped.

BIBLIOGRAPHY

- [1] K. Pickerel. Tesla's 80-MWh energy storage project completed with assist from Swinerton. Solar Power World. [Online]. Available: <https://www.solarpowerworldonline.com/2017/02/teslas-80-mwh-energy-storage-project-completed-assist-swinerton/>
- [2] N. Ammendola. INAUGURATA IN MAROCCO LA CENTRALE SOLARE PIÙ GRANDE DEL MONDO. gli STATI GENERALI. [Online]. Available: <https://www.glistatigenerali.com/innovazione/inaugurata-in-marocco-la-centrale-solare-piu-grande-del-mondo>
- [3] lidovky.cz. Z predpovede počasia pre solárne a veterné elektrárne vzniká biznis. Napalete. [Online]. Available: <https://www.napalete.sk/z-predpovede-pocasia-pre-solarne-veterne-elektrarne-vznika-biznis/>
- [4] "FINAL REPORT of the Investigation Committee on the 28 September 2003 Blackout in Italy," UCTE, Tech. Rep., April 2004.
- [5] "BLACK SYSTEM SOUTH AUSTRALIA 28 SEPTEMBER 2016," AEMO-Australian Energy Market Operator, Tech. Rep., March 2017.
- [6] J. Nesheiwat and J. S. Cross, "Japan's post-Fukushima reconstruction: A case study for implementation of sustainable energy technologies," ELSEVIER ScienceDirect - Energy Policy, 2013.
- [7] M. M. Adibi and D. P. Milanicz, "ESTIMATING RESTORATION DURATION," IEEE Transactions on Power Systems, Vol. 14, No. 4, 1999.
- [8] "DIgSILENT PowerFactory Seminar HVDC and FACTS," DIgSILENT GmbH, Tech. Rep., June 2018.
- [9] H. Polinder. Sustainable Energy: Design a Renewable Future. Lecture "Electrical aspects". Technische Universiteit Delft. [Online]. Available: https://courses.edx.org/courses/course-v1:DelftX+EnergyX+3T2017/courseware/8boff754981f4364a80eec39b14ede03/bc9d6f14c0904ffe9554c74f847911fe/1?activate_block_id=block-v1%3ADelftX%2BEnergyX%2B3T2017%2Btype%40vertical%2Bblock%40bba9e9bda36741e2afb71c96be7ebb15
- [10] A. Viré. Sustainable Energy: Design a Renewable Future. Lecture "Power curve". Technische Universiteit Delft. [Online]. Available: https://courses.edx.org/courses/course-v1:DelftX+EnergyX+3T2017/courseware/8boff754981f4364a80eec39b14ede03/1f753051b5fc45de852698492e6089cc/1?activate_block_id=block-v1%3ADelftX%2BEnergyX%2B3T2017%2Btype%40vertical%2Bblock%40e8679d2b9d274daea497aaba152fe8a8
- [11] "ABB review: Special Report 60 years of HVDC," ABB Group R&D and Technology, Tech. Rep., July 2014.
- [12] "RENEWABLES, POWER AND ENERGY USE FORECAST TO 2050 - Energy Transition Outlook 2017," DNV GL, Tech. Rep., April 2018.
- [13] "Application Example - Battery Energy Storing Systems BESS," DIgSILENT GmbH, Tech. Rep., January 2010.
- [14] F. M. Gonzalez-Longatt and S. M. Alhejaj, "Enabling Inertial Response in Utility-Scale Battery Energy Storage System," Loughborough University Institutional Repository, 2016.
- [15] "DIgSILENT PowerFactory 2018 User Manual," DIgSILENT GmbH, Tech. Rep., February 2018.
- [16] S. P. Teeuwsen, I. Erlich, M. A. El-Sharkawi, and U. Bachmann, "Genetic Algorithm and Decision Tree based Oscillatory Stability Assessment," 2005 IEEE Russia Power Tech, 2005.
- [17] F. Gonzalez-Longatt and J. L. Rueda-Torres, Advanced Smart Grid Functionalities Based on PowerFactory. Springer, 2017. [Online]. Available: <https://www.springer.com/gp/book/9783319505312>
- [18] I. Erlich, A. Korai, T. Neumann, B. Paz, M. K. Sadeh, S. Vogt, C. Buchhagen, C. Rauscher, A. Menze, and J. Jung, "Novel Direct Voltage Control by Wind Turbines," IEEE TRANSACTIONS ON ENERGY CONVERSION, VOL. 32, NO. 3, 2017.

- [19] I. Erlich, A. Korai, T. Neumann, M. K. Sadeh, S. Vogt, C. Buchhagen, C. Rauscher, A. Menze, and J. Jung, "New Control of Wind Turbines Ensuring Stable and Secure Operation Following Islanding of Wind Farms," *IEEE TRANSACTIONS ON ENERGY CONVERSION*, VOL. 32, NO. 3, 2017.
- [20] I. Erlich, A. Korai, and F. Shewarega, "Control Challenges in Power Systems Dominated by Converter Interfaced Generation and Transmission Technologies," *2017 IEEE Power & Energy Society General Meeting*, 2017.
- [21] I. Erlich and A. W. Korai, "Description, Modelling and Simulation of a Benchmark System for Converter Dominated Grids (Part I)," *Universität Duisburg-Essen*.
- [22] A. W. Korai, "Dynamic Performance of Electrical Power Systems with High Penetration of Power Electronic Converters: Analysis and New Control Methods for Mitigation of Instability Threats and Restoration," PhD dissertation, Universität Duisburg-Essen, 2018.
- [23] H. Pustjens, "REDUCING THE RISKS OF NETWORK RESTORATION," DNV GL, Tech. Rep., July 2016.
- [24] "CONTROL METHODOLOGIES FOR DIRECT VOLTAGE AND POWER FLOW IN A MESHERD HVDC GRID," CIGRE, Tech. Rep., September 2017.
- [25] J. L. Rueda-Torres, A. Perilla, and D. Gusain, "ET4113 POWER SYSTEM DYNAMICS - LAB SESSION 4: DYNAMIC MODELING OF SYNCHRONOUS MACHINE - 2," Technische Universiteit Delft, Lecture Notes, 2017.
- [26] "Description, Modelling and Simulation of a Benchmark Test System for Converter Dominated Grids (Part II) 98% - RES Benchmark on Basis of Fast Voltage Source controlled Converters (EMT & RMS)," DIgSILENT GmbH, Tech. Rep., June 2018.
- [27] "Power System Restoration Dynamics (Issues, Techniques, Planning, Training & Special Considerations)," IEEE, Tech. Rep., July 2014.
- [28] J. N. Niang, Z. Zhang, M. Fan, G. Harrison, C. Lin, M. Tamayo, and V. Perumalla, "Power System Restoration Planning and Some Key Issues," *2012 IEEE Power and Energy Society General Meeting*, 2012.
- [29] F. Hernandez, "Models of Battery Storage Systems for Power System Analysis: International Seminar on "Energy Storage Options for Renewable Energy Integration"," DIgSILENT GmbH, Seminar, 2018.
- [30] "Guide for the Development of Models for HVDC Converters in a HVDC Grid (604)," CIGRE, Tech. Rep., December 2014.
- [31] S. Liu, Y. Hou, C.-C. Liu, and R. Podmore, "The Healing Touch," *IEEE Power & Energy Magazine*, 2014.
- [32] J. Latson, "Why the 1977 Blackout Was One of New York's Darkest Hours," *TIME Magazine*, 2015. [Online]. Available: <http://time.com/3949986/1977-blackout-new-york-history/>
- [33] Commission Européenne. (2018) Accord de Paris. [Online]. Available: https://ec.europa.eu/clima/policies/international/negotiations/paris_fr
- [34] European Commission. (2018) The Massive Integration of Power Electronic Devices. [Online]. Available: <https://www.h2020-migrate.eu/>
- [35] Europese Commissie. (2018) Progress on Meshed HVDC Offshore Transmission Networks. [Online]. Available: <https://www.promotion-offshore.net/>
- [36] M. Bahrman and P.-E. Bjorklund, "The New Black Start," *IEEE Power & Energy Magazine*, 2014.
- [37] J. A. Mola-Jimenez, "Evaluation of frequency and transient stability indicators in future power systems with high levels of wind power generation," Master's thesis, Technische Universiteit Delft, 2017.
- [38] I. Erlich and W. Winter, "A Method for Incorporating VSC-HVDC into the Overall Grid Voltage-Reactive Power Control Task," *IEEE 2016 Power Systems Computation Conference (PSCC)*, 2016.
- [39] F. Gonzalez-Longatt and J. L. Rueda-Torres, *PowerFactory Applications for Power System Analysis*. Springer, 2014. [Online]. Available: <https://www.springer.com/gp/book/9783319129570>
- [40] "System Restoration Procedure and Practices," CIGRE, Tech. Rep., December 2017.

[41] S. Ramachandran, S. Joseph, S. Paulraj, and V. Ramaraj, "Handling Overload Conditions in High Performance Trustworthy Information Retrieval Systems," *JOURNAL OF COMPUTING, VOLUME 2*, 2010.

[42] "Current practices in Europe on Emergency and Restoration," ENTSOE, Tech. Rep., May 2014.

[43] P. Pentayya, A. Gartia, A. P. Das, and C. Kumar, "Black Start Exercises Experience in Western Region, India," *2013 Annual IEEE India Conference (INDICON)*, 2013.

[44] M. Muredu, G. Caldarelli, A. Damiano, A. Scala, and H. Meyer-Ortmanns, "Islanding the power grid on the transmission level: less connections for more security," *Nature Scientific Reports*, 2016.

[45] "Report on the blackout in Italy on 28 September 2003," Swiss Federal Office of Energy (SFOE), Tech. Rep., November 2003.

[46] South australia's blackout explained (and no, renewables aren't to blame). The Guardian, author = M. Slezak, url = <https://www.theguardian.com/australia-news/2016/sep/29/south-australia-blackout-explained-renewables-not-to-blame>.

[47] BBC News. (2011) Japan earthquake: Tsunami hits north-east. [Online]. Available: <https://www.bbc.co.uk/news/world-asia-pacific-12709598>

[48] "The Development of and Lessons from the Fukushima Daiichi Nuclear Accident," Tokyo Electric Power Company, Inc., Tech. Rep., March 2013.

[49] World Nuclear Association. (2018) Fukushima Accident. [Online]. Available: <http://www.world-nuclear.org/information-library/safety-and-security/safety-of-plants/fukushima-accident.aspx>

[50] The Japan Times. (2018) Fukushima looks to renewable energy sources in the aftermath of nuclear disaster. [Online]. Available: <https://www.japantimes.co.jp/life/2018/03/10/environment/fukushima-looks-renewable-energy-sources-aftermath-nuclear-disaster/#.W5k5Fuj7SUk>

[51] W. M. Chen, , H. Kim, , and H. Yamaguchi, "Renewable energy in eastern Asia: Renewable energy policy review and comparative SWOT analysis for promoting renewable energy in Japan, South Korea, and Taiwan," *ELSEVIER ScienceDirect - Energy Policy*, 2014.

[52] The Japan Times. (2018) Fukushima powers toward 100% goal on renewables as grid and cost woes linger. [Online]. Available: <https://www.japantimes.co.jp/news/2018/03/11/national/fukushima-powers-toward-100-goal-renewables-grid-cost-woes-linger/#.W5k-2ej7SUk>

[53] "Offshore Wind Power Development in Japan," Japan Wind Power Association, Tech. Rep., March 2017.

[54] C. Grande-Moran and J. W. Feltes, "An Overview of Restoration Issues and Blackstart Analysis," *IEEE Power & Energy Magazine*, 2014.

[55] L. Seca, H. Costa, C. L. Moreira, and J. A. Peças-Lopes, "An Innovative Strategy for Power System Restoration using Utility Scale Wind Parks," *2013 IREP Symposium-Bulk Power System Dynamics and Control -IX (IREP)*, 2013.

[56] A. El-Zonkoly, "Integration of wind power for optimal power system black-start restoration," *Turkish Journal of Electrical Engineering & Computer Sciences*, 2015.

[57] L. Ramirez-Elizondo. Sustainable Energy: Design a Renewable Future. Lecture "Introduction to Power Control". Technische Universiteit Delft. [Online]. Available: https://courses.edx.org/courses/course-v1:DelftX+EnergyX+3T2017/courseware/49d4ec1adce543819eedc707626a340/04594b7f931a4f299df9159732973b27/1?activate_block_id=block-v1%3ADelftX%2BEnergyX%2B3T2017%2Btype%40vertical%2Bblock%4053b7346e01ea4c17a85ee698109e753c

[58] P. Kundur, *POWER SYSTEM STABILITY AND CONTROL*. McGraw-Hill Inc. Series in Electrical and Computer Engineering.

[59] M. A. Perales, M. M. Prats, R. Portillo, J. L. Mora, J. I. Leon, and L. G. Franquelo, "Three-Dimensional Space Vector Modulation in abc Coordinates for Four-Leg Voltage Source Converters," *IEEE POWER ELECTRONICS LETTERS, VOL. 1, NO. 4*, 2003.

[60] Y. Solbakken. (2017) SPACE VECTOR PWM INTRO. [Online]. Available: <https://www.switchcraft.org/learning/2017/3/15/space-vector-pwm-intro>

[61] W. C. Duesterhoeft, J. M. W. Schulz, and E. Clarke, "Determination of Instantaneous Currents and Voltages by Means of Alpha, Beta, and Zero Components," *Transactions of the American Institute of Electrical Engineers (now IEEE)*, 1951.

[62] R. H. Park, "Two-Reaction Theory of Synchronous Machines. Generalized Method of Analysis-Part I," *Transactions of the American Institute of Electrical Engineers (now IEEE)*, 1929.

[63] V. Yaramasu, B. Wu, P. C. Sen, S. Kouro, and M. Narimani, "High-Power Wind Energy Conversion Systems: State-of-the-Art and Emerging Technologies," *Proceedings of the IEEE (Volume: 103, Issue: 5)*, 2015.

[64] F. M. Gonzalez-Longatt, P. Wall, and V. Terzija, "A Simplified Model for Dynamic Behavior of Permanent Magnet Synchronous Generator for Direct Drive Wind Turbines," *PowerTech 2011 IEEE Trondheim*, 2011.

[65] "COMMISSION REGULATION (EU) 2016/631 of 14 april 2016 establishing a network code on requirements for grid connection of generators," ENTSOE, Tech. Rep., April 2016.

[66] "Grid Code - High and extra high voltage -," TenneT TSO GmbH, Tech. Rep., November 2015.

[67] F. H. Kreuger, *Industrial High DC Voltage*. Delft University Press, 1995.

[68] The European Wind Energy Association. (2016) Wind energy's frequently asked questions (FAQ). [Online]. Available: <http://www.ewea.org/wind-energy-basics/faq/>

[69] Green Element Ltd. (2017) Wind vs Solar – Which Green Energy is Winning? [Online]. Available: <https://compareyourfootprint.com/wind-vs-solar-green-energy-winning/>

[70] W. Teng, H. Wang, and Y. Jia, "Construction and Control Strategy Research of Black Start Unit Containing Wind Farm," *TENCON 2015 - 2015 IEEE Region 10 Conference*, 2015.

[71] Ö. Göksu, O. Saborío-Romano, N. A. Cutululis, and P. Sørensen, "Black Start and Island Operation Capabilities of Wind Power Plants," *DTU Wind Energy*, 2017.

[72] W. Sritham, S. Asadamongkol, and T. Sumranwanich, "Application of Battery Energy Storage System in Coordination with MicroEMS for Mae Hong Son Microgrid during Islanding Mode," *CIGRE AORC Technical meeting 2014*, 2014.

[73] Energy Storage NEWS. (2017) California battery's black start capability hailed as 'major accomplishment in the energy industry'. [Online]. Available: <https://www.energy-storage.news/news/california-batterys-black-start-capability-hailed-as-major-accomplishment-i>

[74] R. K. Varma, S. S. Rangarajan, I. Axente, and V. Sharma, "Novel application of a PV Solar Plant as STATCOM during Night and Day in a Distribution Utility Network," *2011 IEEE/PES Power Systems Conference and Exposition*, 2011.

[75] "Sub-national electricity consumption statistics. Regional and local authority level statistics (2012 data)." UK Department of Energy & Climate Change, Tech. Rep., December 2013.

[76] I. The MathWorks. (2018) Three-Phase Harmonic Filter. [Online]. Available: <https://www.mathworks.com/help/physmod/sps/powersys/ref/threephaseharmonicfilter.html>

[77] "IEEE Standard Definitions for Excitation Systems for Synchronous Machines," IEEE, Tech. Rep., July 2007.

[78] A. Hansen, C. Jauch, P. Sørensen, F. Iov, and F. Blaabjerg, "Dynamic wind turbine models in power system simulation tool DiGILENT," DTU-Risø National Laboratory, Tech. Rep., December 2003.

[79] J. J. Grainger and W. D. Stevenson, *POWER SYSTEM ANALYSIS*. McGraw-Hill Inc. Series in Electrical and Computer Engineering, 1994.

[80] "Frequency Sensitive Mode-ENTSO-E guidance document for national implementation for network codes on grid connection," ENTOSE, Tech. Rep., November 2017.

[81] "Damping of Power System Oscillations by VSC-HVDC Multi-Terminal Transmission Networks," Technische Universiteit Delft, Tech. Rep., April 2013.

[82] M. A. Tabrizi. Integration of renewable energy sources: Strong challenge for a weak grid - Energy in Transition. DNV GL. [Online]. Available: <https://blogs.dnvgl.com/energy/integration-of-renewable-energy-sources-strong-challenge-for-a-weak-grid>

A

APPENDIX A: SYNCHRONOUS MACHINE MODELS

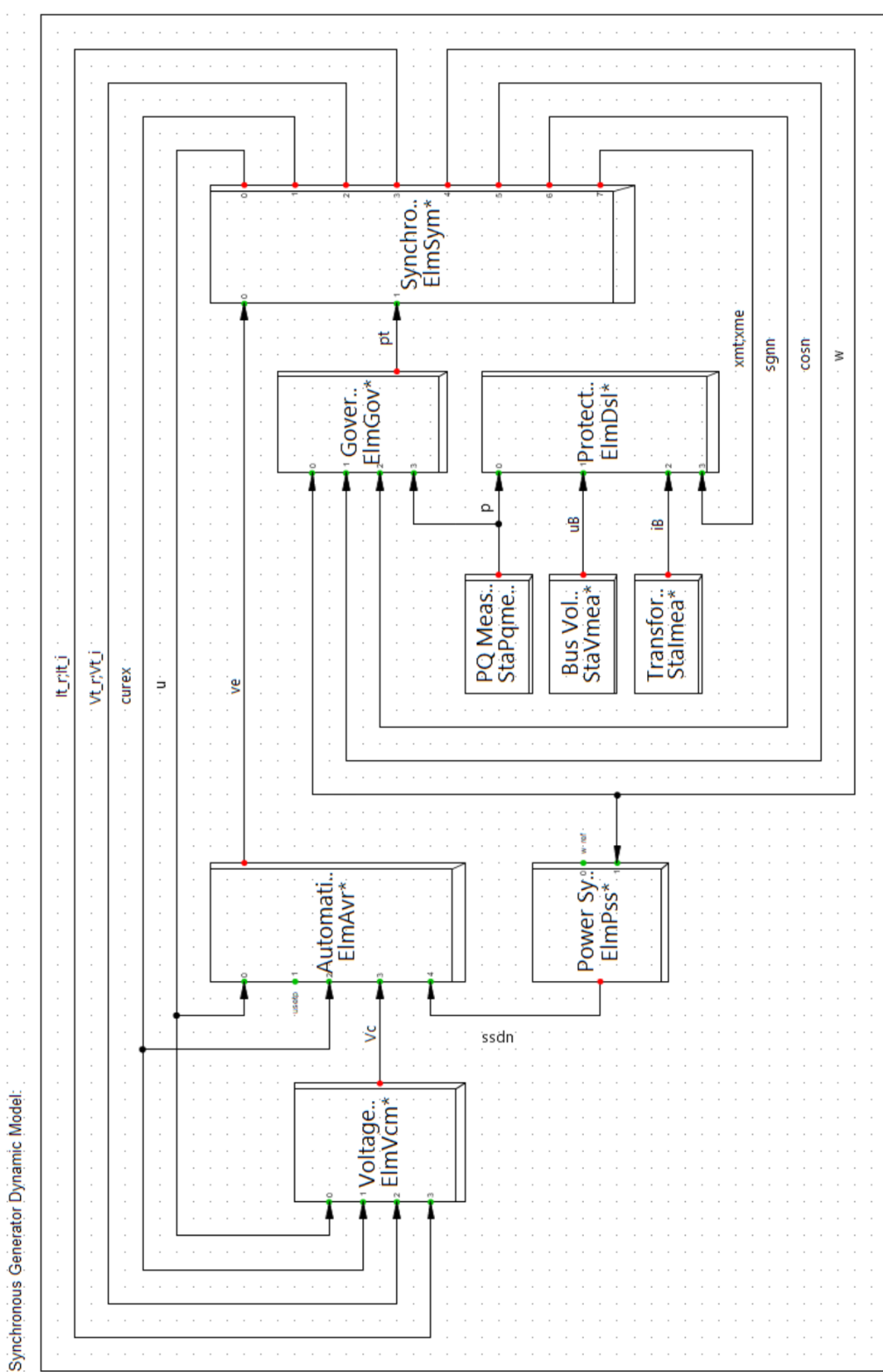


Figure A.1.: Synchronous Generator Dynamic Frame.

avr_EMAC1T: Modified IEEE Type AC1 Excitation System

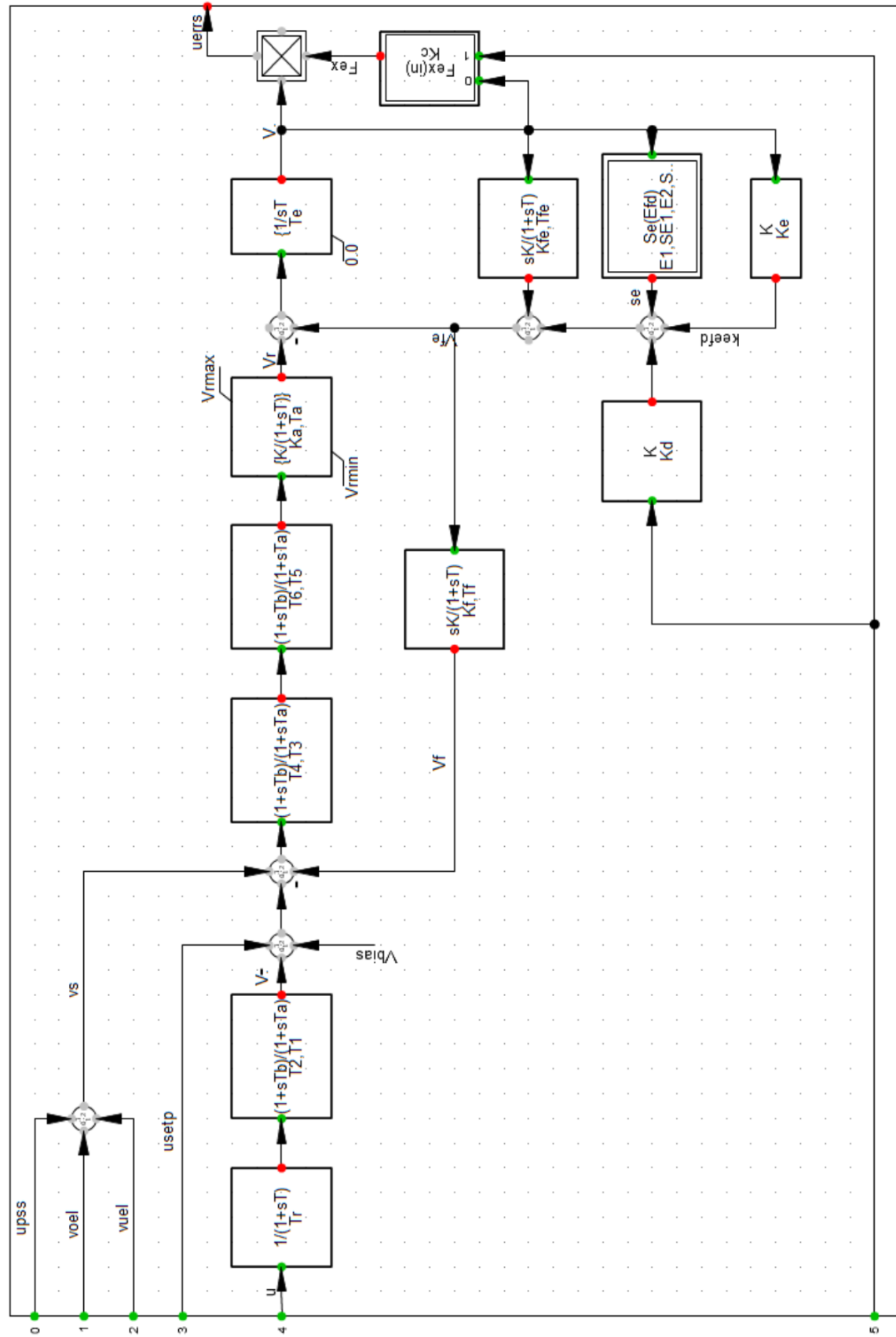


Figure A.2.: Automatic Voltage Regulator System designed as a Block Definition by DPF.

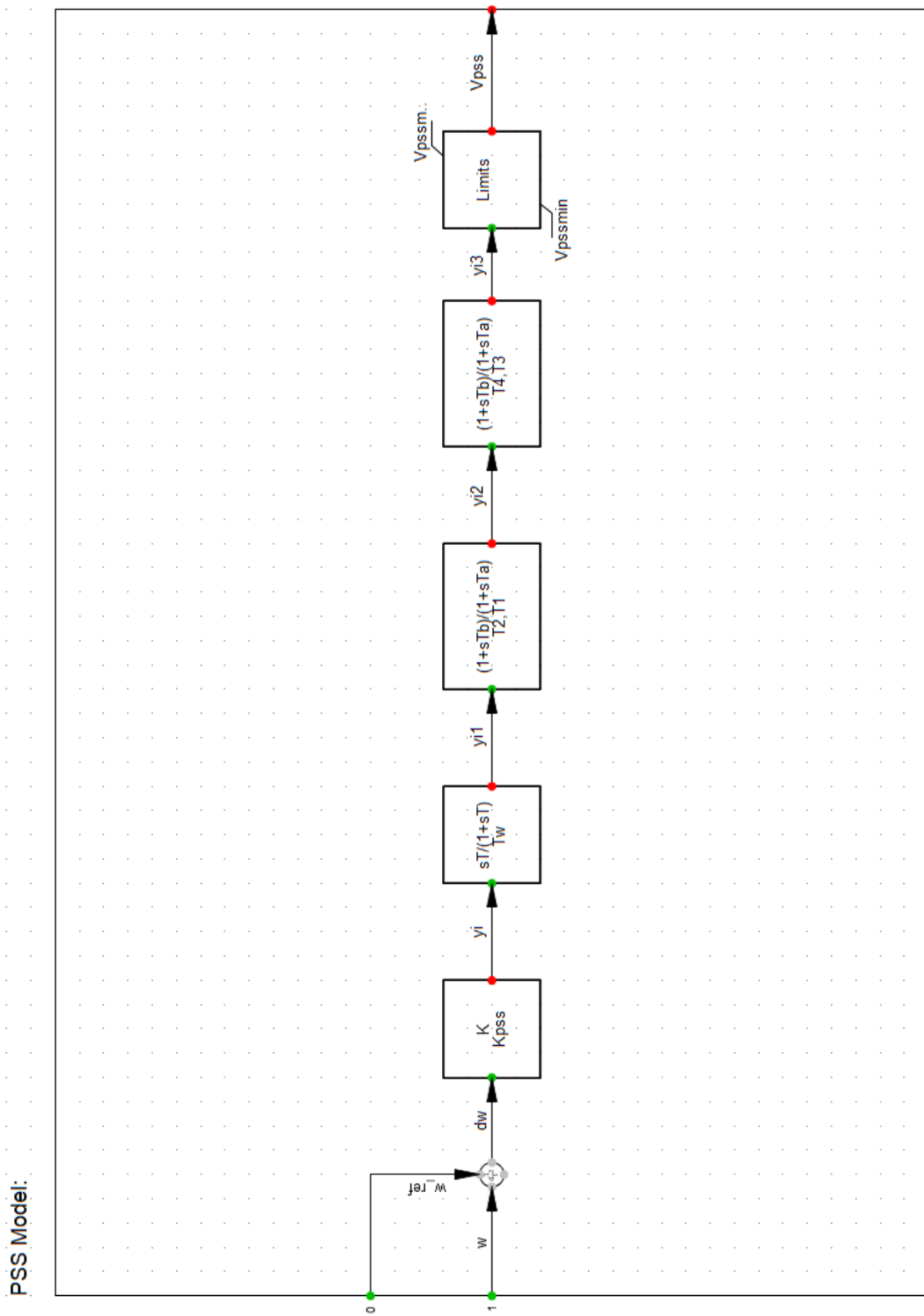


Figure A.3.: Power System Stabiliser designed as a Block Definition by DPF.

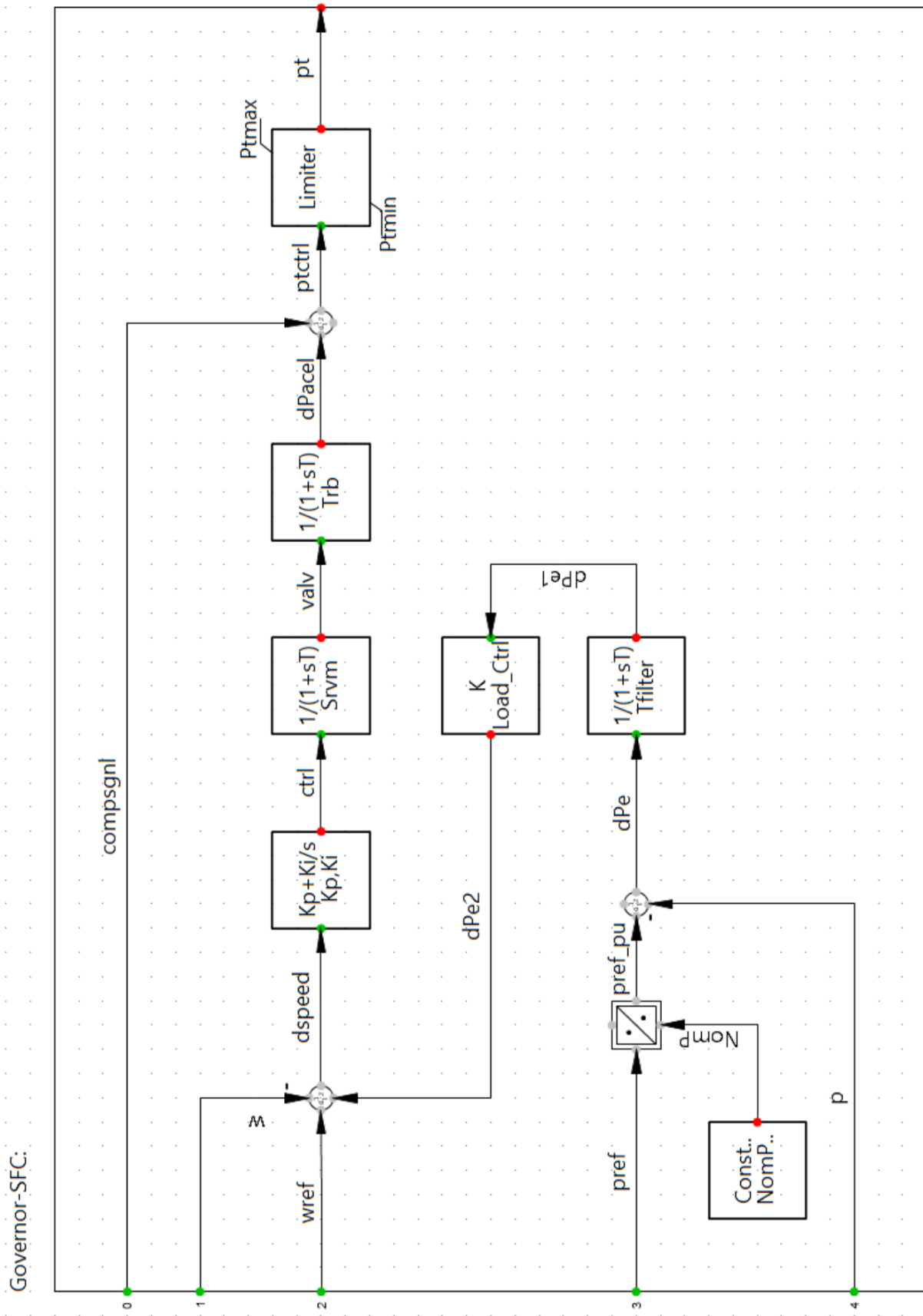


Figure A.4.: Governor with SFC Model [25].

B

APPENDIX B: PERMANENT-MAGNET SYNCHRONOUS GENERATOR WIND TURBINE MODELS

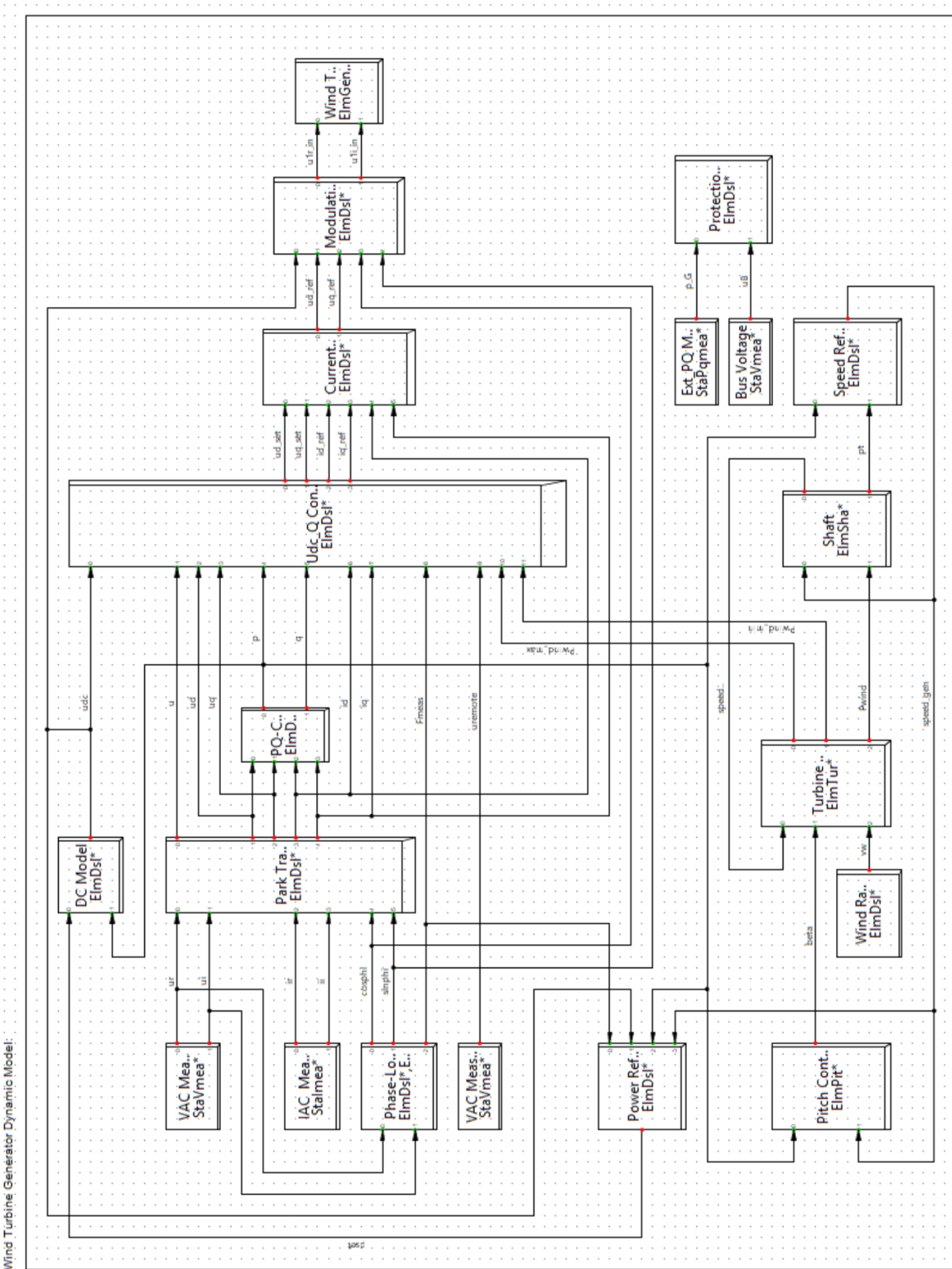


Figure B.1.: Wind Turbine Generator Dynamic Model.

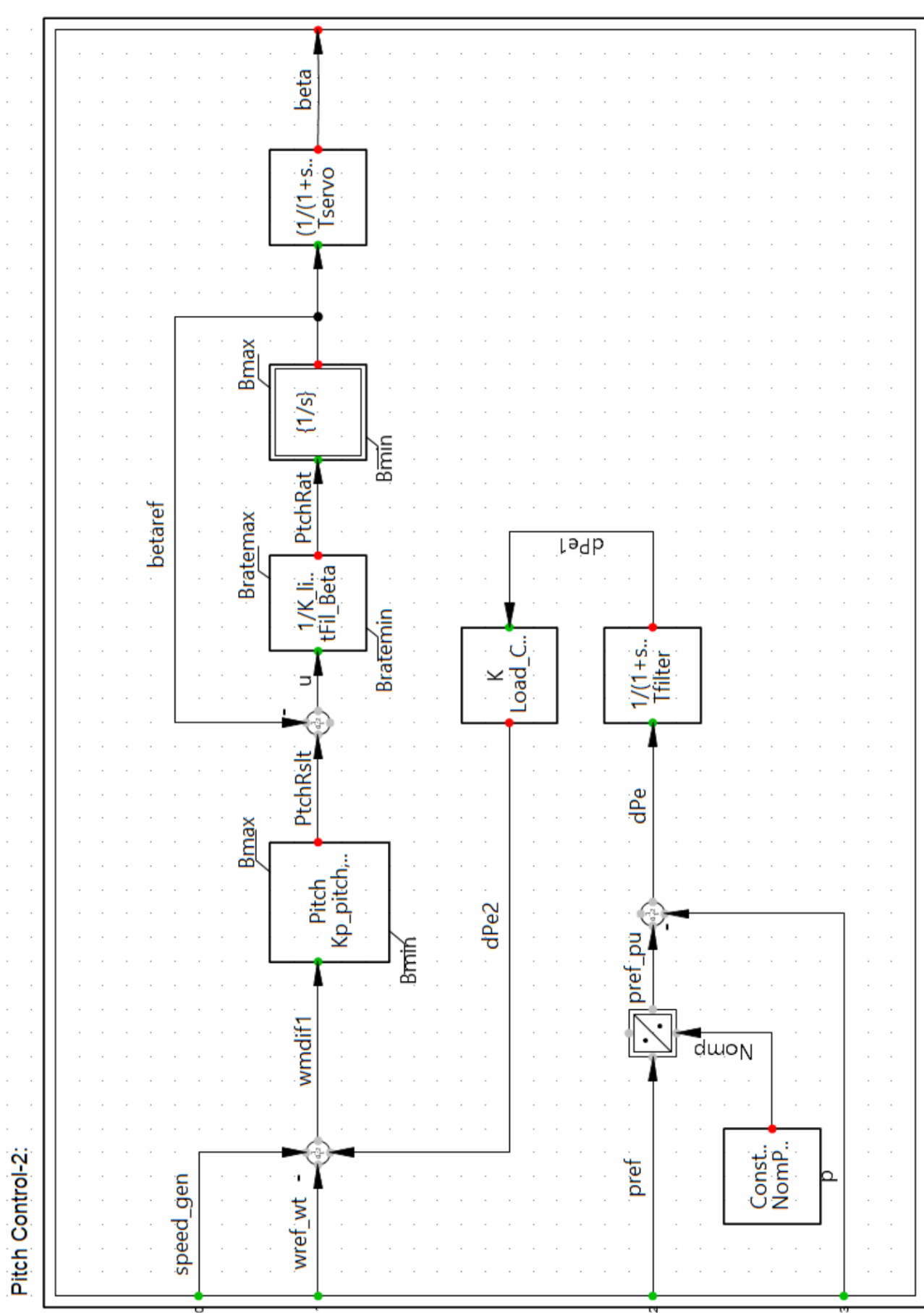


Figure B.2.: Pitch Angle Controller [22].

Turbine-3:

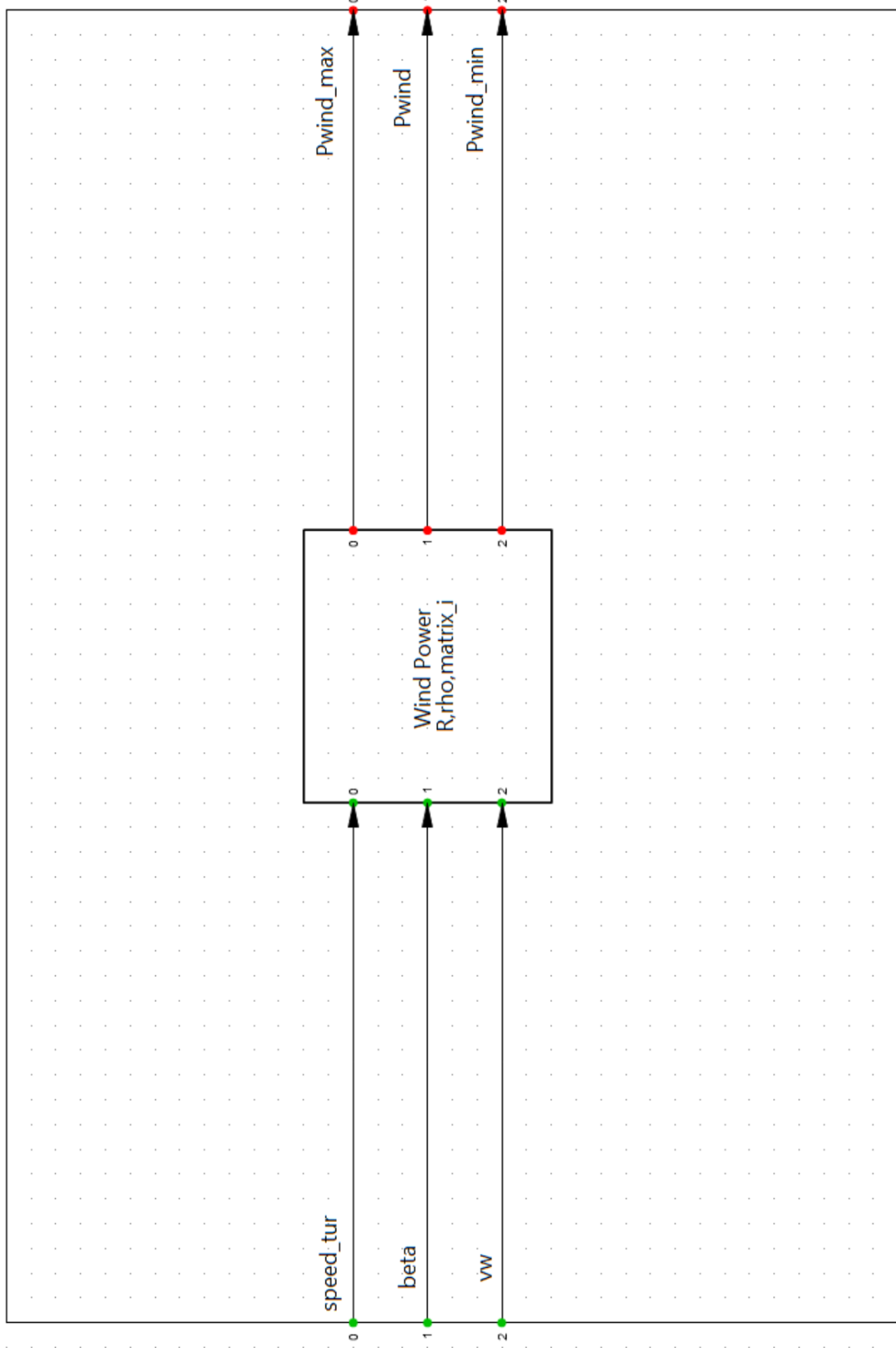


Figure B.3.: Wind Power-Turbine Model.

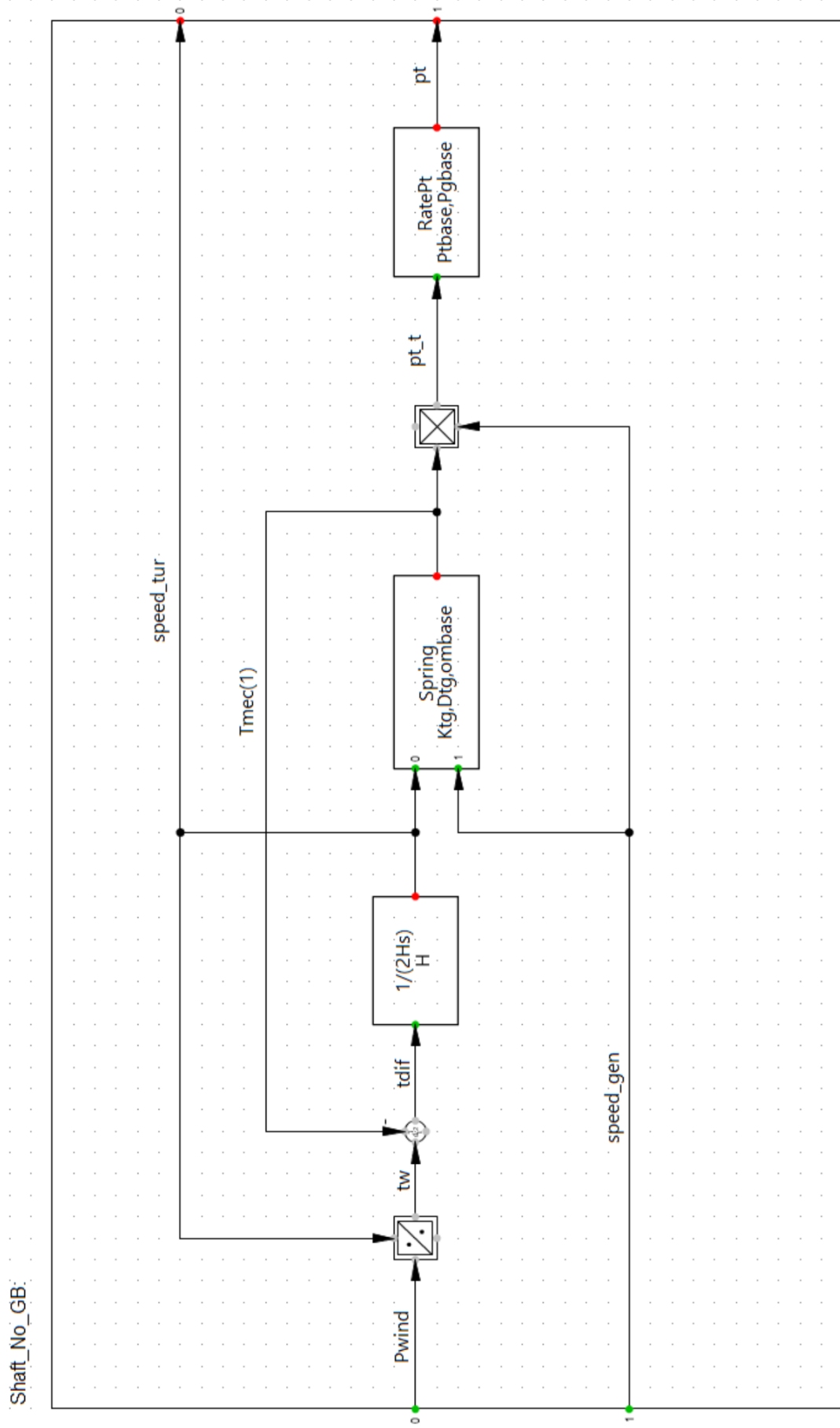


Figure B.4.: WT Shaft Model.

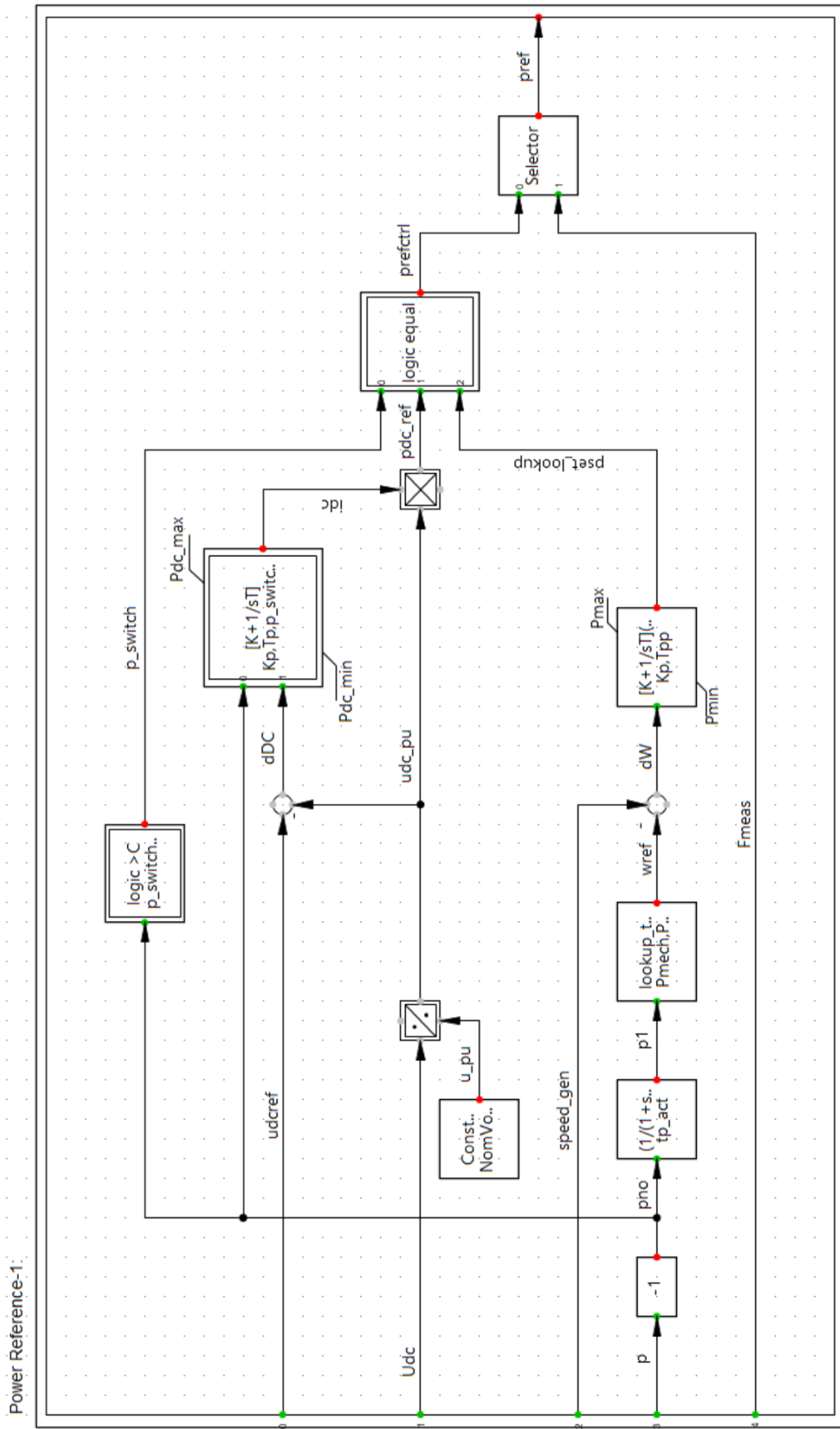


Figure B.5.: WT Power Reference based on Speed or MPPT [22].

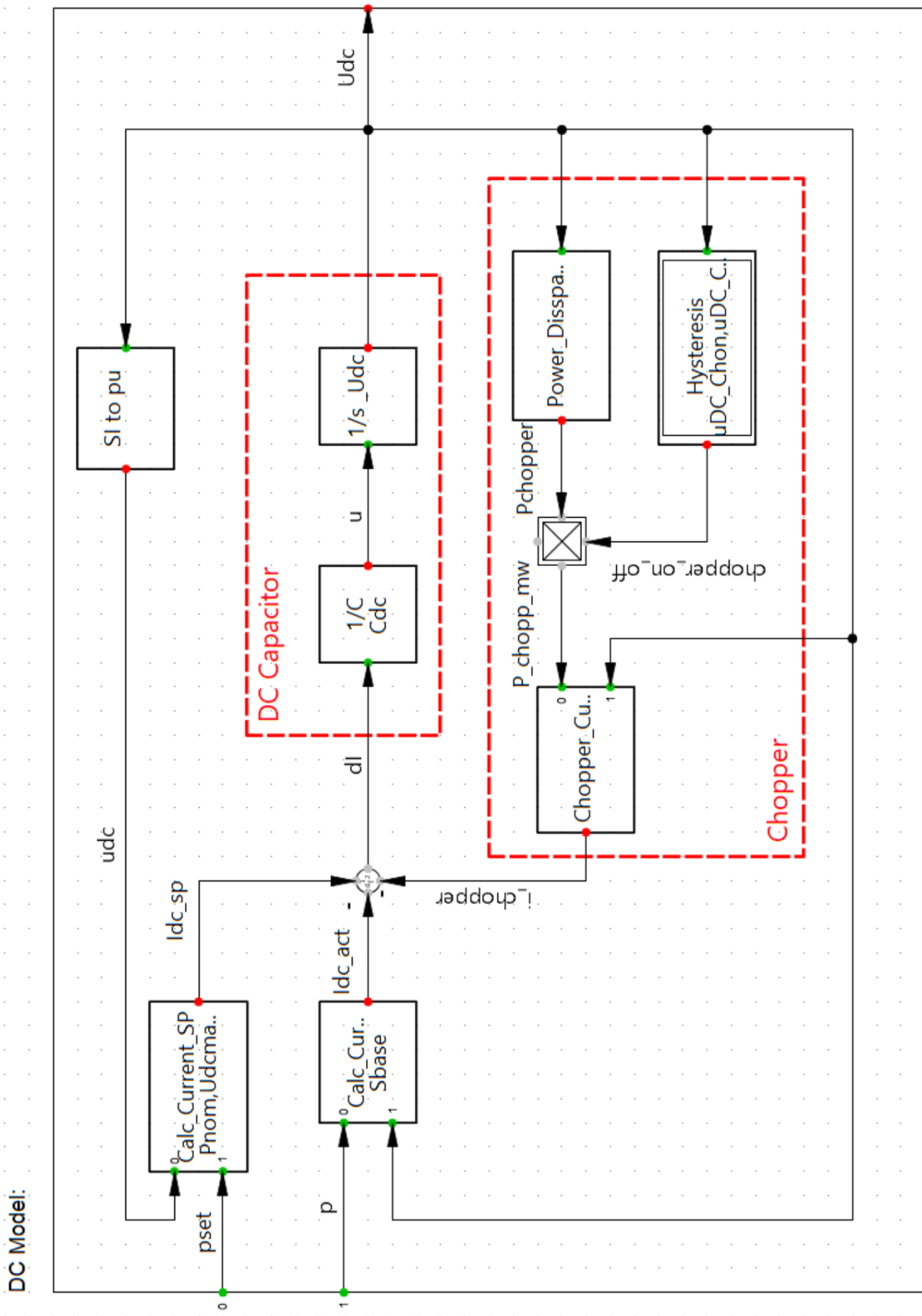


Figure B.6.: WT DC Busbar, Capacitor and Chopper Model [21],[26].

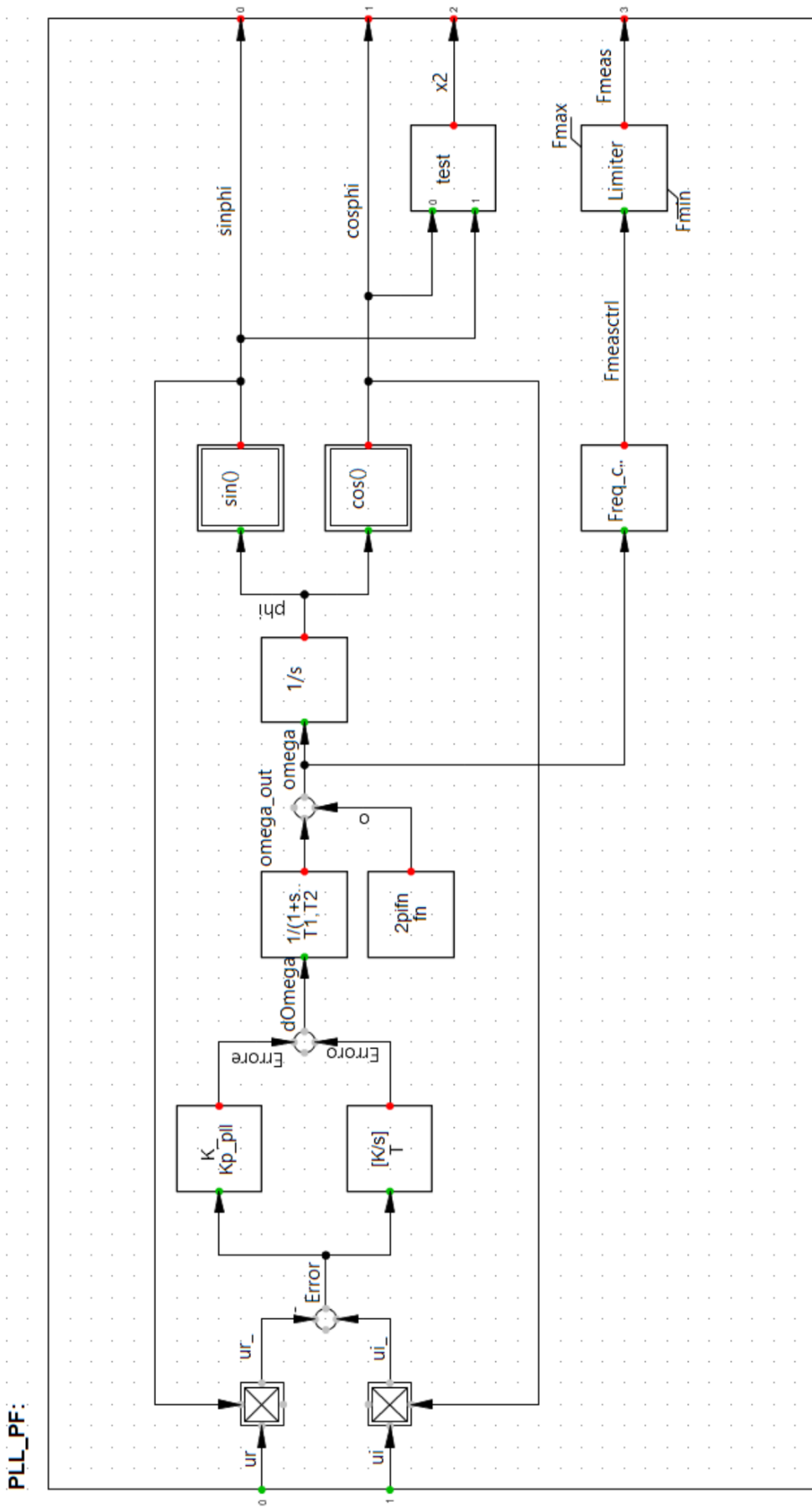


Figure B.7.: Phase-Locked Loop Model [8].

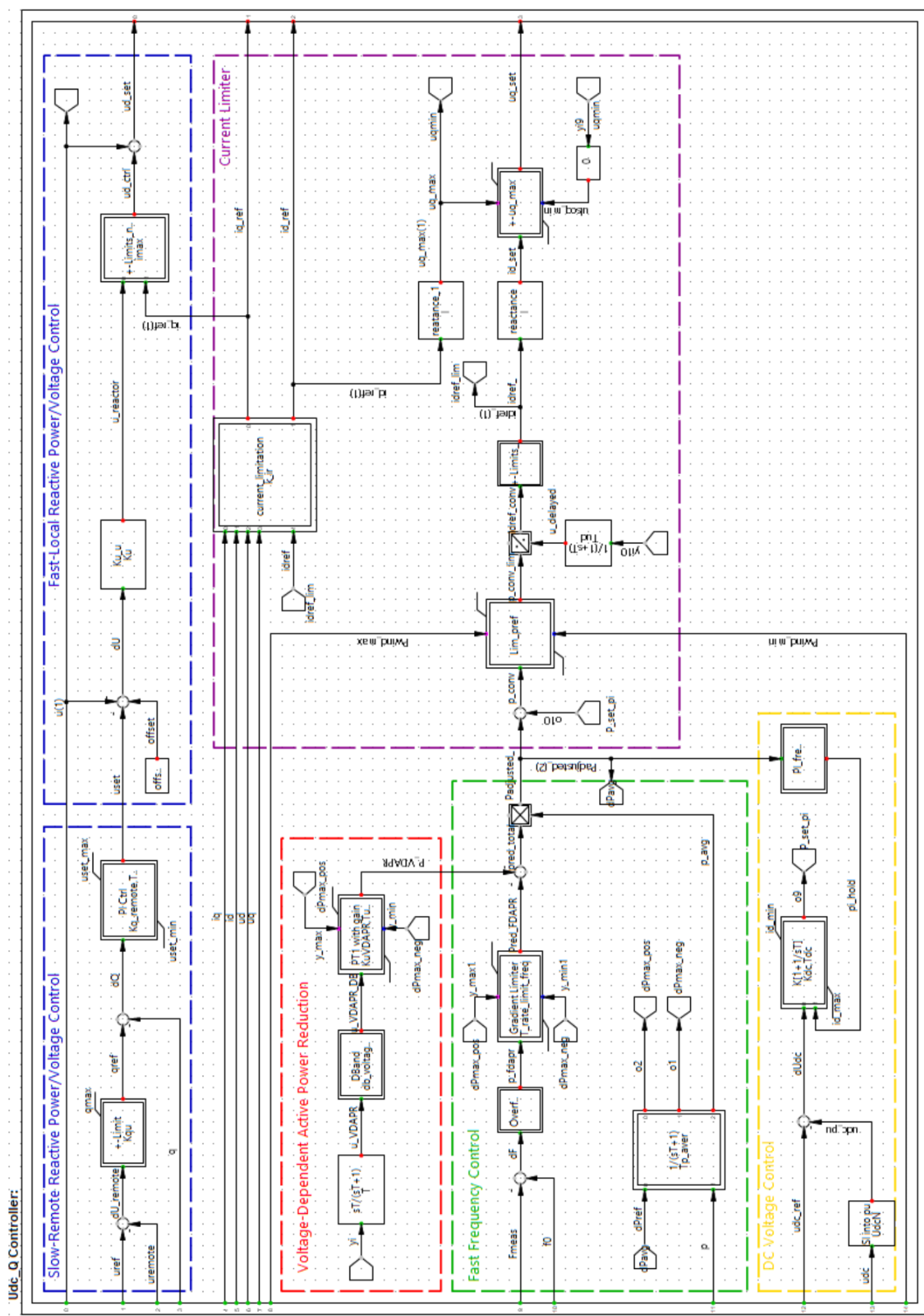


Figure B.8.: Voltage-Reactive Power Controller [21],[26].

Damping Terms:

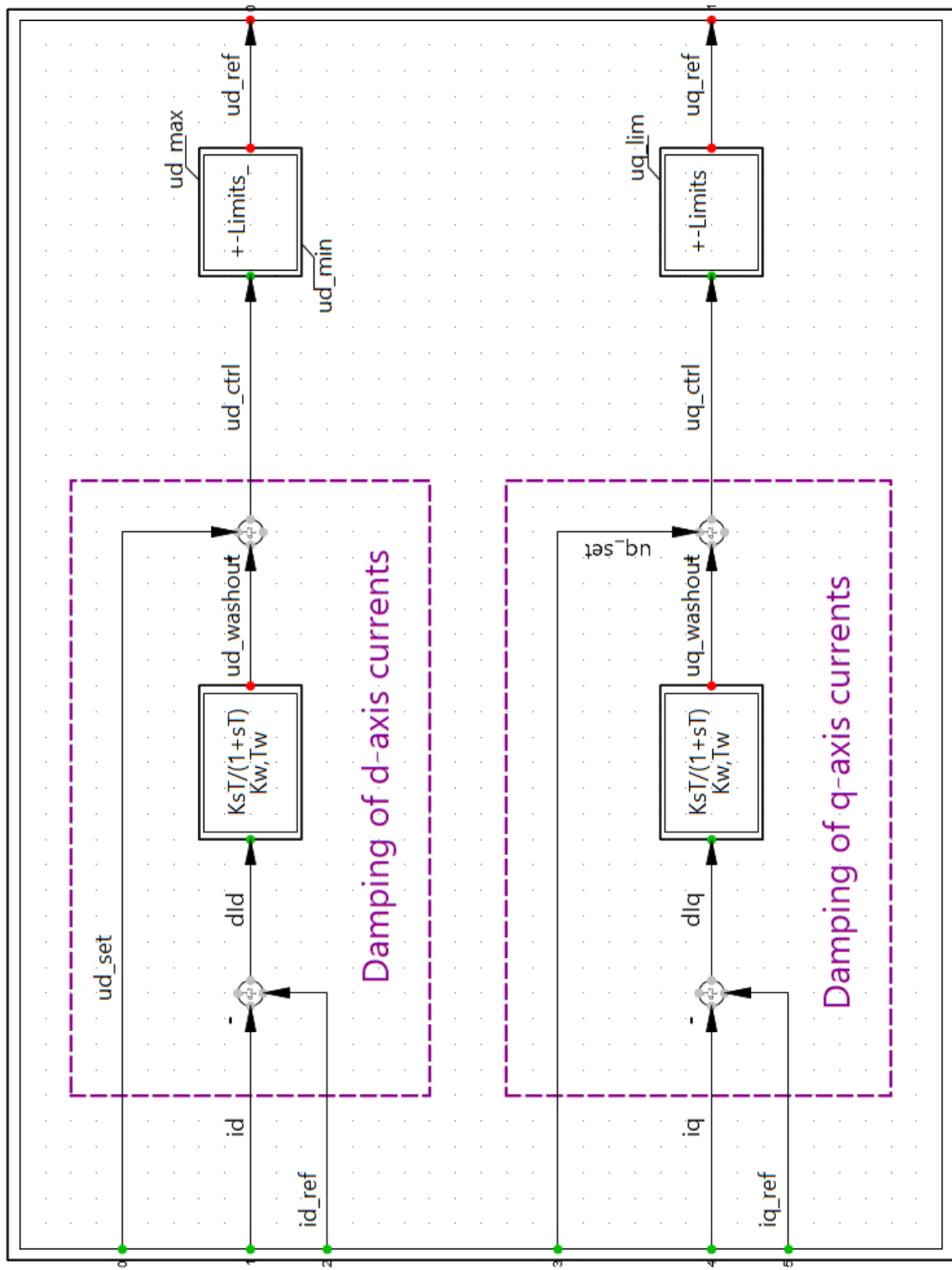


Figure B.9.: Current Limitation and Damping [21],[26].

Modulation Limitation:

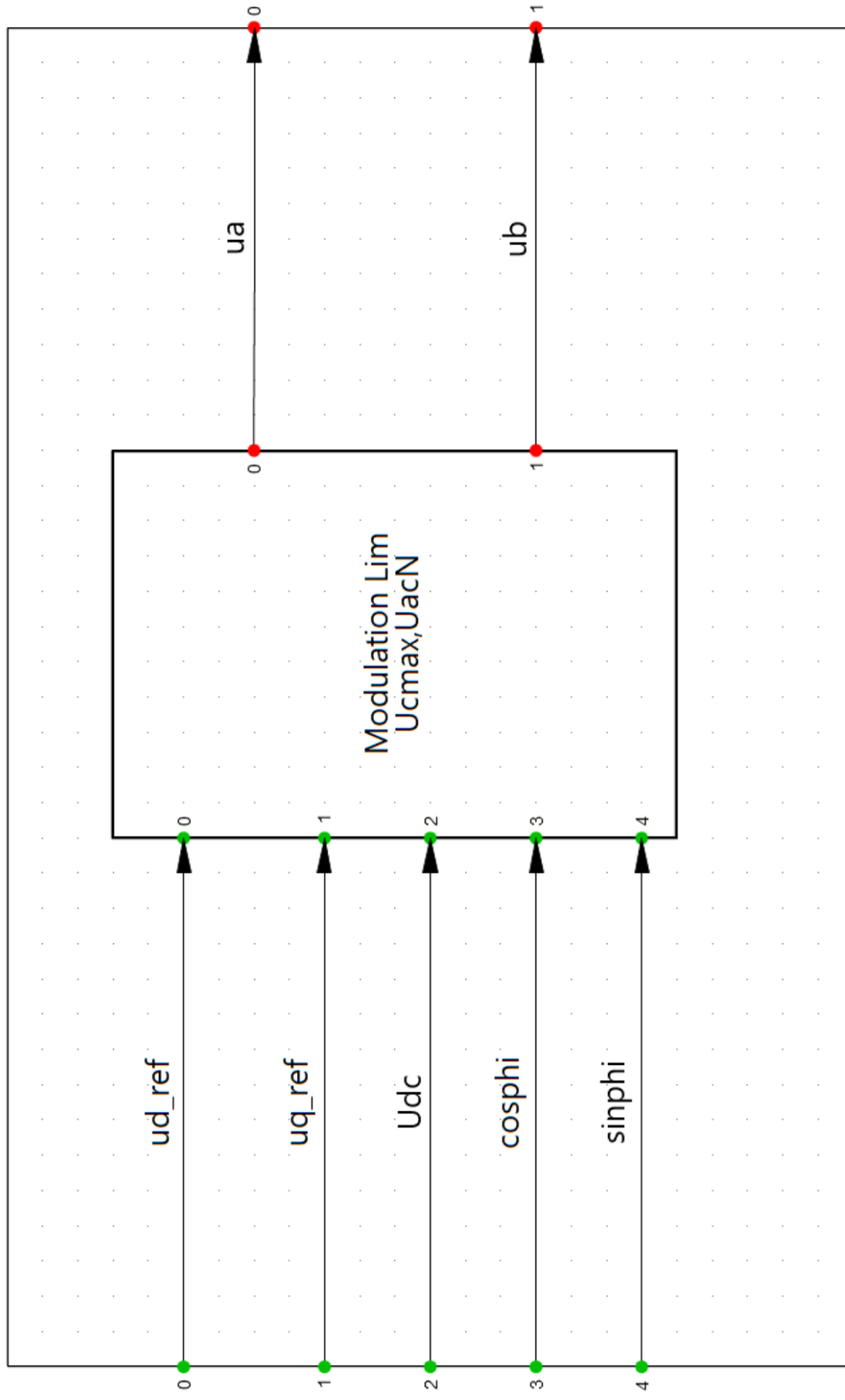


Figure B.10.: WT Voltage Modulation Limiter [21],[26].

C

APPENDIX C: HVDC CONVERTER STATION MODELS

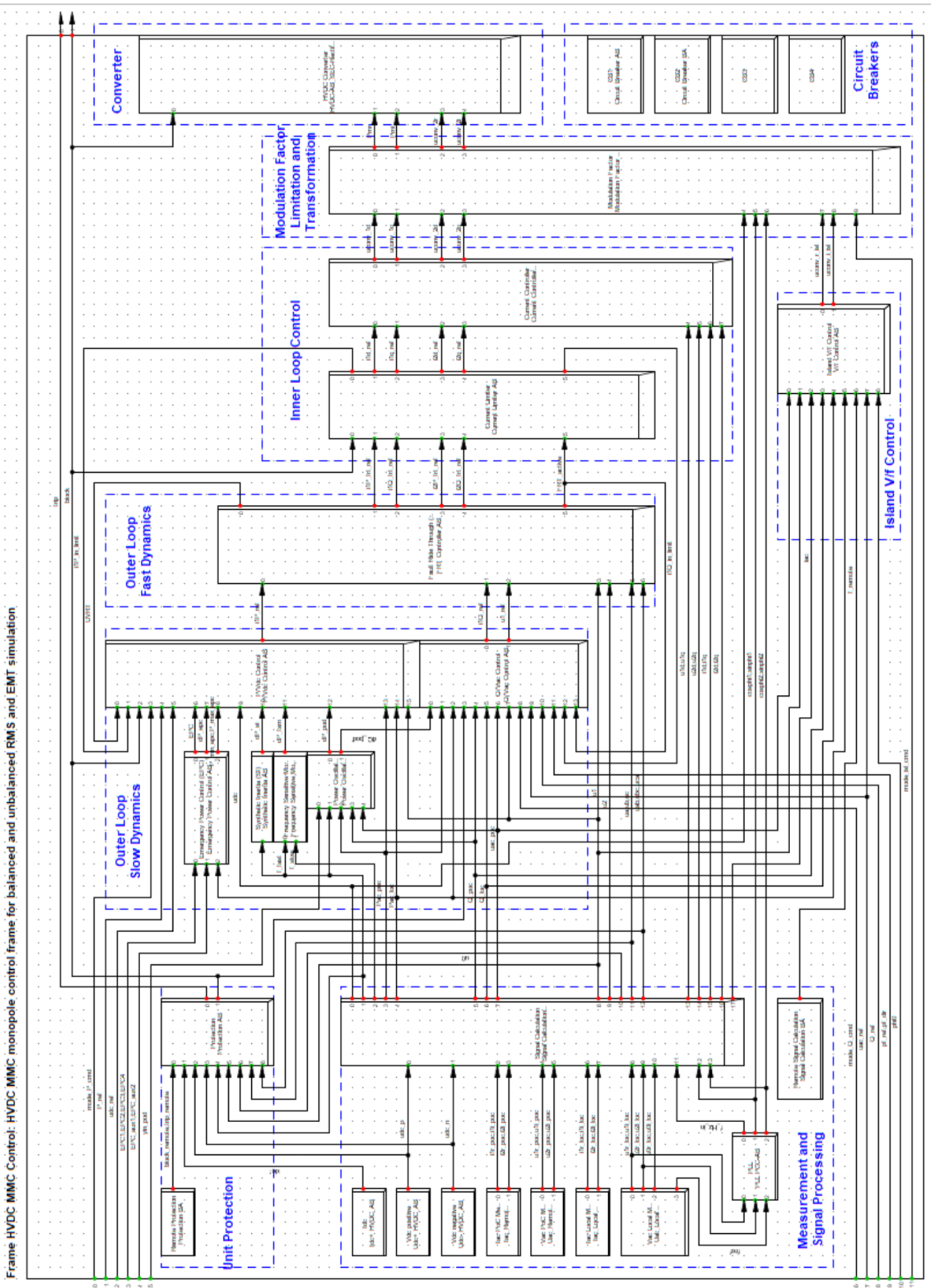


Figure C.1.: HVDC System Composite Frame [8].

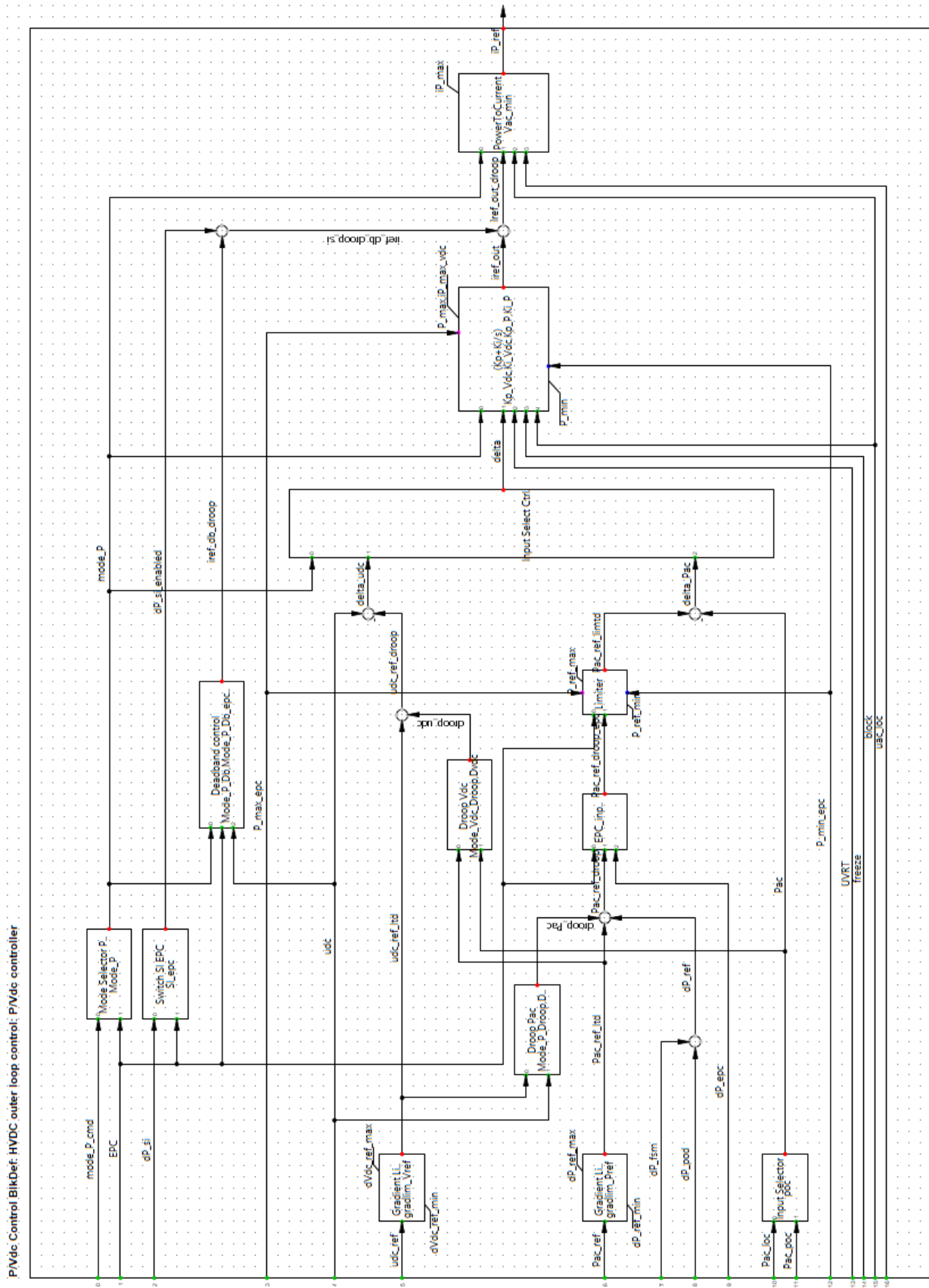


Figure C.2.: HVDC Active Power Control [8].

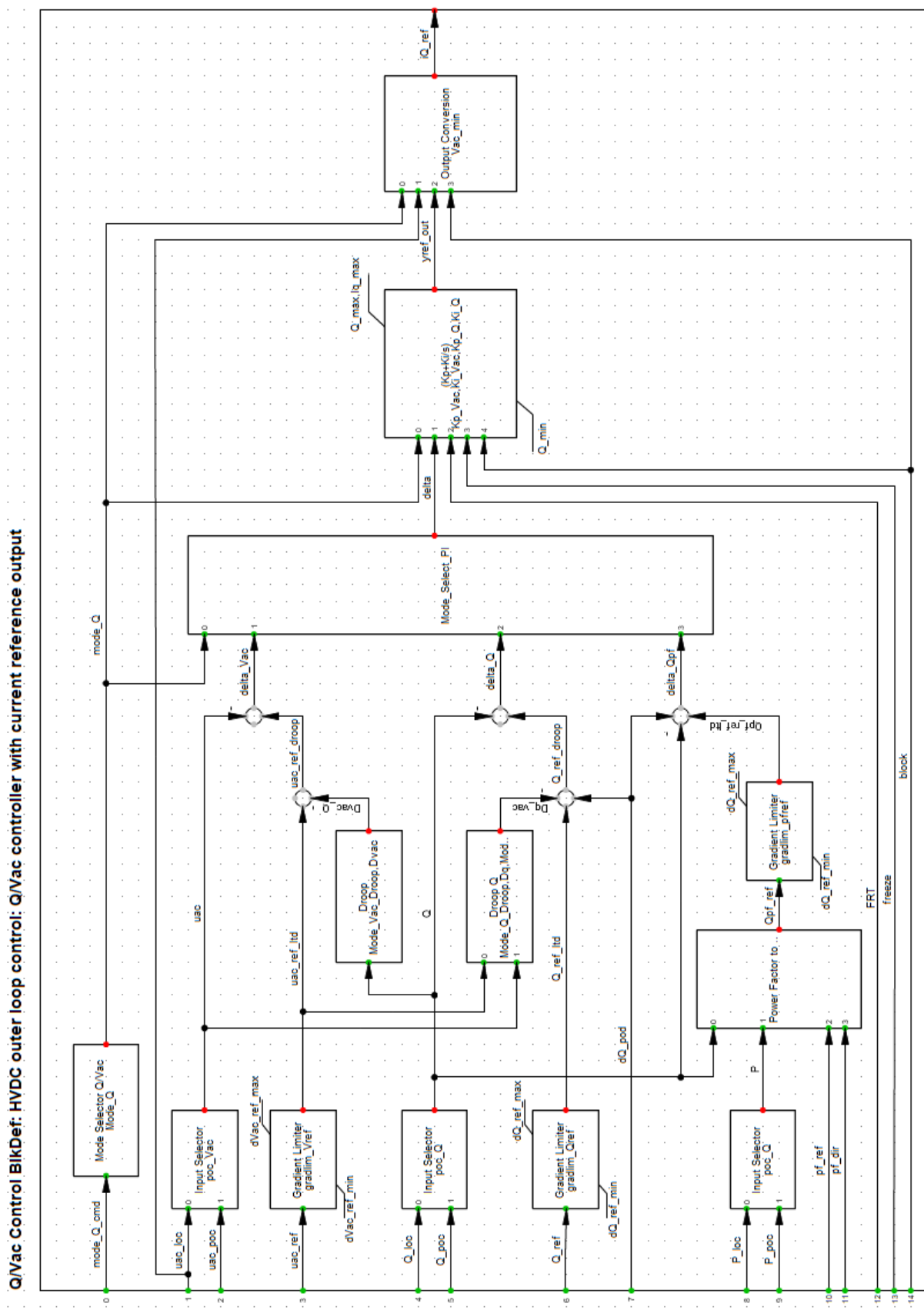


Figure C.3.: HVDC Reactive Power Control [8].

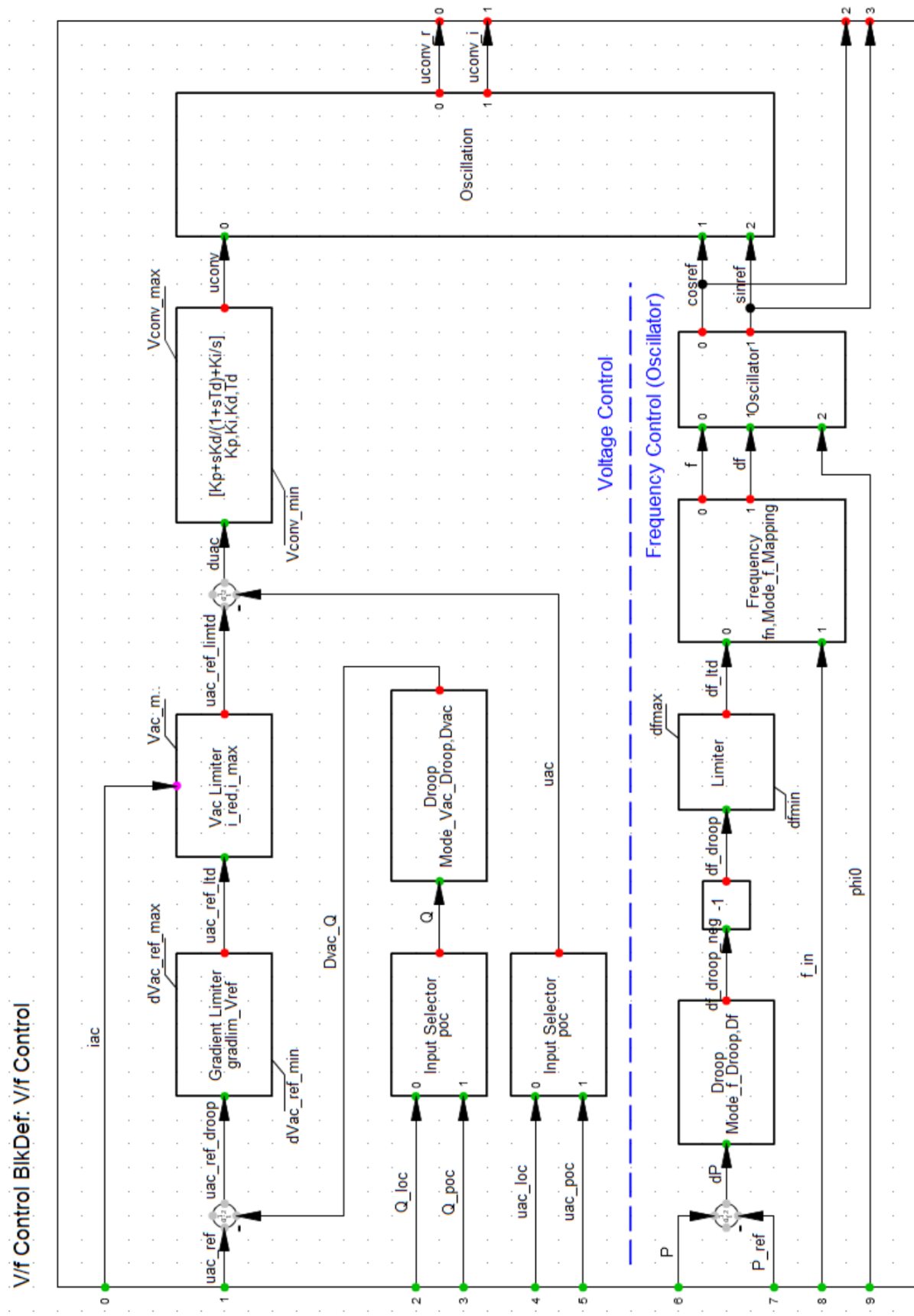


Figure C.4.: HVDC Voltage/Frequency Control [8].

fsm_Frequency Sensitive Mode BlkDef: Frequency Sensitive Mode

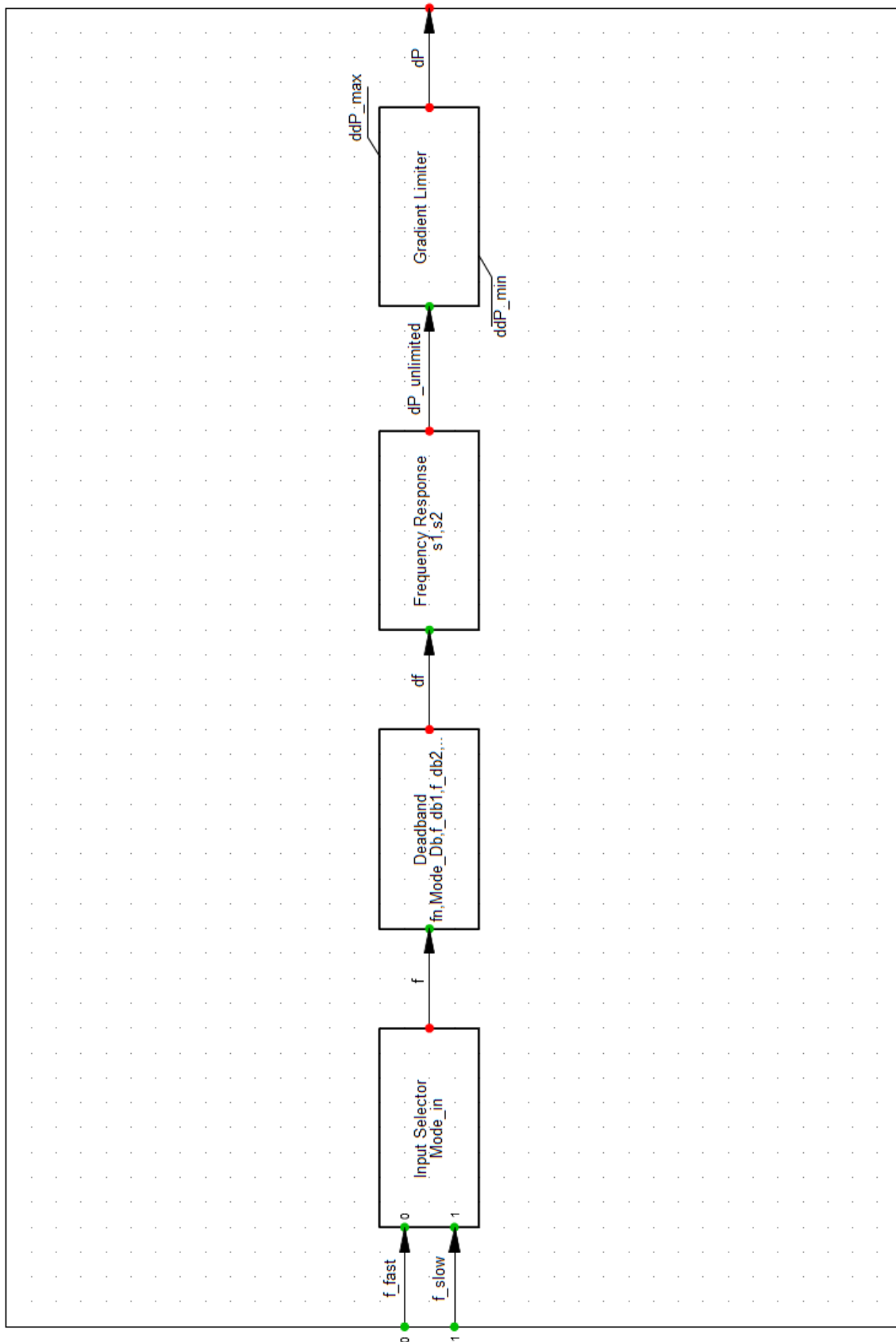


Figure C.5.: HVDC Frequency Sensitive Mode [8].

pod_Power Oscillation Damping BlkDef. Power Oscillation Damping

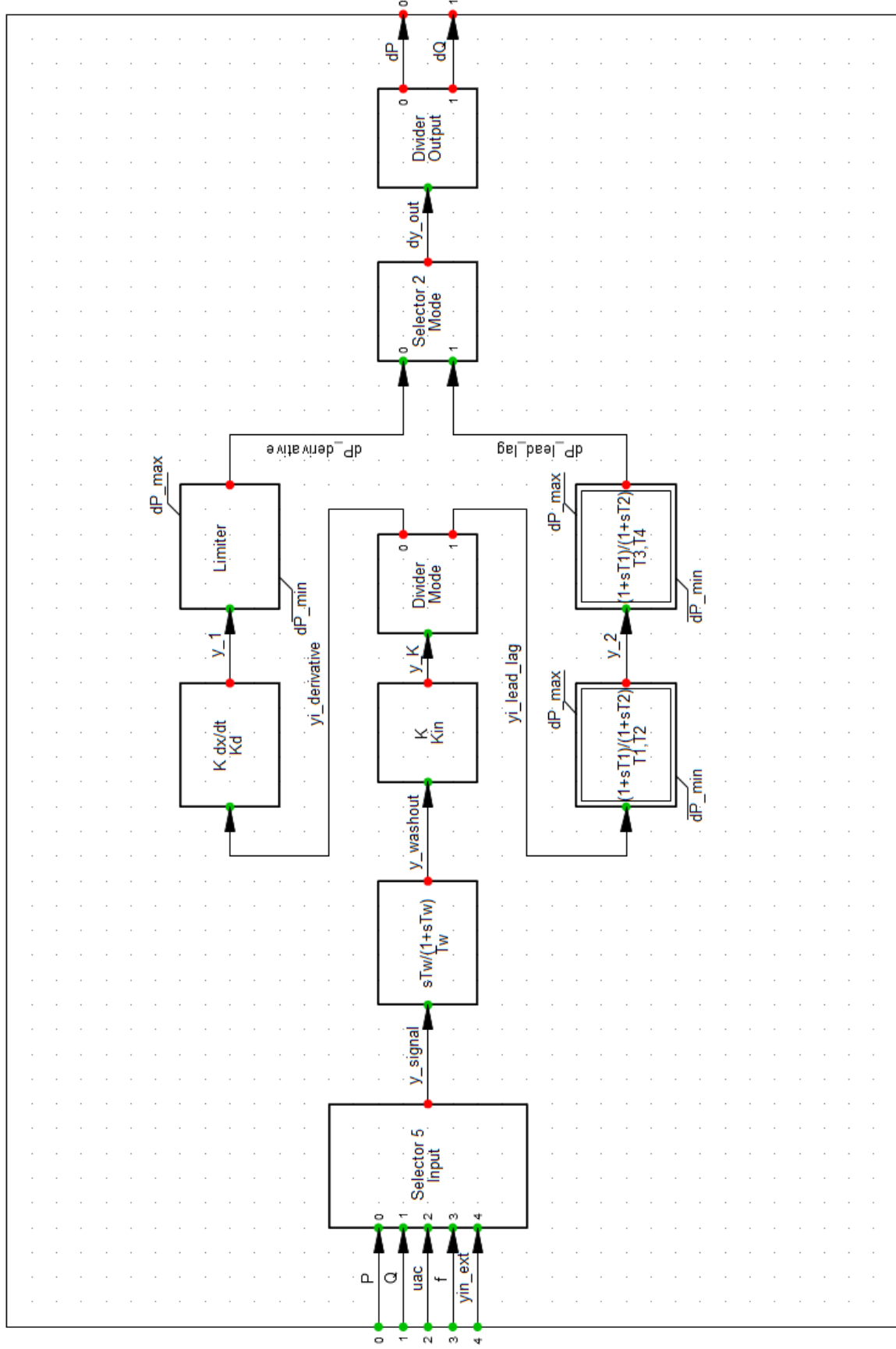


Figure C.6.: HVDC Power Oscillation Damper [8].

FRT Control BlkDef: Controller for Fault-Ride-Through Current Injection

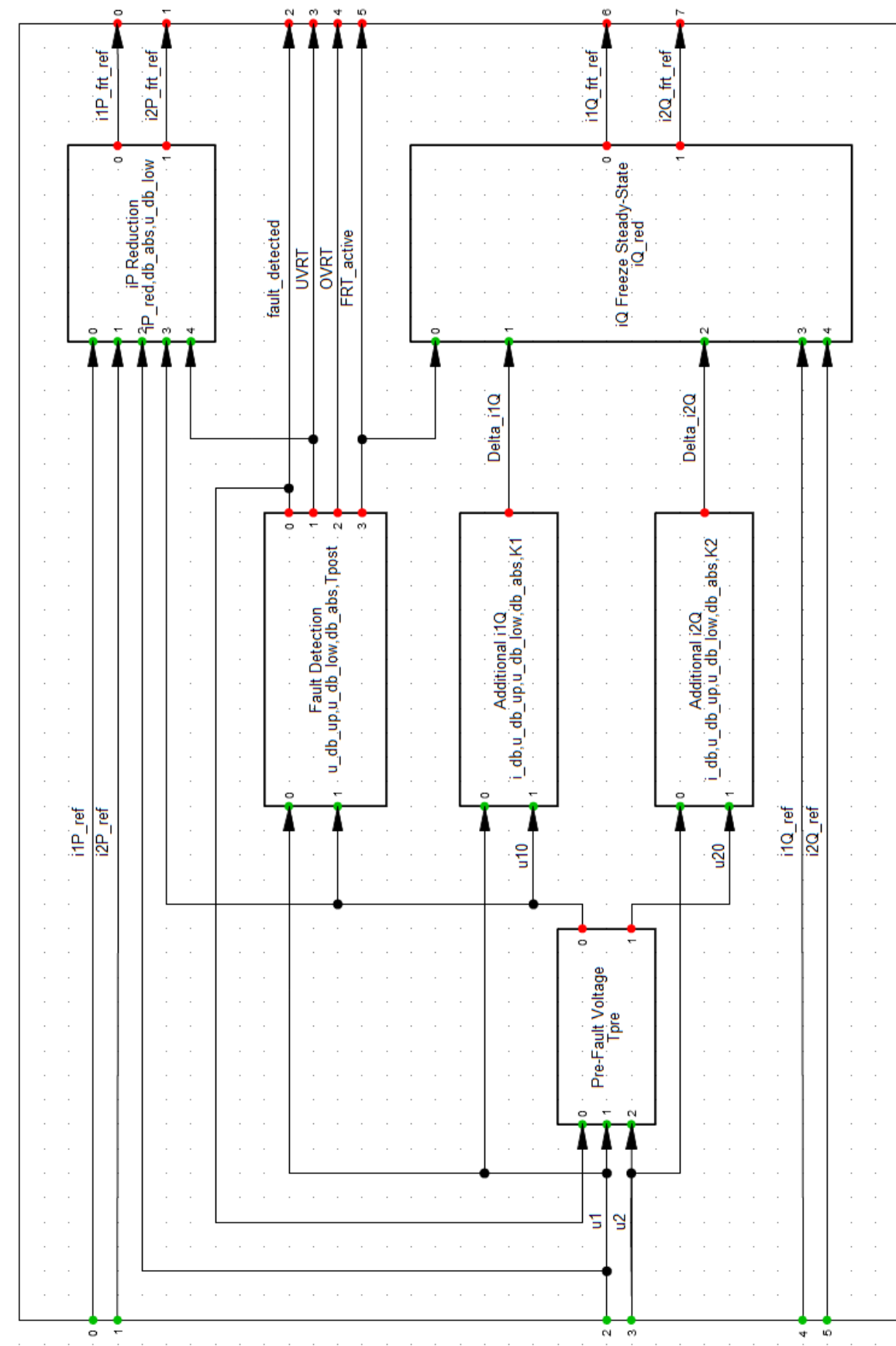


Figure C.7.: HVDC Fault-Ride Through Current Injection [8].

```

vardef(Pmax_EPC1) = '%';'Maximum power EPC function 1'
vardef(Pmax_EPC2) = '%';'Maximum power EPC function 2'
vardef(Pmax_EPC3) = '%';'Maximum power EPC function 3'
vardef(dP_EPC1) = '%/s';'Max. power limitation gradient (EPC1)'
vardef(dP_EPC2) = '%/s';'Max. power limitation gradient (EPC2)'
vardef(dP_EPC3) = '%/s';'Max. power limitation gradient (EPC3)'
vardef(dP_release) = '%/s';'Max. power gradient after EPC release'
vardef(Tmin) = 's' ;'Minimum activation time for starting EPC'

vardef(EPC1) = ;'Trigger Emergency Power Control Function 1'
vardef(EPC2) = ;'Trigger Emergency Power Control Function 2'
vardef(EPC3) = ;'Trigger Emergency Power Control Function 3'
vardef(EPC4) = ;'Trigger Emergency Power Control Function 4'
!vardef(P) = 'p.u.'; 'Active power'

vardef(EPC_flag) = ;'General EPC activation flag'
vardef(dP_epc) = 'p.u.'; 'Additional active power by EPC'
vardef(Pmin_epc) = 'p.u.'; 'Minimum power limitation by EPC'
vardef(Pmax_epc) = 'p.u.'; 'Maximum power limitation by EPC'

vardef(Pmin_epc1) = 'p.u.'; 'Minimum power limitation by EPC function 1'
vardef(Pmax_epc1) = 'p.u.'; 'Maximum power limitation by EPC function 1'
vardef(Pmin_epc2) = 'p.u.'; 'Minimum power limitation by EPC function 2'
vardef(Pmax_epc2) = 'p.u.'; 'Maximum power limitation by EPC function 2'
vardef(Pmin_epc3) = 'p.u.'; 'Minimum power limitation by EPC function 3'
vardef(Pmax_epc3) = 'p.u.'; 'Maximum power limitation by EPC function 3'
vardef(Pmin_inc) = 'p.u.'; 'Minimum power limitation without EPC'
vardef(Pmax_inc) = 'p.u.'; 'Maximum power limitation without EPC'

limfix(Pmax_EPC1) = [0,) ! Pmax_EPC1 >= 0
limfix(Pmax_EPC2) = [0,) ! Pmax_EPC2 >= 0
limfix(Pmax_EPC3) = [0,) ! Pmax_EPC3 >= 0
limfix(dP_EPC1) = (0,) ! dP_EPC1 > 0
limfix(dP_EPC2) = (0,) ! dP_EPC2 > 0
limfix(dP_EPC3) = (0,) ! dP_EPC3 > 0

limits(EPC1) = [0,1] ! 0 <= EPC function 1 <= 1
limits(EPC2) = [0,1] ! 0 <= EPC function 2 <= 1
limits(EPC3) = [0,1] ! 0 <= EPC function 3 <= 1
limits(EPC4) = [0,1] ! 0 <= EPC function 4 <= 1

inc(EPC1) = 0
inc(EPC2) = 0
inc(EPC3) = 0
inc(EPC4) = 0

inc(EPC_flag) = 0
inc(dP_epc) = 0
inc0(Pmin_epc) = -1.0
inc0(Pmax_epc) = 1.0
inc(Pmin_inc) = Pmin_epc
inc(Pmax_inc) = Pmax_epc

inc(epc1_active) = 0
inc(epc2_active) = 0
inc(epc3_active) = 0

epc1_start = picdro_const(flipflop(EPC1.and.(.not.EPC4),EPC4), Tmin, 0.0)
epc2_start = picdro_const(flipflop(EPC2.and.(.not.EPC4),EPC4), Tmin, 0.0)
epc3_start = picdro_const(flipflop(EPC3.and.(.not.EPC4),EPC4), Tmin, 0.0)

epc1_active = epc1_start.or.Pmax_epc1<Pmax_inc.or.Pmax_epc1>Pmax_inc
epc2_active = epc2_start.or.Pmax_epc2<Pmax_inc.or.Pmax_epc2>Pmax_inc
epc3_active = epc3_start.or.Pmax_epc3<Pmax_inc.or.Pmax_epc3>Pmax_inc

EPC_flag = epc1_active.or.epc2_active.or.epc3_active.or.EPC4

Pmax_epc1 = gradlim_const(select(epc1_start, Pmax_EPC1/100, Pmax_inc), -dP_EPC1/100, dP_release/100)
Pmin_epc1 = -Pmax_epc1
Pmax_epc2 = gradlim_const(select(epc2_start, Pmax_EPC2/100, Pmax_inc), -dP_EPC2/100, dP_release/100)
Pmin_epc2 = -Pmax_epc2
Pmax_epc3 = gradlim_const(select(epc3_start, Pmax_EPC3/100, Pmax_inc), -dP_EPC3/100, dP_release/100)
Pmin_epc3 = -Pmax_epc3

dP_epc = 0 ! example, could be used for other emergency power functions

Pmin_epc = max(Pmin_inc,max(Pmin_epc1,max(Pmin_epc2,Pmin_epc3)))
Pmax_epc = min(Pmax_inc,min(Pmax_epc1,min(Pmax_epc2,Pmax_epc3)))

output(epc1_start, 'EPC Function 1 activated.')
output(epc2_start, 'EPC Function 2 activated.')
output(epc3_start, 'EPC Function 3 activated.')
output(EPC4, 'EPC Function 4 activated.')

```

Figure C.8.: HVDC Emergency Power Control Code [8].

D

APPENDIX D: BESS-STORAGE MODELS

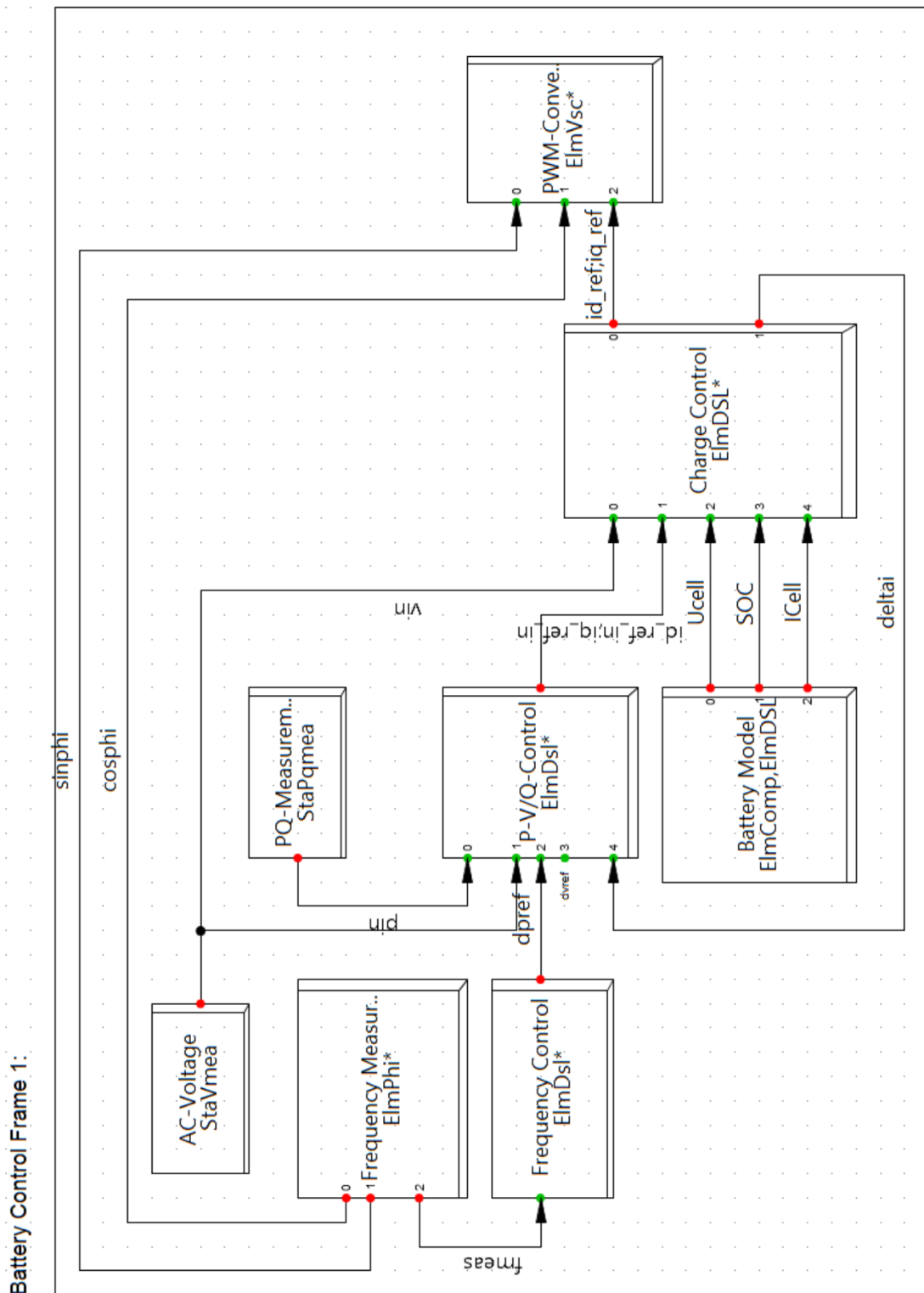


Figure D.1.: Battery-Energy Storage System Frame [13].

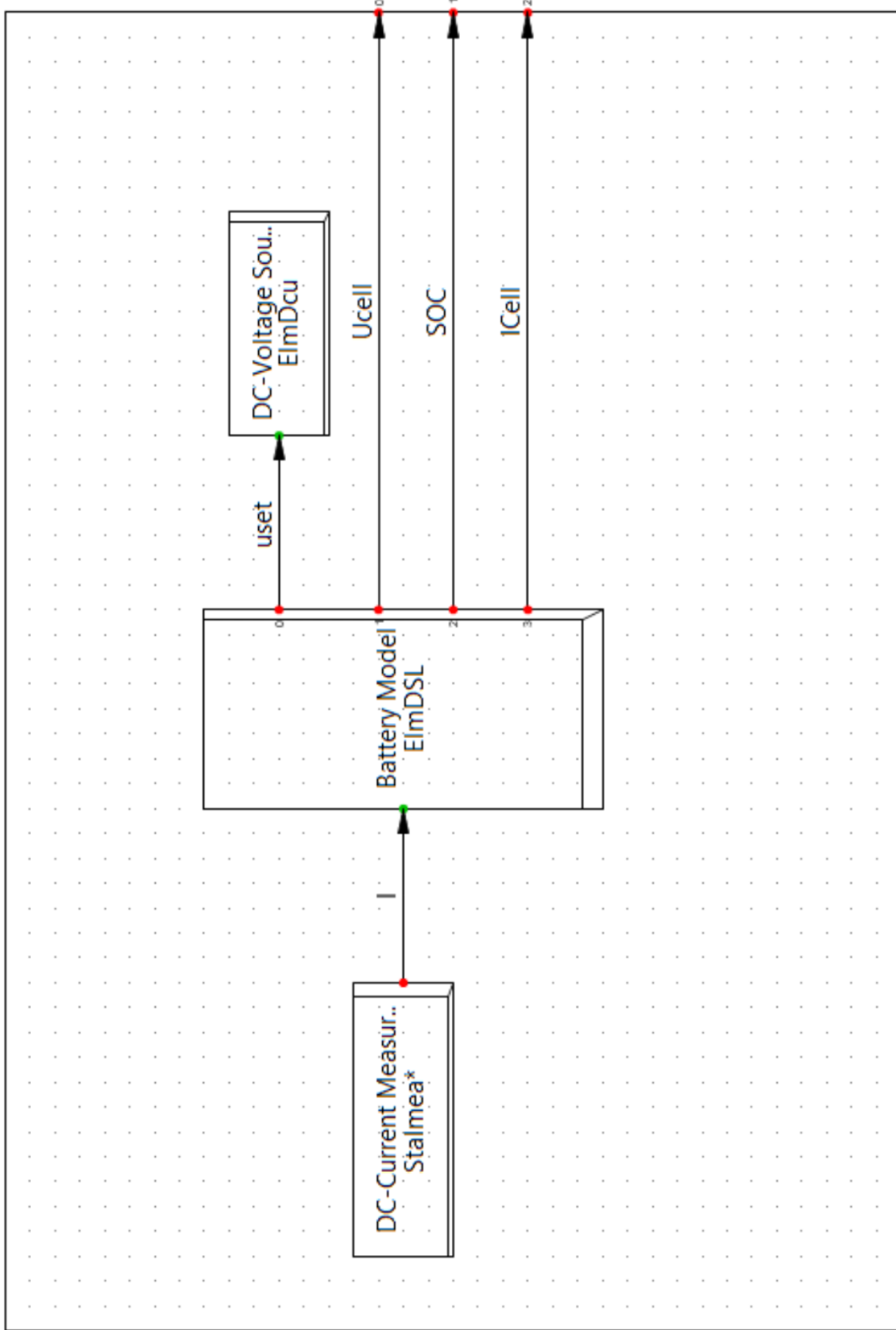
Battery Frame:

Figure D.2.: Battery Frame [13].

Battery cell simple model:

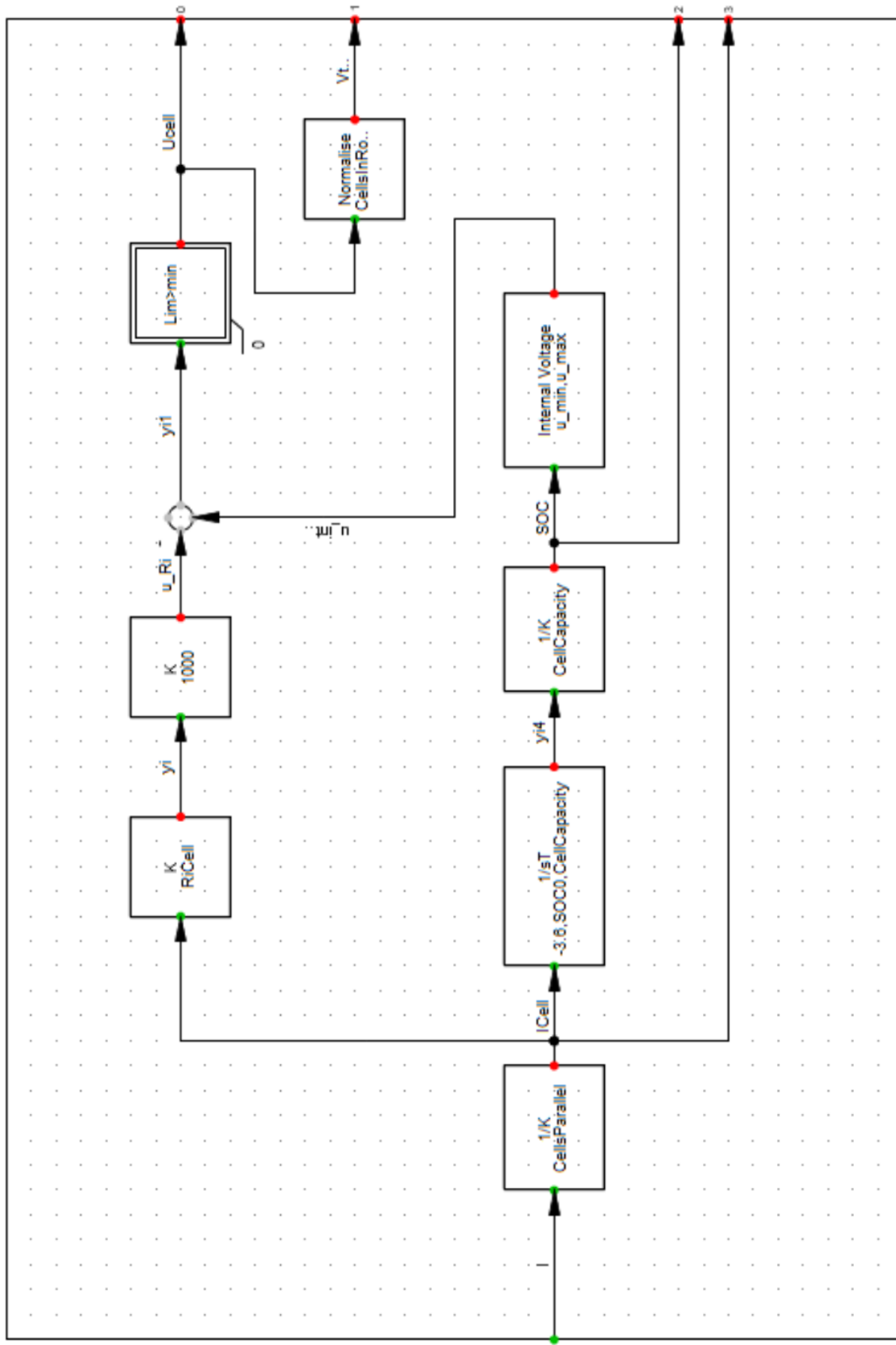


Figure D.3.: Electrochemical Battery Model [13].

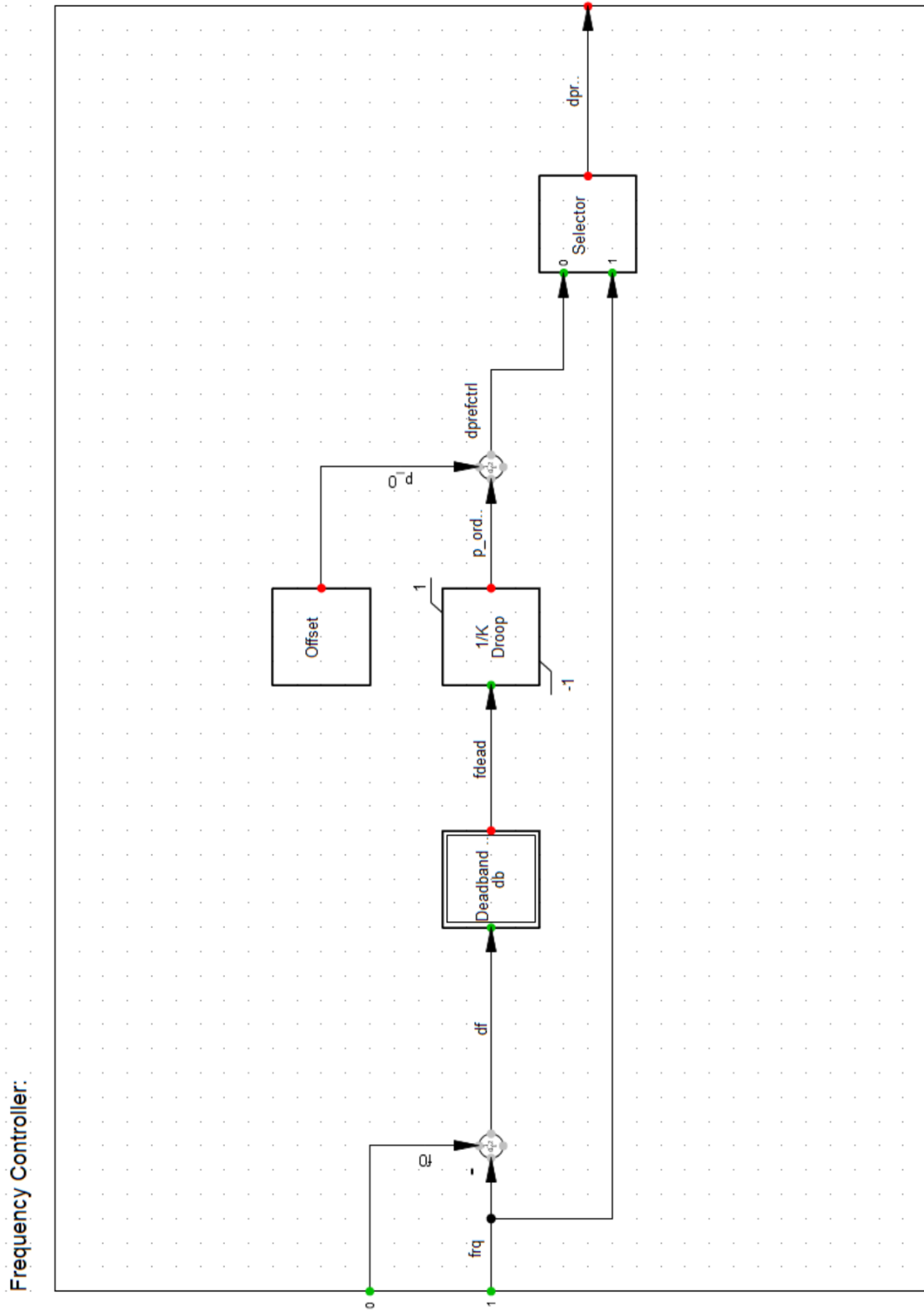


Figure D.4.: BESS Frequency Deviation Regulator [13].

Charge control_charging_FRT:

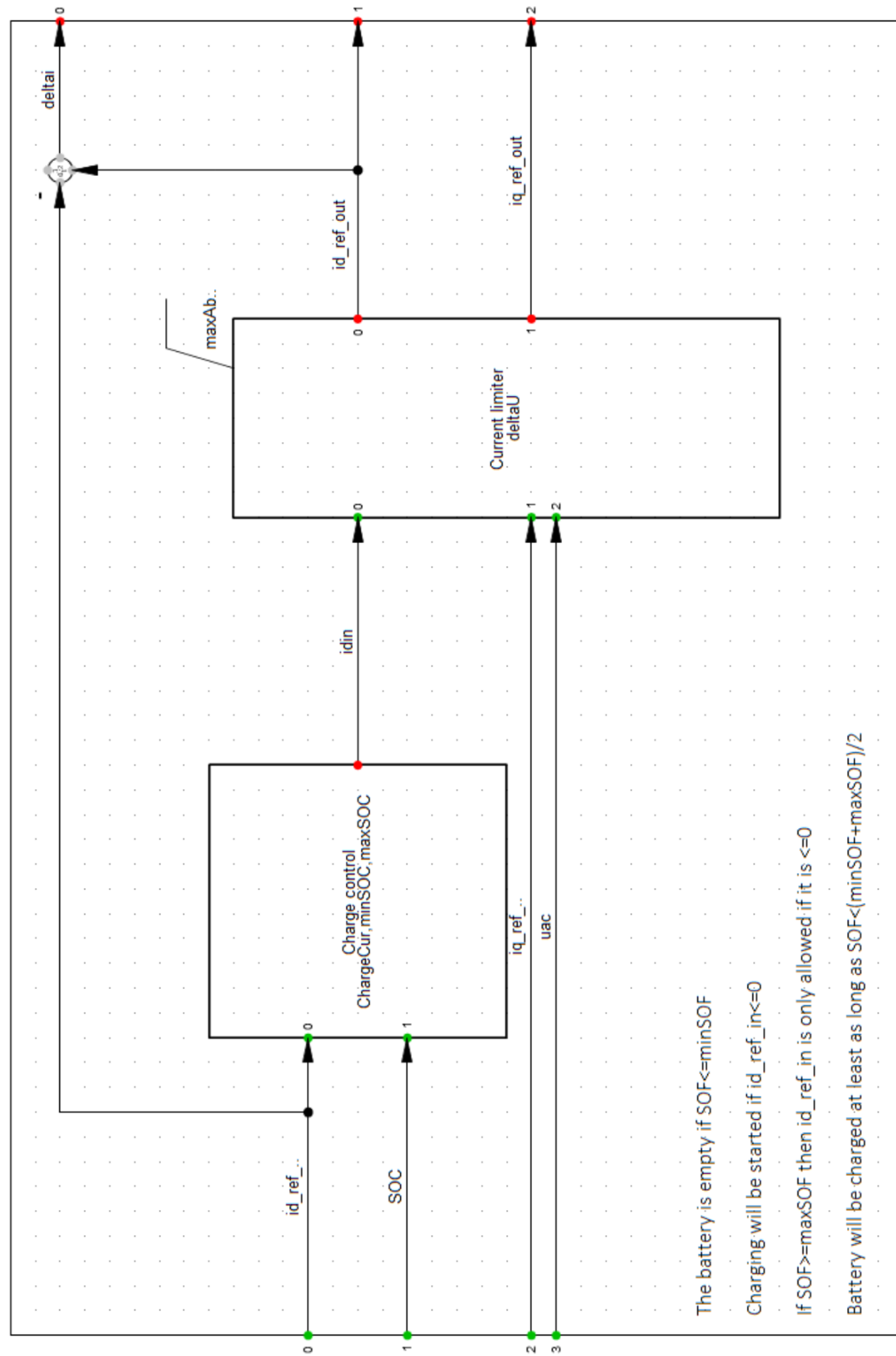


Figure D.5.: BESS Charge Controller [13].

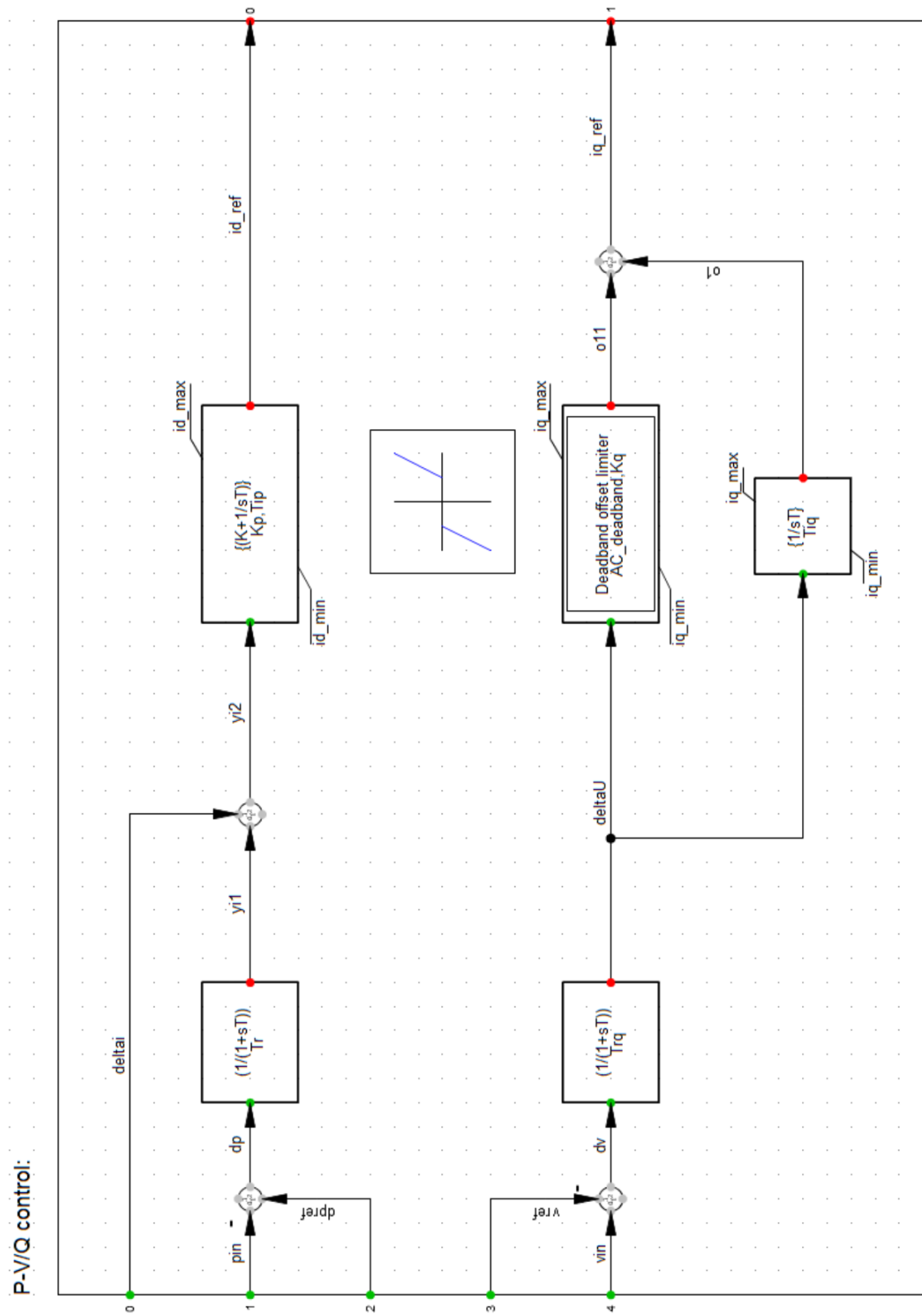


Figure D.6.: BESS Voltage/Power Regulator [13].

E

APPENDIX E: RELAY PROTECTION ALGORITHMS

E.1 RELAY CODE FOR PROTECTION SCHEME IN ZONE A

```
vardef(umin)='p.u.';'Bus Voltage Threshold'  
vardef(pmax)='p.u.';'Permissible Max Active Power'  
vardef(pmin)='p.u.';'Permissible Min Active Power'  
vardef(TSCC)='s';'Short-Circuit Clearing Delay'  
vardef(TMtd)='s';'Generator Torque Decrease Delay'  
vardef(TSwtG)='s';'Switch-off Generator Delay'  
vardef(TIslA)='s';'Area A Isolation Delay'  
vardef(TSwtLA)='s';'Trip A Loads Delay'  
vardef(TSwtEA)='s';'Trip A Elements Delay'  
vardef(Trec1)='s';'Time of Restoration Stage (1)'  
vardef(Trec2)='s';'Time of Restoration Stage (2)'  
vardef(Trec3)='s';'Time of Restoration Stage (3)'  
vardef(Trec4)='s';'Time of Restoration Stage (4)'  
vardef(Trec5)='s';'Time of Restoration Stage (5)'  
vardef(Trec6)='s';'Time of Restoration Stage (6)'  
vardef(Trec7)='s';'Time of Restoration Stage (7)'  
vardef(Trec8)='s';'Time of Restoration Stage (8)'  
vardef(Trec9)='s';'Time of Restoration Stage (9)'  
vardef(Trec10)='s';'Time of Restoration Stage (10)'  
vardef(Trec11)='s';'Time of Restoration Stage (11)'  
vardef(Trec12)='s';'Time of Restoration Stage (12)'  
vardef(Trec13)='s';'Time of Restoration Stage (13)'  
vardef(Trec14)='s';'Time of Restoration Stage (14)'  
vardef(Trec15)='s';'Time of Restoration Stage (15)'  
vardef(Trec16)='s';'Time of Restoration Stage (16)'  
vardef(Trec17)='s';'Time of Restoration Stage (17)'  
vardef(Trec18)='s';'Time of Restoration Stage (18)'  
vardef(Trec19)='s';'Time of Restoration Stage (19)'  
vardef(Trec20)='s';'Time of Restoration Stage (20)'  
vardef(Trec21)='s';'Time of Restoration Stage (21)'  
vardef(Trec22)='s';'Time of Restoration Stage (22)'  
vardef(Trec23)='s';'Time of Restoration Stage (23)'  
vardef(Trec24)='s';'Time of Restoration Stage (24)'
```

```
inc(ptmin)=0  
ptmin=select(time()>9,1,0)
```

```
inc(surgp)=0  
surgp=p>pmax.or.p<pmin
```

```
inc(SCC)=0  
SCC=picdro(u<umin,TSCC,o) !Short-Circuit Clearing
```

```
surgisl=time()>90.56,surgp
```

$!90.56 = \text{Protection Action Time} + \text{TI}_{\text{LA}} (0.15) + 0.01$

$\text{surglid} = \text{time}() > 90.61, \text{surgp}$

$!90.61 = \text{Protection Action Time} + \text{TSwtLA} (0.2) + 0.01$

$\text{surgelm} = \text{time}() > 90.71, \text{surgp}$

$!90.71 = \text{Protection Action Time} + \text{TSwtEA} (0.3) + 0.01$

$\text{recstt} = \text{time}() > 135.01, \text{surgp}$

$!135.01 = \text{Protection Action Time} + \text{Trec2} (75) + 0.01$

$\text{recsyg} = \text{time}() > 165.01, \text{surgp}$

$!165.01 = \text{Protection Action Time} + \text{Trec2} (75) + 0.01$

$\text{recwp3} = \text{time}() > 330.01, \text{surgp}$

$!330.01 = \text{Protection Action Time} + \text{Trec13} (240) + 0.01$

$\text{rechvdc} = \text{time}() > 345.01, \text{surgp}$

$!345.01 = \text{Protection Action Time} + \text{Trec14} (255) + 0.01$

$\text{pul} = \text{time}() > 435.01, \text{surgp}$

$!435.01 = \text{Protection Action Time} + \text{Trec20} (345) + 0.01$

$\text{recend} = \text{time}() > 495.01, \text{surgp}$

$!495.01 = \text{Protection Action Time} + \text{Trec24} (405) + 0.01$

!FAULT STAGE (1)

!EVENTS 1.1: CLEAR SHORT CIRCUIT FAULT

!Clear Short-Circuit Fault in Bus A1 (Area A)

event(1, SCC, 'name=A1_SC_Clear target=A1')

!Clear Short-Circuit Fault in Bus A2 (Area A)

event(1, SCC, 'name=A2_SC_Clear target=A2')

!Clear Short-Circuit Fault in Bus 110_kV_A3 (Area A)

!event(1, SCC, 'name=110_kV_A3_SC_Clear target=110_kV_A3')

!Clear Short-Circuit Fault in Bus A7a (Area A)

event(1, SCC, 'name=A7a_SC_Clear target=A7a')

output(surgp, 'SHORT-CIRCUIT FAULT in Area A. Four faults detected in this Zone. Risk of MASSIVE BLACKOUT')

!EVENTS 1.2: LOSS OF GENERATION A

!Decrease Minimum Mech. Power A1aG Hydro SyM (Area A)

event(1, surgp, 'name=Gov_A1aG_PtminDwn dtime=TMtd')

!Decrease Mech. Torque A1aG Hydro SyM (Area A)

event(1, surgp, 'name=MTorqo_A1aG dtime=TMtd')

!Disconnect A1aG Hydro SyM (Area A)

event(1, surgp, 'name=SyM_1aG_Out dtime=TSwtG')

!Decrease Mech. Torque PMSG WPA1 (Area A)

event(1, surgp, 'name=MTorqo_WPA1 dtime=TMtd')

!Disconnect PMSG WPA1 (Area A)

event(1, surgp, 'name=SyM_WPA1_Out dtime=TSwtG')

!Decrease Mech. Torque PMSG WPA2 (Area A)

event(1, surgp, 'name=MTorqo_WPA2 dtime=TMtd')

!Disconnect PMSG WPA2 (Area A)
 event(1, surgp, 'name=SyM_WPA2_Out dtime=TSwtG')
 !Decrease Mech. Torque PMSG WPA3 (Area A)
 event(1, surgp, 'name=MTorqo_WPA3 dtime=TMtd')
 !Disconnect PMSG WPA3 (Area A)
 event(1, surgp, 'name=SyM_WPA3_Out dtime=TSwtG')
 output(SCC,'Remedial Protection Scheme Started: Short-Circuit Cleared. AREA-A SHEDDING in order to preserve the integrity of the Grid. A BLACK-START and NETWORK RESTORATION will be executed at the proper time.')

!EVENTS 1.3: AREA A ISLAND

!Disconnect HVDC AB Circuit Breaker
 event(1, surgp, 'name=HVDC_AB_Out dtime=TIslA')
 !Disconnect HVDC BA Circuit Breaker
 event(1, surgp, 'name=HVDC_BA_Out dtime=TIslA')
 !Disconnect HVDC AC Circuit Breaker
 event(1, surgp, 'name=HVDC_AC_Out dtime=TIslA')
 !Disconnect HVDC CA Circuit Breaker
 event(1, surgp, 'name=HVDC_CA_Out dtime=TIslA')
 output(surgisl,'Area A is now ISOLATED from the rest of the Network')

!EVENTS 1.4: LOSS OF LOADS A

!Disconnect General Load (Area A)
 event(1, surgp, 'name=GL_Out dtime=TSwtLA')
 !Disconnect General Load 1 (Area A)
 event(1, surgp, 'name=GL_Out(1) dtime=TSwtLA')
 !Disconnect General Load 2 (Area A)
 event(1, surgp, 'name=GL_Out(2) dtime=TSwtLA')
 !Disconnect General Load 3 (Area A)
 event(1, surgp, 'name=GL_Out(3) dtime=TSwtLA')
 !Disconnect General Load 4 (Area A)
 event(1, surgp, 'name=GL_Out(4) dtime=TSwtLA')
 !Disconnect General Load 5 (Area A)
 event(1, surgp, 'name=GL_Out(5) dtime=TSwtLA')
 !Disconnect General Load 6 (Area A)
 event(1, surgp, 'name=GL_Out(6) dtime=TSwtLA')
 !Disconnect General Load 7 (Area A)
 event(1, surgp, 'name=GL_Out(7) dtime=TSwtLA')
 !Disconnect General Load 8 (Area A)
 event(1, surgp, 'name=GL_Out(8) dtime=TSwtLA')
 output(surgld,'Disconnection of Loads in Area A')

!EVENTS 1.5: LOSS OF DEVICES A

!Disconnect M_A1a_2T Trafo (Area A)
 event(1, surgp, 'name=M_A1a_2T_Out dtime=TSwtEA')
 !Disconnect 110_kV_A_TF1 Trafo (Area A)
 event(1, surgp, 'name=A_TF1_Out dtime=TSwtEA')
 !Disconnect 110_kV_A_TF2 Trafo (Area A)
 event(1, surgp, 'name=A_TF2_Out dtime=TSwtEA')
 !Disconnect 110_kV_A_TF3 Trafo (Area A)
 event(1, surgp, 'name=A_TF3_Out dtime=TSwtEA')
 !Disconnect 110_kV_A_TF4 Trafo (Area A)
 event(1, surgp, 'name=A_TF4_Out dtime=TSwtEA')
 !Disconnect 110_kV_A_TF5 Trafo (Area A)
 event(1, surgp, 'name=A_TF5_Out dtime=TSwtEA')
 !Disconnect 110_kV_A_TF6 Trafo (Area A)

```

event(1,surgp,'name=A_TF6_Out dtime=TSwtEA')
!Disconnect A1-A2 Line (Area A)
event(1,surgp,'name=A1-A2_Out dtime=TTSwtEA')
!Disconnect A1-A4 Line (Area A)
event(1,surgp,'name=A1-A4_Out dtime=TSwtEA')
!Disconnect A2-A3 Line (Area A)
event(1,surgp,'name=A2-A3_Out dtime=TSwtEA')
!Disconnect A2-A5a Line (Area A)
event(1,surgp,'name=A2-A5a_Out dtime=TSwtEA')
!Disconnect A2-A5b Line (Area A)
event(1,surgp,'name=A2-A5b_Out dtime=TSwtEA')
!Disconnect A4-A5a Line (Area A)
event(1,surgp,'name=A4-A5a_Out dtime=TSwtEA')
!Disconnect A4T Trafo (Area A)
event(1,surgp,'name=A4T_Out dtime=TSwtEA')
!Disconnect A5a-A5b Line (Area A)
event(1,surgp,'name=A5a-A5b_Out dtime=TSwtEA')
!Disconnect A5a-A7a Line (Area A)
event(1,surgp,'name=A5a-A7a_Out dtime=TSwtEA')
!Disconnect A5b-A7a Line (Area A)
event(1,surgp,'name=A5b-A7a_Out dtime=TSwtEA')
!Disconnect A6T Trafo (Area A)
event(1,surgp,'name=A6T_Out dtime=TSwtEA')
!Disconnect A6-A7 Line (Area A)
event(1,surgp,'name=A6-A7_Out dtime=TSwtEA')
!Disconnect A7T Trafo (Area A)
event(1,surgp,'name=A7T_Out dtime=TSwtEA')
output(surgelm,'Disconnection of all elements in Area A. Now Area A is FULLY OUTAGED.')

```

!RESTORATION STAGE (2)

!EVENTS 2.1

!Reconnect A1aG Hydro SyM (Area A)

event(1,surgp, 'name=SyM_A1aG_Rec dtime=Trec1')

!EVENTS 2.2

!Reconnect M_A1a_2T Trafo (Area A)

event(1,surgp,'name=M_A1a_2T_In dtime=Trec2')

output(recsyg,'Hydro Synchronous Generator A1aG Reconnected.')

output(recstt,'NETWORK RESTORATION STAGE BEGINS.')

!EVENTS 2.3

!Reconnect A1-A2 Line (Area A)

event(1,surgp,'name=A1-A2_In dtime=Trec3')

!Reconnect 110_kV_A_TF2 Trafo (Area A)

event(1,surgp,'name=A_TF2_In dtime=Trec3')

!EVENTS 2.4

!Reconnect PMSG WPA1 (Area A)

event(1,surgp,'name=SyM_WPA1_Rec dtime=Trec4')

!EVENTS 2.5

!Reconnect A2-A3 Line (Area A)

event(1,surgp,'name=A2-A3_In dtime=Trec5')

!Reconnect 110_kV_A_TF3 Trafo (Area A)

```

event(1,surgp,'name=A_TF3_In dtime=Trec5')

!EVENTS 2.6
!Reconnect PMSG WPA2 (Area A)
event(1,surgp,'name=SyM_WPA2_Rec dtime=Trec6')

!EVENTS 2.7
!Reconnect A1-A4 Line (Area A)
event(1,surgp,'name=A1-A4_In dtime=Trec7')
!Reconnect A2-A5a Line (Area A)
event(1,surgp,'name=A2-A5a_In dtime=Trec7')
!Reconnect A2-A5b Line (Area A)
event(1,surgp,'name=A2-A5b_In dtime=Trec7')

!EVENTS 2.8
!Reconnect A4-A5a Line (Area A)
event(1,surgp,'name=A4-A5a_In dtime=Trec8')
!Reconnect A5a-A5b Line (Area A)
event(1,surgp,'name=A5a-A5b_In dtime=Trec8')

!EVENTS 2.9
!Reconnect A5a-A7a Line (Area A)
event(1,surgp,'name=A5a-A7a_In dtime=Trec9')
!Reconnect A5b-A7a Line (Area A)
event(1,surgp,'name=A5b-A7a_In dtime=Trec9')

!EVENTS 2.10
!Reconnect A7T Trafo (Area A)
event(1,surgp,'name=A7T_In dtime=Trec10')

!EVENTS 2.11
!Reconnect A6-A7 Line (Area A)
event(1,surgp,'name=A6-A7_In dtime=Trec11')

!EVENTS 2.12
!Reconnect A6T Trafo (Area A)
event(1,surgp,'name=A6T_In dtime=Trec12')

!EVENTS 2.13
!Reconnect PMSG WPA3 (Area A)
event(1,surgp,'name=SyM_WPA3_Rec dtime=Trec13')
output(recwp3,'Wind Farms of Zone A Reconnected.')

!EVENTS 2.14
!Reconnect HVDC AB Circuit Breaker
event(1,surgp,'name=HVDC_AB_In dtime=Trec14')
!Reconnect HVDC BA Circuit Breaker
event(1,surgp,'name=HVDC_BA_In dtime=Trec14')
!Reconnect HVDC AC Circuit Breaker
event(1,surgp,'name=HVDC_AC_In dtime=Trec14')
!Reconnect HVDC CA Circuit Breaker
event(1,surgp,'name=HVDC_CA_In dtime=Trec14')
output(rechvdc,'HVDC Transmission lines are now Reconnected.')

```

!EVENTS 2.15

```
!Increase Mech. Torque A1aG Hydro SyM (Area A)
event(1, surgp, 'name=MTorqUp_A1aG dtime=Trec15')
!Increase Minimum Mech. Power A1aG Hydro SyM (Area A)
event(1, ptmin, 'name=Gov_A1aG_PtminUp dtime=0.01')
event(1, surgp, 'name=Gov_A1aG_PtminUp dtime=Trec20')
!Increase Mech. Torque PMSG WPA1 (Area A)
event(1, surgp, 'name=MTorqUp_WPA1 dtime=Trec15')
!Increase Mech. Torque PMSG WPA2 (Area A)
event(1, surgp, 'name=MTorqUp_WPA2 dtime=Trec15')
!Increase Mech. Torque PMSG WPA3 (Area A)
event(1, surgp, 'name=MTorqUp_WPA3 dtime=Trec15')
```

!EVENTS 2.16

```
!Reconnect 110_kV_A_TF1 Trafo (Area A)
event(1, surgp, 'name=A_TF1_In dtime=Trec16')
```

!EVENTS 2.17

```
!Reconnect 110_kV_A_TF4 Trafo (Area A)
event(1, surgp, 'name=A_TF4_In dtime=Trec17')
!Reconnect 110_kV_A_TF5 Trafo (Area A)
event(1, surgp, 'name=A_TF5_In dtime=Trec17')
```

!EVENTS 2.18

```
!Reconnect A4T Trafo (Area A)
event(1, surgp, 'name=A4T_In dtime=Trec18')
```

!EVENTS 2.19

```
!Reconnect 110_kV_A_TF6 Trafo (Area A)
event(1, surgp, 'name=A_TF6_In dtime=Trec19')
```

!EVENTS 2.20

```
!Connect Schalter-Ereignis Load (Area A)
event(1, surgp, 'name=Schalter-Ereignis dtime=Trec20')
output(pul, 'Initialisation of Load Pick-Up Process.')
```

!EVENTS 2.21

```
!Reconnect General Load 1 (Area A)
event(1, surgp, 'name=GL_In(1) dtime=Trec21')
!Reconnect General Load 4 (Area A)
event(1, surgp, 'name=GL_In(4) dtime=Trec21')
```

!EVENTS 2.22

```
!Reconnect General Load (Area A)
event(1, surgp, 'name=GL_In dtime=Trec22')
!Reconnect General Load 3 (Area A)
event(1, surgp, 'name=GL_In(3) dtime=Trec22')
!Reconnect General Load 8 (Area A)
event(1, surgp, 'name=GL_In(8) dtime=Trec22')
```

!EVENTS 2.23

```
!Reconnect General Load 2 (Area A)
event(1, surgp, 'name=GL_In(2) dtime=Trec23')
!Reconnect General Load 7 (Area A)
event(1, surgp, 'name=GL_In(7) dtime=Trec23')
```

```
!EVENTS 2.24
!Reconnect General Load 5 (Area A)
event(1,surgp,'name=GL_In(5) dtime=Trec24')
!Reconnect General Load 6 (Area A)
event(1,surgp,'name=GL_In(6) dtime=Trec24')
output(recend,'NETWORK RESTORATION IN ZONE A COMPLETED.')
```

E.2 RELAY CODE FOR PROTECTION SCHEME IN ZONE B/ZONE C

```
vardef(imax)='p.u.';'Permissible Max Current'
vardef(TSwtBC)='s';'Switch B-C Loads/Elements Delay'
vardef(Trec1)='s';'Time of Restoration Stage (1)'
vardef(Trec2)='s';'Time of Restoration Stage (2)'
vardef(Trec3)='s';'Time of Restoration Stage (3)'
vardef(Trec4)='s';'Time of Restoration Stage (4)'
vardef(Trec5)='s';'Time of Restoration Stage (5)'
vardef(Trec6)='s';'Time of Restoration Stage (6)'
vardef(Trec7)='s';'Time of Restoration Stage (7)'

inc(surgi)=0
surgi=i>imax

inc(surgu)=0
surgu=u<0.8

surgisl=time()>94.536,surgi
!94.536 = Protection Action Time (94.226) + TSwtBC (0.3) + 0.01

recend=time()>610.236,surgi
!610.236 = Protection Action Time (94.226) + Trec7 (516) + 0.01
```

!EVENTS 1: LOSS OF LOADS B/C

```
!Increase C12G Governor Limits (Area C)
event(1, surgu, 'name=Gov_C12G_Ptmax1 dtime=0.15')
!Decrease C12G Governor Limits (Area C)
event( 1, surgi, 'name=Gov_C12G_Ptmax2 dtime=0.15')
!Disconnect B1a-B4 Line (Area B)
event(1,surgi,'name=B1a-B4_Out dtime=TSwtBC')
!Disconnect B2c-B4 Line (Area B)
event(1,surgi,'name=B2c-B4_Out dtime=TSwtBC')
!Disconnect 110_kV_B_TF5 Trafo (Area B)
event(1,surgi,'name=110_kV_B_TF5_Out dtime=TSwtBC')
!Disconnect General Load 20 (Area B)
event(1,surgi,'name=GL_Out(20) dtime=TSwtBC')
!Disconnect C3-C5 Line (Area C)
event(1,surgi,'name=C3-C5_Out dtime=TSwtBC')
!Disconnect C5-C6 Line (Area C)
event(1,surgi,'name=C5-C6_Out dtime=TSwtBC')
!Disconnect C5T Trafo (Area C)
event(1,surgi,'name=C5T_Out dtime=TSwtBC')
!Disconnect General Load 41 (Area C)
event(1,surgi,'name=GL_Out(41) dtime=TSwtBC')
```

```
!Disconnect General Load 34 (Area C)
event(1,surgi,'name=GL_Out(34) dtime=TSwtBC')
!Disconnect 110_kV_C_TF13 Trafo (Area C)
event(1,surgi,'name=110_kV_C_TF13_Out dtime=TSwtBC')
!Disconnect C12-C13 Line (Area C)
event(1,surgi,'name=C12-C13_Out dtime=TSwtBC')
!Disconnect C13-C14 Line (Area C)
event(1,surgi,'name=C13-C14_Out dtime=TSwtBC')
!Disconnect General Load 36 (Area C)
event(1,surgi,'name=GL_Out(36) dtime=TdSwtBC')
!Disconnect 110_kV_C_TF8 Trafo (Area C)
event(1,surgi,'name=110_kV_C_TF8_Out dtime=TSwtBC')
output(surgisl,'Load Shedding Relay C12G trips elements for avoid Network Overload')
```

!RECONNECTION STAGE

!EVENTS 2.1: LINES B

```
!Reconnect B1a-B4 Line (Area B)
event(1,surgi,'name=B1a-B4_In dtime=Trec1')
!Reconnect B2c-B4 Line (Area B)
event(1,surgi,'name=B2c-B4_In dtime=Trec1')
```

!EVENTS 2.2: LINES C

```
!Reconnect C3-C5 Line (Area C)
event(1,surgi,'name=C3-C5_In dtime=Trec2')
!Reconnect C5-C6 Line (Area C)
event(1,surgi,'name=C5-C6_In dtime=Trec2')
```

!EVENTS 2.3: LINES C

```
!Reconnect C12-C13 Line (Area C)
event(1,surgi,'name=C12-C13_In dtime=Trec3')
!Reconnect C13-C14 Line (Area C)
event(1,surgi,'name=C13-C14_In dtime=Trec3')
```

!EVENTS 2.4: TRAFOS B/C

```
!Reconnect 110_kV_B_TF5 Trafo (Area B)
event(1,surgi,'name=110_kV_B_TF5_In dtime=Trec4')
!Reconnect 110_kV_C_TF13 Trafo (Area C)
event(1,surgi,'name=110_kV_C_TF13_In dtime=Trec4')
```

!EVENT 2.5: TRAFOS C

```
!Reconnect C5T Trafo (Area C)
event(1,surgi,'name=C5T_In dtime=Trec5')
!Reconnect 110_kV_C_TF8 Trafo (Area C)
event(1,surgi,'name=110_kV_C_TF8_In dtime=Trec5')
```

!EVENT 2.6: LOADS B/C

```
!Reconnect General Load 20 (Area B)
event(1,surgi,'name=GL_In(20) dtime=Trec6')
!Reconnect General Load 41 (Area C)
event(1,surgi,'name=GL_In(41) dtime=Trec6')
```

!EVENT 2.7: LOADS C

```
!Reconnect General Load 34 (Area C)
event(1,surgi,'name=GL_In(34) dtime=Trec7')
!Reconnect General Load 36 (Area C)
event(1,surgi,'name=GL_In(36) dtime=Trec7')
output(recend,'NETWORK RESTORATION IN ZONES B-C COMPLETED.')
```

COLOPHON

This document was typeset using \LaTeX . The document layout was generated using the `arsclassica` package by Lorenzo Pantieri, which is an adaption of the original `classicthesis` package from André Miede.

